Blast Resistance of Non-Composite Tilt-Up Sandwich Panels and Their Connections

José Barreiro

Thesis Submitted to the
Faculty of Graduate and Postdoctoral Studies
in partial fulfillment of the requirements for the degree of
Master of Applied Science
In Civil Engineering

uOttawa

Abstract

Blast risk associated with terrorist threats and accidental explosions has become an international concern over the past decade and has provoked structural engineers to implement protective design measures. Recent advances in this area of research has seen tremendous improvements in mitigating this risk through the installation of retrofits, advanced structural design, or pre-emptive protective measures. Tilt-up and precast panel walls are constructed using a unique approach in which the walls are cast horizontally and lifted, or tilted, into their final vertical position. These unique structures are cost effective, energy efficient, and can be rapidly constructed. This approach is commonly applied to the construction of large industrial facilities and the construction of schools which are categorized as high importance structures in the National Building Code of Canada. These panels are inherently flexible and have a surplus of mass making them desirable for protective design applications, however their behaviour under blast induced loads is not well defined.

This experimental research project investigates the behaviour of non-composite tilt-up sandwich (NCTS) panels and solid reinforced concrete (SRC) panels with realistic support conditions subjected to blast-induced shockwaves. Previous research shows that NCTS panels, identifiable by their large structural wythe, exhibit some degree of composite behaviour and require between *5%* to *10%* composite action for successful erection.

Five scaled specimens were constructed following common procedures used in practice, equipped with identical data acquisition instruments, and tested at the University of Ottawa shock tube testing facility under similar blast pressure-impulse combinations. Test results for the NCTS and SRC panels are compared graphically in terms of displacement–time histories and sectional strain distributions. The data is evaluated to approximate the composite behaviour at mid-span of the NCTS panel. Analytical results generated, using "RC Blast," single-degree-of-freedom analysis software developed at the University of Ottawa, were validated with empirical data and are presented graphically.

Each specimen was equipped with connections similar to those commonly used in the construction of NCTS panels. These connections were experimentally studied under simulated blast pressures and analysed using CSA A23.3-04 guidelines for punching shear capacity. Modified support

reinforcement layouts and surface bonded FRP laminates were evaluated as strengthening and retrofit techniques to prevent support failure. Dynamic support reactions and predicted support resistances are tabulated for each shot of every panel.

The results indicate that it is possible to accurately predict the flexural behaviour and support resistance of a NCTS panel using RC Blast and CSA A23.3-04 guidelines. Several factors considered in this analysis include boundary conditions, dynamic material properties, and shear tie degradation. This analysis of flexural behaviour is highly dependent on shear stiffness, which is directly related to the composite action within NCTS panels. Support resistance was increased significantly through application of the strengthening techniques outlined in this thesis.

Acknowledgements

I would like to thank my thesis supervisor, Dr. Murat Saatcioglu, for his unending support and encouragement in the realization of this research project. My gratitude extends beyond his technical guidance and financial support. I have learned much and more during this endeavor, and I have him to thank for it.

I cannot thank my parents enough for providing me with the necessary tools and foundation I needed throughout this process. I would also like to extend my gratitude to Ms. Tesia Bryski for motivating and encouraging me time-and-time again. Finally, to Tara and Peter Barreiro for your unprecedented generosity. I am indebted to you all for your continuous support and unending love.

Lastly, I would like to thank my graduate colleagues, specifically Eric Jacques, for their technical guidance, the educational discussions we've had, and the time and effort they've contributed to this research. I am equally grateful for the advice and help of the lab technicians in the Structural Engineering Research Laboratory at the University of Ottawa.

Table of Contents

List of Tables

List of Figures

List of Symbols

Symbol	Definition	Unit of Measure
$\ddot{x}$	Acceleration	(m/s^2)
$\dot{x}$	Velocity	(m/s)
a	Depth of concrete compressive zone	(mm)
A_L	Load area exposed to blast loads	(mm^2)
A_N	Projected concrete failure area of an anchor or group of anchors, for calculation of resistance in tension	(mm^2)
A_{N0}	Projected concrete failure area of one anchor, for calculation of resistance in tension, when not limited by distance or spacing	(mm^2)
A_s	Area of steel reinforcement	(mm^2)
A_{se}	Effective area of steel reinforcement	(mm^2)
A_v	Projected concrete failure area of an anchor or group of anchors, for calculation of resistance in shear	(mm^2)
A_{v0}	Projected concrete failure area of once anchor, for calculation of resistance in shear, when not limited by corner influences, spacing, or member thickness	(mm^2)
A_{vs}	Cross-sectional area of headed shear reinforcement on a line parallel to the perimeter of the column	(mm^2)
b	width of concrete section	(mm)
b_0	Perimeter of critical section for shear in slabs and footings	(mm)
c	Damping coefficient	(N-s/m)
C_{cr}	Critical damping	(N-s/m)
d	Depth of tensile reinforcement	(mm)
d	Depth of reinforcement	(mm)
e	Eccentricity of axial load applied at the top of the panel	(m)
E_c	Elastic modulus of concrete	(MPa)
F	Equivalent static load (P_r x A_L)	(kN)
$F(t)$	Force	(N)
f_c'	Specified compressive strength of concrete	(MPa)
fr	Concrete Modulus of Rupture	(MPa)
f_y	Yield strength of reinforcing steel	(MPa)
f_{yv}	Specific yield strength of headed shear reinforcement	(MPa)

h	Clear span of specimen	(mm)
h	Overall thickness/height of panel cross-section	(mm)
I_e	Effective Moment of Inertia	(mm^4)
I_g	Gross Moment of Inertia	(mm^4)
I_r	Positive impulse	(kPa-ms)
I_{tr}	Transformed Moment of Inertia	(mm^4)
k	System stiffness	(N/m)
k	Panel stiffness	(N/m)
K_{actual}	Shear tie stiffness based on experimental data and applied forces	(N/m)
K_{bf}	Cracked bending stiffness of panel	(kN-m/m)
K_{rigid}	Shear tie stiffness with fully composite behaviour	(N/m)
K_{soft}	Shear tie stiffness with no composite behaviour	(N/m)
l	Clear span of specimen	(m)
L	Length	(mm)
L_D	Shock tube driver length	(mm)
m	System mass	(kg)
M	System Mass	(kg)
M	Bending moment	(kN-m)
M_b	Factored moment excluding the P-Δ effects	(kN-m)
M_f	Factored moment including the P-Δ effects	(kN-m)
M_{FC}	Fully composite moment	(kN-m)
M_i	Moment at shear tie location	(kN-m)
M_{NC}	Non-composite moment	(kN-m)
M_{PC}	Partially composite moment	(kN-m)
M_r	Bending resistance	(kN-m)
n	Number of supports	
N_{br}	Factored concrete breakout resistance in tension of a single anchor in cracked concrete	(kN)
N_{cbr}	Factored concrete breakout resistance in tension of a single anchor	(kN)
P_D	Shock tube driver pressure	(kPa)
P_f	Factored axial load at panel mid-span	(kN)

P_r	Peak reflected pressure	(kPa)
PS	Prestressed	
P_{tf}	Factored axial load at the top of the panel	(kN)
R	Panel Resistance	(kN)
t_{ana}	Analytical Time-to-Maximum Displacement	(ms)
t_{ar}	Architectural wythe thickness	(mm)
t_d^+	Positive phase duration from pressure time history	(ms)
t_E	Time to strain (i.e. Time to peak strain, time to yield strain)	(ms)
t_{exp}	Experimental Time-to-Maximum Displacement	(ms)
t_{st}	Structural wythe thickness	(mm)
t_{total}	Total thickness of panel	(mm)
V_{br}	Factored concrete breakout resistance in shear of a single anchor in cracked concrete	(kN)
v_c	Factored shear stress resistance provided by the concrete	(MPa)
V_{cbr}	Factored concrete breakout resistance in shear of a single anchor in cracked concrete	(kN)
V_{conn}	Shear resistance of a single connection	(kN)
V_{conn}	Shear strength of individual connections	(kN)
V_f	Factored shear load applied to connections	(kN)
v_f	Factored shear stress applied to connections	(MPa)
Vij	Shear strength in shear ties	(kN)
V_r	Shear resistance of support	(kN)
v_r	Factored shear resistance	(MPa)
V_r	Factored shear load	(kN)
v_s	Factored shear stress resistance provided by shear reinforcement	(MPa)
V_{sup}	Factored load applied to individual connection	(kN)
w	Uniformly distributed out-of-plane load	(kN/m)
w_f	Factored lateral uniformly distributed load	(kN/m)
α_s	Factor that adjusts v_c for support dimensions	
β_c	Ratio of long side to short side of concentrated load or reaction	
Δ_0	Initial deflection at panel mid-height determined iteratively	
δ_{ana}	Maximum analytical mid-span displacement	(mm)

δ_b	Moment magnification factor	
δ_{exp}	Maximum experimental mid-span displacement	(mm)
δ_r	Residual displacement	(mm)
ε_0	Strain at peak compressive strength, 0.2%	(mm/mm)
ε_{cc}	Compressive strain of concrete, used in Hognestad's model	(mm/mm)
ε_{ct}	Tensile strain of concrete	(mm/mm)
ε_s	Strain in reinforcement	(mm/mm)
ε_s'	Experimental strain rate in steel reinforcement (mm/mm/ms) or (%/ms)	(%/ms)
λ	Factor to account for variations in concrete density	
σ_b	Stress at bottommost fibre of panel cross-section	(MPa)
σ_t	Stress at uppermost fibre of panel cross-section	(MPa)
ϕ_c	Resistance factor for concrete	
ϕ_{FC}	Fully composite curvature	(m^{-1})
ϕ_m	Member resistance factor = 0.75	
ϕ_{NC}	Non- composite curvature	(m^{-1})
ϕ_{PC}	Partially composite curvature	(m^{-1})
ϕ_s	Resistance factor for steel reinforcement	
$\Psi_{c,N}$	Modification factor for resistance in tension to account for cracking	
$\Psi_{c,P}$	Modification factor for pullout resistance to account for cracking	
$\Psi_{cp,N}$	Modification factor for concrete breakout resistance to account for premature splitting failure	
$\Psi_{ec,N}$	Modification factor for resistance in tension to account for anchor groups loaded eccentrically	
$\Psi_{ec,V}$	Modification factor for resistance in tension to account for anchor groups loaded eccentrically	
$\Psi_{ed,N}$	Modification factor for resistance in tension to account for edge distances smaller than h_{ef}	
$\Psi_{ed,N}$	Modification factor for resistance in shear to account for edge distances smaller than $1.5h_{ef}$	

List of Common Acronyms

Acronym	Description
CFRP	Carbon Fibre Reinforced Polymer
CM	Strain gauge series located at mid-span on compressive reinforcement
DIF	Dynamic Increase Factor
FRP	Fibre Reinforced Polymers
HSS	Hollow steel section
LVDT	Linear Variable Displacement Transducers
NCTS Panel	Non-Composite Tilt-Up Sandwich Panel
NRC	Normally Reinforced Concrete
SDOF	Single-Degree-of-Freedom
SRC Panel	Solid Reinforced Concrete Panel
TB	Strain gauge series located at the lower quarter-span on tensile reinforcement
TM	Strain gauge series located at mid-span on tensile reinforcement
TT	Strain gauge series located at the upper quarter-span on tensile reinforcement
WWM	Welded Wire Mesh Reinforcement
XPS	Extruded Polystyrene Insulation

1.0 Introduction

1.1 General

The mitigation of blast risk, associated with both intentional acts of terror and accidental explosions, has become a primary societal focus over the course of the 21st Century. The geographical uncertainties, social impacts, and political scope associated with these extreme events are key contributors to the sheer complexity of this multidisciplinary field. As a result, the strength and integrity of infrastructure subjected to blast loads has been an area of interest for government research institutions both within Canada and Internationally. The primary objective of this research is to generate standards to regulate and improve the construction of new structures and retrofitting of existing structures to resist blast induced loads.

Aesthetic properties, historical characteristics, and the associated costs often make it impractical to replace existing structures with new blast resistance buildings. In which case, performing a complete dynamic blast assessment will diagnose the inherent blast resistance of structural elements and identify elements with insufficient resistance. Based on the results of the risk and blast assessments, a combination of protective measures and structural enhancement may be instituted to alleviate or minimize the risks. The most common and effective preventative measure is increasing stand-off distance. Stand-off distance, defined as the distance from the centroid of the explosion to the point of interest (i.e. the structural element), can be increased to reduce the effect of blast loads on a structure. Improving the blast resistance of structural elements, typically the less cost effective approach, can be achieved by increasing the ductility, resistance, and/or the mass of the element.

Exterior tilt-up panel walls are commonly used on low to mid-rise structures with large floor plans such as schools and warehouses. Tilt-up construction is cost effective, energy efficient, and expeditious, compared to other construction methods for similar buildings. The large mass and high flexural resistance of reinforced concrete tilt-up panels make them inherently resistant to blast loads. However, two questions arise when designing new tilt-up panels or analysing existing panels against blast loads. How does the architectural wythe influence the resistance of the panel? and, can supports be designed to resist dynamic support loads generated under extreme blast loads?

This thesis presents the results of a comprehensive research project conducted at the University of Ottawa investigating the behaviour of non-composite tilt-up sandwich panels under extreme blast loads.

1.2 Concrete Tilt-up Construction

Concrete tilt-up buildings use a unique construction method in which reinforced concrete wall panels are constructed horizontally at ground level and erected into a final vertical position. Tilt-up wall panels can be designed as non-loadbearing or loadbearing walls capable of resisting out-of-plane wind loads and in-plane seismic loads depending on their desired application. These wall panels have become a staple façade component for one to four storey structural steel buildings and are widely used for their inherent advantageous characteristics, the most notable of which is the ease and speed of construction. The construction of formwork, installation of reinforcing steel, and placement of concrete in vertical wall construction are labour intensive, expensive, and difficult. Tilt-up panel construction eliminates these disadvantages by casting walls horizontally at ground level. This results in shallow forms, accessible reinforcement, and a high level of control during concrete placement. Concrete tilt-up panels can be stacked to expedite construction, minimize erection time and reduce bracing requirements.

Both tilt-up and precast wall panels (which are constructed off site and delivered for erection), can be designed as sandwich panels. These unique panels embed a layer of insulation between two concrete faces to capitalize on these advantageous construction practices. It is common practice for precast sandwich walls to exhibit composite behaviour between the two faces. This practice, however, is less widely used in tilt-up construction where a thinner architectural face is supported by a more robust structural face. Furthermore, unlike precast concrete wall panels, tilt-up panels are formed, poured, and erected onsite while precast panels are constructed in a plant and delivered to site. As a result, tilt-up panels are typically much larger panel and have few connections, details for which vary considerably between these two construction methods. Figure 1.1 and Figure 1.2 show connection details typical to tilt-up construction.

Tilt-up and precast construction use a combination of embedded plates and anchors to effectively connect panels to supporting steel structures. Tilt-up connections are typically less rigid than

precast panels as the additional size of tilt-up panels inherently resistance overturning or sliding. There is wide array of these connections used for various framing, placement, and loading scenarios:

- Panel-to-Frame Connection – There is a wide variety of panel-to-frame connections available in industry, the most common of which are joist seats. These connections come in a variety of forms depending on the number of floors, framing members, and loading conditions. The key design purposes of these connections are for the transfer of axial load into the wall member and out-of-plane lateral loads into the steel frame. However, they can also be designed to transfer seismic loads from the structures frame. The specimens tested in this study were non-loadbearing panels with joist seats designed to mimic industry standard to resist typical out-of-plane loads (i.e. wind). Additional details regarding the specific joist seats used in this study are provided in Section 3.3.
- Panel-to-Panel Connection – There are two primary types of panel-to-panel connections. Welded shear connectors are commonly used in high seismic zones where panel overturning is of concern. It is common to use slotted bolt connections where overturning due to seismic loads can be resisted by individual panels. These connections allow some movement between panels. Similar connections can be found for edge panels. While these connections may be susceptible to blast loads, they were not included within the scope of this study.
- Panel-to-Footing/Slab Connection – As is the case with panel-to-panel connectors, there are two primary types of base connectors. Common industry practice uses shear keys embedded in the foundation to meet moderate seismic design requirement. Welded shear connectors can also be used to provide additional resistance to in-plane shear loads and help prevent overturning. This practice is more typical to precast panel which are smaller and do not have the inherent weight to resist overturning. The specimens tested in this study were non-loadbearing panel with a bearing base support using shear keys embedded into the foundation. Additional details regarding the base connection used in this study are provided in Section 3.3.

1.3 Concrete Tilt-up Behaviour

There are two categories of tilt-up and precast panels: solid reinforced concrete panels consist of a single reinforced concrete wythe while sandwich panels consist of two reinforced concrete wythe that sandwich a layer of rigid insulation. Figure 1.3 shows a 3-Dimensional section of a sandwich panel. The two concrete wythes in a sandwich panel are connected to each other using small connectors, known as shear ties, which protrude through the insulation and are embedded in both layers of concrete. There are three sub-categories of sandwich panels, non-composite, partially composite, and fully composite panels, which describe the sectional behaviour of the specimen under flexural loads.

The composite behaviour of a sandwich panel is dependent on the ability of the shear ties to transfer shear forces between the wythes. Figure 1.4 illustrates the sectional behaviour associated with each sub-category. A sandwich panel is considered partially or fully composite when the two concrete wythes act in unison to resist flexural loads. A fully composite section behaves as if it were a solid reinforced section which a partially composite specimen achieves only partially achieves this behavior. A sandwich panel is considered non-composite when the two concrete wythes act separately to resist flexural loads. There are two types of sectional behaviour in non-composite failure. When each wythes behaves as its own section and experiences both tensile and compressive forces, this is typical behaviour of non-composite behaviour. When the sectional behaviour become irregular, as in Figure 1.4 (4), the shear tie capacity has been exceeded and the wythes each wythe experience only tensile or compressive forces. Panels with these sectional properties exhibit a significant strength decrease similar to non-composite panel.

Composite action is a complex behaviour which varies along the span of the panel and is dependent on shear tie type, spacing and capacity, as well as the wythe capacity and moment distribution. As a result, all panels exhibit some degree of composite behaviour at some locations along the span. Section 5.4.2 provides additional information in regards to the evaluation of composite behaviour within sandwich panel.

1.4 Literature Review

Structural integrity and resistance to blast loads is a rapidly growing field of civil engineering design and research. Extensive research, including experimental and analytical studies, has been conducted on reinforced concrete elements. As a result, the overall behaviour of normal reinforced concrete elements is well understood and methodologies have been applied in practice.

Blast Standards: CSA S850-12 Design and Assessment of Buildings Subjected to Blast Loads

CSA S850-12, the leading standard in Canada for buildings subjected to blast loads and provides guidelines for the design of new buildings and assessment of existing buildings. This standard focuses on limiting potential for progressive collapse, defining degrees of damage for structural systems, mitigating damage to the building envelope, and minimizing flying or falling debris. These performance objectives are specified based on a design basis threat and level of protection, specified by the building owner.

CSA S850 provides performance evaluation guidelines for a wide variety of materials and member, which are defined by the ratio of maximum displacement-to-typical yield displacement and support rotations. These evaluation guidelines are referred to as response limits. While there are no standardized response limits defined for tilt-up or precast construction, similarities can be drawn with other members specified in the code; Standards for double-reinforced slabs without shear reinforcement and walls with combined flexure and axial compression were used in the determination of response limits for non-loadbearing and loadbearing panels, respectively.

The response limits used in this experimental study are tabulated in Table 1.2.

Naito et al. 2008

In this investigative study full-scale tests were conducted on prestressed concrete wall panels to evaluate their performance under blast induced loading. Tests were performed on four panels: two identical solid reinforced control panels designed for testing purposes only and two dissimilar sandwich panels. Each of the sandwich panels was designed using industry standards, such that the architectural wythe and structural wythe acted as one unit to resist loading. This type of sectional behaviour is referred to as composite action. The first sandwich panel was constructed

using a solid zone method in combination with carbon fibre reinforced polymers (CFRP) anchors to achieve composite actions. In this method concrete sections connect the faces. The second sandwich panel type was constructed using only CFRP anchors, providing enhanced thermal performance. The control specimen used conventional reinforcement placed longitudinally at the centroid of the section. Each sandwich panel was reinforced in the longitudinal direction with *8 – 3/8"* strands, four in each wythe, prestressed to *71.6kN* each. All panels were constructed using welded wire mesh reinforcement (WWM) in each wythe to accommodate horizontal temperature and shrinkage demands.

The *30ft* by *8ft* wall panels were mounted to a reaction structure with idealized simple support conditions as shown in Figure 1.5 and Figure 1.6. Specimens were instrumented with external and internal pressure gauges and internal displacement gauges were installed at quarter- and mid-spans. In total four panels were constructed and tested using bare live explosives at varying standoff distances to induce a variety of pressure-impulse combinations. Tests were conducted on two panels simultaneously, one control panel and one sandwich panel, such that results could be compared directly without having to replicate exact pressures and impulses.

The solid zone wall panels performed desirably under blast loading conditions. Solid zone panel results were indicative of full composite action as flexural cracking extended only on the structural wythe. While both panels sustained permanent deformation, the sandwich panel exhibited considerably less deflection than the control specimen.

Three tests were conducted on the CFRP panel and the corresponding control panel. The CFRP exhibited vertical cracking at the base support, indicative of two-way bending, after initial testing of the specimen. Panels exhibited a centralized plastic hinge region at approximately mid-height. The ratio of maximum deformation of the CFRP panel to the control panel ranged from 0.84-0.89. The third and final test performed in this portion of the experiment displayed permanent deformations of approximately *6"* in the CFRP panel opposed to 10.5" in the control panel. Specimens were subjected to considerably higher deformations than the solid zone tests with span-to-deflection ratios close to *20*, however the walls remained intact.

In conclusion of the investigation it was found that the wall panels provided a high level of protection against blast induced loading. The measured results were modelled using a finite

element analysis to assess the response for prestressed precast concrete elements. Composite sandwich panels performed significantly better than the SRC control panels.

Naito et al. 2011

This extensive research project was undertaken to assess the inherent blast resistance of conventional insulated concrete sandwich panels. Fifty-eight panels were tested under quasi-static loading conditions to verify the capacity of wall systems subjected to blast loads and determine recommendations for acceptable deformation, rotation and ductility limits. The results of the investigation facilitated the development of static resistance functions and dynamic performance limits for sandwich walls constructed with different types of insulation, shear connectors, spans, and design techniques. Specifically, forty-six single- and twelve double-span panels were tested, five types of shear ties were used, and three insulation types were used in the investigation to reflect common practice. Furthermore, panel designs follow three general configurations: Non-composite non-prestressed, partially composite non-prestressed walls, and partially composite prestressed walls.

Tests were performed on *16"* and *32"* subsections of wall panels and included:

- Forty-two single-span panels with idealized supports,
- Four single-span panels with end connections, and
- Twelve double-span panels with intermediate connections.

Of these three sets of specimen, twelve used tilt-up design methodology, including partially composite (TS2), non-composite (TS1), and two-span sections (TS3). TS1 was designed to be non-composite 16" wide panel with a *6"* structural wythe, *2"* of expanded extruded polystyrene (XPS) insulation, and a *3"* architectural wythe. The structural face was longitudinally and transversely reinforced using *#3* deformed bars spaced at *12"* and *18"*, respectively. The architectural face was connected to the structural face using a non-composite CFRP shear ties and reinforced with *W2.9xW2.9 6x6* WWM. TS2 was designed as a partially composite panel with a *3"* structural wythe, *2"* of XPS insulation, and *a 3"* architectural wythe. The two concrete faces had *#3* longitudinal and transverse reinforcement spaced at *12"* and *18"*, respectively. Wythes were connected using composite CFRP ties. TS3 was designed as a non-composite section and had the

same details as TS1. Furthermore, four single-span panels with end connections were fabricated using precast design methodologies and utilized the same connection at the top and bottom of the panel to ensure symmetric failure. Connections were tested for both positive and negative phase response. All panels were loaded to failure using a loading tree fixture that applied a uniformly distributed load across the entire span of the panel at a rate of *0.01*" per second. Experimental setup details are shown in Figure 1.7 through Figure 1.10. Specimens were instrumented to record the mid- and quarter-span displacement and the applied loads on the panels. Furthermore, relative shear deformation between wythes was recorded at end-span.

The partially composite tilt-up panels maintained a higher resistance than the non-composite counterpart exhibiting greater load capacity under similar deformations. Furthermore, the partially composite tilt-up panel demonstrated greater strength at higher rotations and postponed strength degradation when compared with similar precast panels. Panels with end connections performed better when subjected to inbound pressures as opposed to rebound pressures. Inbound pressures, applied during the positive blast phase, caused ductile failure of the concrete and steel near the stud group area while rebound pressures caused a less ductile stud group weld failure. Similarly, multi-span specimens were found to fail at the mid-span connection. In the thinner wythe sections shear punching was observed at the connection, this was only observed for the Halfen connection in the *6"* wythe tilt-up panel.

The investigative study concluded that changes in the current design limits are required. Table 1.1 provides a summary of current design limits specified in CSA S850-12 [1] and recommended modifications based on the results of this study. Blowout of specimens is defined by [1] as *10 degrees* for non-loadbearing normally reinforced concrete (NRC) members and *3 degrees* for prestressed (PS) specimens. This is due to the inherently higher ductility in NRC members compared to PS members. However, Naito et al. recommend that the blowout limits be reduced to *7.6 degrees* for non-loadbearing NRC member and increased to *3.6 degrees* for non-loadbearing PS members. These recommendations are based on a Z-distribution of experimental displacements with a *90%* confidence level.

The use of multilayered foam or XPS was found to reduce the overall flexural capacity of panels while increasing the deformation capabilities. In general, panels provided adequate capacity to meet current blast response criteria. In all cases, composite deformation calculations did not agree

with results and were unconservative. Non-composite and partially composite tilt-up panels also suffered similar disagreements between theoretical and experimental deformations. These inconsistencies were a result of the failure to incorporate shear tie behaviour and composite degradation into the analysis. The incorporation of these parameters into panel analysis is further detailed in Section 5.4.2.

E. Jacques (2010)

The objective of this research project was to evaluate and compare the resistance of as-built and retrofitted one- and two-way reinforced concrete members subjected to blast loading. Thirteen panels were constructed and tested using shock tube simulated blast loads. Seven one-way panels, four *80mm* (CS1) and three *120mm* thick (CS2), 440mm wide with a clear span of *2232mm* were tested. All one-way panels were doubly reinforced with *6.3mm* diameter non-deformed steel reinforcement. For each companion set one specimen was an un-strengthened control panel while the others were retrofitted with surface bonded CFRP laminate.

Testing was conducted using a pneumatically driven shock tube capable of simulating blast induced shockwaves. Specimens were clamped between two *19mm* diameter steel rods at either end, restraining the panel from lateral movement but allowing free rotation, attributes consistent idealized simple-support conditions. Additionally, a load transfer device was used to effectively transfer pressures distributed over the *2032x2032mm* opening of the shock tube to the surface of the specimen. Pressure sensors were installed at the bottom and side walls of the shock tube to measure the reflected pressure-time histories. Specimens were instrumented with linear variable displacement transducers (LVDT) at mid-height, lower quarter, and lower end-span to monitor the deformations of the panels. Spring loaded wire gauges were used as an alternative to LVDTs for large destructive tests. Additionally, strain gauges were installed on reinforcing steel and CFRP laminate to measure the longitudinal elongation during loading. Panels were loaded to failure through the application of increasingly destructive blast pressures.

In conclusion it was found that the installation of a CFRP retrofit produced significant reductions in maximum displacement and increased the overall performance of the wall. The maximum support rotation for as-built one-way panels at failure were between *7°* and *10°*. A single degree of freedom (SDOF) analysis was performed on all panels for comparison with experimental

results. Results of the SDOF analysis for one-way panels were found to be reasonably comparable with those obtained experimentally, confirming the validity of a SDOF analysis.

C. J. Oswald & M. Bazan

This investigative research studied the behaviour of solid precast concrete wall panels with several different precast connection details. Specifically, six precast connections were tested for blast response criteria including: bolted angles, bolted gusseted angles, direct bearing, welded angles, welded gusseted, angles and Halfen connections. Panel connections were designed to resist the panel reactions caused by blast loading. Shock tube testing was performed on thirteen precast panels connected to the shock tube frame using conventional precast connectors.

Tests were conducted using a pneumatically driven shock tube to apply simulated blast loads on *8x8ft* panels. Two *5"* and eleven *6"* thick full-scale panels were tested with varying reinforcement layouts and connections details. Testing of panels did not push panels to failure; rather a similar pressure-impulse combination was applied to all panels for sake of comparison. All panels were instrumented such that the pressure-time history, mid-span acceleration, and deflections could be recorded.

Panels exhibited a range of damage and support rotation dependant on the type and layout of steel reinforcement. In general, conventional bolted and welded angles designed to resist reaction forces corresponding to the ultimate resistance of the panel had the capacity to resist dynamic blast loads. One scenario, with asymmetric support conditions (Halfen top connection and a bolted angle bottom connection) failed prematurely due to bolt failure. Upon comparing these with the results of panels with similar connections (i.e. bolted angles) and reactions, this was attributed to a potentially flawed bolt. Failure of panels was flexural in nature with displacements and support rotations ranging from *2.8"* to *6"* and *3.3º* to *7.1º*. Experimental data was compared with analytical results using an SDOF approach. Results were somewhat comparable to the SDOF results with a variance of approximately *16%* and *20%* for maximum reactions and peak mid-span deflections, respectively. It was found that doubly reinforced concrete panels performed significantly better than single-mat reinforcement.

Newberry et al. (2010)

This research project focused on the development and validation of a finite element model to simulate the response of precast insulated concrete sandwich panels under blast loading. The model was based on results from Naito et al. [2] for simple reinforced concrete beams, conventionally reinforced sandwich panels, and prestressed sandwich panels. Other input parameters used empirical data from shear tests performed on a variety of wythe connectors to determine their contribution to composite action. Full-scale results from Naito et al. [3] were used to validate the dynamic analysis approach. The objective of the analytical model was to accurately model the effects of various design techniques, loading scenarios, and boundary conditions on the response of precast/tilt-up wall panels.

Three conventionally reinforced concrete beam designs (nine total), *18"* wide with a clear span of *144"*, were tested under uniformly distributed loads. Specimens were instrumented to measure total applied load and mid-span deflections. In general results from the finite element analysis were found to be generally acceptable. Data input for static tests of sandwich panels relies on the composite performance of the section, which is based primarily on the behaviour of rigid insulation and shear ties. Compressive testing of insulation was used to define the stress/strain relationship. Static shear tests, using three concrete wythes, were performed to determine the shear resistance of the connectors. Modelling of statically loaded precast panels proved to agree well with experimental data, being generally conservative prior to peak capacity.

1.5 Research Needs

The literature review presented in the preceding section is indicative of the insufficient data collected for Non-Composite Tilt-up Sandwich (NCTS) panels subjected to blast induced shock waves:

- Despite the name, NCTS panels typically exhibit some degree of composite behaviour. The application of sectional analysis methods to predict this behaviour has not been verified for dynamic tests of NCTS panels under simulated blast loading.

- Experimental data for NCTS panels subjected to blast loading is limited to quasi-static or static loading conditions. Consequentially the effects of dynamic loads on NCTS panel displacement-time behaviour is unknown.
- The limited amount of experimental research that has been performed for NCTS panels were conducted with idealized symmetric support conditions, unrealistic to tilt-up construction practice.
- Research of sandwich panel support capacities have been limited to pre-cast panel design methodologies. NCTS panels have unique connections that introduce material discontinuity within the panels. There is no previous research for the effects of extreme blast loads on these connections.

1.6 Objectives and Scope

The primary objective of the research project is to investigate the performance of tilt-up wall panels subjected to simulated blast shock waves. The objective also includes the assessment of the level of composite action attained in sandwich panels, as well as the adequacy of panel connections, while also developing retrofit strategies for improved performance of connections.

The scope of the project includes large-scale tests of NCTS panels under simulated blast shock waves using the University of Ottawa Shock Tube. The specimens are equipped with conventional tilt-up support details and are instrumented to capture the longitudinal internal moment-distribution and cross sectional strain profiles within the panel. Composite behaviour within the panel is compared with theoretical results from analytical methods used in previous research.

The resistance of conventional tilt-up supports are experimentally investigated and compared with analytical studies. The results are used to formulate design recommendations for blast-resistant tilt-up construction. Finally, a full-scale analysis of two panels subjected to various pressure-impulse combinations is conducted to determine general flexural performance and corresponding support behaviour. Design procedures for support strengthening techniques are evaluated analytically.

Table 1.1– Summary of Naito et al. 2008 Test Results

Specimen	*Test*	*Peak Mid-Span Displacement (inch)*	*Residual Mid-Span Displacement (inch)*
Control 1	1	2.24	0.5
	2	2.86	1.3
Solid Zone	1	1.74	0.1
	2	3.64	0.3
Control 2	1	5.49	1.8
	2	7.00	1.6
	3	19.3	10.6
CFRP	1	4.62	0.9
	2	6.21	1.4
	3	16.9	6.2

Table 1.2 – CSA S850-12 Design Limits vs. Naito et al. 2011 Proposed Design Limits for Non-Loadbearing NRC Panels and Prestressed Panels

		Flexural		***Prestressed Panel***	
		CSA S850-12	***Naito et Al. 2011***	***CSA S850-12***	***Naito et Al. 2011***
Superficial	B1	$\mu_{max} \leq 1.0$	$\mu_{max} \leq 1.0$	$\mu_{max} \leq 1.0$	$\mu_{max} \leq 1.0$
Moderate	B2	$\theta_{max} \leq 2°$	$\theta_{max} \leq 3.1°$	$\theta_{max} \leq 1°$	$\theta_{max} \leq 1.3°$
Heavy	B3	$\theta_{max} \leq 5°$	$\theta_{max} \leq 5.7°$	$\theta_{max} \leq 2°$	$\theta_{max} \leq 3.1°$
Hazardous	B4	$\theta_{max} \leq 10°$	$\theta_{max} \leq 7.6°$	$\theta_{max} \leq 3°$	$\theta_{max} \leq 3.6°$
Blowout	-	$\theta_{max} \geq 10°$	$\theta_{max} \geq 7.6°$	$\theta_{max} \geq 3°$	$\theta_{max} \geq 3.6°$

Table 1.3 – C.J Oswald & M. Bazan Specimen Outline

Panel #	***Panel Thickness (mm)***	***Reinforcement Details***	***Connection (2 per support)***
1	150	#4 @ 300mm Each Face	Bolted Angles
2	150	#4 @ 300mm Each Face	Direct Bearing
5	150	#4 @ 300mm Each Face	Bolted Gusseted Angles
8	150	#4 @ 300mm Each Face	Welded Gusseted Angles
9	150	#4 @ 300mm Each Face	Welded Angles
10	150	#4 @ 300mm Each Face	Bolted Angles
6	150	(2) 4x4 W2.1xW4 Each Face	Bolted Angle (Bot.), Halfen w/rod (Top)
7	150	(2) 4x4 W2.1xW4 Each Face	Welded Angles
14	150	(2) 4x4 W2.9xW2.9	Welded Angles
11	150	#6 @ 125mm Each Way	Bolted Angles
12	150	#6 @ 125mm Each Way	Welded Angles
3	125	#5 @ 200mm	Bolted Angles
4	125	#5 @ 200mm	Direct Bearing

Figure 1.1 – Tilt-Up Panels used in Practice (Panel-to-Frame Upper Connections)

Figure 1.2 – Typical Panel-to-Panel Connections for Precast (left) and Tilt-up (right) Panels (FireEngineering.com)

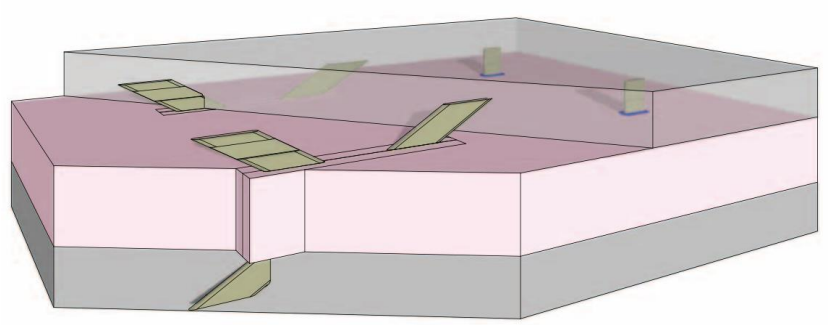

Figure 1.3 – 3-Dimensional Section of Sandwich Panels (Thermomass.com)

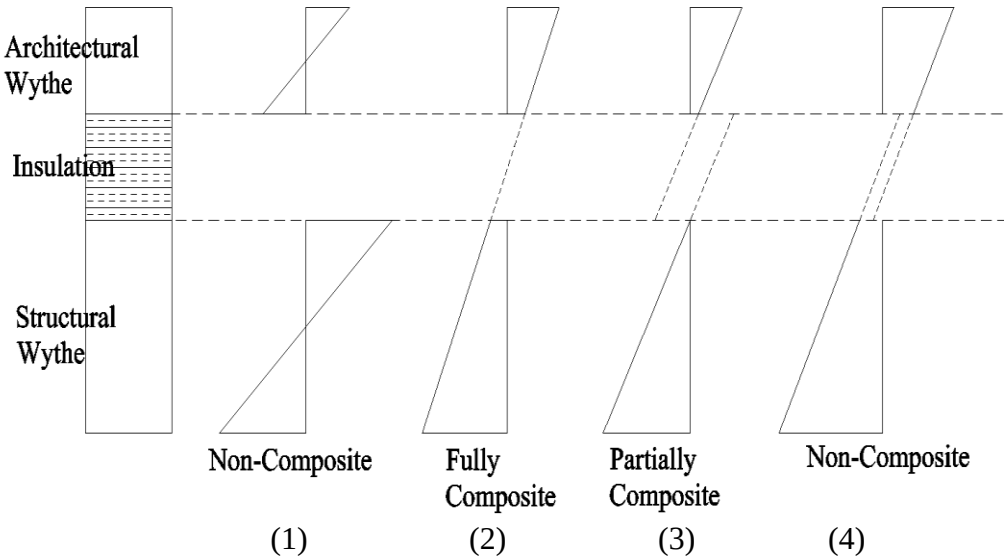

Figure 1.4 – Sectional Strain Profiles for Tilt-up and Precast Panels

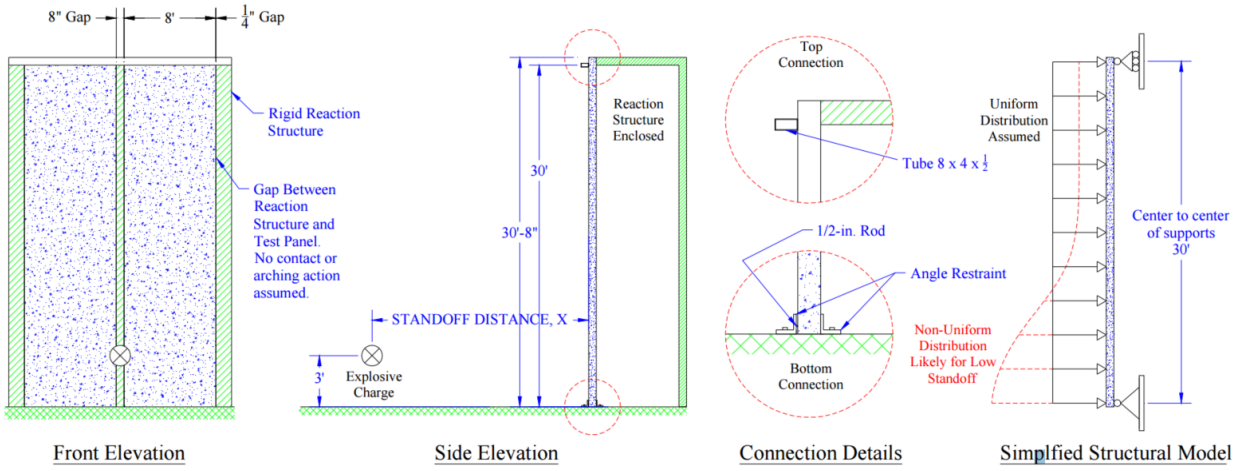

Figure 1.5 – Naito et al. 2008 Experimental Setup Schematics

Figure 1.6 – Naito et al. 2008 Experimental Setup

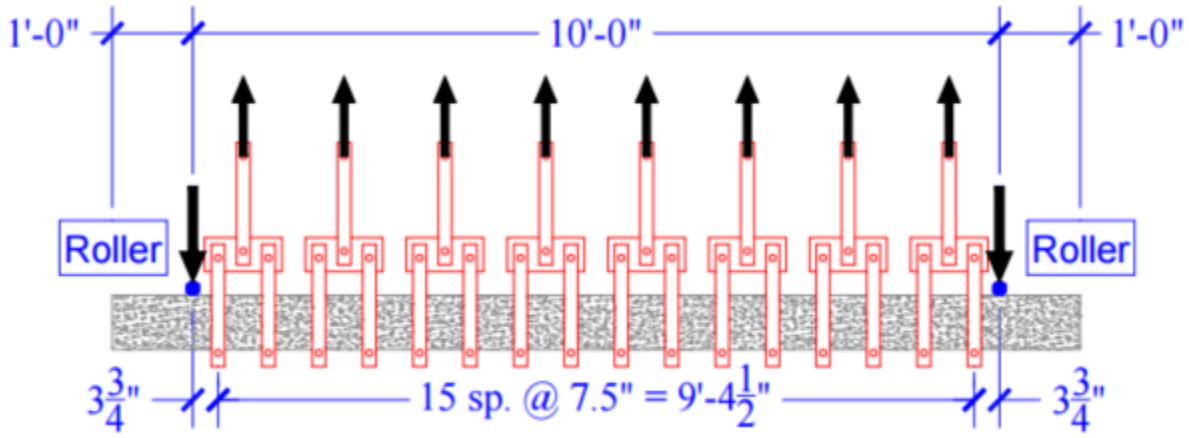

Figure 1.7 – Naito et Al. 2011 Experimental Setup Schematic for Single Span Panels without Connections

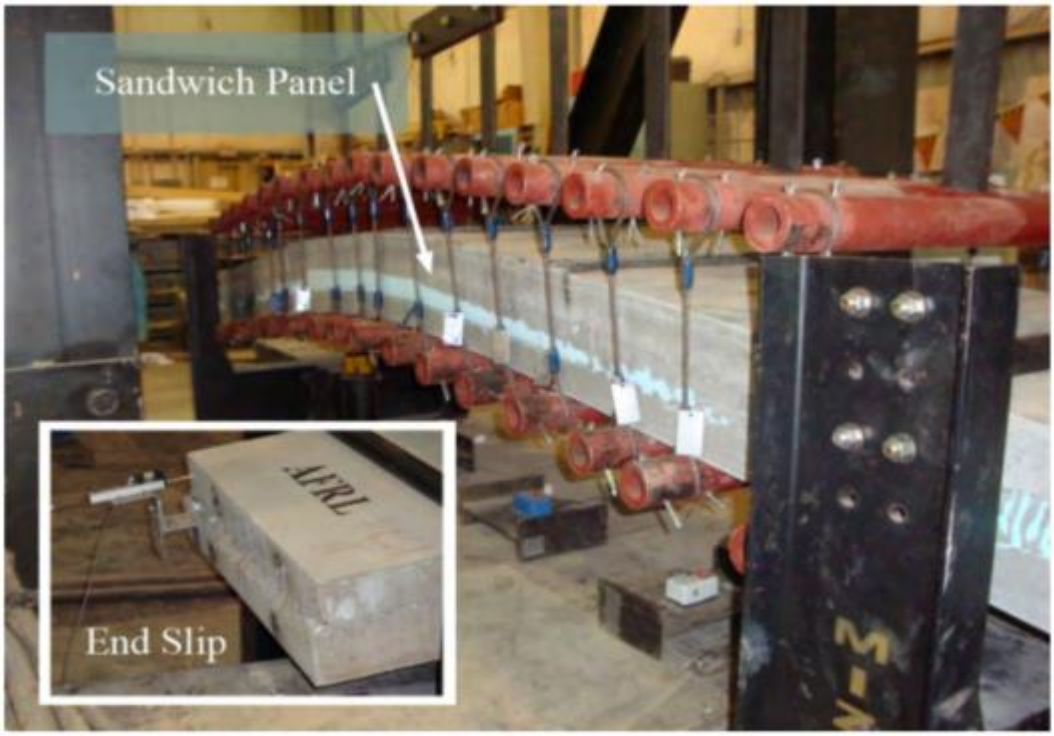

Figure 1.8 – Naito et Al. 2011 Experimental Setup for Single Span Panels without Connections

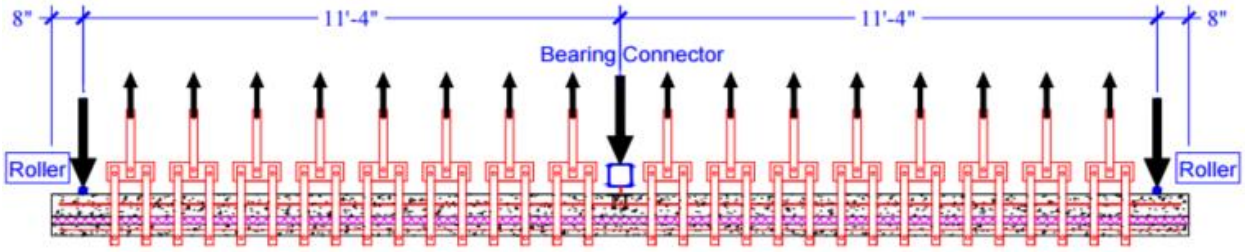

Figure 1.9 – Naito et Al. 2011 Experimental Setup Schematic for Double Span Panels without Connections

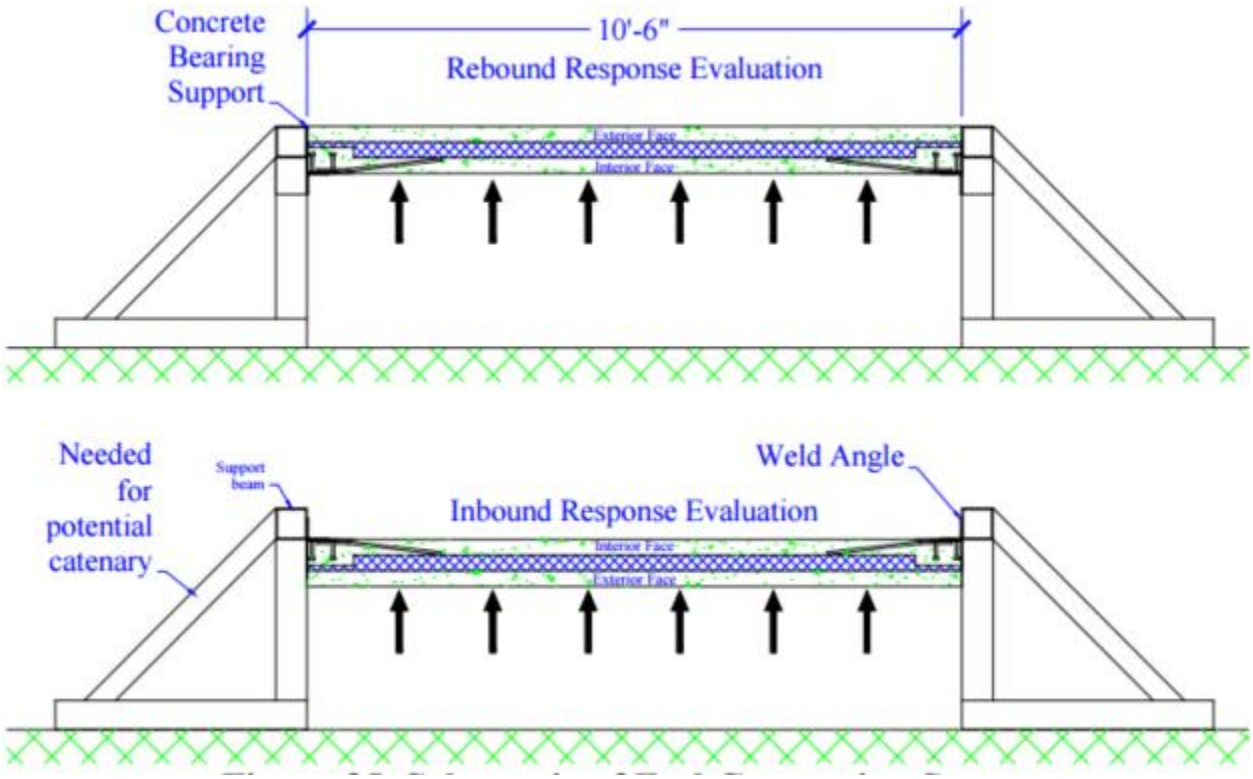

Figure 1.10 – Naito et Al. 2011 Experimental Setup Schematic for Single Span Panels without Connections

(a) Front view (b) Side view

Figure 1.11 – E. Jacques Experimental Setup for 400mm One-Way Specimens

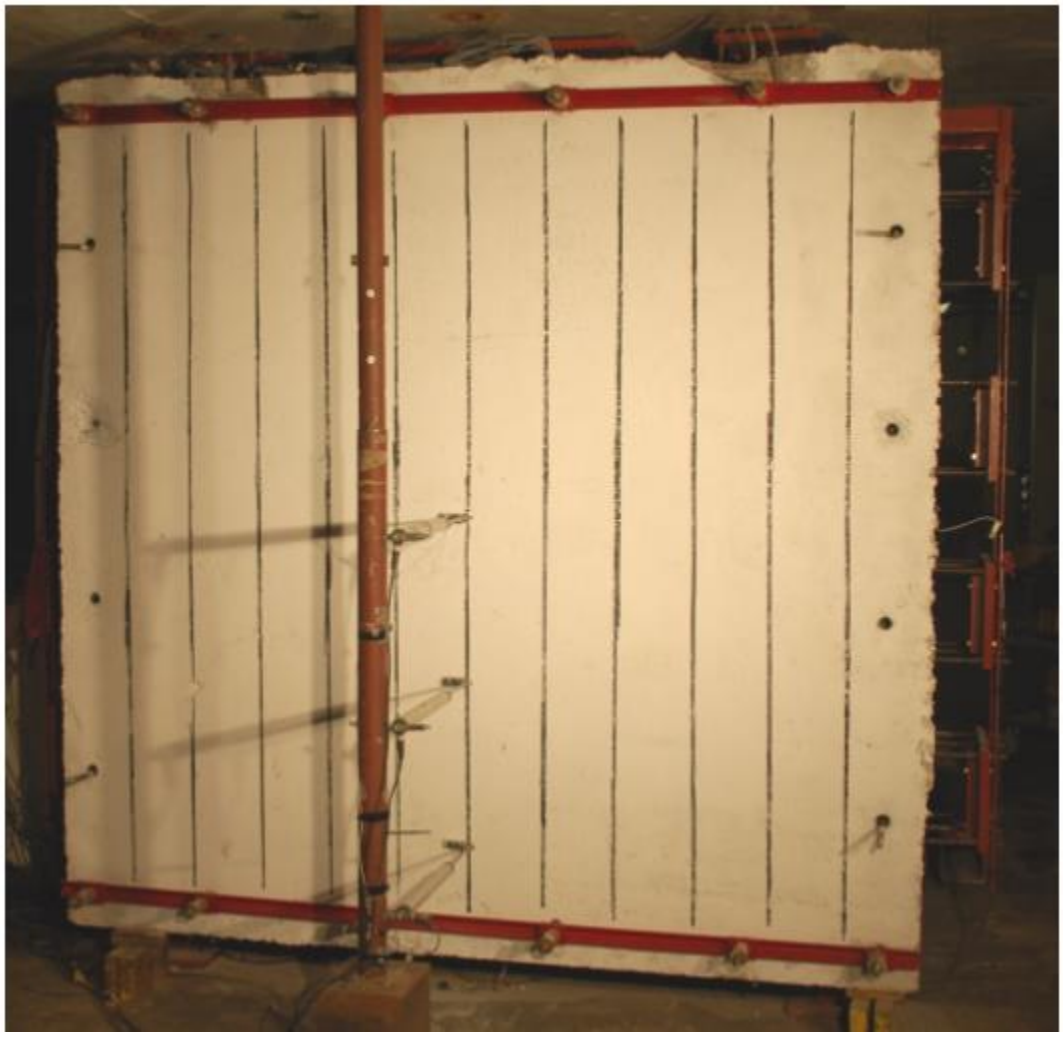

Figure 1.12 – E. Jacques Experimental Setup for 2440mm One-Way Specimens

Figure 1.13 – E. Jacques Experimental Setup for Two-Way Specimens

2.0 Tilt-up Panel Design

2.1 General

Concrete tilt-up wall panels are slender members that act predominately in flexure and can be designed as load bearing or non-load bearing. Panels can be designed as solid reinforced concrete or insulated sandwich panels. Tilt-up and precast wall panels have two unique design requirements in comparison with cast in-place concrete walls. Firstly, tilt-up wall panels must be designed for flexural stresses generated from erection of the panels. Secondly, panels are typically fastened to a structural steel skeleton rather than monolithic concrete connections causing a discontinuity in materials which must be adequately designed for. The following chapter briefly outlines the basic design requirements for non-composite tilt-up panels considered in this research program.

2.2 Code Design Requirements

Non-composite load bearing walls are designed such that there is minimal interaction between the architectural and structural wythes. This method is widely used in construction for three primary reasons: i) the ease of constructing an architectural face without structural reinforcement, ii) the lack of in-field quality control, and iii) the uncertainties of composite behaviour. In this method the architectural face is provided simply for aesthetics and functionality whereas the structural wythe is responsible for bearing loads.

Tilt-up panels are designed using the moment magnification approach outlined in CSA A23.3-04 [1]:

- Factored Moment: Concrete tilt-up panels are designed as slender members therefore P-Δ effects must be considered. The P-Δ effect takes into account secondary bending moments due to the lateral mid-span deflection caused by applied loads and can be applied to structural design by determining a magnified moment. This is an iterative process using Equations 2.1 through 2.3.

$$M_f = M_b\left(\frac{1}{1 - P_f/K_{bf}}\right) = M_b \cdot \delta_b \ (kN \cdot m) \quad \textbf{2.1}$$

$$M_b = \frac{w_f l^2}{8} + P_{tf}\frac{e}{2} + \left(P_{wf} + P_{tf}\right)\Delta_0 \quad \textbf{2.2}$$

$$\delta_b = \frac{1}{1 - P_f/\phi_m K_{bf}} \geq 1.0 \quad \textbf{2.3}$$

- Resisting Moment: Bending moment resistance can be calculated through application of Equation 2.4. In axial load bearing wall panels bending moment resistance is increased through the use of an equivalent tensile steel area shown in Equation 2.5.

$$M_r = \phi_s A_{se} f_y \left(d - \frac{a}{2}\right) \geq M_f \quad \textbf{2.4}$$

$$A_{se} = \frac{\phi_s A_s f_y + P_f}{\phi_s f_y} \quad \textbf{2.5}$$

2.3 Lifting Load Design

During erection, panels rotate from a horizontal position on the slab to a final vertical position causing various loading scenarios and moment distributions similar to those shown in Figure 2.1. The following is a brief summary of the iterative lifting load determination process outlined in TM-34 [4]. Using the procedure outlined below lifter locations can be specified to minimize bending moments. Other important design considerations not covered here include the resistance of lifting inserts.

Forces within the panel in its original horizontal position can be determined using static equilibrium equations. Lifter line locations should be specified to minimize bending moments at this stage. From this, the shear and bending moment diagrams can be generated.

As the panel is lifted from the ground it rotates from its initial horizontal position to a final vertical position. Multiple shear and bending moment distributions can be generated due to changes in the support loads as the panel rotates. It is important to find the critical angle of rotation with the maximum bending moment using the iterative process outlined in TM-34 [4]. In practice it is important to design the panel such that it remains uncracked under these loading conditions. This

prevents the development of early cracks which can propagate, causing degradation of the panel's thermal and moisture resistant properties.

For additional information regarding the lift design of tilt-up panel please refer to TM-34 [4].

2.4 Connection Design

While connection design is common for all structural components there is a higher degree of discontinuity in tilt-up and precast panel connections. Panel connections are typically achieved through the use of embedded plates which are either bolted or welded to the supporting structural frame and are designed to resist lateral wind loads, shear forces, and to transfer gravity loads to loadbearing panels. In this investigation two connections commonly used in practice are designed to reflect industry standards and are scaled for testing. The base (bottom) connection replicates a footing which bears the weight of the panel and an interior slab which the panel bears against under lateral load. The top connection mimics commonly practiced roof-panel connection details and consists of embedded joist bearing seats welded to a supporting system.

The base connection utilizes the shear and pullout capacities of dowels embedded into the footing and grouted to fasten the panel down. The top connection consists of an angle embedded on the top corner with two headed studs extending 45 degrees from each leg of the angle. CSA A23.3-04 Annex D [5] outlines a design approach for anchors embedded 90 degrees into a flat concrete surface, however this approach needs to be modified to accommodate anchors embedded at different angles. The embedment angle influences the propagation of the failure crack which can ultimately be used to determine the effective embedment depth. The effective embedment depth is defined as the depth of the anchor to its failure surface. Anchor location also influences strength in that it limits the projected concrete failure area (A_N) and alters the modification factors (Ψ_x). It is important to accurately capture these characteristics in 45-degree corner embedded anchors to avoid premature failure. Figure 2.2 illustrates some of the different theoretical crack propagations and failure planes for 90 and 45 degree embedded anchors

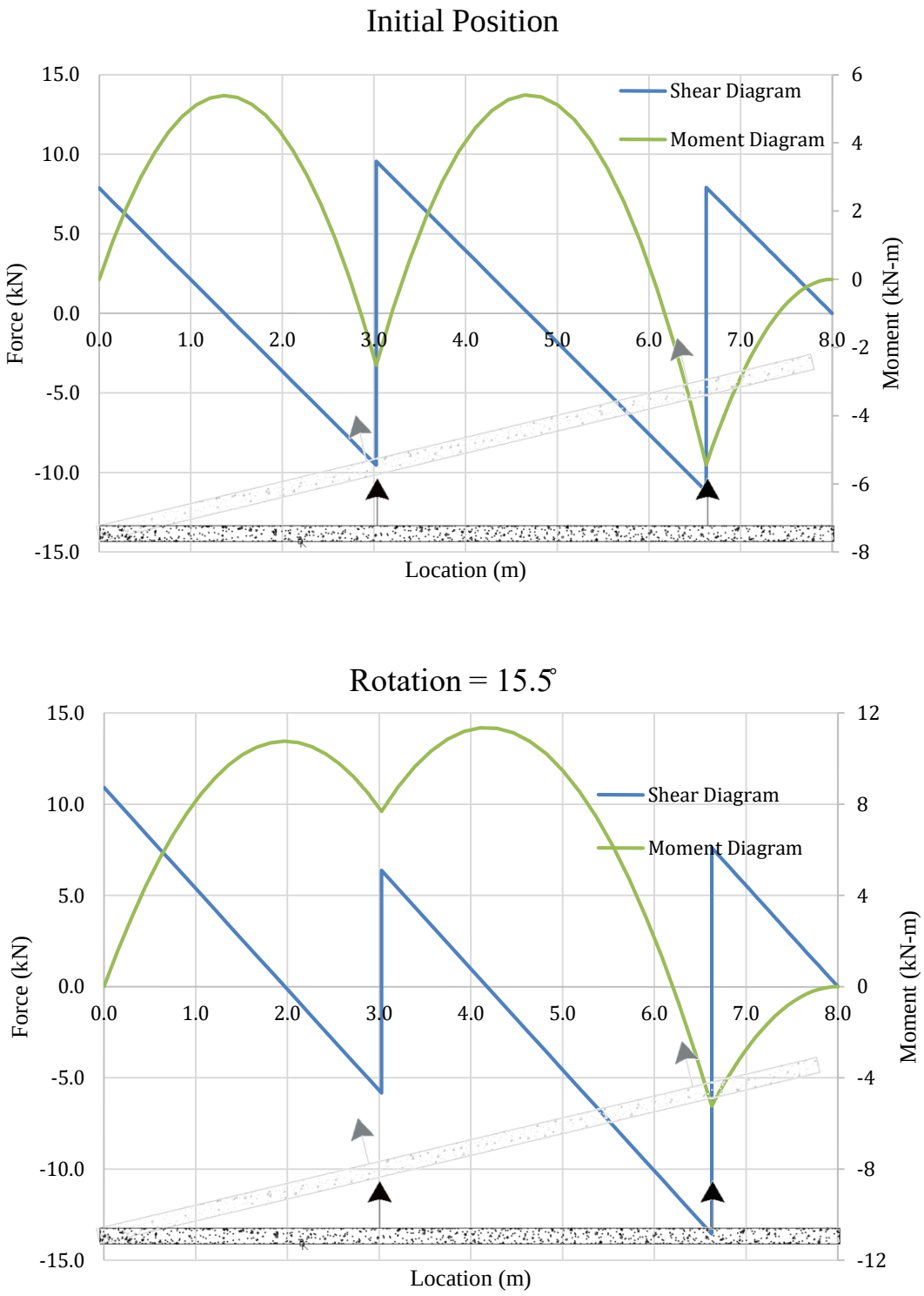

Figure 2.1 – Lifting Shear Force and Moment Diagram from Horizontal (top) and Rotational (bottom) Positions

90 Degree Surface Embedded Anchor 45 Degree Corner Embedded Anchor

$$N_{cbr} = \frac{A_N}{A_{N0}} \Psi_{ed} \Psi_c \Psi_{cp} \Psi_{ec} N$$

Tensile Concrete Breakout

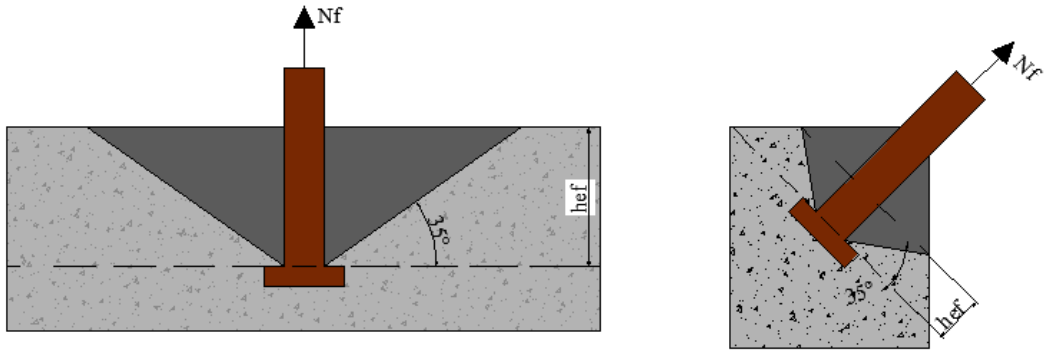

$$V_{cbr} = \frac{A_v}{A_{v0}} \Psi_{ec} \Psi_{ed} \Psi_c V_{br}$$

Shear Concrete Breakout

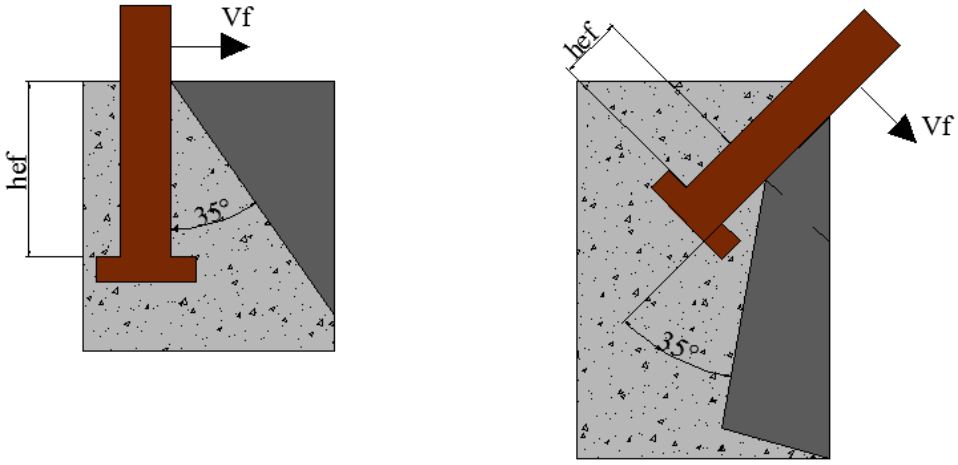

Figure 2.2 Embedded Anchor Theoretical Crack Propagation and Failure Plane

3.0 Experimental Program

3.1 University of Ottawa Blast Research Facility

3.1.1 Shock Tube

The blast research facility, located in the University of Ottawa Structural Engineering Laboratory, has a pneumatically driven shock tube with the ability to test full-size and scaled structural members under simulated blast loads. The shock tube simulates blast induced shock waves by reproducing the fundamental mechanisms of high explosive detonation through the rapid release of compressed air.

The shock tube is comprised of a variable length driver section, a spool section, and an expansion section equipped with a rigid test frame. The driver section consists of six circular steel section, allowing its overall length to range from *305mm* to *5185mm* in *305mm* increments. Each steel section has a thickness of *12.7mm* and an inner diameter of *597mm*. The spool section, fixed at a *90mm* length, is the connecting portion between the driver and expansion sections which ultimately controls the firing of the shock tube. The expansion section is *6096mm* in length, connecting to the spool section at one end with a rigid test frame located at the opposite end. The cross section of the expansion section varies from the *597mm* circular diameter of the spool section to the *2032x2032mm* test frame opening. Both the test frame and expansion section are constructed with *12.7mm* thick stiffened steel plate. Specimens can be bolted to the shock tube using twenty *19mm* holes located on the test frame.

Shock waves are generated within the shock tube using a double diaphragm firing mechanism to allow the development and nearly instantaneous release of compressed air. In this firing process two aluminum diaphragms are installed on either end of the spool section (i.e. driver-spool section and spool-expansion section). While the driver length and pressure govern the pressure-time history of the shockwave produced, it is critical to select an adequate spool pressure and diaphragm rupture capacity to prevent premature firing of the shock tube. Based on the driver and spool pressures the diaphragms must be selected such that the rupture capacities are marginally larger than the pressure differential between the expansion-spool section and the driver-spool section,

respectively. The diaphragms are fastened between flanges that connect the various sections of the shock tube with twenty *31.75mm* bolts.

Firing of the shock tube is controlled from the upper floor of the Structural Engineering Laboratory. Pressure in the spool and driver sections are incrementally increased, ensuring the pressure differential between the driver-spool and spool-expansion interface does not exceed the rupture capacity of the respective diaphragm. Upon achieving the desired driver and spool pressures, the firing process is initiated by draining the air pressure in the spool. The pressure differential between the driver and spool section increases causing the first diaphragm to rupture. Immediately the pressure increase in the spool area causes the second diaphragm to rupture allowing the compressed air to enter the expansion area. This instantaneous expansion of compressed air produces a shockwave which propagates through the expansion section where it ultimately contacts the specimen at the test frame.

There are twelve sliding pressure relief vents located at the end of the expansion section before the testing frame, which slide open as the shock wave passes. These vents allow the pressurized air to enter the surrounding atmosphere, producing a negative pressure phase and reducing the effects of reflected shock waves within the shock tube.

Lloyd et al. [6] reported that the peak reflected over pressure and positive phase duration of shock wave produced were primarily related to the driver pressure and driver length, respectively. For further information regarding the shock tube's properties and capabilities refer to Lloyd et al. [6].

3.2 Description of Test Specimens

Five scaled test specimens were constructed to represent a single storey panel and designed to reflect general tilt-up panels commonly used in industry. The full-scale specimens, designed using CSA A23.3 standards as a *4000x4000x290mm* non-composite reinforced concrete sandwich panel with a *165mm* thick structural wythe, were scaled to accommodate the *2032x2032mm* shock tube dimensions. A scaling factor of *0.5* was used for the sizing of connections and the length and width of the panel. This was increased to *0.6* for the thickness of the panel to achieve a structural wythe thickness of *100mm* with adequate space for reinforcing steel. Scaled panels were designed to have the same reinforcement ratio at the full-scale specimens.

3.2.1 SRC-1 (Control Panel)

SRC-1 is a one-way solid reinforced concrete panel consisting of a single *100mm* thick structural wythe. SRC-1, also referred to as the control specimen, had a total length of *2032mm* and a clear span (height) of *1862mm*.

The specimen was doubly reinforced with six 10M deformed reinforcing steel bars, spaced at *400mm* c/c in each principle direction. Transverse reinforcement was staggered between the two layers. *180º* end hooks with an interior diameter of *70mm* and a *200mm* extension were used to ensure full development of the bar and prevent pullout. The clear cover of the transverse longitudinal reinforcement was maintained at *10mm* and *20mm*, respectively.

All panels were constructed using concrete with a specified 28-day compressive strength of *25MPa* and a maximum aggregate size of *10mm*. The concrete compressive strength at the time of testing was 39.2MPa, based on an average of three test cylinders. Panel properties are summarized in Table 3.1.

3.2.2 NCTS-1

NCTS-1 is a one-way reinforced concrete non-composite sandwich tilt-up panel with a total thickness of *200mm* and consists of: a 100mm structural wythe, a *50mm* layer of insulation, and a *50mm* architectural wythe. Each specimen has an overall length of *2032mm* with a clear span of *1862mm*. The structural wythe of the specimen is identical to SRC-1 to ensure the comparability of data.

The structural wythe of specimen NCTS-1 is doubly reinforced with six 10M deformed steel reinforcement, spaced at *400mm* c/c in the principle directions on each face of the panel. Transverse reinforcement was staggered between each mat. *180º* end hooks with an interior diameter of *70mm* and a *200mm* extension ensured full development of the reinforcing bars. The clear cover of concrete to the transverse and longitudinal reinforcement was maintained at *10mm* and *20mm*, respectively.

The architectural wythe of NCTS-1 is reinforced with a single mat of *9/9x6x6* (1*52x152xMW11.1/11.1*) WWM, with strands running in the principle directions. Mats were placed such that there were no joints in the panel's longitudinal direction and joints in the

transverse direction were overlapped *150mm*. The WWM was placed in the centre of the *50mm* architectural face with a clear cover of approximately *25mm* from either face.

The architectural and structural wythes were connected using shear ties, typical to non-composite design. Shear ties were constructed from *6.3mm* diameter non-deformed steel reinforcement. Shear ties were spaced at *300mm* c/c as shown in Figure 3.3. All ties were cut and bent on site such that the insulation was clamped between the ends of the bend as shown in Figure 3.5 and Figure 3.6.

Concrete with a 28-day compressive strength of *25MPa* and a maximum aggregate side of *10mm* was used in the construction of the panels. The concrete compressive strength at the time of testing was 41.8MPa, based on an average of three test cylinders. Panel properties are summarized in Table 3.1.

3.2.3 NCTS-2

The design of NCTS-2 is identical to specimen NCTS-1; however, the actual thickness of the specimen was *110mm* due to construction related issues. Refer to Section 3.2.2 for a description of specimen NCTS-2.

The concrete compressive strength at the time of testing was 34.3MPa, based on an average of three test cylinders. Panel properties are summarized in Table 3.1.

3.2.4 NCTS-M (Modified Connection Reinforcement)

NCTS-M is a one-way reinforced concrete non-composite sandwich tilt-up panel with a total thickness of *200mm*. NCTS-M is made up of three layers: a *100mm* structural wythe, a *50mm* layer of insulation, and a *50mm* architectural wythe and an overall length of *2032mm* with a clear span of *1862mm*. NCTS-M is identical to NCTS-1 and NCTS-2, with modified reinforcement details surrounding the three upper connections.

The structural wythe of specimen NCTS-M is doubly reinforced with six 10M deformed steel reinforcement, spaced at *400mm* c/c in the principle directions on each face of the panel. Transverse reinforcement was staggered between each reinforcement layer. *180º* end hooks with an interior diameter of *70mm* and a *200mm* extension were used to fully develop the reinforcing

bars. The clear cover of concrete to the transverse and longitudinal reinforcement was maintained at *10mm* and *20mm*, respectively.

The architectural wythe of NCTS-M is reinforced with a single mat of *9/9x6x6* (*152x152xMW11.1/11.1*) WWM, with strands running in the principle directions. Mats were placed such that there were no joints in the panel's longitudinal direction and joints in the transverse direction were overlapped *150mm*. The WWM was placed in the centre of the *50mm* architectural face.

The architectural and structural wythes were connected using shear ties, typical to non-composite design. Shear ties were constructed from *6.3mm* diameter non-deformed steel reinforcement. Shear ties were spaced at *300mm* c/c as shown in Figure 3.3. All bars were cut and bent on site such that the insulation was clamped between the ends of the bend as shown in Figure 3.5 and Figure 3.6.

A modified reinforcement detail was used to increase the ductility and overall capacity of the embedded joist seats in the three upper connections. The additional reinforcement installed in this panel consisted *6.3mm* diameter nondeformed steel bent and placed as shown in Figure 3.7 and Figure 3.8 , respectively.

Concrete with a 28-day compressive strength of *25MPa* and a maximum aggregate side of *10mm* was used in the construction of the panels. The concrete compressive strength at the time of testing was 42.7MPa, based on an average of three test cylinders. Panel properties are summarized in Table 3.1.

3.2.5 NCTS-R (Retrofitted Support)

NCTS-R was constructed by repairing and retrofitting the previously tested NCTS-1 with unidirectional Carbon Fibre Reinforced Polymer (CFRP) sheets. Upon failure of NCTS-1, the concrete in the upper span of the panel was removed in an attempt to eliminate the effects of damage caused in previous tests and return the panel to like new conditions. New upper connections were installed in the panel while the existing flexural reinforcement was reused in the repair. Upon casting and curing of the structural wythe four layers of CFRP sheets, two in either principal direction, were installed on the compressive face to prevent the punching shear failure experienced in NCTS-1. This retrofit option was designed as a solution that could easily be

installed on existing panels with minimal labour. CFRP sheets were installed such that, where possible, there was a *100mm* extension beyond the connections failure plane to ensure that it would not break off during support failure. The *100mm* extension was calculated based on equations recommended by Shadravan [7] to prevent debonding of the retrofit. Figure 3.9 illustrates the location and directions of the CFRP layers while its properties are summarized in Section 3.4.6.

Similarly, to the other sandwich panel specimens NCTS-R is a one-way reinforced concrete panel consisting of a *100mm* structural wythe, a *50mm* insulation layer, and a *50mm* architectural wythe for an overall thickness of *200mm*. The actual overall thickness of the panel around the upper supports was *210mm* due to a construction error during the panel repair which resulted in a *110mm* thick structural wythe. Specimen NCTS-R is a square NCTS-1*032mm* high and wide with a clear span of *1862mm*.

The structural wythe of specimen NCTS-R is doubly reinforced with six 10M deformed steel reinforcement, spaced at *400mm* c/c in the principle directions on each face of the panel. Transverse reinforcement was staggered between each mat. *180º* end hooks with an interior diameter of *70mm* and a *200mm* extension were used to fully develop the reinforcing bars. The clear cover of concrete to the transverse and longitudinal reinforcement was maintained at *10mm* and *20mm*, respectively.

The architectural wythe of NCTS-R is reinforced with a single mat of *152x152xMW11.1/11.1* WWM, with strands running in the principle directions. The WWM in the upper portion of the panel was discarded during the repair process. Anchors, made of the same gauge steel as the WWM, were embedded and anchored into the remaining portion of the architectural face. The *350mm* anchors were embedded *150mm* into the existing concrete using Quickrete® FastSet Anchor Epoxy at one end and bent *180º* to ensure sufficient bond with new concrete. A single sheet of WWM was then placed in the repaired section of the panel overlapping the anchors by *150mm*. The WWM was placed in the centre of the *50mm* architectural face.

The repaired architectural and structural wythes were connected using a generic shear tie similar to those in previous panels. However, this unique tie consists of a *50mm* straight extension epoxy anchored into the structural face and an end with a *180º* bend cast into the architectural face. Details and schematics are provided in Figure 3.11.

Concrete with a 28-day compressive strength of *25MPa* and a maximum aggregate side of *10mm* was used in the construction of the panels. The concrete compressive strength at the time of testing was 40.4MPa, based on an average of three test cylinders. Panel properties are summarized in Table 3.1.

3.3 Connection Details

The panel connections used in this investigative study were selected to represent a significant portion of connections used in non-composite reinforced concrete tilt-up panel construction. Based on this, a combination of two connections was selected: joist bearing seats and direct bearing. Connection details were reviewed and designed for generic two storey 4*000x4000mm* panel and scaled to accommodate the *2032x2032mm* shock tube test frame. The connections used in this experimental study were designed to be pinned supports.

3.3.1 Joist Seat Connection Details (Top Connection)

Each specimen is equipped with three joist bearing seats embedded at the base of *50mm* deep pockets along the top edge of the panel. The joists bearing seats consist of a *150mm* long *63.5x63.5x6.5mm* angle. The angles are equipped with two *75mm* long headed studs welded at *45º* from the inside of either leg of the angle. All components of the joist seats were fabricated at the University of Ottawa Structural Engineering Research Laboratory. Headed studs were built using *10mm* non-deformed steel reinforcement with a *25x25mm* plate welded at the end

Joist seats are embedded into the bottom-corner of *50mm* deep pockets located along the top edge of the panel. A *76mm* x *8kg*/*m* standard steel I-section were used to simulate open web steel joists as sizing restriction movement of the shock tube made it impractical to use scaled joists. The I-sections were welded to the top of the plate using a robust fillet weld along the entire bearing length, *45mm* on either flange. A robust fillet weld was used along the top of the I-sections to mechanically fasten the specimen to a *152.4x152.4x4.78mm* shock tube support beam to simulate the structural skeleton of the building (i.e. the roof or floor system providing lateral restraint). The HSS was connected to the shock tube test frame with six *19mm* threaded rods. Photos of the

completed inserts are shown in Figure 3.12 while support locations and details can be found in Figure 3.1 and Figure 3.2.

3.3.2 Direct Bearing Connection Details (Base Connection)

The base connection of the panels consists of the concrete support structure shown in Figure 3.14, which is designed to reproduce the in-situ footing/slab connection details commonly used in practice. The base support is comprised of a reinforced concrete support structure and shear keys. To adequately reflect the location where the slab and footing meet, and to allow direct bearing, a step was cast into the base support. Details and schematics for the base support are provided in Figure 3.13.

The side and base of the step, or the slab and footing, are *120mm* and provides approximately *100x2032mm* of direct bearing area. Each specimen is equipped with three *25mm* PVC pipes embedded *200mm* into the panel. *300mm* dowels were embedded *150mm* into the footing with *20mm* generic plastic shims placed directly beside them to ensure adequate space for grout placement. Specimens were placed on the support structure such that the dowels were inserted *150mm* in the PVC pipe with the panel bearing directly on the shims *20mm* from the face of the slab. The panel was then mechanically connected to the support base by filling the *20mm* void and PVC pipes with non-shrink construction grout. Six *1100lb* casters were installed on the base support for ease of mobility. Furthermore, PVC pipe was cast-in the base to accommodate four *19mm* threaded rod, allowing direct installation to the shock tube test frame.

3.4 Material Properties

3.4.1 Concrete

Panels SRC-1 and NCTS-1 were cast as a set, followed by NCTS-2 and NCTS-M. All Panels were cast using concrete with a specified 28-day compressive strength of *25MPa* and *10mm* crushed limestone aggregates.

Concrete repairs for NCTS-2 and the architectural face of NCTS-R were cast using KING MS-S10 Self Consolidating Concrete to achieve the required concrete capacity quickly. The KING

MS-S10 mixture contains *10mm* aggregate and Silica fume with specified 3-day and 28-day compressive strengths of *25MPa* and *40MPa*, respectively.

The results of cylinder compressive strength tests performed for each panel at the time of testing are shown in Table 3.1.

3.4.2 Grout

KING Non-Shrink Grout ™, used to connect specimens to the base support, was prepared onsite following manufacturer guidelines to achieve a fluid grout mixture:

- Dust and debris was removed from the concrete surface to reduce the potential of reduced bond strength.
- Approximately *75%* of the required water was added to the wheel barrel. The cement based mixture was gradually added to the water and mixed until a consistent slurry was achieve. Finally, the remaining water was added to the mix.
- Shovel mixing of the grout continued for a minimum of three minutes until a homogeneous mixture was achieved.

The 3-day and 28-day compressive strength specified by KING are *25MPa* and *35MPa*, respectively for a liquid mix. A minimum of four grout cylinders were tested for each specimen during the experiment. Actual compressive strength at time of testing are provided in Table 3.1.

3.4.3 Deformed Steel Reinforcement

All specimens were reinforced with 10M deformed steel reinforcing bars with a tensile yield capacity and strain of *489MPa* and *0.282%*, respectively. The ultimate capacity of *589MPa* occurred at a strain of *14.8%*. The stress-strain properties of the flexural steel, shown in Figure 3.15 were found from an average of three test coupons.

3.4.4 Shear Ties

Generic shear ties used in the construction of NCTS panels were fabricated from *6.3mm* non-deformed steel reinforcing bars with a tensile yield capacity of *480MPa* at a strain of *0.245%*. The

ultimate capacity of the nondeformed steel bars was *650MPa* at a strain of *4.59%*. The stress-strain relationship is provided in Figure 3.16.

3.4.5 Welded Wire Mesh

The architectural wythe of each sandwich panel was reinforced with *152x152xMW11.1/11.1* non-deformed welded wire mesh with a tensile yield capacity of *592MPa* and strain of *0298%*. The welded wire mesh registered an ultimate capacity of *728MPa* at a strain of *1.78%*. The stress-strain relationship, shown in Figure 3.17, is based on the average of three test coupons.

3.4.6 CFRP Sheets

SikaWrap® -230 C/45 is a unidirectional carbon fibre fabric used as a support retrofit for NCTS-R. The manufacturer specified tensile strength and elastic modulus of dry fibres are *4300MPa* and *234GPa* respectively. Laminated CFRP layers are *1.0mm* thick with a *25.0GPA* modulus of elasticity. Concrete surfaces were primed and CFRP fibres were impregnated with Sikadur® resin as specified by the manufacturer.

3.4.7 Insulation

Styrofoam™ CLADMATE™ Insulation was selected as the insulation layer between the architectural and structural wythes of all sandwich panels. This *50mm* thick extruded polystyrene foam insulation has an R-value of *10* and a minimum compressive strength of *110kPa*, specified by the manufacturer.

3.5 Construction of Test Specimens

All test specimens and supports were constructed and tested at the University of Ottawa Structural Engineering Laboratory. Fabrication of panels is identical for the early stages of construction however vary considerably near completion of the panels. This section will briefly outline the construction methods used throughout this project in a step-by-step manor.

3.5.1 Panels SRC-1, NCTS-1, NCTS-2, and NCTS-M

The construction of each specimen was carried out using the materials outlined in Section 3.4. There are three primary steps in the construction process common to all panels: construction of formwork, preparation and installation of rebar and inserts, and placement of concrete. There are two addition steps unique to the sandwich panels: preparation and installation of insulation and the placement of welded wire mesh.

Formwork consisted of a flat base *2440x2440mm* with *200mm* high edges, enclosing a *2032x2032mm* area constructed on top of the base. Two sets of formwork were constructed to accommodate simultaneous construction of test specimens.

Rebar was cut to *2550mm* lengths, bent *180º* at either end with an extension of *200mm* beyond the bend. Rebar mats were prepared individually with a *400mm* centre-to-centre spacing in each direction. Transverse reinforcement was staggered *200mm* between the compressive and tensile mats, a standard commonly used in tilt-up practice. Strain gauges were then installed on reinforcement at the locations shown in Figure 3.18 and Figure 3.19. Rebar was installed using generic plastic chairs to maintain desired cover in the first layer while custom steel chairs were used for the second layer. Finally, the inserts, PVC Pipe and embedded connections, were installed in the panel as shown in Figure 3.20.

In addition to the above steps specimen NCTS-M required the cutting, bending, and installation of additional reinforcement around the three joist seats. Figure 3.7 shows the schematics for the modified reinforcement details.

Sandwich panel specimens required two additional steps prior to the placement of concrete. The welded wire mesh, used to meet minimum reinforcement requirements in the architectural face, was cut from *1220x2440mm* sheets to fit the opening. Sheet were cut such that there was no longitudinal joints and transverse joints overlapped by a minimum *150mm*. Generic shear ties fabricated by cutting *6.3mm* non-deformed bars to approximate lengths of *260mm*. The ties were then bent using a conventional manual rebar bender such that there was a *50mm* space to accommodate the insulation. Finally, the insulation was cut to *1932x300mm*, with shear ties installed along their length at a *300mm* c/c spacing.

Concrete was placed directly from the back of the truck. Thickness of the panels was monitored to maintain desired thicknesses. Levelling of the structural wythe was required for sandwich panels to allow placement of insulation and shear ties. Insulation was installed such that there was *100mm* of concrete at their base. Finally, WWM was installed above the insulation and the architectural face was cast. Panels were poured in pairs, SRC-1 and NCTS-1 were first cast and tested followed by NCTS-2 and NCTS-M. Concrete was wet cured for seven days and dry cured a minimum of 21 days prior to testing.

3.5.2 Panel NCTS-R

Specimen NCTS-R is a repaired and retrofitted panel constructed from the relatively undamaged lower half of NCTS-1 and therefore required the removal, disposal, and replacement of the damaged portion of the panel. The process involved:

1) Removing the structural, insulation, and architectural wythes to approximately *950mm* from the top of the panel. The architectural face was cut in the transverse direction and removed along with the insulation. The concrete of the structural wythe was then removed while maintaining the original reinforcing steel.
2) Constructing formwork around the remaining portion of the panel to allow the recasting of the structural wythe.
3) Examining the reinforcement to confirm the spacing of the steel was retained and restoring original spacing if necessary. Reinforcement chairs were installed to ensure original depths would be maintained and new embedded plates were installed at the previous connection locations.
4) Casting concrete for the structural wythe.

Installation of the support retrofit was done as to replicate actual retrofit procedures potentially used in practice. The structural face was allowed to cure for a minimum of 28-days after which point four layers of *500x500mm* CFRP sheets were installed at the upper support locations in interchanging directions. The following procedure was used in the installation of the CFRP retrofit:

1) Remove irregularities on the concrete surface using an angle grinder with a concrete and masonry grinding blade to ensure high quality bond.

2) Remove dust and debris from concrete surface. This was done using compressed air to remove loose debris.
3) Apply epoxy to the concrete surface using a paint roller.
4) Saturate CFRP sheets with epoxy by rolling each side with paint roller.
5) Apply CFRP sheet to the concrete surface and remove air bubbles by scraping surface of sheets in the direction of the fibres. This also serves to force the epoxy into and between the fibres further saturating the sheets.
6) Apply additional epoxy to the exposed surface of the applied CFRP sheet.
7) Repeat step 4 through 5 alternating fibre direction for each successive layer.

Insulation was installed on the structural wythe upon hardening of the FRP retrofit. Shear ties used in the repair of NCTS-1 consisted of a straight end anchored in the existing structural wythe and a *180º* bend extending beyond the insulation into the architectural face. Details for this are provided in Figure 3.11. Following installation of the insulation, anchors were installed in the existing portion of the architectural face in such a way to ensure a mechanical bond with new concrete and WWM.

Finally, the architectural face was cast using KING MS-S10 Self Consolidating Concrete and allowed to wet cure for three days prior to testing.

3.5.3 Base Connection

Construction of the base connection was performed concurrently with the test specimens SRC-1 and NCTS-1, and followed similar stages in construction: construction of formwork, installation of rebar and inserts, and placement of concrete. Additional preparation of the base was required to allow the placement of the panels and to facilitate mobility of the entire system.

The construction of the formwork followed the same principals as the test specimens: preparation of a *2440x500mm* base and a *500mm* high enclosure. In addition to this, steps were installed at either end of the base and along the top edges to accommodate the installation of casters and to simulate the slab/footing area. A detailed design of the base support is provided in Figure 3.13.

Although the base was designed to remain uncracked under all load scenarios four *2400mm* 10M rebar were installed, three along the bottom and one along the top. Ten additional U-shaped rebar were inserted at equal spacing along the base as shown in Figure 3.14. PVC pipes were installed to allow mounting of the base to the shock tube using threaded rod as discussed in Section 3.1.1. Finally, threaded rod was embedded in the bottom step such that casters could be fastened to a plate. Concrete was cast and wet cured for a minimum seven days.

Due to the spatial in the blast research facility, the overall weight of the test setup, and the capacity of the available forklift, a plate fashioned with three *1100lb* casters was fastened at either end of the base after 28 days of curing. This provided the system with inherent mobility and maneuverability, and allowed the setup to be moved to and attached to the shock tube without exceeding the forklift capacity. Following this the bearing surface was prepared, shear keys were drilled and installed, and the wall was placed as described in Section 3.3.2.

3.5.4 Mounting Specimen to Shock tube

Mounting the panel to the shock tube testing frame required three primary steps: fastening the panel to the base support, connecting the base to the testing frame, and installing the upper supports to the panel. The following section explains these steps in detail.

Firstly, the panel was installed on the base support using the mechanic connection details discussed in Section 3.3.2. Installation involved lifting the specimen vertically and resting it on the base connection, the panel must be accurately positioned and level such that dowels are correctly placed in the wall and that the spacers provide adequate room for grout. Formwork was constructed and fluid form grout was poured into the space between the base and the panel.

Secondly, the system was connected to the shock tube using four *19mm* diameter threaded rods. The system was adjusted so that it aligned with the opening of the shock tube and the base support was braced using spacers to minimize support rotation and prevent damage to the casters.

Finally, *70-80mm* long *S75x8* I-beam sections were welded to a rigid steel section. The rigid steel section, with I-beam sections resting on the joist seats, was then connected to the shock tube using six *19mm* threaded rods. Lastly, the I-beam sections were welded to the embedded plates.

Due to the additional thickness of the sandwich panel, a spacer was fastened to the shock tube test frame prior to installation of the panel. Figure 3.21 through Figure 3.24 show the final test setup typical to all panels.

3.6 Instrumentation

Experimental data was recorded at *100,000* samples per second using a Yokogawa SL1000 High-Speed Data Acquisition Unit with 16 available data channels. A typical system setup consisted of ten strain gauges, two pressure sensors and four LVDT units. The data acquisition sequence was initiated when sensors recorded pressure exceeding a predetermined threshold. Data was recorded to a desktop computer at the shock tube control station on the upper level of the Structural Engineering Laboratory. Pressure fluctuations and data were measured by two PCB Piezotronic Piezoelectric Pressure Sensors located on the side and bottom of the expansion section 50mm away from the specimen.

All specimens were equipped with a minimum of ten Tokyo Sokki Kenkyujo Co., Ltd. FLA-6-350-11 350Ω electrical resistance strain gauges. The basic layout of strain gauges consisted of four units on tensile steel at mid-span, two units on compressive steel at mid-span, and two units on tensile steel at upper and lower quarter-span. Additional redundant units were installed to accommodate potential malfunction or damage to concurrent strain gauges. The locations of strain gauges were selected to capture maximum moments, provide a strain profile along the length of the beam, and record the sectional strain profile at mid-span. General strain gauge locations and orientations are illustrated in Figure 3.18 and Figure 3.19 .

Panel displacement profiles were measured using Celesco CLWG-300 Linear Variable Displacement Transducers (LVDT's). LVDT's were calibrated with the SL1000 data acquisition software prior to testing each specimen to accurately measure displacement to a tenth of a millimeter. Panel displacements were measured at the upper quarter-span (LVDT-1), mid-span (LVDT-2), and lower quarter-span (LVDT-3) with a fourth LVDT to measure the overall displacement of the shock tube. For high pressure shots where excessive damage was expected, LVDTs were removed from the panel and displacement was visually recorded using ruled steel HSS section mounted to the shock tube.

An AOS Technologies X-PRI full colour high-speed camera recorded the panel's reaction to the shockwave at *500* frames per second and a resolution of *800x600* pixels. The video recording sequence was triggered by the Yokogawa SL1000 with a pre-buffer of 15 percent. Video data was recorded to a Laptop Computer located near the shock tube on the lower level of the Structural Engineering Laboratory.

Table 3.1 – Panel Description and Properties

Specimen	*Length* *L* *mm*	*Clear Span* *h* *mm*	*Width* *b* *mm*	*Total Thickness* t_{total} *mm*	*Structural Wythe Thickness* t_{st} *mm*	*Architectural Wythe Thickness* t_{ar} *mm*	*Concrete Compressive Strength* f_c' *MPa*		*Description*
							Concrete	*Grout*	
SRC-1	2033	1862	2033	100	100	-	39.2	45.3	- Structural control panel
NCTS-1	2033	1862	2033	200	100	50	41.8	25.6	- Sandwich panel
NCTS-2	2033	1862	2033	200	110	40	34.3 55.4[1]	41.2	- Sandwich panel -Structural depth increased due to over vibration of architectural face.
NCTS-M	2033	1862	2033	200	100	50	42.7	47.4	- Sandwich panel - Modified supports with additional reinforcement.
NCTS-R	2033	1862	2033	210[2]	110	50	40.4[1]	40.9	- Repaired sandwich panel retrofitted with four interchanging layers of FRP sheets.

[1] Repaired portion of the panel
[2] Increased thickness near repaired portion of the panel.

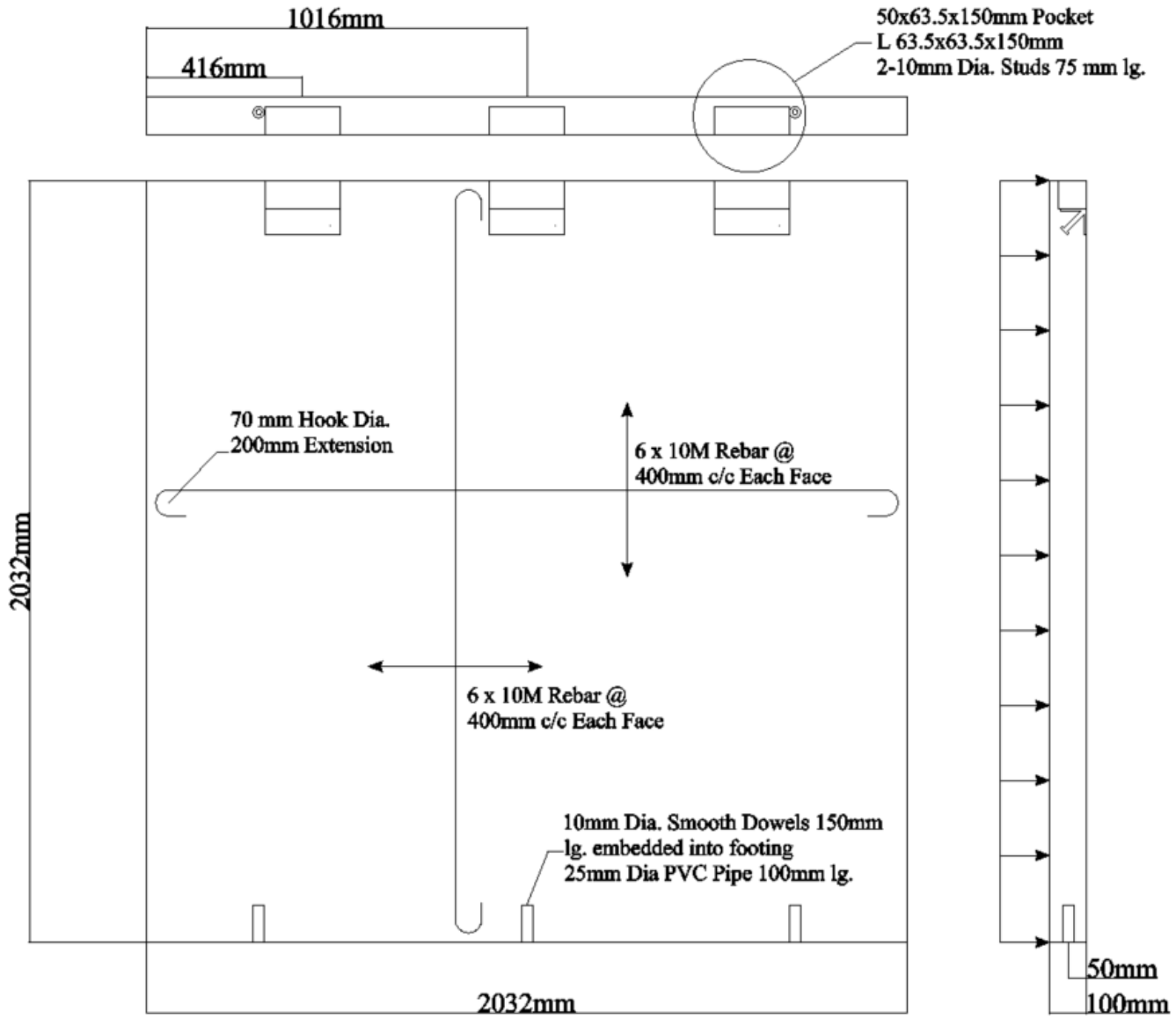

Figure 3.1 - Reinforcement and Connection Details for Control Panel SRC-1

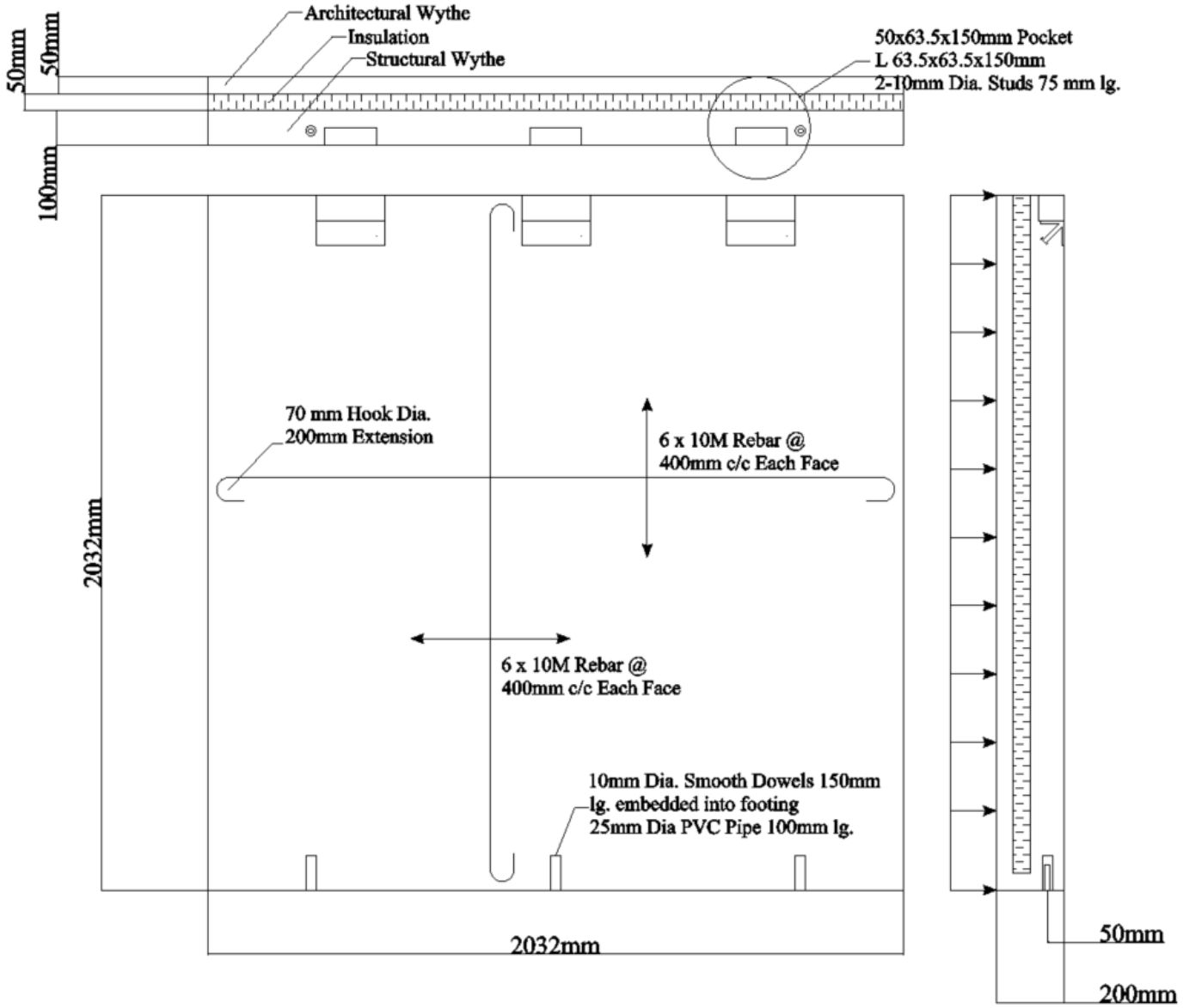

Figure 3.2 – Typical Reinforcement and Connection Details for Sandwich Panels

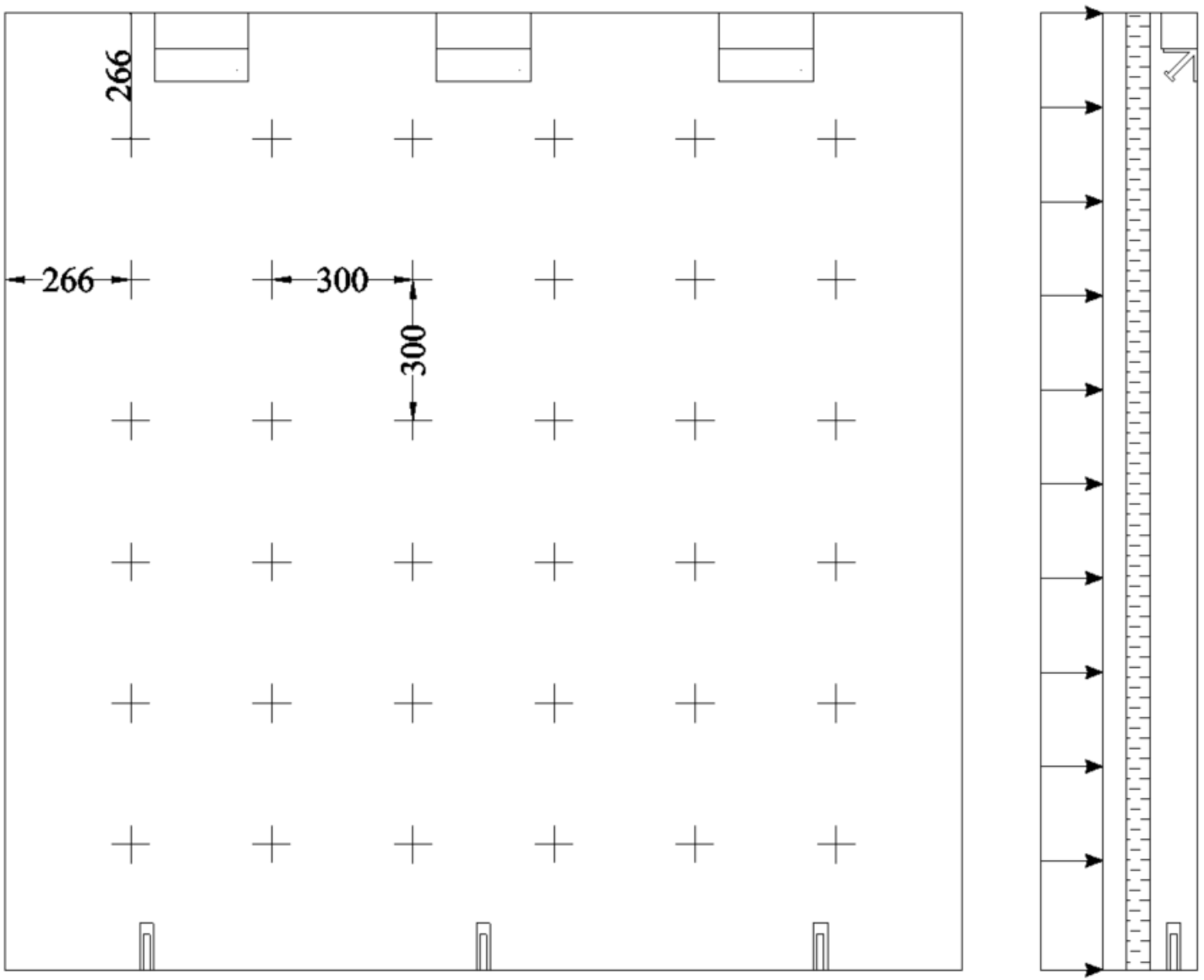

Figure 3.3 – Typical Shear Tie Locations for Sandwich Panels

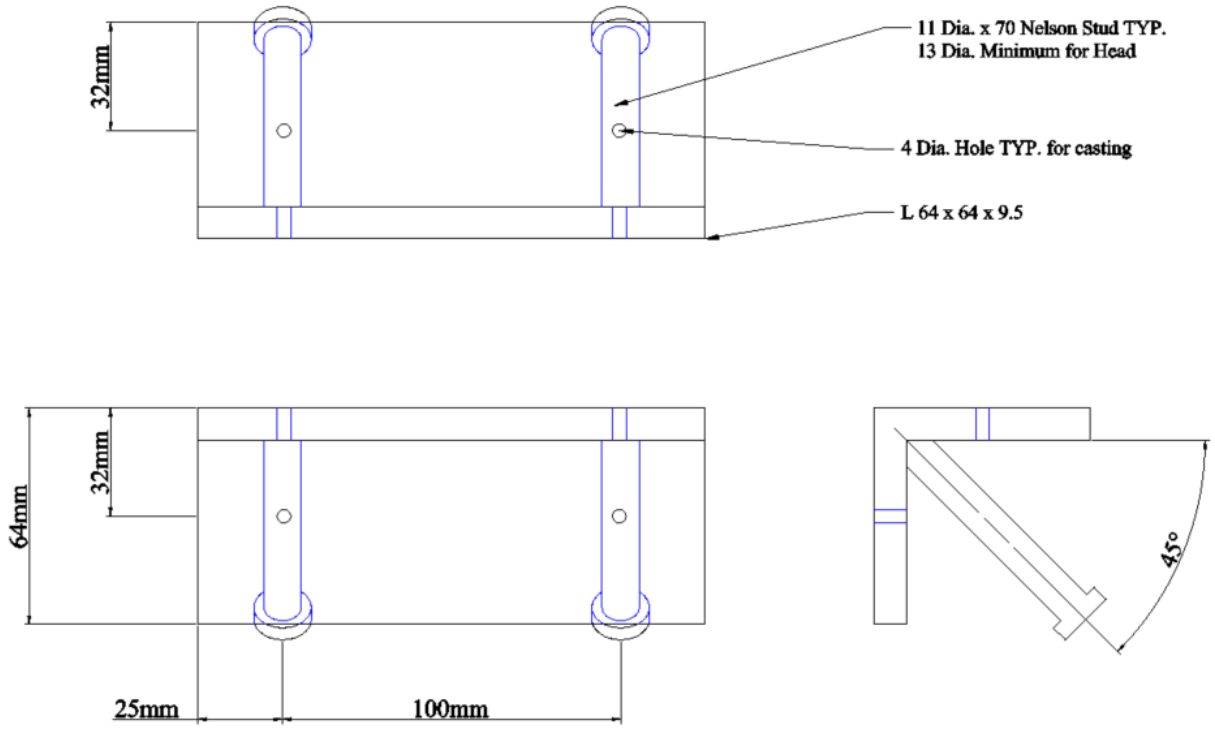

Figure 3.4 – Joist Seat Schematic

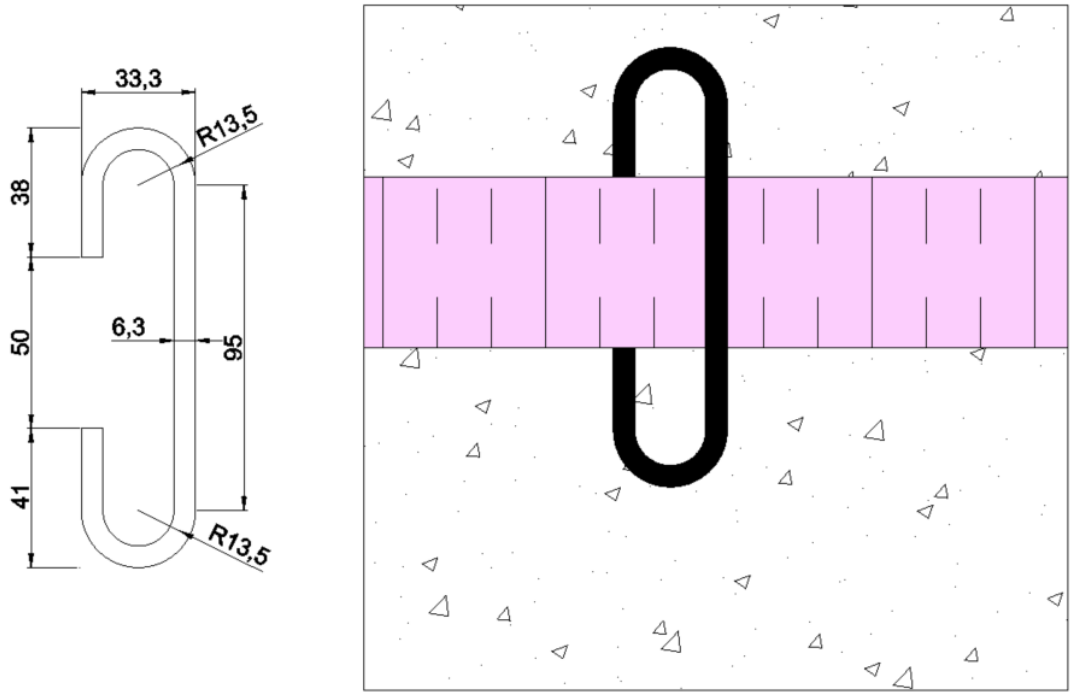

Figure 3.5 – Typical Shear Tie Details and Installation Schematic

Figure 3.6 – Typical Installation of Shear Ties Prior to Casting

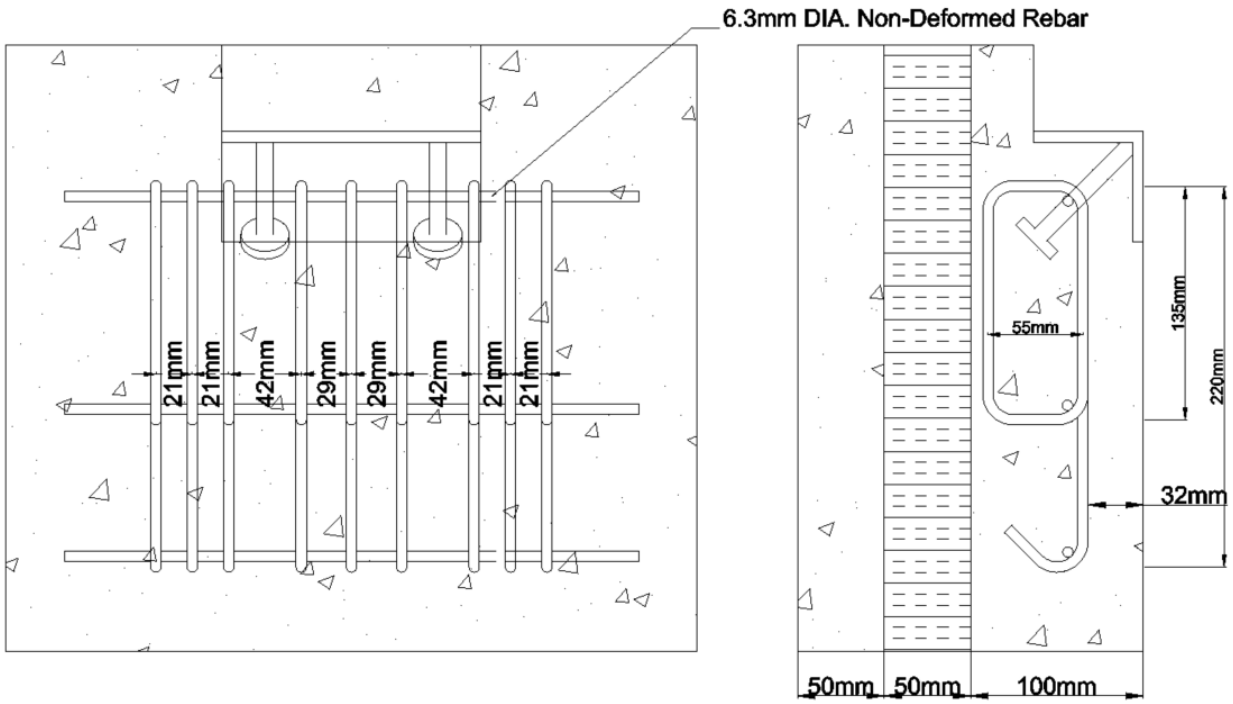

Figure 3.7 – Modified Support Reinforcement for NCTS-M

Figure 3.8 – Modified Support Reinforcement for NCTS-1 & NCTS-2 (Left) and NCTS-M (Right) Installed Prior to Casting

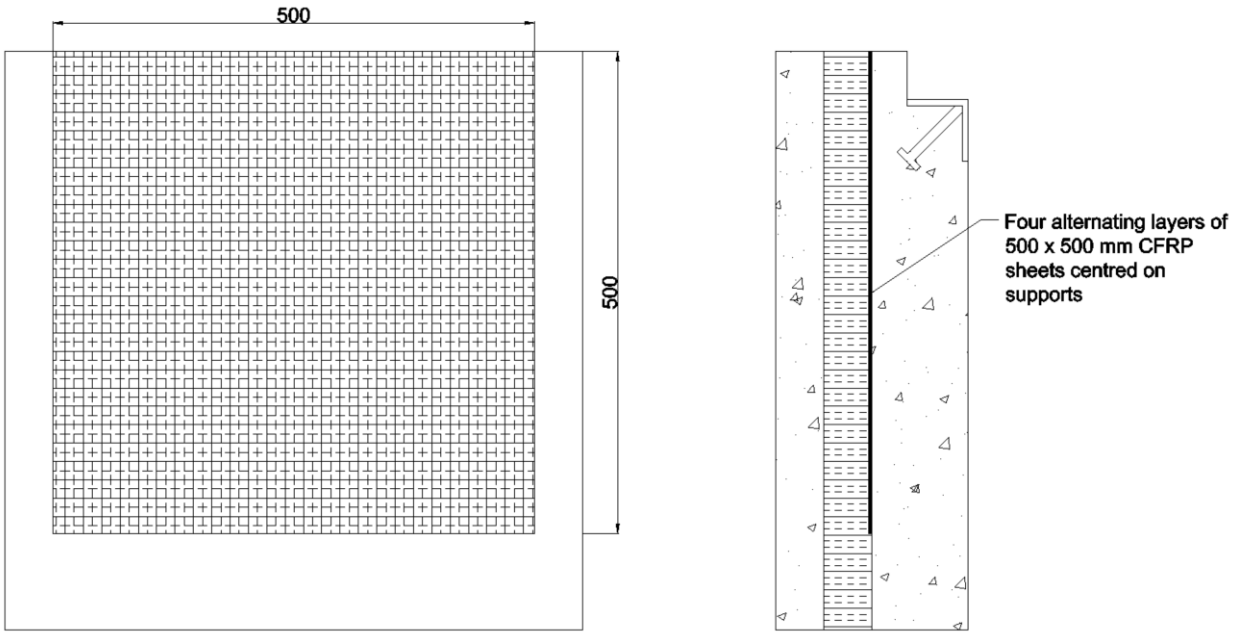

Figure 3.9 – FRP Support Retrofit Details for NCTS-R

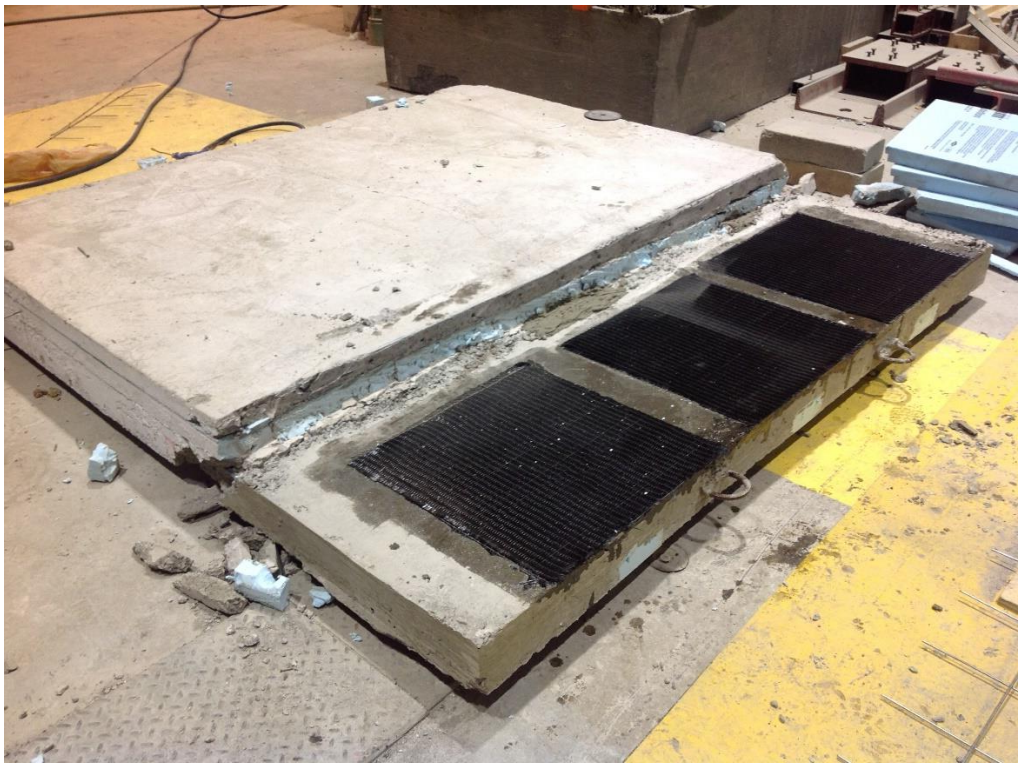

Figure 3.10 – FRP Support Retrofit Installed Prior to Casting of Architectural Face

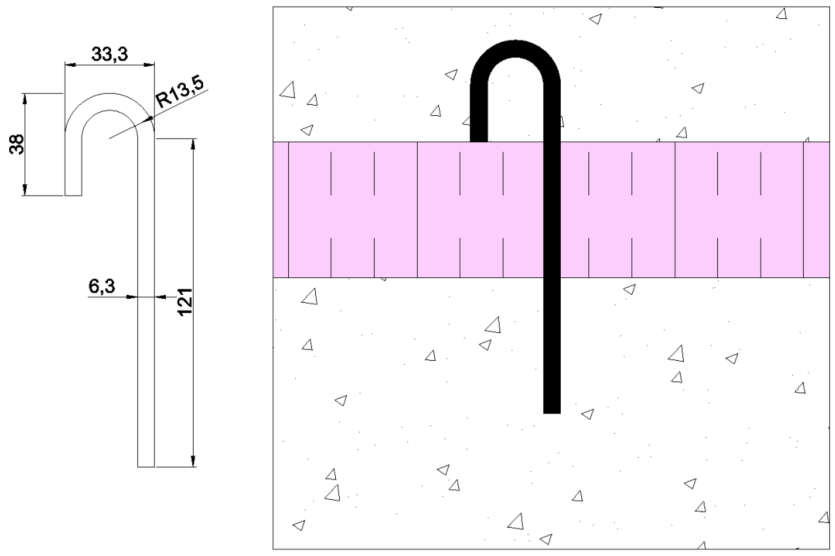

Figure 3.11 – Shear Tie Details and Installation Schematics for NCTS-R Repair

Figure 3.12 – Close-Up of Joist Seat (Upper Connection)

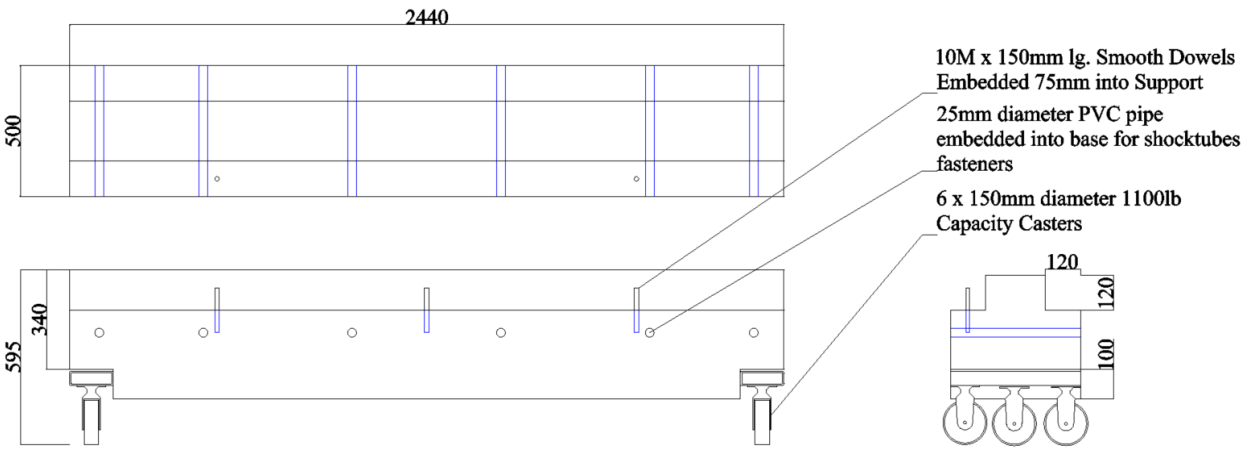

Figure 3.13 – Details and Schematics for Base Support

i) Construction of formwork and installation of reinforcement

ii) Completed base support with dowels and panel layout marking

iii) Complete installation of panel with base connected to shock tube

Figure 3.14 – Base Connection Overview

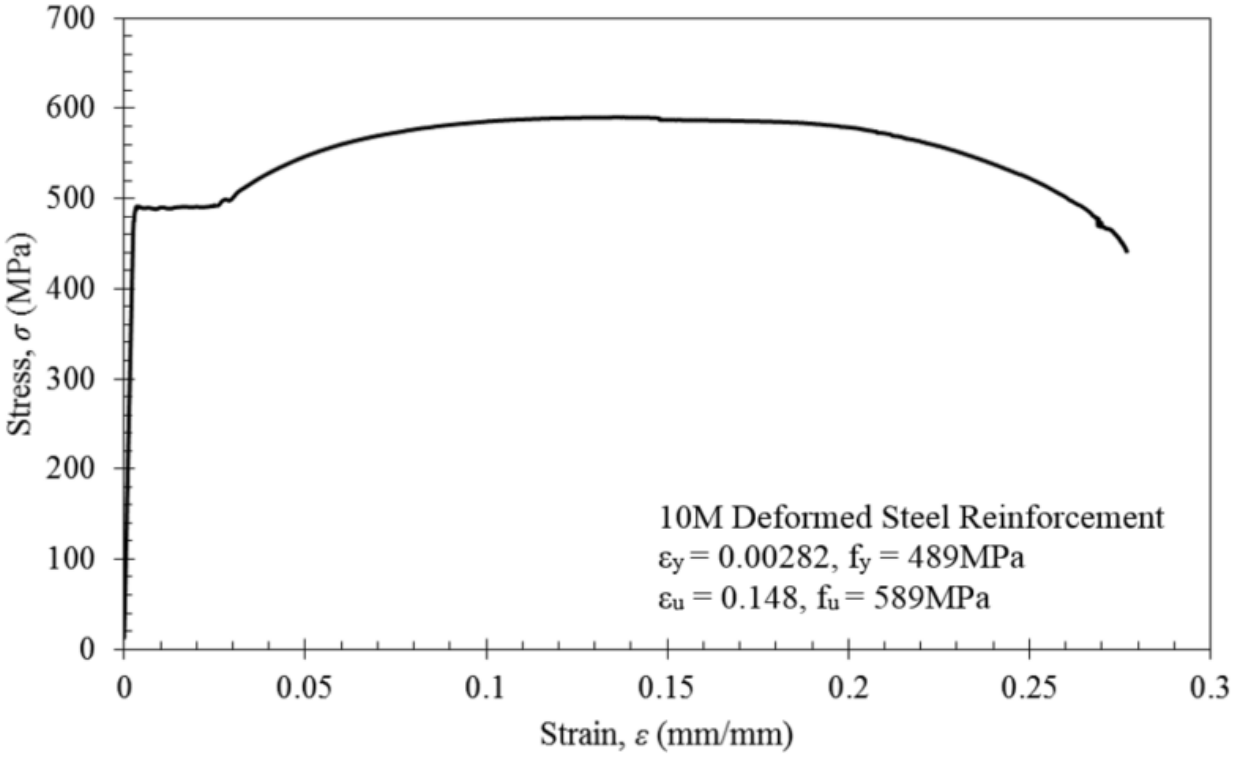

Figure 3.15 – Stress-Strain Relationship of Flexural Reinforcement

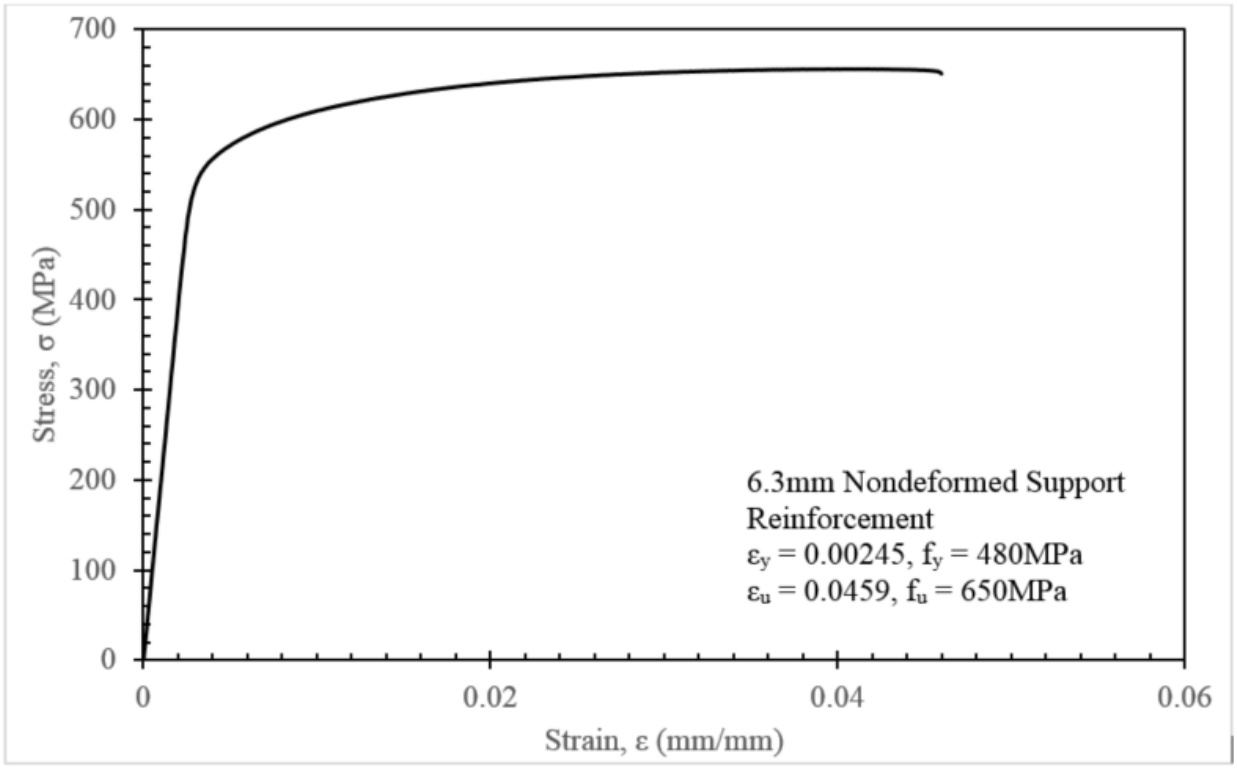

Figure 3.16 – Stress-Strain Relationship of Modified Support Reinforcement

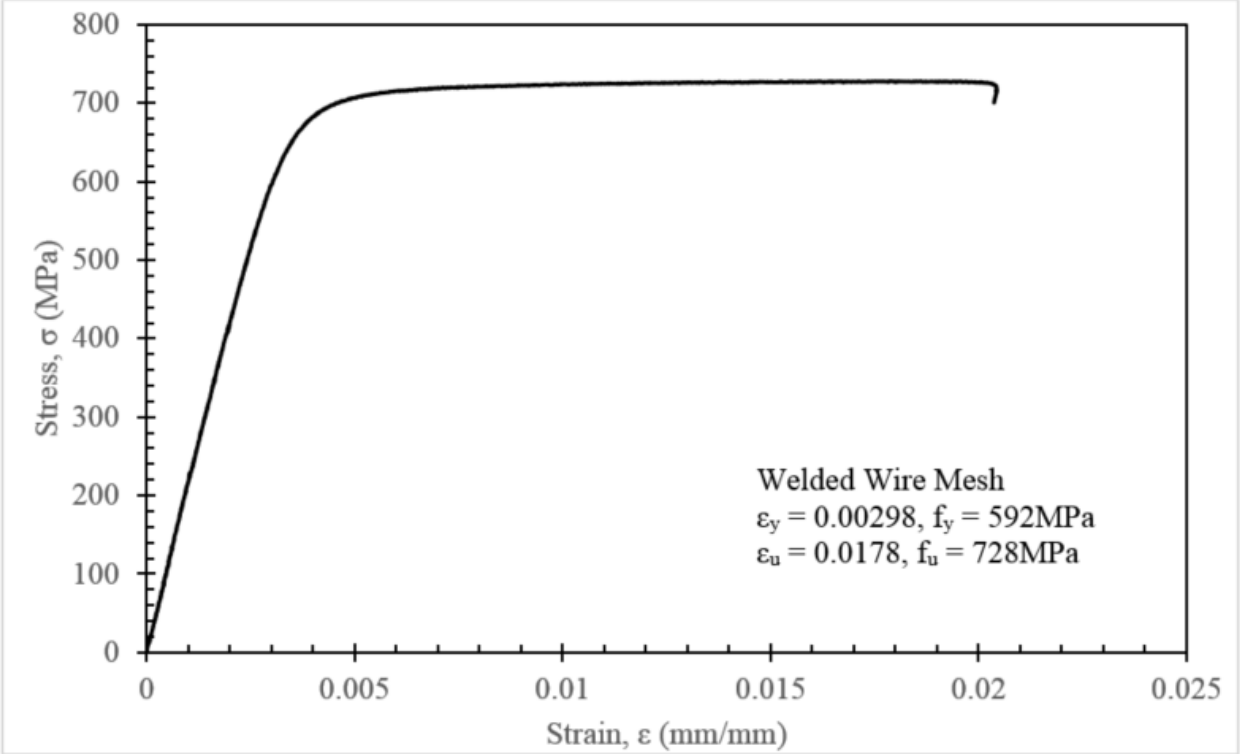

Figure 3.17 – Stress-Strain Relationship of Welded Wire Mesh Reinforcement

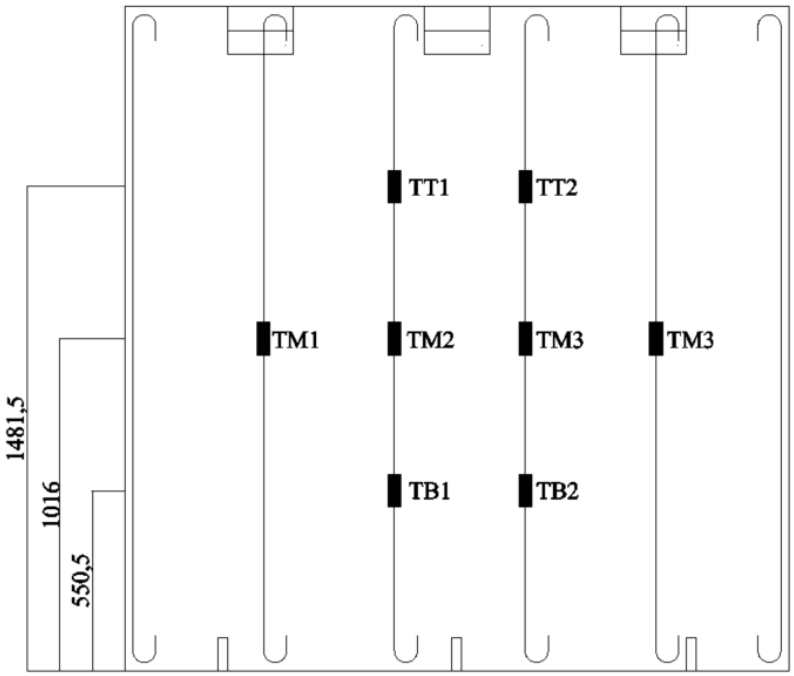

Figure 3.18 – Strain Gauges Locations on Tensile Flexural Reinforcement

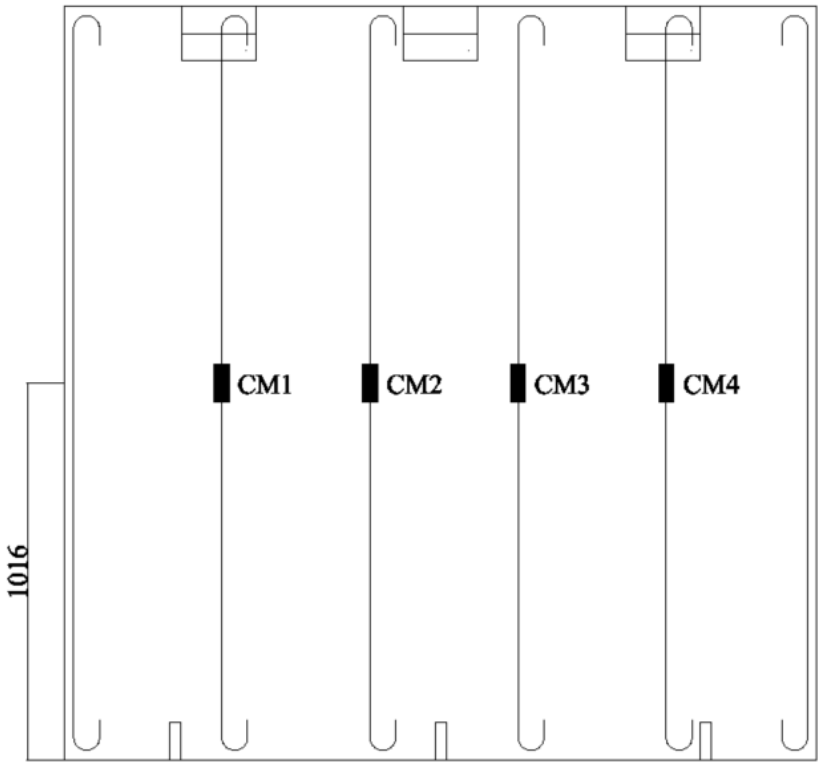

Figure 3.19 – Strain Gauge Locations on Compressive Flexural Reinforcement

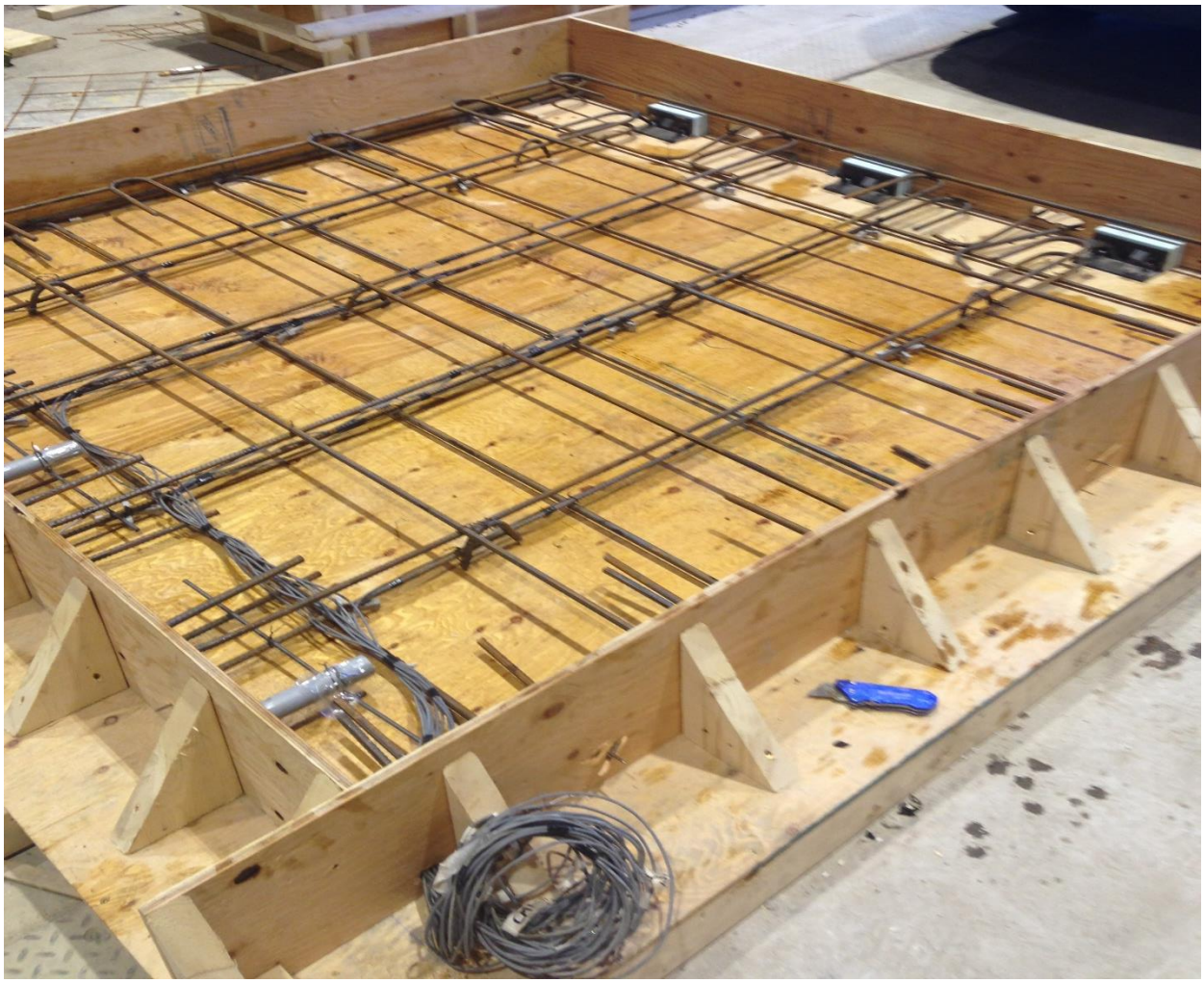

Figure 3.20 – Typical Reinforcement and Insert Layout

Figure 3.21 – Complete test Setup for Specimen SRC-1

Figure 3.22 – Typical Test Setup for Sandwich Panel Series

Figure 3.23 – Close-Up of Upper Support System

Figure 3.24 – Close-Up of Base Support System

4.0 Experimental Results

Five scaled reinforced concrete tilt-up panels were tested under simulated blast loads to determine and evaluate the applicability of current analysis procedures on concrete sandwich panels and the susceptibility of connections used in practice. Modifications, in the form of enhanced reinforcement details and the application of a surface bonded FRP retrofit, were applied to two of the specimens to enhance connection capacity and prevent catastrophic failure of the panel.

Each specimen was subjected to a series of shockwaves with increasing pressure-impulse combinations. The five specimens were split into two test series which followed distinct regiments. In the first series, SRC-1 and NCTS-1 were subjected gradually increased pressure-impulse combination, selected to induce a range of failure in the panel. This series allowed for a direct comparison between SRC and NCTS panels at various degrees of failure. In the second series, NCTS-2, NCTS-M, and NCTS-R were subjected to gradually increased pressure-impulse combinations, similar to those which induced failure in NCTS-1. This allow for a compare the effects of the damage induced by previous tests and to evaluate the panel and connection behaviour of undamaged specimens. The panels reactions to the shock wave were documented through internal strain readings, displacement measurements, and high speed video recordings.

Table 4.2 summarizes the average maximum elastic strain and the time to reach maximum elastic strain recorded during each test. Data is presented in terms of the average values for each strain gauge series (i.e. TB, TT, TM, and CM). Strain rates calculated from these results are also presented in the table. This data is presented for the sake of completeness and is not discussed further.

4.1 Discussion of Experimental Data

4.1.1 SRC-1 (Control Panel)

Specimen SRC-1 consists of a single *100mm* doubly reinforced concrete section. This panel was tested a total of five times with gradually increased driver pressure, driver length, or both. A detailed summary of the tests performed on SRC-1 is provided in Table 4.1

SRC-1: Test 1 – 16psi Driver Pressure

A peak reflected pressure of *18.2kPa* with a positive phase duration of *19.8ms* was recorded during Test 1 of SRC-1. A maximum mid-span displacement of *3.12mm* occurred at *17.8ms* with a residual displacement of *0.31mm*. The average strains recorded by the *TM* gauge series indicates a peak tensile strain at mid-span of *0.117%* at *19.6ms*. The *TT* and *TB* stain gauge series registered their greatest readings of *0.013%* and *0.008%* at *21.96ms* and *21.96ms*, respectively. Strain gauges *TM6* malfunctioned and were not used in the determination of average strain values.

Blast pressures induced minor flexural cracks at mid-span along transverse reinforcement. Low cover likely contributed to these effects. In addition to flexural damage, small hairline cracks developed along the interface of the embedded face plate of the joist seat and the panel. It is unlikely that this is indicative of internal damage but rather discontinuity in the materials. Figure 4.1 through Figure 4.7 show damage sustained by the panel during testing.

SRC-1: Test 2 – 30psi Driver Pressure

A peak reflected pressure of *39.6kPa* with a positive phase duration of *23.2ms* was recorded during Test 2 of SRC-1. A maximum mid-span displacement of *15.6mm* occurred at *25.6ms* with a residual displacement of 3.98*mm*. The average strain recorded by the *TM* gauge series indicated a peak tensile strain at mid-span of *0.312%* at 14.91*ms*. The greatest strain reading registered by the *TT* and *TB* series were *0.105%* and *0.064%* at 14.91*ms* and *14.91ms*, respectively. Strain gauges *TM6*, *TT1*, and *CM1* malfunctioned and were not used in the determination of average strain values.

The increased pressure generated in the second test caused a noticeable increase in damage to specimen SRC-1. Additional flexural cracking centralized around mid-span developed at locations with transverse reinforcement and low cover. Cracks observed on the side of the panel extended further toward the compressive face of the panel. The damage incurred by specimen SRC-1 is shown in Figure 4.1 through Figure 4.7.

SRC-1: Test 3 – 70psi Driver Pressure

A maximum reflected pressure of *70.6kPa* with a positive phase duration of *27.8ms* was recorded during Test 3 of SRC-1. A maximum mid-span displacement of *50.8mm* occurred at *32.4ms* with a residual displacement of 22.0*mm*. The average strains recorded by the *TM* gauge series indicated

a peak tensile strain at mid-span of *0.647%* at *20.0ms*. The greatest strain readings registered by the *TT* and *TB* series were *0.150%* and *0.156%* at *30.0ms* and *34.4ms*, respectively. Strain gauges TM6, *TB1*, and *CM1* malfunctioned and were not used in the determination of average strain values.

The third test of SRC-1 produced a considerable increase in damage causing existing crack to widen and propagate deeper into the panel in addition to the creation of more flexural cracks. As should be expected with larger pressures, new flexural cracks are more well-defined than in previous test.

Connections continue to appear unaffected by the applied load, experiencing no notable increase in damage. Figure 4.1 through Figure 4.7 show the damage sustained by specimen SRC-1 through the first three tests.

SRC-1: Test 4 – 100psi Driver Pressure

A maximum reflected pressure of *91.2kPa* with a positive phase duration of *25.0ms* was recorded during Test 4 of SRC-1. The panel which deformed about a plastic hinge developed a maximum mid-span displacement of *110.8mm* occurred at *43.4ms* with a residual displacement of *66.1mm*. This corresponds to a maximum and residual support rotation of approximately *13.4º* and *8.1º*, respectively. The maximum mid-span displacement exceeded the blowout limit of *10º* for double-reinforced members without shear reinforcement. The average strain reading recorded by the *TM* series indicated a maximum tensile strain at mid-span of *0.451%* at *28.4ms*. Data from the *TM* series is erratic compared to previous tests and should be considered with skepticism. The greatest strains registered by the *TT* and *TB* series were *0.428%* and *0.228%* at *19.4ms* and *19.6ms*, respectively. Strain gauges *TM1*, *TM6*, *TB2*, and *CM1* malfunctioned and were not used in the determination of average strain values.

The fourth test of specimen SRC-1 produced significant damage causing flexural crack to widen to the point where reinforcement was visible within the concrete. The compression face of the panel began to crush and concrete breakout was observed at locations of transverse reinforcement.

The connections appear unaffected by the applied loads, experiencing no notable increase in damage. However, when observing the test footage, there is visible rotation in the base support due to the incapability of the casters to sustain the rotational forces associated with high reflected

pressures. The lack of rotational rigidity in the base support could result in the potential loss of partial fixity that may be observed in practice. Rigid supports were installed to support the base and significantly reduce the potential for rotation.

SRC-1: Test 5 – 80psi Drive Pressure with 16ft Driver

Using an increased drive length generates similar reflected pressures to shorter driver but with an increased positive phase duration and corresponding impulse. While a longer driver produces positive phase durations which unrealistically represent large quantities of far explosives, the data collected can be extrapolated and applied to similar close range blast parameters above the capable threshold of the shock tube. Due to the large impulse associated with these driver properties, only one LVDT mounted at mid-span was used to minimize damage. While the specimen had exceeded the blowout limits outlined in CSA S850-12 [1], the panel was subjected to one additional test in an attempt to further evaluate support damage.

A maximum reflected pressure of *71.25kPa* with a positive phase duration of *47.2ms* was recorded during Test 5 of SRC-1. The panel which deformed about a plastic hinge developed a maximum mid-span displacement in excess of the LVDT's *258.5mm* stroke capacity at *40.4ms*. The residual displacement at mid-span was approximately *223.8mm*. These correspond to a maximum and residual support rotations of greater than *29.0º* and equal to *25.7º*, respectively. The average strains recorded by the *TM* gauge series indicated a maximum tensile strain at mid-span of *0.406%* at *40.2*. Strain data recorded in the *TM* series is erratic compared to previous tests. The greatest strains registered by the *TT* and *TB* series were *0.218%* and *0.223%,* at *47.8ms* and *38.2ms*, respectively. Strain gauges *TM1*, *TM6*, *TT1*, *CM1*, and CM2 malfunctioned and were not used in the determination of average strain values.

The fifth, and final, test of specimen SRC-1 resulted in flexural blowout of the panel with deeper crack propagation and concrete crushing rendering the panel incapable of sustaining any further loads.

Figure 4.2 shows the complete destruction of either side of the panel left tensile and compressive reinforcement completely exposed.

The recorded video provides evidence that shimming the base support prevented rotation observed in previous tests. This forced the panel to rotate independently of the base about the top corner of

the slab. The video also clearly shows the uplift of the panel from the base causing a complete separation of the panel from the grout infill. The dowels, however, effectively prevent any significant lateral movement. The upper connection remained intact with little to no concrete cracking while the I-beam supports warped slightly. Upon removal of the wall and the support beam it was observed that the top leg of the embedded angle rotated slightly away from the panel. This could be prevented by providing additional anchorage into the concrete from each leg of the angle, however this effect may be beneficial as it reduces stress in the concrete while allowing the panel to rotate.

Damage observed in the panel following testing is shown in Figure 4.1 through Figure 4.7.

4.1.2 NCTS-1: Sandwich Panel

Specimen NCTS-1 consisted of a *100mm* doubly reinforced structural wythe, a *50mm* layer of rigid insulation, and a *50mm* architectural wythe for an overall thickness of *200mm*. The panel followed a similar regimen as specimen SRC-1 and was tested a total of six times under gradually increasing driver pressures and/or driver lengths. A detailed summary of test parameters and detailed results are provided in Table 4.1.

.

NCTS-1: Test 1 – 16psi Driver Pressure with 8ft Driver

A peak reflected pressure of *20.6kPa* with a positive phase duration of *19.2ms* was recorded during Test 1 of NCTS-1. A maximum mid-span displacement of *1.49mm* occurred at *18.4ms* with a residual displacement of *0.411mm*. However, the maximum displacement likely occurs slightly above mid-span. This is evidenced by the difference in *LVDT-1* and *LVDT-3* which have maximum recorded displacements of *1.49mm* and *0.94mm*, respectively. Strain values recorded in test 1 were erratic and registered minimal values due to the low applied pressure.

The panel displayed no observable signs of damage.

NCTS-1: Test 2 – 30psi Driver Pressure

A peak reflected pressure of *39.49kPa* with a positive phase duration of *23.2ms* was recorded during Test 2 of NCTS-1. A maximum mid-span displacement of *3.90mm* occurred at *19.2ms* with a residual displacement of *1.05mm*. Similarly, to test 1 the differences in values recorded by *LVDT-*

1 and *LVDT-3*, indicate a maximum displacement between *LVDT-1* and *LVDT-2*. Strain values recorded in test 1 appear erratic and register minimal values, due to the low applied pressure.

The panel displayed no observable signs of damage.

NCTS-1: Test 3 – 70psi Driver Pressure with 8ft Driver

A peak reflected pressure of *72.3kPa* with a positive phase duration of *44.2ms* was recorded during Test 3 of NCTS-1. A maximum mid-span displacement of *12.0mm* occurred at *25.16ms* with a residual displacement of *3.46mm*. *LVDT-1* recorded similar displacements with a maximum and residual of *12.53mm* and *4.64mm*, respectively while *LVDT-2* recorded a much smaller maximum displacement of *6.18mm*. The average strains recorded by the *TM* gauge series indicate a maximum tensile strain at mid-span of *0.168%* at *23.0ms*. The greatest readings registered by the *TT* and *TB* series were *0.086%* and *0.014%* at *24.2ms* and *20.8ms*, respectively. Strain gauges *TM1* and *TM4* malfunctioned and were not used in the determination of average strain values.

Various signs of damage were visible in NCTS-1 following the third test. Flexural cracks developed at approximately *400mm* above mid-span following transverse reinforcement on the tensile face of the panel. Observation of the side of the panel revealed deeper cracks in the upper portion of the wall than at mid-span while there were no observable flexural cracks in the architectural wythe. Cracking was localized in the upper half of the panel, this combined with the distribution of recorded displacement data provide evidence of partial fixity in the base.

All three upper supports showed no notable signs of damage to the concrete, plate, I-beam, or weld. Cracks along the grout and panel interface formed in the base support due to the independent rotation of the panel. These cracks, shown in Figure 4.14, were visible on either end of the panel and did not propagate along the face of the panel.

Figure 4.8 through Figure 4.14 show the damage sustained by NCTS-1 following the third test.

NCTS-1: Test 4 – 100psi Driver Pressure with 8ft Driver

A peak reflected pressure of *88.1kPa* with a positive phase duration of *29.6ms* was recorded during Test 4 of NCTS-1. A maximum mid-span displacement of *25.2mm* occurred at *28.8ms* with a residual displacement of *10.1mm*. *LVDT-1* recorded similar displacements with a maximum and residual of *23.4mm* and *12.31mm*, respectively while *LVDT-2* recorded a much smaller maximum displacement of *12.1mm*. The average strains recorded by the *TM* gauge series indicated a

maximum tensile strain at mid-span of *0.198%* at *23.4ms*. The greatest strain values registered by the *TT* and *TB* series were *0.147%* and *0.022%* at *17.4ms* and *16.4ms*, respectively. Strain gauges *TM1* and *TM4* malfunctioned and were not used in the determination of average strain values.

Specimen NCTS-1 exhibited a considerable increase in flexural damage in both the structural and architectural face following the fourth test. Intermediate lateral cracks formed around and between the flexural cracks observed in Test 3. Cracks were clearly visible in the structural and architectural wythes from the side of the panel. Figure 4.9 clearly shows that the tensile cracks in the structural face do not propagate the entire depth prior to tensile cracking in the architectural wythe. This could indicate that the panel is not fully composite. As with observations made in previous tests LVDT, strain, and video data provide evidence of partial fixity at the base of the panel.

In addition to the widening of cracks observed in previous tests, a long crack formed between the grout and panel along the base support. Further to this the left side of the panel shows failure and breakout of a small portion of the grout infill. Cracks, propagating toward the edge of the panel from the bottom outside corner of the embedded joist seat, formed in Connections 1 and 3 during the test. Connections 1 and 3 also had minor concrete cracking at the back corner of the joist pockets. There was no observable damage to Connection 2.

Figure 4.8 through Figure 4.14 show the damage sustained by specimen NCTS-1.

NCTS-1: Test 5 – 80psi Driver Pressure with 16ft Driver

A peak reflected pressure of *78.8kPa* with a positive phase duration of *64.6ms* was recorded during Test 5 of NCTS-1. A maximum mid-span displacement of *45.6mm* occurred at *39.4ms* with a residual displacement of *23.6mm*. *LVDT-1* recorded similar displacements with a maximum and residual of *39.8mm* and *24.7mm*, respectively while *LVDT-3* recorded a much smaller maximum displacement of *22.1mm*. The average strains recorded by the *TM* gauge series indicate a maximum tensile strain at mid-span of *0.249%* at *34.3ms*. The greatest strain readings registered by the *TT* and *TB* series were *0.270%* and *0.047%* at *34.3ms* and *16.7ms*, respectively. Strain gauges *TM1* and *TM4* malfunctioned and were not used in the determination of average strain values.

Existing flexural cracks in the mid- to upper quarter-span region widened considerably, with the most defined cracks centralized at approximately *620mm* from the upper support. As Figure 4.9 indicates, cracks observable from the sides of the panel propagated deeper into the compressive

face of both the architectural and structural wythes of the panel. It is clearly visible in the high-speed video that the maximum displacement occurs between the upper and middle LVDTs. Further evidence is provided towards this through observation of strain gauge and LVDT data. This data is indicative of pin-fixed support conditions and is discussed further in Section 5.3.

No additional damage to the base connection was observed following the fifth test, while the upper connections displayed various signs of damage. Connection 1 showed a slight separation of the face plate from the panel as well as the formation of a crack propagating from the bottom corner of the face plate into the panel. Connection 3 displayed similar traits with cracks developing around the faceplate. Moreover, hairline cracks in the back corners of the joist pockets, observed following the fourth test, widened and propagated toward the compressive face of the structural panel. While Connection 2 did not show any signs of concrete damage, the weld at this support showed minor signs of rupturing.

Damaged sustain by the panel and its connections are shown in Figure 4.8 through Figure 4.14.

NCTS-1: Test 6 – 115psi Driver Pressure with 16ft Driver

Due to the high pressure and impulse associated with these driver properties *LVDT-2* and *LVDT-3* were removed from the panel to reduce damage to the units.

A peak reflected pressure of *96.1kPa* with a positive phase duration of *58.2ms* was recorded during Test 6 of NCTS-1. Connection failure caused the panel to blowout almost instantaneously. As a result, LVDT and strain data should be regarded unusable.

show the panel failure plane and the remaining pieces of Connections 1, 2, and 3. It can be seen that the embedded angles of Connections 1 and 3 remained attached to the support while Connection 2 did not. This can be attributed the failure modes of the connections. Connection 1 and 3 experienced a brittle concrete failure, with a failure plane propagating away from the joist pocket at approximately *35 degrees*, similar to punching shear. Connection 2 also shares similar traits with the other connection but with a much smaller concrete failure plane and the clear failure of the weld. While it is impossible to confirm which connection initially failed it can be concluded that the weld was the first portion of Connection 2 to fail. Following failure of the weld, the impact of the I-beam support on the concrete at the back of the joist pocket caused it to fail in shear. Figure 4.10 through Figure 4.14 illustrate the concrete failure plane of the three connections, failure of

the architectural face at *180* to *320mm* from the top of the panel, pullout failure of grout and dowels from the base connection, and severe bending of the dowels.

Figure 4.8 through Figure 4.14 illustrate the catastrophic damage sustained by the panel and connections at the conclusion of testing.

4.1.3 NCTS-2: Sandwich Panel

Specimen NCTS-2 was designed with connection details, reinforcement layout, wythe thicknesses, and concrete properties identical to specimen NCTS-1. Table 3.1 outlines the actual wythe thicknesses of the specimens which vary slightly as a result of construction error. NCTS-2 was tested with gradually increased pressures similar to the failure pressures found in previous tests. Due to the failure mode of specimen NCTS-1 a single LVDT was installed at mid-span to avoid potentially destroying the unit. At higher test pressures the LVDT was removed and a ruled bracket was mounted to the shock tube. This enables the approximation of maximum deflections using footage recorded by the high speed camera. A detailed summary of the tests performed on specimen NCTS-2 is provided in Table 4.1.

NCTS-2: Test 1 – 70psi Driver Pressure with 16ft Driver

A peak reflected pressure of *72.4kPa* with a positive phase duration of *57.9ms* was recorded during Test 1 of NCTS-2. The maximum mid-span displacement of *25.5mm* occurred at *44.8ms* and resulted in a residual displacement of *7.51mm*. The average strains recorded by the *TM* gauge series indicated a maximum tensile strain at mid-span of *0.146%* at *21.9ms*. The greatest strain reading registered by the *TT* and *TB* series were *0.091%* and *0.026%* at *29.3ms* and *22.5ms*, respectively. The initial test performed on Specimen NCTS-2 instigated weld failure in two of the three top connections and considerable deformation of the I-beam support in the third. Therefore, LVDT and strain data collected during this test is inaccurate.

Weld failure did not result in complete panel failure with damage localized to the upper supports alone. Several flexural cracks formed in the panel at and *400mm* above mid-span, locations with transverse reinforcement and a low cover. As is evidenced through observation of the video, the failure of the weld appears to occur first with flexing of the panel beginning only after the top of the panel has stopped moving. This is likely due to the I-beam support's impact with the back of the joist pocket.

The damage sustained by the panel and connections during this test are shown in Figure 4.15 through Figure 4.21.

To evaluate the magnitude of the damage sustained at the supports the panel was removed from the shock tube and the top *100mm* of the architectural wythe and insulation was removed. NCTS-2 was repaired after the initial test to mitigate the effects of premature damage which clearly propagated into the expected failure plane of the connections. The repair implemented to mitigate the reduction of strength around the connections involved:

- Removing all remaining concrete within the cracked portion of the panel to accommodate the recasting the damaged area,
- Constructing formwork to contain the damaged portion of the joist seat,
- Cleaning the damaged surface of the concrete with compressed air to eliminate any concrete and dust particles,
- Preparing the surface by applying KING Concrete Adhesive to increase the bond between new and existing concrete,
- Mixing and casting King MS-S10 Self Consolidating Concrete with partial water content replaced with KING Concrete Adhesive to enhance bonding,
- Curing of the concrete and removing formwork,
- Installing new insulation to portion the portion previously removed, and
- Repeating the second through sixth step for the concrete removed from the architectural wythe.

Figure 4.21 outlines the reparation procedure described above.

NCTS-2: Test 2 – 105psi Driver Pressure with 16ft Driver

LVDTs were removed due to the catastrophic failure experienced in Specimen NCTS-1 when subjected to shockwaves generated from similar shock tube parameters. A ruled bracket installed on the shock tube at mid-span allows the approximate determination of displacement using high speed video footage.

A peak reflected pressure of *91.05kPa* with a positive phase duration of *56.8ms* was recorded during Test 2 of NCTS-2. The maximum mid-span displacement sustained by the panel was approximately *52.8mm* with a residual displacement of *10mm*. However, the largest residual displacement of *13mm* was located *200mm* above mid-span. The average strains recorded by the *TM* gauge series recorded a peak tensile strain at mid-span of *1.13%* at *19.8ms*. The *TT* and *TB* series registered their greatest strain values of *0.905%* and *0.144%* at *15.8ms* and *22.8ms*, respectively. Strain gauges *TM1*, *TM2*, and *TM4* malfunctioned and were not used in the determination of average strain values.

Flexural cracks developed in the upper half of the panel, with a single yield crack approximately *400mm* below mid-span. The formation pattern of flexural cracks in the architectural and structural wythes indicate partial composite action within the panel. NCTS-2 also suffered significant movement between the architectural and structural wythes as a consequence of the large shear forces during flexing of the panel. This shear slippage is evidenced in Figure 4.17 which shows typical connection damage at the conclusion of testing.

Notable damage, similar to specimen NCTS-1, developed around the upper connections. Each connection experienced minor separation of the face plate from the concrete with hairline cracks extending from the bottom corners of the plate. Cracks propagating at 35 *degrees* could be observed in all connections, however, the repaired portions of Connections 1 and 3 make the cracks more difficult to distinguish. Cracks following the grout-panel interface in the base connection developed for the on the sides of the panel implying the panel rotated independently of the base.

Figure 4.15 through Figure 4.21 show the extent of damage suffered by the NCTS-2.

NCTS-2: Test 3 – 105psi Driver Pressure with 16ft Driver

A third test was performed on this panel in an attempt to induce failure by using a higher driver pressure. Due to a leak in the shock tube and this risk associated with draining it at such a high pressure, the test was carried out with a driver pressure of *105psi*. A peak reflected pressure of *88.6kPa* with a positive phase duration of *63.1ms* was recorded during Test 3 of NCTS-2. The maximum mid-span displacement sustained by the panel was approximately *77mm* with a residual displacement of *32mm*. This corresponds to maximum and residual support rotations of *13.6º* and *3.9º*, respectively. The largest residual displacement of *39mm* was located at *211mm* above mid-span. The average strains recorded by the *TM* gauge series indicate a peak tensile strain at mid-

span of *0.693%* at *38.9ms*. The *TT* and *TB* series registered their largest strains of *0.514%* and *0.134%* at *30.1ms* and *38.9ms*, respectively. Strain gauges *TM2* and *TM4* malfunctioned and were not used in the determination of average strain values.

At the conclusion of testing specimen NCTS-2 suffered appreciable amounts of damage with flexural cracking centralized around the mid- to upper quarter-span of the panel extending through the entire depth of the structural and architectural wythes. The location of residual deformed shape of the panel and the concentration of flexural cracks the maximum moment appears to occur at approximately *200mm* above mid-span.

Cracks in the panel-grout interface at the base connection widened with a crack forming along the face of the panel where it connects to the base. The face-plate separation in Connection 1 further increased to approximately *3-4mm*. Cracks propagating at 35 *degrees* could be observed in all connections, however, the repaired portions of Connections 1 and 3 make the cracks more difficult to distinguish. Similar face plate separation of lesser severity was noticeable in Connection 2. Connection 2, shown in Figure 4.17, incurred serious damage with a complete breakoff of the back and exposure of the rebar. There was no further notable damage to Connection 2, nor was there observable signs of damage to the welds in any of the upper connections.

While the connections remained intact and residual deflection is less than prescribed failure criteria, testing of the specimen was stopped due to the combination of damage to the specimen, damage to the connections, and decrease in strength due to excessive testing.

Figure 4.15 through Figure 4.21 outline the damage incurred by the panel at the conclusion of testing.

4.1.4 NCTS-M: Sandwich Panel with Modified Connection Reinforcement

NCTS-M consisted of a *100mm* doubly reinforced structural wythe, a *50mm* layer of rigid insulation, and a *50mm* architectural wythe for an overall thickness of *200mm*. Reinforcement modifications designed to capture and control crack propagation in the upper connections were installed to prevent failure. The test regimen was very similar to that used for NCTS-2, with gradually increasing driver pressures. A detailed outline of test parameters is provided in Table 4.1.

NCTS-M: Test 1 – 70psi Driver Pressure with 16ft Driver

A peak reflected pressure of *73.9kPa* with a positive phase duration of *62.0ms* was recorded during Test 1 of NCTS-M. A maximum mid-span displacement of *13.4mm* occurred at *25.6ms* with a residual displacement of *1.98mm*. *LVDT-1* recorded similar data with a maximum displacement of *13.7mm* at *25.6ms*, and a residual displacement of *1.96mm*. The average strains recorded by the *TM* gauge series indicated a peak tensile strain at mid-span of *0.266%* at *21.5ms*. The *TT* and *TB* series registered largest strain readings of *0.374%* and *0.144%*, at *22.3ms* and *17.5ms*, respectively. Strain gauge *CM2* malfunctioned and was not used in the determination of average strain values.

Flexural cracks developed across the entire panel with an apparent focal point of approximately *400mm* above mid-span. A vertical hairline crack formed between Connections 1 and 2, however this is likely due to the reduced cover produced by the bent reinforcement at this location. Minor cracks in the architectural wythe were visible from the side of the panel.

The cracks, shown in Figure 4.27, propagating at approximately *50* to *30 degrees* from the back corners of the joist pockets developed in Connections 2 and 3 during the first test. Signs of face plate separation were also visible in Connections 2 and 3. There was no notable damage to the base supports.

The damage incurred by the panel during test 1 are outlined in Figure 4.22 through Figure 4.29.

NCTS-M: Test 2 – 115psi Driver Pressure with 16ft Driver

A peak reflected pressure of *98.0kPa* with a positive phase duration of *56.2ms* was recorded during Test 2 of NCTS-M. A maximum mid-span displacement of 68.5*mm* occurred at *46.5ms* with a residual displacement of *37.5mm*. *LVDT-1* recorded similar data with a maximum displacement of *58.8mm* at *45.3ms*, and a residual displacement of *34.0mm*. The average strains recorded by the *TM* gauge series recorded a peak tensile strain at mid-span of *1.76%* at *29.0ms*. The *TT* and *TB* series registered their greatest strain readings of *0.403%* and *0.134%*, at *39.0ms* and *39.0ms*, respectively. Stain gauges *TM1*, *TM2*, *TM4*, *TT2*, and *CM2* malfunctioned and were not used in the determination of average strain values.

Specimen NCTS-M experienced a considerable increase of damage provoking the formation of intermediate flexural cracks centralized at *400mm* above mid-span. Cracks developed in the architectural wythe while existing cracks in the structural wythe propagated deeper into the panel.

Significant shear slippage between the architectural and structural wythes is visible along the top of the panel.

Shear cracks developed near in the back of the joist pockets in Connection-1. There is no visible damage to the welds. Rotation of the panel caused cracking between the panel and the base support.

Photos of the damage sustained by specimen NCTS-M through the second the series of testing are shown in Figure 4.22 through Figure 4.29.

NCTS-M: Test 3 – 105psi Driver Pressure with 16ft Driver

A third test was performed on this panel in an attempt to induce failure by using a higher driver pressure. Due to a leak in the shock tube and this risk associated with draining it at such a high pressure, the test was carried out with a driver pressure of *105psi*. A peak reflected pressure of *71.3kPa* with a positive phase duration of *49ms* was recorded during Test 3 of NCTS-M. *LVDT-2* and *LVDT-3* were removed from the panel to prevent any loss of equipment in case of failure. *LVDT-1* recorded a maximum displacement of *72.5mm* at *34.9ms*, and a residual displacement of *45.65mm*. The average strains recorded by the *TM* gauges' series indicated a peak tensile strain at mid-span of *0.430%* at *23.4ms*. The *TT* and *TB* series registered their greatest strain reading of *0.336%* and *0.106%*, at *28.1ms* and *34.5ms*, respectively. Strain gauges *TM2*, *TM4*, *TM6*, and *CM2* malfunctioned and were not used in the determination of average strain values.

Specimen NCTS-M experienced an extensive increase in damage during the third test including the development of cracks on the side of the panel and the widening of existing cracks. The most severe cracks were localized between *250mm* and *450mm* above mid-span. Cracks in the architectural wythe propagated deeper into the compressive face and insulation split in several locations. The shear slippage between the structural and architectural wythes, shown in Figure 4.27, varied between *15* and *20mm* along the top of the panel.

In addition to the formation of a crack along the face of the panel rotation of about the base support caused existing to crack to widen. Cracks in the upper connections widened slightly with no additional visible damage. The modified connections performed significantly better than those installed in NCTS-1 and NCTS-2, showing significantly lower signs of damage.

Figure 4.22 through Figure 4.29 show the damage sustained by specimen NCTS-M at the conclusion of testing

4.1.5 NCTS-R: Repaired Sandwich Panel with FRP Retrofit

Specimen NCTS-R is a *200mm* thick sandwich panel consisting of a *100mm* thick structural wythe, *50mm* thick insulation layer, and a *50mm* thick architectural wythe reconstructed from the lower half of NCTS-1. NCTS-R was subjected to gradually increasing blast pressures at a constant driver length. A detailed summary of test parameters is provided in Table 4.1.

NCTS-R: Test 1 – 70psi Driver Pressure with 16ft Driver

A peak reflected pressure of *74.9kPa* with a positive phase duration of *57.1ms* was recorded during Test 1 of NCTS-R. A maximum mid-span displacement of *39.8mm* occurred at *44.5ms* with a residual displacement of *14.2mm*. *LVDT-1* recorded similar data with a maximum displacement of *34.75mm* at *46.5ms,* and a residual displacement of *15.5mm*. The average strains recorded by the *TM* gauge series indicated a peak tensile strain at mid-span of *0.304%* at *34.3ms*. The *TT* and *TB* series registered their greatest strain readings of *0.215%* and *0.162%,* at *34.7ms* and *22.9ms*, respectively. Strain gauges *TM1*, *TM2*, and *CM2* malfunctioned and were not used in the determination of average strain values. Furthermore, strain gauges from specimen P-2 were reused and overall strain readings may be inaccurate though strain distribution data can still be used.

Specimen NCTS-R experienced extensive flexural cracking localized about the repair joint. Figure 4.32 illustrates the cover cracks running vertically along the side of the repaired portion of the panel. Flexural cracks in the architectural wythe of the panel appear to extend through the entire repaired section. Existing cracks in the lower portion of the wall widened slightly following the test.

There is no notable damage to the upper or lower connections.

Photos outlining the damage sustained by the panel and connections following the first test are provided in Figure 4.31 through Figure 4.36.

NCTS-R: Test 2 - 105psi Driver Pressure with 16ft Driver

A peak reflected pressure of *99.5kPa* with a positive phase duration of *57.9ms* was recorded during Test 2 of NCTS-R. A maximum mid-span displacement of *124mm* occurred at *62.6ms* with a residual displacement of *97.1mm*. *LVDT-1* recorded similar data with a maximum displacement of *122.0mm* at *62.7ms,* and a residual displacement of *102.9mm*. The average strains recorded by the *TM* gauge series indicated a peak tensile strain at mid-span of *0.355%* at *25.4ms*. The *TT* and *TB*

series registered their greatest strain readings of *0.178%* and *0.201%*, at *29.7ms* and *30.4ms*, respectively. Strain gauges *TM1*, *TM4*, and *CM2* malfunctioned and were not used in the determination of average strain values. Furthermore, strain gauges from specimen NCTS-1 were reused and overall strain readings may be inaccurate though strain distribution data can still be used.

Specimen NCTS-R suffered a flexural failure at the repair joint during the second test. Extensive cracking occurred at the repair interface with little damage to the rest of the panel. Transverse and longitudinal reinforcement was visible on the tensile face of the panel as crack widths increased considerably. The architectural wythe suffered severe concrete crushing and cracking through the entire section at *400mm* above mid-span.

Cracks developed along the entire perimeter of the grout/panel interface as the panel rotated independently of the base. There was no visible damage to the concrete or welds in the upper connections, however the I-beam support in all three connections warped under the compressive loads in flexure.

The damage observed in specimen NCTS-R following the second test are provided in Figure 4.31 through Figure 4.36.

4.2 Comparison of Experimental Results

In total, five scaled reinforced concrete tilt-up panels with realistic connections were tested under a series of simulated shockwaves with incrementally increasing pressures-impulses combination. Tests were conducted at the shock tube facility in the Structural Engineering Research Laboratory at the University of Ottawa. Four of the five panels tested were designed as non-composite tilt-up sandwich panels consisting of a *100mm* structural wythe, a *50mm* layer of insulation, and a *50mm* architectural wythe. The control panel consisted only of a single *100mm* structural wythe. To ensure comparability of data, specimens followed similar test regimens with comparable driver pressures and length combinations. Design details and a description of all five test specimen is provided in Section 4.1.

Panels SRC-1 and NCTS-1 were subjected to gradually increased driver pressures until failure to evaluate and compare panel properties. SRC-1 was tested a total of five times with pressure-

impulse combinations similar to the first five tests conducted on NCTS-1. A sixth test was performed on NCTS-1 due the limited amount of damage observed following the fifth shot. Alternatively, specimens NCTS-2, NCTS-M, and NCTS-R were tested using driver pressures similar to those which induced failure in the first two specimens. The first and second shots on NCTS-2, NCTS-M, and NCTS-R were analogous with the fifth and sixth shots performed on NCTS-1. Figure B.1 through Figure B.7 illustrate the ability to reproduce blast parameters (i.e. reflected pressure and impulse) for similar driver pressures and lengths.

Observing the displacement-time histories presented in Figure A.5 through Figure A.9, clearly indicates an increased blast resistance in sandwich panels compared to the control specimen. This increased capacity can be attributed to several properties:

a) Added mass provided by the architectural wythe. This directly reduces the effects of shockwaves due to an increase in the inertial force of the panel.

b) Composite behaviour within the panel produces a significant increase in the blast resistance and overall structural capacity of the panel.

c) Panels that do not achieve composite behaviour would still experience an increase in structural capacity caused by the flexural strength of the architectural face.

These factors are not currently incorporated into the design of non-composite sandwich panels and the applied loads are assumed to be resisted by the structural wythe alone. Consequentially the design of connections does not incorporate the additional flexural capacity provided by non-composite action. So while sandwich panels capably sustain larger blast loads, connection design does not currently accommodate these increased pressures.

Rotation in the base support during testing of the control panel SRC-1, provoked a potential reduction in fixity untrue to realistic conditions. The based support was shimmed in subsequent tests to eliminate the transfer of rotational forces to the casters and ultimately prevent this rotation. As a result, experimental strain and displacement data as well as crack patterns indicated fixed-pinned support conditions. These conditions better reflected actual field conditions and allowed the development of partial fixity in the base support. Discrepancy arises from the comparison of the failure behaviour of the control panel and the sandwich panels. All specimens experienced similar damage to the base support excluding NCTS-1, which as a result of upper support failure

lifted off of the base support and collapsed as shown in Figure 4.10. Failure criteria varied considerably. Specimen SRC-1 failed strictly in flexure with little or no damage to the upper connections while NCTS-1 suffered a catastrophically brittle connection failure with little flexural damage. Similarly, specimen NCTS-2 sustained significant damage at the upper connections with little residual flexural displacement.

Specimens NCTS-1, NCTS-2, and NCTS-M suffered similar flexural damage, crack patterns, and highly comparable strain and displacement distributions. The upper quarter- to mid-span displacement ratio varied by less than *2%,* indicating partial fixity in the base connection. The displacement-time histories of the NCTS panels, plotted in Figure A.10 to Figure A.12, reveal substantial inconsistencies in panel response to similar blast loads. The large mid-span displacements suffered by NCTS-1 can be attributed to reduced resistance caused by consecutively testing the specimen. The failure plane observed in NCTS-1 is reminiscent of punching shear failure typically found in elevated slabs. Prior to failure, specimen NCTS-1 sustained a maximum mid-span displacement of only *45.6mm*, which corresponds to an approximate support rotation of relatively *5.5º*.

NCTS-2 suffered premature weld failure in two of the upper supports during the first shot. This can be seen in the panel response plotted in Figure A.10. Initially the response of the panel is very similar to NCTS-M, but as weld failure occurs the displacement of the panel increases significantly. This can be seen in the inflection point of the response at approximately *25ms*. Although specimen NCTS-2 did not fail, damage around the upper connections was comparable with NCTS-1. Cracks propagating at approximately *35º*, toward the compressive face of the wythe developed and widened considerably in the back corners of the support pockets.

The modified connection reinforcement in specimen NCTS-M significantly reduced damage by effectively capturing and controlling these cracks, preventing them from expanding as they did in NCTS-1 and NCTS-2. While mid-span displacement and support rotation properties of NCTS-M are analogous with previous specimens, damage in the upper connections was notably less at the conclusion of testing. Providing reinforcement cages in the upper connections reduces damage and prevents premature failure of the panel.

The application of FRP sheets on the compressive face of the structural wythe is a viable retrofit solution to increase the blast resistance of sandwich panels. Previous research indicates that the

application of FRP strips spanning the failure plane can reduce the potential of punching shear failure. Unfortunately, due to the reduced strength at the repair interface, NCTS-R failed in flexure prior to developing significant stresses in the upper connections. As a result, it is impossible to conclude if the FRP retrofit was a success based on experimental data. Unlike previous tests performed on sandwich panels, NCTS-R suffered considerable plastic deformation about the repair joint *400mm* above mid-span. A maximum mid-span displacement of *122mm* with a corresponding support rotation of *14.7º* was registered at *62.6ms*.

It was also found that for most tests the I-beam, which represented an open web steel joist framing into the section, buckled as the panel rotated. This could have been alleviated by using a thicker stiffer section, however due to spatial limitations this was not possible. Also, it was deemed to be acceptable, as similar bending or damage would likely be found in practice as the open web steel joist bent to accommodate panel rotation.

Table 4.1 – Shock Tube Test Parameters, Resulting Shockwave Properties, and Test Result Summary

Specimen	*Driver Pressure* P_D *kPa*	*Driver Length* L_D *mm*	*Peak Reflected Pressure* P_r *kPa*	*Positive Phase Duration* t_d^+ *ms*	*Peak Reflected Impulse* I_r *kPa-ms*	*Peak Mid-Span Displacement (LVDT-2)* δ_{mid} *Mm*	*Peak Upper Quarter-Span Displacement LVDT-1* δ_{upper} *mm*	*Maximum Upper Support Rotation* θ_{max} *Degrees*	*Residual Mid-Span Displacement* δ_{max} *mm*
SRC-1: 1	103	2438	18.2	19.8	181.9	3.12	1.68	0.385	0.309
SRC-1: 2	207	2438	39.6	23.2	405.7	15.6	8.51	1.95	3.98
SRC-1: 3	482	2438	70.6	27.8	781.2	50.8	24.1	5.51	22.96
SRC-1: 4	689	2438	91.3	25.0	1038.4	110.8	46.1	10.45	66.06
SRC-1: 5	551	4879	71.2	47.2	1376.4	>258.5	-	>15.52	223.8
NCTS-1: 1	103	2438	20.6	19.2	191.6	1.49	1.79	0.25	0.412
NCTS-1: 2	207	2438	39.5	23.2	403.2	3.90	5.14	0.91	1.05
NCTS-1: 3	482	2438	72.6	44.2	973.3	12.0	12.5	1.72	3.46
NCTS-1: 4	689	2438	88.1	29.6	1079.8	25.2	23.4	3.23	10.12
NCTS-1: 5	551	4879	78.8	64.6	1859.2	45.6	39.8	5.5	23.64
NCTS-1: 6[*]	689	4879	96.1	58.2	2365.9	-	-	-	-
NCTS-2 1	482	4879	72.4	57.9	1590.1	25.5	-	2.75	7.51
NCTS-2 2	723	4879	91.0	56.8	2343.1	~52.8[**]	-	~5.68	10
NCTS-2 3	720[***]	4879	88.6	63.1	2254.4	~85[**]	-	~9.09	32
NCTS-M: 1	482	4879	73.9	62.0	1759.1	13.4	13.7	1.68	1.98
NCTS-M: 2	792	4879	98.0	56.2	2410.4	68.5	58.8	7.21	37.5
NCTS-M: 3	551	4879	71.3	49	1596.2	-	72.5	8.86	45.6[****]
NCTS-R: 1	482	4879	74.9[*****]	57.1	1687.0	39.8	34.8	4.28	14.2
NCTS-R: 2	723	4879	99.5[*****]	57.9	2271.3	124.8	122.0	14.7	97.1

[*] Test caused connection failure at upper support resulting in the complete blowout of the panel.
[**] Based on visual observation of video data using a ruled bracket mounted to the shock tube.
[***] A leak in the shock tube's driver section resulted in lower test pressure than desired.
[****] Residual displacement recorded in LVDT-1.
[*****] Only pressure reading from the side gauge were used in the determination of the pressure-time relationship.

Table 4.2 – Experimental Strain Data

Specimen	*Test*	*Lower Quarter-Span Tensile Reinforcement*			*Mid-Span Tensile Reinforcement*			*Upper Quarter-Span Tensile Reinforcement*			*Mid-Span Compressive Reinforcement*		
		Time t_E *(ms)*	*Strain* ε_s *(%)*	*Strain Rate* ε_s' *(%/ms)*	*Time* t_E *(ms)*	*Strain* ε_s *(%)*	*Strain Rate* ε_s' *(%/ms)*	*Time* t_E *(ms)*	*Strain* ε_s *(%)*	*Strain Rate* ε_s' *(%/ms)*	*Time* t_E *(ms)*	*Strain* ε_s *(%)*	*Strain Rate* ε_s' *(%/ms)*
SRC-1	1	22.0	0.008	0.0004	19.6	0.117	0.0060	22.0	0.01300	0.0006	22.0	0.035	0.0016
	2	14.9	0.064	0.0043	14.9	0.313	0.0210	14.9	0.10500	0.0070	14.9	0.177	0.0119
	3	34.4	0.156	0.0045	11.8	0.285	0.0242	30.0	0.15000	0.0050	31.6	0.240	0.0076
	4	19.6	0.228	0.0116	24.8	0.286	0.0115	12.6	0.284	0.0225	26.2	0.261	0.0100
	5	38.2	0.223	0.0058	37.6	0.281	0.0075	47.8	0.21800	0.0046	49.8	0.175	0.0035
NCTS-1	3	20.8	0.014	0.0007	23.0	0.169	0.0074	24.2	0.08600	0.0036	22.8	0.138	0.0061
	4	16.4	0.022	0.0013	23.4	0.198	0.0085	17.4	0.14700	0.0085	28.0	0.119	0.0043
	5	16.7	0.047	0.0028	34.3	0.249	0.0073	34.3	0.27000	0.0079	43.1	0.177	0.0041
NCTS-2	1	22.5	0.026	0.0012	21.9	0.146	0.0067	29.3	0.09100	0.0031	22.4	0.096	0.0043
	2	22.8	0.144	0.0063	8.65	0.433	0.0501	8.65	0.368	0.0425	39.2	0.278	0.0071
	3	38.9	0.134	0.0034	13.27	0.281	0.0212	8.97	0.28	0.0312	30.1	0.219	0.0073
NCTS-M	1	17.5	0.144	0.0082	21.5	0.266	0.0124	14.57	0.281	0.0193	13.8	1.231	0.0894
	2	39.0	0.134	0.0034	18.05	0.29	0.0161	9.65	0.321	0.0333	38.2	0.271	0.0071
	3	34.5	0.106	0.0031	20.67	0.282	0.0136	19.57	0.281	0.0144	32.6	0.173	0.0053
NCTS-R	1	22.9	0.162	0.0071	26.97	0.281	0.0104	34.7	0.21500	0.0062	34.7	0.137	0.0040
	2	30.4	0.202	0.0066	19.4	0.286	0.0147	29.7	0.17800	0.0060	25.2	0.126	0.0050

i) Prior to testing

ii) Test 1

iii) Test 3

iv) Test 5

Figure 4.1 – SRC-1: Panel Overview

Figure 4.2 – SRC-1: Side View at Conclusion of Testing (Test 5)

Figure 4.3 – SRC-1 Test 5: Compressive Face from Inside Shock Tube

i) Test 1

ii) Test 2

iii) Test 3

iv) Test 5

Figure 4.4 – SRC-1: Upper Connection-1

i) Test 1

ii) Test 2

iii) Test 3

iv) Test 5

Figure 4.5 – SRC-1: Upper Connection-2

i) Test 1

ii) Test 2

iii) Test 3

iv) Test 5

Figure 4.6 – SRC-1: Upper Connection-3

i) Prior to Testing ii) Test 5 = 71.2kPa & 47.2ms

Figure 4.7 – SRC-1: Base Connection

i) Prior to testing

ii) Test 3 – 72.6kPa & 44.2ms

iii) Test 4 – 88.1kPa & 64.6ms

iv) Test 5 – 78.8kPa & 64.6ms

Figure 4.8 – NCTS-1: Panel Overview

i) Test 4 ii) Test 5

Figure 4.9 – NCTS-1: Side View with Flexural Cracks

i) Complete failure of upper panel supports

ii) Upper supports following

iii) Base support

Figure 4.10 – NCTS-1: Overview of Panel Damage at Failure

i) Prior to Testing

ii) Test 3

iii) Test 4

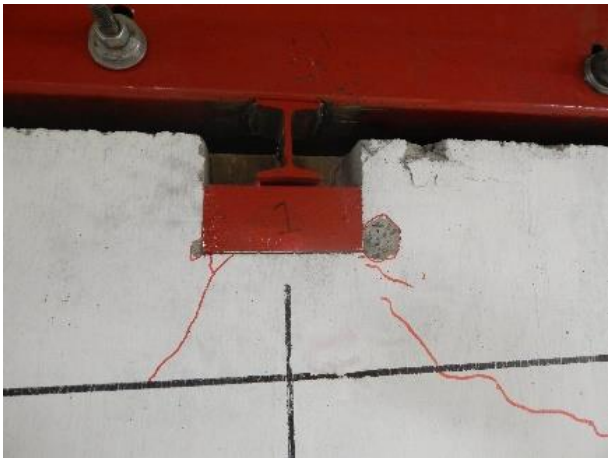

iv) Test 5

Figure 4.11 – NCTS-1: Upper Connection-1

i) Test 1

ii) Test 2

iii) Test 3

iv) Test 4

Figure 4.12 – NCTS-1: Upper Connection-2

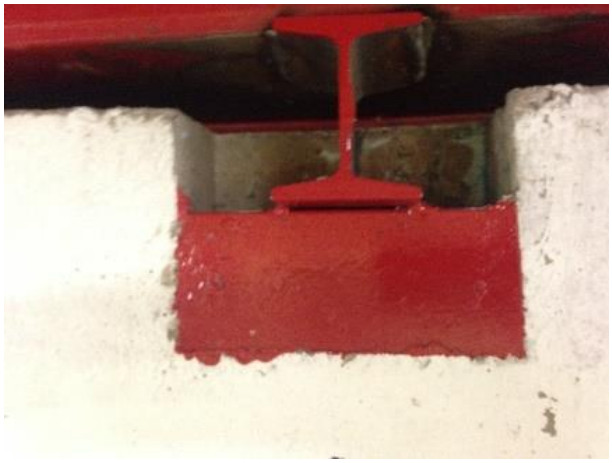

i) Test 1

ii) Test 2

iii) Test 3

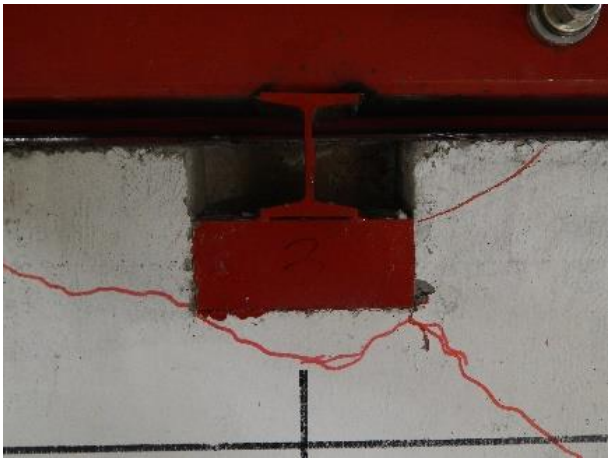

iv) Test 4

Figure 4.13 – NCTS-1: Upper Connection-3

i) Prior to testing

ii) Test 3 – 72.6KPa & 44.2ms

iii) Test 4 – 88.1kPa & 29.6ms

iv) Test 5 – 78.8kPa & 64.6ms

Figure 4.14 – NCTS-1: Base Connection

i) Test 1 – 72.4kPa & 57.9ms
Prior to repair

ii) Test 2 – 91.0kPa & 56.8ms

iii) Test 3 – 88.6kPa & 63.1ms

Figure 4.15 – NCTS-2: Panel Overview

i) Test 1

ii) Test 2

iii) Test 3

Figure 4.16 – NCTS-2: Upper Connection-1

i) Test 1

ii) Test 2

iii) Test 3

Figure 4.17 – NCTS-2: Upper Connection-2

i) Test 1

ii) Test 2

iii) Test 3

Figure 4.18 – NCTS-2: Upper Connection-3

i) Test 1 – 72.4kPa & 57.9ms

ii) Test 2 – 91.0kPa & 56.8ms

iii) Test 3 – 88.6kPa & 63.1ms

Figure 4.19 – NCTS-2: Base Connection

Figure 4.20 – NCTS-2: Typical Damage to Upper Connections and Shear Slip

i) Upper Connection-3

ii) Upper Connection-1

Inspection and removal of concrete near damaged connections

ii) Installation of formwork

iii) Recasting concrete into the damaged area

Figure 4.21 – NCTS-2: Repair of Connection-1 and -3

i) Test 1 – 73.9kPa & 62ms

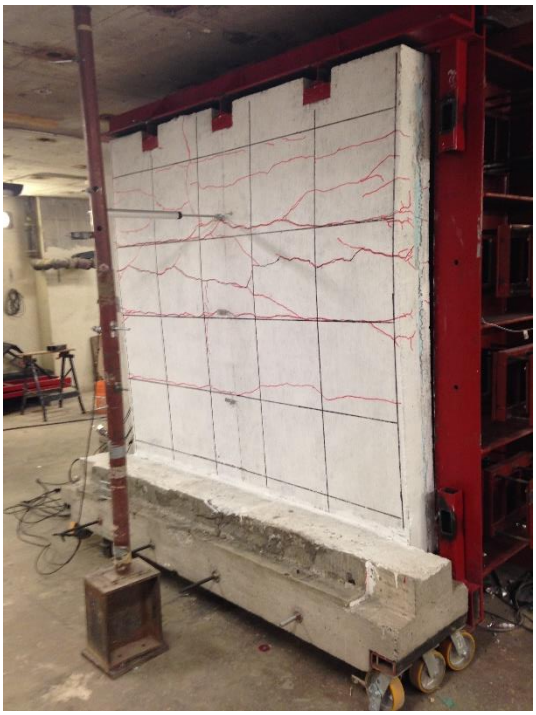

ii) Test 2 – 98.0kPa & 56.2ms

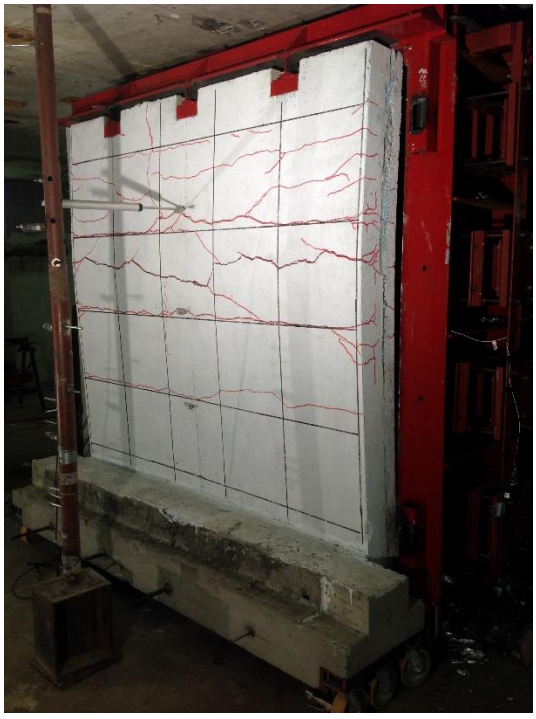

iii) Test 3 – 71.3kPa & 49.0ms

Figure 4.22 – NCTS-M: Panel Overview

Figure 4.23 – NCTS-M: Side View with Flexural Cracks (Test 3)

i) Test 1

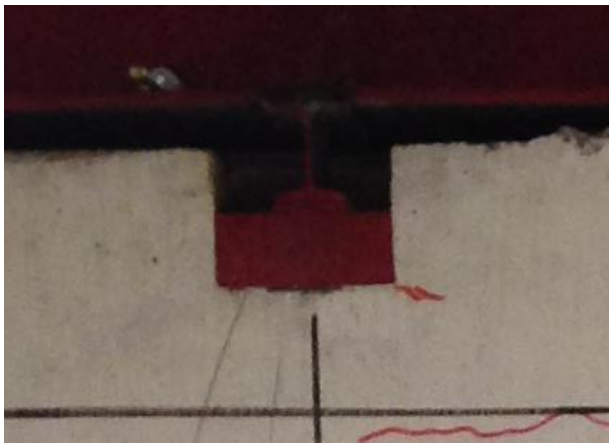

ii) Test 2

iii) Test 3

Figure 4.24 – NCTS-M: Upper Connection-1

i) Test 1 ii) Test 3

Figure 4.25 – NCTS-M: Upper Connection-2

i) Test 1

i) Test 2

iii) Test 3

Figure 4.26 – NCTS-M: Upper Connection-3

Figure 4.27 – NCTS-M: Typical Crack Development near Upper Supports during Test 1

Figure 4.28 – NCTS-M: Cracks near the Upper Support and Shear Slippage between the Architectural and Structural Wythes following Test 3

i) Prior to testing

ii) Test 1 – 73.9kPa & 62.0ms

iii) Test 2 – 98.0kPa & 56.2ms

iv) Test 3 – 71.3kPa & 49ms

Figure 4.29 – NCTS-M: Base Connection

Figure 4.30 – NCTS-2 (Bottom) and NCTS-M (Top): Side-by-Side View of Upper Connection Damage

i) Test 1 – 74.9kPa & 57.1ms ii) Test 2 – 99.5kPa & 57.9ms

Figure 4.31 – NCTS-R: Panel Overview

Figure 4.32 – NCTS-R: Side View with Flexural Cracks

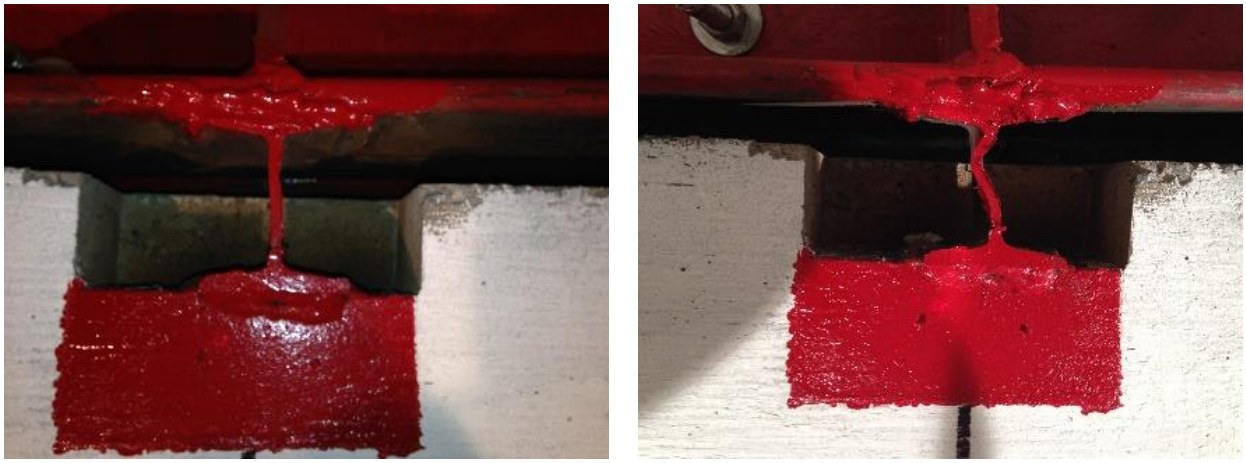

i) Test 1 ii) Test 2

Figure 4.33 – NCTS-R: Upper Connection-1

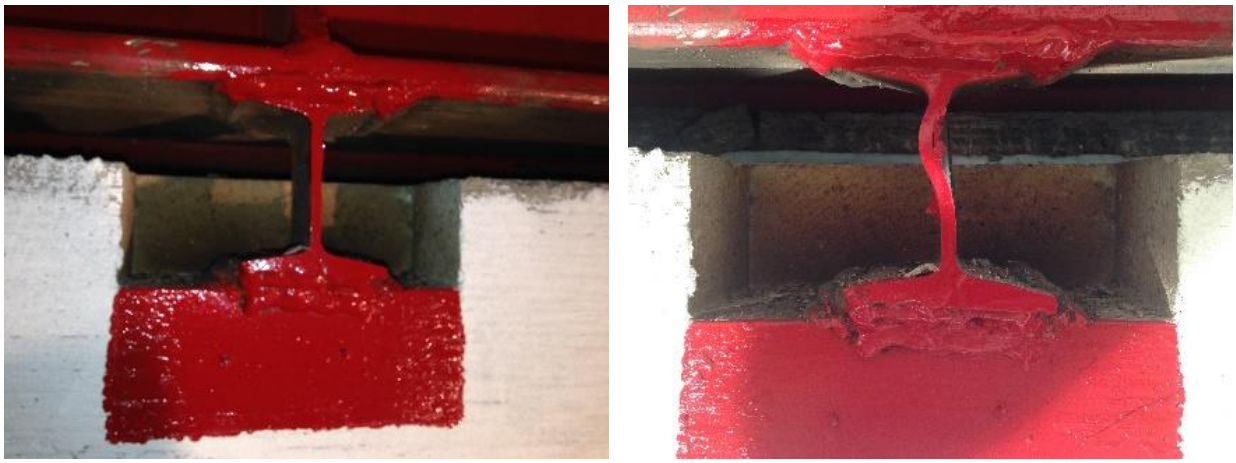

i) Test 1 ii) Test 2

Figure 4.34 – NCTS-R: Upper Connection-2

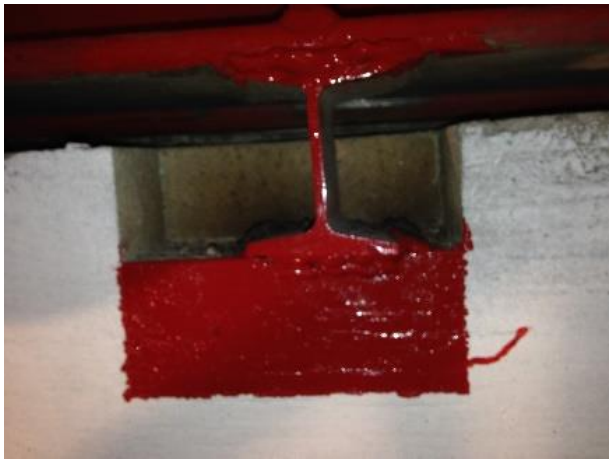

i) Test 1

ii) Test 2

Figure 4.35 – NCTS-R: Upper Connection-3

i) Test 1

ii) Test 2

Figure 4.36 – NCTS-R: Base Connection

5.0 Analysis of Panels

5.1 General

This section discusses the analytical study conducted to complete the evaluation of reinforced concrete tilt-up panels subjected to blast induced shock waves. Included in this section is an outline of the procedures and methodologies used in the analysis of the five reinforced concrete tilt-up panels described in Section 3.2. Due to the extremely short duration of blast induced pressures, members are loaded individually at extremely high strain rates and can therefore be analyzed using a single degree-of-freedom approach.

A SDOF system refers to a system with force-deformation properties that can be idealized as an independent Mass-Spring system with a range of motion in a single direction similar to Figure 5.1. Multi degree-of-freedom systems on the other hand are idealized as several dependent Mass-Spring systems and require complex matrices to accurately define the behaviour of motion. The motion of a SDOF system can be described by equation 5.1, where *m* is the mass of the system, *c* is the damping coefficient within the system, *k* is the stiffness, *F(t)* is the forcing function, and $\ddot{x}$, $\dot{x}$, and *x* are the acceleration, velocity, and displacement, respectively.

$$m\ddot{x} + c\dot{x} + kx = F(t) \qquad \textbf{5.1}$$

Previous research has found the accuracy of analytical evaluations of reinforced concrete members to be highly dependent on the accuracy of the load-deformation properties. Strain, displacement, and pressure data found in the experimental portion of this research study have been extracted and applied to the analytical process.

An analytical evaluation of the upper support capacity was performed to predict the failure criteria of NCTS panel connections subjected to blast loads. Included in this study is an in depth assessment of modified support reinforcement details and retrofit techniques designed to increase the blast resistance of the embedded supports. Code specified procedures to analyze the effects of punching shear in RC flat slabs can be applied to accurately predict the failure criteria of the panel's connections. Application of these ideologies caters to the skillset of many structural

engineers and will allow designers to easily incorporate these methods into their current design procedures.

5.2 Determination of Material Properties

The analytical evaluation of structural behaviour is highly dependent on accurately modelling material properties and panel characteristics. These properties include the stress-strain relationship of the reinforcing steel, the compressive strength of concrete, and the mass of the system. This section outlines how these properties are modelled and specifies how they are applied to the analysis.

5.2.1 Dynamic Increase Factors

The dynamic increase factor, DIF, is the ratio of dynamic strength to static strength which accounts for the change in material properties caused by high strain rates. The DIF is a material dependant property that increases with increasing strain rates. UFC [8], recommends DIFs of *1.17* and *1.05* for the yield and ultimate stresses of reinforcing steel and *1.19* for concrete compressive strength in members subjected to bending. UFC also recommend a DIF of *1.1* for concrete, *1.1* for yield stresses and *1.0* for ultimate stresses of reinforcing steel subjected to direct shear. These factors were used to perform the structural analysis discussed in the proceeding subsections.

5.2.2 Stress-Strain Relationship of Reinforcing Steel

Determining the force-deformation properties for a reinforced concrete member requires accurate interpretation of the internal force interaction within the member. A key component of this is the stress-strain relationship of the reinforcing steel. The stress-strain relationships shown in Figure 3.15 through Figure 3.17, were used in the sectional analysis of all specimens.

5.2.3 Concrete Strength Parameters

The concrete compressive cylinder strength, f_c', for each panel are presented in Table 3.1. The compressive stress distribution within the concrete was modelled using Hognestad's Parabolic Stress Block with a peak compressive strength at a strain equal to *0.2%*. Once exceeding this strain,

the compressive strength decreased linearly until reaching a strain of *1.0%*. Strength remained constant and was assumed to be 10% of the peak compressive strength after this point. The ascending branch of the stress strain relationship (i.e. $0 \leq \varepsilon_{cc} \leq \varepsilon_0$) is defined by Equation 5.2. Figure 5.2 illustrates the stress-strain relationship modelled using Hognestad's Parabola. The modulus of rupture, f_r, and modulus of elasticity, E_c, were calculated using the methods prescribed by CSA A23.3-04 [5] shown in Equations 5.3 and 5.4.

$$\boldsymbol{f_c = f_c^{'} \left[\frac{2\epsilon_c}{\epsilon_0} - \left(\frac{\epsilon_c}{\epsilon_0}\right)^2\right]} \quad \textbf{5.2}$$

$$\boldsymbol{f_r = 0.6\sqrt{f_c^{'}}} \quad \textbf{5.3}$$

$$E_c = 4500\sqrt{f_c'} \quad \textbf{5.4}$$

5.3 Analysis of Experimental Strain Data

As discussed in Section 3.6 strain gauges were installed on compressive and tensile steel to capture the strain profile at mid-span. Additional strain gauges installed on tensile reinforcement at the lower- and upper-quarter span provide insight into the distribution of moments along the span of the panel. This section discusses the interpretation of this data and its application to the overall analysis of the panels.

5.3.1 Analysis of Sectional Strain Data

Experimental compressive and tensile strain data, details sectional strain behaviour at mid-span and provides insight into the composite behaviour of the specimen. A sectional analysis was performed for every test on each panel to determine the compressive forces required to achieve equilibrium with stresses in the reinforcing steel. The equilibrated sectional strain profiles for every test on each panel are plotted in Figure 5.3 through Figure 5.7.

Internal forces in the reinforcing steel are calculated from peak experimental strain data at mid-span and a neutral axis depth is assumed. Compressive forces in the concrete are determined using Hognestad's parabolic stress block and the internal force differential is calculated. The neutral axis is adjusted accordingly until the internal force differential is zero and the system reaches

equilibrium. This iterative procedure requires assumptions in regards to the strain distribution across the section. Firstly, the strain distribution within a continuous portion of the section is continuous and linear in nature. Secondly, the strain distribution on either side of a discontinuity (i.e. insulation) in the member will share the same linear properties. Lastly, in the event a discontinuity in the section causes disproportionate strain distributions in either wythe the member should be considered to behave without composite action (e.g. the wythes will no longer act together). A visual explanation of these assumptions is provided in Figure 1.4.

The sectional strain distributions of specimen SRC-1 for shots 1 through 4 disagreed with typical distributions, with tensile strains measured in both the tensile and compressive steel. This is shown in Figure 5.3. SRC-1 behaved as expected, in terms of sectional strain, with tensile and compressive forces near equilibrium. Data for subsequent tests follows a same linear pattern however all strains are tensile. This may be a result of erratic strain readings or failure of the specimen.

Sectional strain data for NCTS-1 from tests 1 through 4 show that the panel is nearly fully composite. The dashed lines in Figure 5.4 represent the insulation which does not contribute to the flexural capacity of the specimen. The sectional strain data for shot 5 indicates that the shear tie capacity has been exceed and non-composite behaviour is predominant. This can be seen by the change in the strain offset between the architectural and structural wythes.

NCTS-2, NCTS-M, and NCTS-R all demonstrated lower composite behaviour than those observed in NCTS-1. This can be attributed to the higher blast loads induced by these tests and the result degradation of shear tie capacity as the panel are forced to resist higher loads.

In general, all of the NCTS panels demonstrate a reduction in composite behaviour. This is evidenced by the widening offset between the architectural wythe, as well as the introduction of tensile and compressive forced in bother wythes. These sectional strain distributions were recorded at mid-span and are not used in the analysis of displacement-time histories. The distributions are rather to illustrate the typical behaviour of the NCTS panels and are confirmed with analytical results which show that as resistance is increased, composite behaviour changes.

5.3.2 Analysis of Strain Distribution

The distribution of moments along the span of the panel was recorded using strain gauges installed on tensile steel at quarter-, mid-, and three-quarter-span. This data provides information essential to the determination of support reactions and the construction of load-deformation characteristics.

Strain values were averaged over a predetermined period of time (e.g. duration at which mid-span displacement is above *50%* of the peak) to reduce the effects of erratic fluctuations in the data. Moments were approximated at each location based on experimental strain data using the rectangular stress block theorem outlined in CSA A23.3-04 [5]. The moment at each data point was divided by the moment at mid-span (i.e. M_{top}/M_{mid}, M_{mid}/M_{mid}, and M_{bot}/M_{mid}) to normalize data. This distribution was then plotted and the boundary conditions were determined through trial-and-error by fitting a mid-span moment ratio distribution to the plotted experimental data. Typical moment distributions are plotted in Figure 5.8 and Figure 5.9. Results are presented in Table 5.1, as a percentage of $wl^2/8$.

The moment distribution for specimen SRC-1, plotted in Figure 5.8, shows a reduction in support fixity as blast magnitude is increased. As a result, SRC-1 shifts from a nearly fully fixed panel in the initial test to a simply supported panel in the concluding test. Loss of rotational capacity in the base support was do to the inability of casters to resist the extreme blast loads. This was remedied by shimming the support so that the casters remained unloaded. Moment distributions for NCTS-1 followed a similar pattern, however, the base support remained partially fixed while the upper support suffered a loss in rotational stiffness and acted as a pinned support.

Support reactions can be calculated by differentiating the moment-distribution, this is discussed in further detail in Section 5.6.5.

5.4 Deriving Force-Deformation Properties

Precision of force-deformation properties is reliant on the accuracy of defined material and sectional properties. Determining these parameters for reinforced concrete sandwich panels is a complex process sensitive to the interpretation of composite behaviour within the panel. This section discusses in detail, the methods and procedures used to derive the force-deformation characteristics of the tilt-up panels.

5.4.1 Sectional Analysis of Moment-Curvature Relationship

The load-deformation characteristics of a flexural member can be derived directly from its moment-curvature relationship. Performing a sectional analysis on a reinforced concrete member is an iterative process used to construct the moment-curvature relationship. In conventional methods, internal forced are equilibrated iteratively for increasing extreme compressive fibre strains, ε_{cc}. This process is continued until predetermined failure criterion are reached. The primary disadvantage of this method arises at later stages in the analysis as interpolating between moment-curvatures of panels with varying composite behaviour becomes complex. Sandwich panels experience sudden degradation in flexural capacity due to the relationship between the two concrete wythes and the discontinuity introduced by the insulation layer. As a result, a five-line idealized moment-curvature relationship, shown in Figure 5.10, should be used to reflect the flexural behaviour of NCTS panels. Moment-curvature relationships for each panel are plotted in Figure 5.11 through Figure 5.15.

Sectional Analysis of SRC Panel

An initial extreme compressive fibre strain was selected based on the tensile capacity of concrete and the neutral axis was calculated at the centroid of the section. The cracking moment and corresponding curvature were calculated using Equation 5.5 and 5.6, respectively. The extreme compressive fibre strain was then incremented a predetermined amount and a corresponding neutral axis was assumed. A strain profile was generated and the internal force differential within the specimen was calculated. Compressive stresses above the neutral axis were divided into sections dependant on the strain level and material behaviour: prior to peak compressive strength, strength decay region post peak, and crushing or spalling of concrete. The neutral axis depth was then adjusted accordingly until the internal force differential was equal to zero and equilibrium was achieved. The moment was equated by multiplying the force in a portion of a section by the distance between its centroid and the neutral axis. This procedure was repeated until tensile reinforcement ruptured and the system could no longer reach equilibrium.

$$M = \frac{f_r I_{tr}}{\bar{y}} \qquad \textbf{5.5}$$

$$\phi = \frac{\epsilon_{ct}}{\bar{y}} \qquad \textbf{5.6}$$

Sectional Analysis of NCTS panels

The moment-curvature relationship generated in the sectional analysis consisted of six points joined by five straight lines. These points were representative of concrete cracking, yielding of tensile reinforcement, ultimate concrete capacity, a compressive strain of *1%*, and a compressive strain in excess of *1%*. This combination of data points was selected because a trilinear approach did not accurately represent the rebound behaviour of the NCTS panels. Figure 5.10 demonstrates the accuracy of using this method to predict moment-curvature relationships.

Sectional properties were calculated for an initial tensile strain equal to the strain at concrete cracking and a neutral axis was calculated at the sections centroid. Forces within the specimen were equilibrated by performing a transformed sectional analysis and moment-curvature properties were calculated using Equations 5.5 and 5.6, respectively. The strain was adjusted to the represent yielding of tensile reinforcement and a neutral axis was assumed. A strain profile was generated and the internal force differential was calculated. Compressive stresses above the neutral axis were divided into sections dependant on the strain level and material behaviour: prior to peak compressive strength, strength decay region post peak, and crushing or spalling of concrete. The neutral axis depth was then adjusted accordingly until the internal force differential was equal to zero and equilibrium was achieved. The moment was equated by multiplying the force in a portion of a section by the centroidal distance to neutral axis. This procedure was repeated for each of the six points or until tensile reinforcement ruptured and equilibrium could no longer be reached.

Several assumptions regarding the behaviour of material and strain properties were required to generate this relationship for the NCTS series: Firstly, the strain distribution in the architectural and structural wythes of non-composite sandwich panels are assumed to be parallel. Secondly, the foam core does not contribute structurally to the flexural resistance of the panel and is an architectural feature only. Finally, rupture of the architectural reinforcement does not constitute failure under negative loading due to the remaining structural integrity of the structural wythe.

Additional complications arise in the derivation of moment-curvature relationships for partially composite sandwich panels due to the complex relationship between the structural and architectural wythes. Furthermore, as a member is exposed to flexural forces the composite behaviour varies along its span producing an intricate distribution of moment-curvature behaviour along the panel. Benayoune et al. [9] found that the moment-curvature moment can be determined

by iterating between the fully composite and non-composite moment-curvature, using the following procedure:

- Calculate the moment-curvature assuming the panel is fully composite;
- Calculate the moment-curvature assuming the panel is non-composite;
- Determine the percentage of composite action within the panel using the procedure outlined in 5.4.2; and
- Calculate the partially composite moment-curvature relationship for the panel using Equations 5.7 and 5.8.

$$M_{PC} = (M_{FC} - M_{NC}) \cdot \frac{\%_{composite}}{100\%} + M_{NC} \quad \textbf{5.7}$$

$$\phi_{PC} = (\phi_{FC} - \phi_{NC}) \cdot \frac{\%_{composite}}{100\%} + \phi_{NC} \quad \textbf{5.8}$$

5.4.2 Evaluating Composite Action within a Sandwich Panel

Contrary to the name, non-composite tilt-up panels are typically capable of maintaining some degree of composite action. Composite action is a function of the shear tie stiffness; therefore, all panels experience it to some degree. Dayton Superior [10] recommends a minimum of *5* to *10 percent* composite action to achieve a flat lift and many proprietary shear ties achieve partial composite action with the maximum spacing guidelines. Assuming that a panel experienced no composite behaviour would result in an under estimation of support loading and could potentially result in catastrophic support failure similar to that experienced by NCTS-1.

Benayoune et al. [9] conducted an experimental and analytical investigation of the behaviour of partially composite precast panels in flexure. In partial completion of this study a finite element analysis was conducted to evaluate the composite behaviour within sandwich panels. Findings indicate that the composite action within the elastic region of a sandwich panel can be approximated using the relationship expressed in Equation 5.9. While this evaluative method can be applied to approximate composite action it lacks applicability to classic analytical methods used in practice. Benayoune et al. also found that directly interpolating between fully composite and

non-composite resistance curves yielded a reasonable approximation of flexural behaviour within a partially composite panel.

$$\%_{composite} = \frac{I_e}{I_g} = \frac{\left(\frac{Mh}{\sigma_b - \sigma_t}\right)}{I_g} \quad \textbf{5.9}$$

Alternative approaches recommended by Naito et Al. [11] expanded on these concepts incorporating conventional sectional analysis methods into the evaluation of composite behaviour within sandwich panel. Moreover, the force-deformation properties of shear ties, similar to those used in the construction of the NCTS panel series, were considered in the analysis. Figure 5.16 shows the backbone of the shear tie force-deformation relationship used in the analysis of the NCTS panel series. The steps prescribed to approximate the composite action within a sandwich panel with shear tie degradation are:

1) Apply a uniformly distributed force along the span of the panel and compute the moment between each shear tie,
2) Calculate the shear force acting on each shear tie using the expression provided in Equation 5.10,
3) Determine the slip in each tie using the force-deformation relationship plotted in Figure 5.17,
4) Calculate the partially composite properties based on tie stiffness, *k*, calculated by dividing the shear force acting on the tie by the total slip.

$$V_{ij} = \frac{(M_{i+1} - M_i)_j}{0.9h \; or \; 0.72d} \quad \textbf{5.10}$$

Composite behaviour is defined by the relationship between rigid stiffness (e.g. within the elastic region) and soft stiffness of the tie (e.g. shear forces exceed ultimate strength of the tie) and can be evaluated using Equation 5.11. This method can be applied to panels with various support conditions provided the force-deformation of the shear ties is known.

$$\%_{composite} = \frac{K_{actual} - K_{soft}}{K_{rigid} - K_{soft}} \quad \textbf{5.11}$$

Applying this method on scaled panels yielded poor results due to the small quantity and large spacing of the shear ties with respect to the size of the specimen. To account for this and better define the motion within the panel, the tributary area (e.g. half the distance between ties) was divided into multiple regions and the backbone of the ties were adjusted accordingly. The forces in each region were calculated and the composite behaviour was assessed.

5.4.3 Derivation of Resistance Curve

A load-displacement relationship specific to each panel was generated based on empirical support conditions and the theoretical moment-curvature properties. The SDOF analysis uses the resistance curve to model the displacement-time history of a member subjected to an impulsive forcing function. The resistance curves for each panel are plotted in Figure 5.17 through Figure 5.21. Typical theoretical degradation of composite behaviour with an NCTS panel is presented in Figure 5.22.

Each panel was divided into *250* length increments with a total of *251* data points at a spacing of approximately *7.5mm*. The panel was subjected to a uniformly distributed load of *1kN/m* and the moment at each length increment was calculated based on the specified support conditions. The shear force at each data point was calculated using Equation 5.10 and the composite behaviour at each point was assessed with Equation 5.11. A curvature distribution was then constructed along the span of the panel by interpolating between the non-composite and fully composite moment-curvature relationship at each data point. Mid-span displacements of the panel were determined by numerically integrating the curvature-distribution. The load-mass factor was adjusted from *0.78* to *0.66* once any data point exceeded the yield capacity. This procedure was repeated until failure of the panel with uniformly distributed load increments of *1kN/m*.

5.5 Single Degree of Freedom Analysis

An SDOF analysis was performed to evaluate and compare theoretical displacement-time histories with empirical data. RC Blast, a versatile and user friendly SDOF software, was used to analyze the dynamic response of the SRC and NCTS panels. This section discusses in detail, the procedures and assumptions used in the dynamic analysis.

5.5.1 RC Blast

RC Blast is a software developed at the University of Ottawa to perform dynamic SDOF analysis of reinforced concrete members subjected to blast induced shock waves. RC Blast is composed of a structural analysis module and SDOF analysis modules. The structural analysis module allows users to model sectional behaviour and construct resistance curves for one-way members. The structural analysis module also generates the load-mass transformation factors coinciding with each load stage of the resistance curve. This module was not designed to model the complex sectional behaviour of NCTS panels.

The SDOF analysis module allows users to perform a dynamic time-history analysis on members subjected to impulsive forcing functions. Direct integration of the dynamic equation of motion, provided in Equation 5.1, produces displacement-time history for members with specified load-deformation characteristics subjected to a given pressure-time history. While RC Blast recognizes custom pressure-time properties it is also capable of generating these properties based on charge weight and stand-off distance. The experimental pressure-time histories recorded during testing were input into RC Blast to ensure accurate reproduction of experimental test parameters.

Another feature of RC Blast is the ability to generate pressure-impulse diagrams for given structural elements. A PI diagram is a useful design tool that plots the pressure-impulse combinations that induce the same levels of structural response. PI diagrams were constructed by iteratively adjusting reflected pressure, P_r, with a constant positive phase duration, t_d^+, until the specified deflection was achieved. For more information regarding RC Blast refer to Jacques et Al. [12].

5.5.2 Transformation Factors

Load and mass factors are used to transform multi degree of freedom systems into an equivalent SDOF systems based on mode shape. The factors range between *0.78* in the elastic region, *0.66* in the plastic region, and a variety of values in the elasto-plastic region of the typical members subjected to uniformly distributed loads. The factors recommended by UFC [8] and Biggs [13] for each load region were used in the analysis of the panel.

These factors were assigned to specific deformations during the construction of the resistance curve. Tensile strains varied considerably due to the variation of composite behaviour along the span of the panel. The panel was considered to be elastic prior to any yielding in the member regardless of location and composite behaviour.

5.5.3 System Damping

Damping is an integral property, required to accurately modelling the free vibration behaviour of a member subjected to dynamic loads. While damping has very little effect on the system response prior to the first peak it is a crucial component in predicting the displacement-time history post-peak. Even so, ignoring damping is a conservative design approach that will ultimately produce greater displacement within the panel. UFC, [8], recommends that if damping is to be considered it should range between *1%* and *5%* of the systems critical damping. A system that is critically damped approaches zero as quickly as possible without oscillating. This phenomenon can be applied to structural members using Equation 5.12. Therefore, critical damping is reliant on the sectional properties of the member which, for NCTS panels, varies considerably along the span of the panel. As a result, the complex degradation of structural capacity must be incorporated into the analysis of the specimen. SDOF analysis software, RC Blast, does not permit the use of a displacement dependant damping function. Figure 5.23 illustrates the large difference between the critical damping of fully-composite fully-fixed specimens and non-composite simply supported specimens.

$$C_{cr} = \sqrt{4kM} \qquad \textbf{5.12}$$

To account for this an average effective moment of inertia was calculated at each load stage during construction of the resistance curve. This relationship is plotted in Figure 5.24. The members damping was iteratively calculated based on the peak mid-span displacement determined by the SDOF analysis. The effective moment of inertia and system damping for each shot is tabulated in Table 5.2.

5.5.4 Pressure-Time History

For sake of comparison the experimental pressure-time history recorded for each shot was used as the impulsive forcing function for the SDOF analysis. Only the positive phase of the shock wave

was used to avoid the complexities associated with the reflection and venting of pressures within the shock tube.

5.5.5 Panel Mass

Panel mass was calculated assuming concrete and insulation densities of $2440kg/m^3$ and $30kg/m^3$, respectively. A total mass of *1010kg* for the control panel and *1519kg* for the sandwich panels were used in the analysis. These masses were verified using a lifting scale in the Structural Engineering Laboratory and were found to be within 6% of the assumed mass.

5.5.6 Exposed Surface Area

The exposed surface area, or loaded area, is the surface area impacted by shock wave. Both the SRC and NCTS panels were constructed to cover the entire opening of the shock tube. The exposed surfaced area of each specimen is $4.13m^2$.

5.6 Modelling Support Capacity

The support failure plane exhibited by NCTS-1 were analogous to the punching shear failure in a flat slab. To facilitate a smooth transition from well-established design requirements, support punching shear failure was analysed using CSA A23.3-04 [5] guidelines. Predicted support capacities and support loads for each panel are summarized in Table 5.4 through Table 5.7.

5.6.1 Comparison of Theoretical and Experimental Failure Plane

Punching shear is a common failure mode of flat slabs or foundations subjected to concentrated lateral loads. This failure mode is characterized by the propagation of cracks between 30^o and 45^o from the contact surface through the slab to the failure surface.

The support failure plane, shown in Figure 4.10, observed in NCTS-1 propagated at approximately 35^o to 40^o *65mm* from the compressive face of the panel to the failure surface. The three-dimensional model presented in Figure 5.25 provides a visual comparison between the theoretical and observed failure planes. Initiation of cracking at mid-depth of the panel can be attributed to the mechanics of the joist seat embedded in the panel. Firstly, the presence of the pocket above the

embedded angle reduces the required crack propagation. Secondly, each leg of the angle is embedded in the concrete, one at *6.35mm* and another at *63.5mm* into the wall. Finally, the headed studs extend *75mm* at *45º* from the angle joint or *60mm* from the face of the panel. This effectively results in a *short circuiting* effect which allows shear cracks to bypass this portion of the depth. This can be directly observed by the concrete cone remaining on the embedded support after failure, the impressions of the studs in the failure plane, and the *90º* failure surface parallel to the legs of the angle.

Figure 5.25 also shows that cracks propagate at a smaller angle near the bottom of the support than at the sides. This is related to the embedment angle of the headed studs into the panel. The transfer of the shear forces between the panel and the supports produces a *45-degree* resultant force causing the unique crack development in this region.

Considering these differences, analysing the support using conventional punching shear application will produce slightly lower capacities. The degree of error already associated with blast response analysis and the uncertainties surrounding material properties, make these differences acceptable. The small error produced in this analysis is conservative and does not overestimate the capacity of the supports.

5.6.2 Analysis of Unmodified Supports

Analysis of the conventional supports used in panels SRC-1, NCTS-1, and NCTS-2 was performed following CSA A23.3-04 [5] guidelines for punching shear of flat slabs. Two analytical methods were reviewed; conventional punching shear of flat slabs and anchorage failure of embedded studs. This approach was selected because it best reflected the empirical failure plane suffered by NCTS-1. This method was also applied to panels NCTS-M and NCTS-R to evaluate increase in support capacity and to facilitate a direct comparison of the results. Figure 5.25, which shows the theoretical punching shear breakout vs. the experimental failure surface. The critical section assumed for punching shear failure extended to the surface of the upper edge of the panel and was determined using the thickness of the panel minus the depth of the embedded support. This resulted in a failure plane that was smaller than those observed in panel NCTS-1 and was likely due to the orientation of the embedded studs. Orienting the studs at *45°*likely contributed to the propagation

of the punching shear failure plane further toward mid-span of the panel. The smaller failure plane results in a more conservative theoretical analysis.

Punching shear resistance is based on the shear capacity of the concrete along the critical section and was calculated from Equations 5.13 through 5.15.

$$v_r = v_c \leq \left(1 + \frac{2}{\beta_c}\right) 0.19\lambda\phi_c\sqrt{f_c'} \quad \textbf{5.13}$$

$$v_r = v_c \leq \left(\frac{\alpha_s d}{b_0} + 0.19\right)\lambda\phi_c\sqrt{f_c'} \quad \textbf{5.14}$$

$$v_r = v_c \leq 0.38\lambda\phi_c\sqrt{f_c'} \quad \textbf{5.15}$$

Where β_c is the ratio of the long and short edges of the support (i.e. *150mm/63.5mm*), α_s incorporates edge effects and is equal to *3* for edge columns, b_0 is the critical perimeter *d/2* away from the support, and λ describes concrete density (i.e. *1.0* for normal density concrete). Calculations were performed to evaluate current design methods; therefore, design reduction factors were taken as unity.

5.6.3 Analysis of Reinforced Supports

The upper supports of panel NCTS-M were modified with a reinforcement cage similar to stirrups in a beam designed to capture and reinforce the failure plane experienced in the support failure of specimen NCTS-1. Shear reinforcement was installed at *30º*, *45º*, and *60º* from the outside of either stud as well as *30º* and *55º* from the inside. This is illustrated in Figure 5.26. The lower layer of shear reinforcement was designed to capture the deep crack propagation at the bottom of the support.

The theoretical analysis performed on panel NCTS-M follows CSA A23.3-05 guidelines for analysing punching shear in flat slabs reinforced with stirrups. Modifications to previous approach for unreinforced supports included adjusting the shear resistance of concrete within the reinforced zone and including the shear resistance of reinforcement. These modifications are shown in Equations 5.16 through 5.18, where A_{vs} is the cross-sectional area of shear reinforcement parallel to the column perimeter and f_{yv} is the yield strength of the steel.

$$v_c = 0.19\lambda\phi_c\sqrt{f_c'} \quad \textbf{5.16}$$

$$v_s = \frac{\phi_s A_{vs} f_{yv}}{b_0 s} \quad \textbf{5.17}$$

$$v_r = v_c + v_s \quad \textbf{5.18}$$

5.6.4 Analysis of FRP Retrofit Supports

The upper supports of panel NCTS-R were retrofitted with four layers of surface bonded FRP laminates on the tensile face of the structural wythe. Each layer consisted of *500mm* FRP sheets bonded in alternating directions centred on the support. The FRP retrofit was designed to extend beyond the failure plane suffered by specimen NCTS-1 to ensure sufficient bond strength. El-Salakawy et Al. [14] conducted a research study to evaluate the punching shear behaviour of flat slabs retrofitted with surface bonded FRP laminates. The experimental portion of the study consisted of seven full-scaled reinforced concrete slab-column edge connections. Results were dependent on fibre type (i.e. glass or carbon) and laminate layout. Specimens retrofitted with surface bonded FRP laminates experienced a small boost in capacity. Salakawy et Al. also found CSA A23.3-04 conservatively predicted punching shear capacity with consistently lower failure loads. Another study performed by Farghaly and Ueda [15] examined the punching shear capacity of flat slabs retrofitted with surface bonded FRP sheets. The study included an experimental program in which three RC slabs, one control slab and two retrofitted slabs, were tested under a monotonic load. The slabs were simply supported along the four edges of the panel with load applied in the centre. Results indicated a significant improvement in the punching shear resistance when retrofitted with surface bonded FRP laminate. The amount of FRP applied to the specimen is proportional to the increase in capacity. The theoretical portion of the study developed a new analysis method to better model the punching shear capacity of flat slabs with surface bonded FRP laminates. Data shows that compared with ACI and JSCE predictions, Farghaly and Ueda's equation more accurately predicted punching shear behaviour by *8%* and *16%*, respectively.

5.6.5 Determining Support Loading

A summary and comparison of the applied shear forces and the punching shear resistance is presented in Table 5.7. Support reactions were calculated based on the empirical moment distribution and the peak resistance experienced by the panel. These parameters were dependant on experimental strain gauge readings and the displacements recorded by LVDTs during testing.

Evaluation of strain data is discussed in Section 5.3.2. The resistance function was calculated using the experimental displacement-time history for each function, following three steps:

1. Generate a trend line for the first inbound and rebound peaks of the experimental displacement-time history. Sixth-order polynomials were found to accurately represent experimental data.
2. Double differentiate the polynomial to generate the velocity-time and acceleration-time histories for the panel. Typical displacement-, velocity-, and acceleration-time histories are shown in Figure 5.27.
3. Calculate inertial force and resistance at each time interval. Figure 5.28 shows typical force-, inertial force-, and resistance-time histories.

Support reactions were then calculated using the peak resistance and the support conditions found in Section 5.3.2. The equations recommended by Biggs [13] can be used to approximate dynamic support reaction in the elastic, elasto-plastic, and plastic strain range as a function of panel resistance and static forces. The static force acting on the panel is equal to the product of pressure and area.

5.7 Comparison of Analytical Results and Experimental Data

Theoretical and experimental mid-span displacement-time histories a plotted in Figure C.1 through Figure C.18 in Appendix C. Maximum displacements and time-to-maximum-displacements results are tabulated in Table 5.8 and are plotted in Figure 5.30 and Figure 5.31. Analytical support punching shear capacities are summarized against experimental support reactions in Table 5.4 through 5.6.

5.7.1 Comparison of Experimental Data and Theoretical Displacements

Maximum mid-span displacements were consistently predicted within *26%* of the experimental results with two minor exceptions. The predicted maximum mid-span displacements for shot 1 and 2 on NCTS-1 were *0.26mm* and *0.44mm* of the experimental peak. While these predictions produce the highest percentage of error, there is only *1.1mm* and *2.2mm* a difference between the experimental and theoretical results. Overall the average predicted peak mid-span displacements

were *0.933* of the experimental values with a standard deviation of *0.27*. However, displacement predictions were more accurate for high pressure blast loads, even after numerous shots. Tests with an impulse greater than *500kPa-ms* show increased accuracy. Maximum mid-span displacement predictions for these tests were on average *1.04* of experimental data with a standard deviation of *0.16*. Predictions for shots with and impulse in excess of *1000kPa-ms* were on average *1.08* of experimental results with a standard deviation of *0.15*. This trend indicates that as blast pressures become more destructive, theoretical analyses produce more conservative results.

Time-to-maximum displacements were consistently predicted within *22%* of the experimental results with similar discrepancies to those observed in maximum mid-span displacements. The average predicted time-to-maximum displacement for all tests is 0.84 of the experimental data with a standard deviation of 0.19. Accuracy increase considerably for shots with an impulse over *500kPa-ms* and in excess of *1000kPa-ms* with averages of 0.92 and 0.94. The corresponding standard deviations were *0.115* and *0.117*, respectively. Time-to-maximum displacement were consistently under predicted.

Simple observation of Figure C.1 through Figure C.18 in Appendix C shows that the accuracy of free vibration displacement-time histories vary considerably for each panel and shot. The average residual displacement for all shots, shots with an impulse over *500kPa-ms*, and shots with an impulse over *100kPa-ms* of were equal to *0.90*, *1.14*, and *1.19* of the predicted values, respectively. These results appear to agree with experimental data and become more conservative under higher impulse loads. However, the corresponding standard deviations of *0.74*, *0.67*, and *0.71* indicate a large variance in data. This error is produced from the sensitivity of the system's free vibration to unloading stiffness and damping. RC Blast uses a constant system damping to calculate displacement-time histories for specimens subjected to blast load. As composite behaviour within NCTS panels degrade the system loses stiffness and as a results damping is reduced. The unloading stiffness of a specimen significantly impacts its peak displacement and motion in free vibration. As NCTS panel deform composite strength decays and sectional properties of the panel change. This complex change is not captured by the analytical tools and result in inconsistent behaviour post peak displacement. Unloading stiffness was changed between shots (i.e. based on previous peak displacement) in an attempt to capture this behaviour however a composite behaviour dependent stiffness would be ideal.

There are several potential causes of the inaccuracies in the predictive models of low pressure shots for specimens SRC-1 and NCTS-1:

- Over estimation of the rotational stiffness of supports due to the erratic and inconsistent strain readings associated low pressure tests would result in stiffer resistance curves.
- Difficulty capturing the cracking capacity of sandwich panels and its relationship to shear tie capacity, resulted in extremely high uncracked stiffness. Incorporating uncracked sectional stiffness into the construction of resistance curves produced smaller displacements for low pressure-impulse shots. Thus, uncracked stiffness was not included incorporated into the resistance curve.
- Lastly, shear tie load-deformation characteristics were based results from Naito et al. [11]. Minor variations in the stiffness of shear ties would expedite or postpone degradation of composite behaviour in the panel. This phenomenon is more critical in earlier stages of the resistance curve when fully composite behaviour dominates. Erecting panels may also cause premature shear tie degradation resulting in a lower initial flexural stiffness.

Shot 6 of NCTS-1 and tests conducted on NCTS-2 were not included in this comparison due to the panel's behaviour during tests. NCTS-1 suffered a catastrophic support failure during its sixth test, as a result instrumental data was considered unusable. The initial test of NCTS-2 caused a premature weld failure in the supports producing unrealistically large deformation, therefore results contained a high degree of error. LVDTs were not installed on NCTS-2 for subsequent tests to avoid the loss of critical instrumentation.

5.7.2 Comparison of Analytical Connection Capacities and Experimental Results

CSA A23.3-04 [5] guidelines for analysing the punching shear capacity of flat slabs were applied to the assessment of NCTS panel supports. Analytical results are summarized in Table 5.4 through

Table 5.6. As discussed in Section 5.6 this approach conservatively predicts the failure criteria of NCTS panel joist seat supports under blast induced loads.

Results coincide with experimental observations for damage and panel failure. For more information regarding the support behaviour in the experimental portion of this study please refer to Section 4.2. The peak support reactions, *92.4kN* and *114.0kN*, experienced by SRC-1 and NCTS-2 through the first five tests were well below their respective support capacities of *113.5kN* and *141.3kN*. However, the support reaction of specimen NCTS-2 is approximate due to the absence of displacement-time history data. Analytical results correlate well with the amount of damage observed in SRC-1 during testing. The damage incurred by NCTS-2 is representative of higher pressures, however this can be attributed the repaired section of the support discussed in Section 4.1.3. The support capacity of panel NCTS-1, *128.0kN*, was exceeded in the sixth test by *23.9kN*.

The theoretical support capacity of the modified supports in NCTS-M increased to 715.0*kN* from the *124.2kN* capacity of the unmodified support. NCTS-M was subjected to the most severe blast scenarios, with a *98.0kPa* reflected pressure and *154.4kN* upper support reactions. These pressures would have exceeded capacity had the support not been modified. As a result, the specimen did not suffer catastrophic support failure similar to NCTS-1 and experienced only minor damage in this region. The analysis was performed using only the six outer stirrups in the upper layer to adhere to CSA A23.3-04 spacing requirements, otherwise theoretical resistance would be approximately *1686kN*. CSA A23.3-04 however limits shear resistance of the section to $v_r = 0.55\lambda\phi_c\sqrt{f_c'}$, resulting in a reduced allowed design capacity of *194.0kN* per support or *582.1kN* overall.

The analytical approach used in the analysis of the retrofitted support of NCTS-R followed equations outlined by Farghaly and Ueda [15]. Retrofitted supports achieve a theoretical support resistance of *372.9kN* compared to the non-retrofitted support capacity of *146.2kN*. While specimen NCTS-R was subjected to *99.5kPa* blast pressures, the corresponding support reactions were only *103.6kN*. This was a product of the reduced capacity of the repair section and the dissipation of energy associated with the extent of flexural failure. As a result, retrofitted support experienced minor damage.

Overall, the modified support performed substantially better than the other specimens with an overall strength increase of *590.8kN*. It also outperformed other panels, exhibiting very minor damage to the supports under extremely load scenarios. Analytical results show that the application

of a surface bonded FRP retrofit would produce an approximate increase of *226.7kN*. Alternatively, small fluctuations in the depth of the punching shear failure plane produce large variations in punching shear resistance. Therefore, increasing the concrete thickness around the supports is an alternate design measure to increase support capacity.

Table 5.1 – Support Fixity from Analysis of Strain Data

	Support Fixity: %wl²/8									
	SRC-1		***NCTS-1***		***NCTS-2***		***NCTS-M***		***NCTS-R***	
Test	***Bot***	***Top***	***Bot***	***Top***	***Bot***	***Top***	***Bot***	***Top***	***Bot***	***Top***
1	0.67	0.67	0.21	0.33						
2	0.4	0.2	0.42	0.68						
3	0.45	0.3	0.67	0.5						
4	0	0	0.7	0.22	0.9	0.35	0.8	0	0.57	0.45
5	0	0	0.85	0	0.88	0.35	0.7	0	0.7	0.34
6					0.9	0	0.7	0		

Table 5.2 – Summary of I_{eff} and System Damping

Specimen	***Peak Reflected Pressure*** P_r ***kPa***	***Maximum Inbound Impulse*** I_r ***kPa-ms***	***Effective Moment of Inertia*** I_{eff} ***x 10⁶ mm⁴***	***System Damping*** c ***N-s/m***
NCTS-1: 1	20.6	191.6	419.6	18821.8
NCTS-1: 2	39.5	403.2	325.3	16573.2
NCTS-1: 3	72.6	973.3	247.4	14453.7
NCTS-1: 4	88.1	1079.8	227.2	13850.2
NCTS-1: 5	78.8	1859.2	215.7	13493.9
NCTS-2 1	72.4	1590.1	237.6	13481.1
NCTS-2 2	91.0	2343.1	211.1	12705.9
NCTS-2 3	88.6	2254.4	211.1	12705.9
NCTS-M: 1	73.9	1759.1	237.3	14231.6
NCTS-M: 2	98.0	2410.4	210.5	13403.7
NCTS-M: 3	71.3	1596.2	210.5	13403.7
NCTS-R: 1	74.9	1687.0	210.3	13324.2
NCTS-R: 2	99.5	2271.3	210.3	13324.2

Table 5.3 – Composite Behaviour of NCTS Panels from Analysis of Experimental Strain Data

Test	***Composite Behaviour: Percentage of Fully Composite***			
	NCTS-1	***NCTS-2***	***NCTS-M***	***NCTS-R***

1	100			
2	100			
3	41			
4	45	32.4	32.1	34.1
5	0	15.8		31.4
6		17.2	29.6	

Table 5.4 – Theoretical Punching Shear Resistance of Unmodified and Non-Retrofitted Supports

Panel	*Compressive Strength* f_c' *MPa*	*βc*	α_c	*Depth of Shear Plane* d *mm*	*Critical Section Perimeter* b_0 *mm*	*Shear Resistance* *CSA A23.4 (13-5)* v_{r1} *MPa*	*CSA A23.4 (13-6)* v_{r2} *MPa*	*CSA A23.4 (13-7)* v_{r3} *MPa*	*Shear Resistance per Support* V_{conn} *(kN)*	*Total Shear Resistance* $V_r = n \cdot V_{conn}$ *(kN)*
SRC-1	39.2	2.36	3	36.5	450.0	2.31	2.84	2.50	37.9	113.5
NCTS-1	41.8	2.36	3	36.5	450.0	2.38	2.93	2.58	39.1	117.2
NCTS-2	34.3	2.36	3	46.5	470.0	2.15	2.99	2.34	47.1	141.3
NCTS-M	42.7	2.36	3	38.0	453.0	2.40	3.03	2.60	41.4	124.2
NCTS-R	40.4	2.36	3	46.5	470.0	2.34	3.24	2.54	51.1	153.3

Table 5.5 – Theoretical Punching Shear Resistance of Reinforced Supports for NCTS-M

Panel	*Compressive Strength* f_c' *MPa*	*Depth of Shear Plane* d *mm*	*Critical Section Perimeter* b_0 *mm*	*Area of Shear Rebar* A_{yv} mm^2	*Yield Strength of Shear Rebar* f_{yv} *MPa*	*Shear Resistance of Concrete* V_c *kN*	*Shear Resistance of Steel* V_s *(kN)*	*Single Support Shear Resistance* V_{conn} *(kN)*	*Total Shear Resistance* $V_r = n \cdot V_{conn}$ *(kN)*
NCTS-M	42.7	38.0	453.0	187.0	480.0	22.4	215.9	238.3	715.0

Table 5.6 – Theoretical Punching Shear Resistance of Retrofitted Supports for NCTS-R

Panel	*Compressive Strength* f_c' *MPa*	*Depth of Shear Plane* d *mm*	*Critical Section Perimeter* b_0 *mm*	*FRP Reinforcement Ratio* ρ_f mm^2	ξ	k	*Single Support Shear Resistance* V_r *(kN)*	*Total Shear Resistance* $V_r = n \cdot V_{conn}$ *(kN)*
NCTS-R	42.7	46.5	470.0	0.016	0.157	0.15	124.3	372.9

Table 5.7 – Peak Applied Load, Static Support Reactions, Dynamic Support Reactions, and Support Punching Shear Resistance

Specimen	*Shot*	*Peak Reflected Pressure* P_r *kPa*	*Peak Applied Load* $F = P_r \cdot A_L$ *kN*	*Dynamic Support Reaction* V_f *kN*	*Support Shear Stress* v_f *MPa*	*Upper Support Shear Resistance* V_r *kN*
SRC-1	1	18.2	75.2	35.0	0.71	**113.5**
	2	39.6	163.7	54.8	1.01	
	3	70.6	291.8	81.7	1.65	
	4	91.3	377.4	**92.4**	**1.88**	
	5	71.2	294.3	82.5	1.67	
NCTS-1	3	72.6	300.1	74.1	4.5	**117.2**
	4	88.1	364.1	93.2	5.7	
	5	78.8	325.7	116.0	7.1	
	6	96.1	397.2	**141.1**	**8.6**	
NCTS-2	1	72.4	299.2	100.1	4.6	**141.3**
	2	91.0	376.1	110.4	5.1	
	3	88.6	366.2	**114.0**	**5.2**	
NCTS-M	1	73.9	305.4	108.7	6.3	**715.0**
	2	98.0	405.0	**154.4**	**9.0**	
	3	71.3	294.7	100.2	5.8	
NCTS-R	1	74.9	309.6	89.2	4.1	**372.9**
	2	99.5	411.2	**103.6**	4.7	

Table 5.8 – Summarized Comparison of Experimental Data and Analytical Results; Maximum Displacement and Time-to-Maximum-Displacement

Specimen	*Shot*	*Maximum Mid-Span Displacement*			*Time-to-Maximum Displacement*			*Residual Mid-Span Displacement*		
		Experimental δ_{exp} *mm*	*Analytical* δ_{ana} *mm*	$\delta_{ana}/\delta_{exp}$	*Experimental* t_{exp} *ms*	*Analytical* t_{ana} *ms*	t_{ana}/t_{exp}	*Experimental* $\delta_{r,exp}$	*Analytical* $\delta_{r,ana}$	$\delta_{r,ana}/\delta_{r,exp}$
SRC-1	1	3.12	2.7	0.86	17.8	14	0.79	0.309	0	0
	2	15.6	14.6	0.94	25.6	21.5	0.84	3.98	0.59	0.15
	3	50.8	42.7	0.84	32.4	30	0.92	22.96	14.1	0.61
	4	110.8	111.7	1.01	43.4	41	0.94	66.06	52.3	0.79
	5	>258.5	190.7	0.74	-	49	-	223.8	121.3	0.542
NCTS-1	1	1.49	0.39	0.26	19.6	6.5	0.33	0.412	0	0
	2	3.90	1.7	0.44	19.2	11.5	0.60	1.05	0.53	0.5
	3	12.0	10.8	0.90	25.6	20	0.78	3.46	4.3	1.24
	4	25.2	31.2	1.24	28.8	25.8	0.90	10.12	15.5	1.53
	5	45.6	49.6	1.09	39.4	27	0.68	23.64	30.3	1.28
	6	-	-	-	-	-	-	-	-	-
NCTS-2	1	25.5	15.90	-	45.1	30.8	-	7.51	7.53	1.00
	2	~52.8	64.5	-	-	44.4	-	17	27.7	1.63
	3	~77.7	110.6	-	-	48.8	-	37	63.2	1.70
NCTS-M	1	13.4	15.84	1.18	33.5	31.5	0.94	1.98	6.03	3.05
	2	68.5	81.8	1.19	47.7	48.5	1.02	37.5	30.18	0.80
	3	72.5	91.3	1.26	36.5	40.5	1.11	45.6	38.55	0.84
NCTS-R	1	39.8	39.6	0.99	47.5	48	1.01	14.2	14.9	1.05
	2	124.8	132.8	1.06	62.6	58	92.6	97.1	77.45	0.80

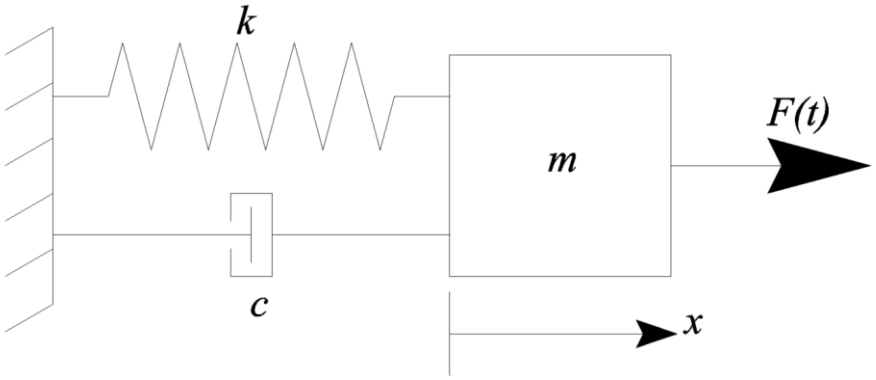

Figure 5.1 – Idealized Spring-Mass Single Degree-of-Freedom Systems

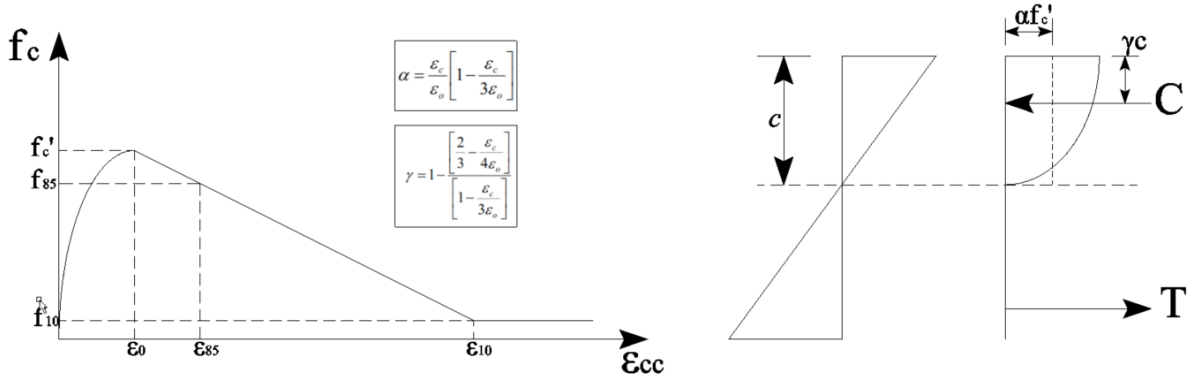

Figure 5.2 - Hognestad's Parabolic Stress Block

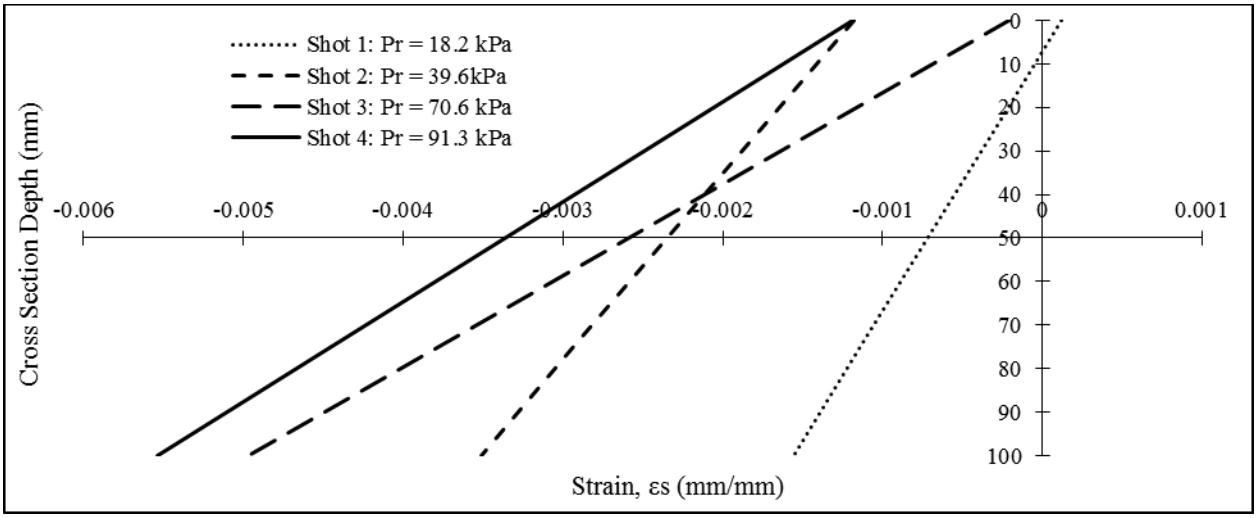

Figure 5.3 - SRC-1 Sectional Strain Profile

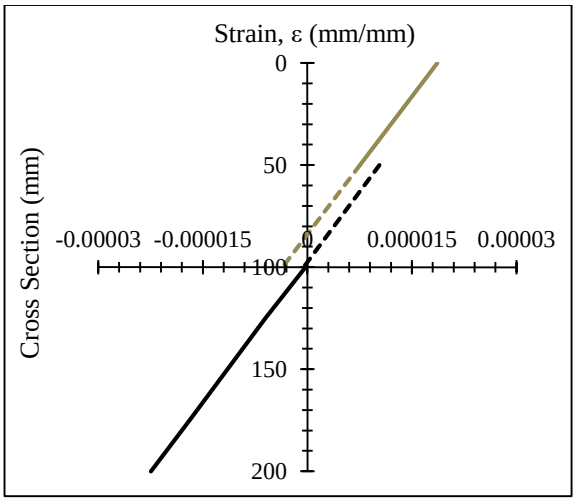

a) Shot 1: P_r = 20.6kPa

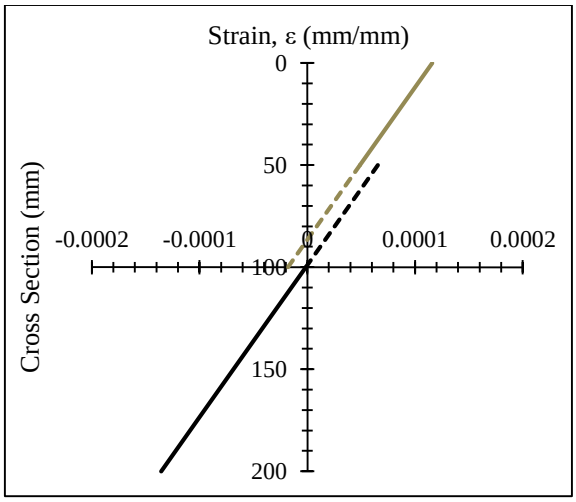

b) Shot 2: P_r = 39.5kPa

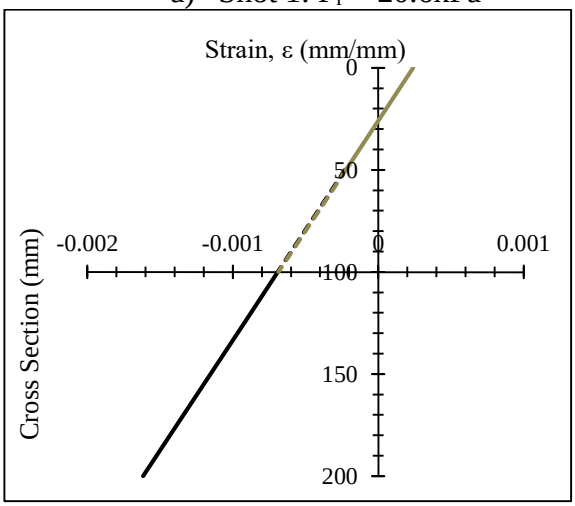

c) Shot 3: P_r = 72.6kPa

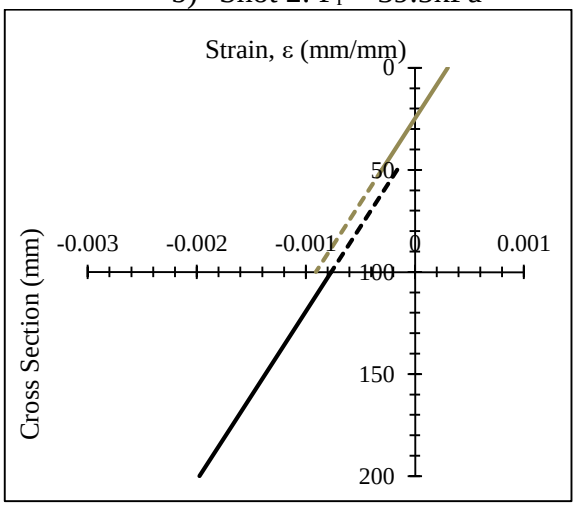

d) Shot 4: P_r = 88.1kPa

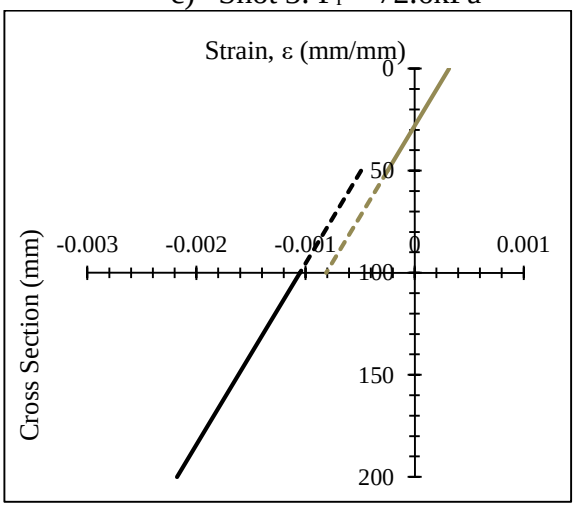

e) Shot 5: P_r = 78.8kPa

-

Figure 5.4 – NCTS-1: Equilibrated Section Strain Profile

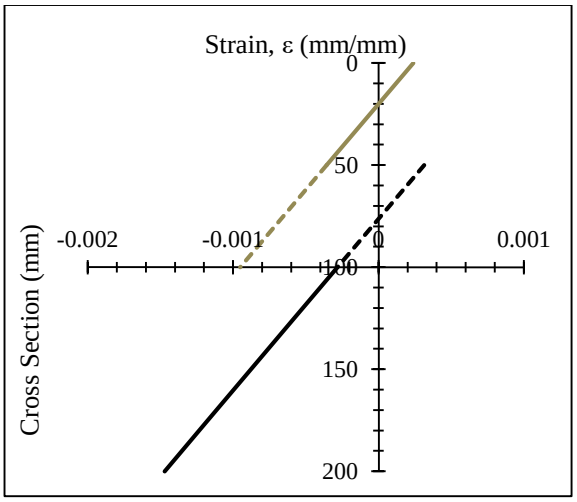

a) Shot 1: P_r = 72.4kPa

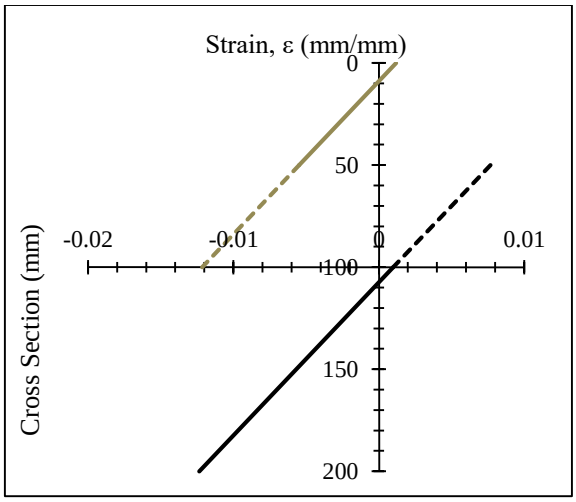

b) Shot 2: P_r = 91.0kPa

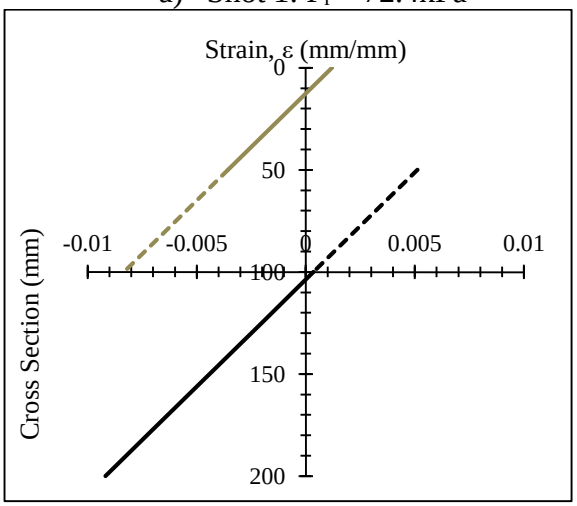

c) Shot 3: P_r = 88.6kPa

Figure 5.5 – NCTS-2: Equilibrated Section Strain Profile

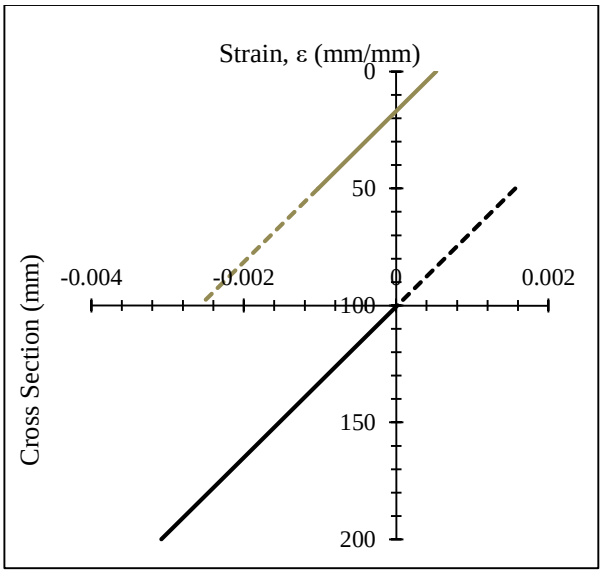

a) Shot 1: P_r = 73.9kPa

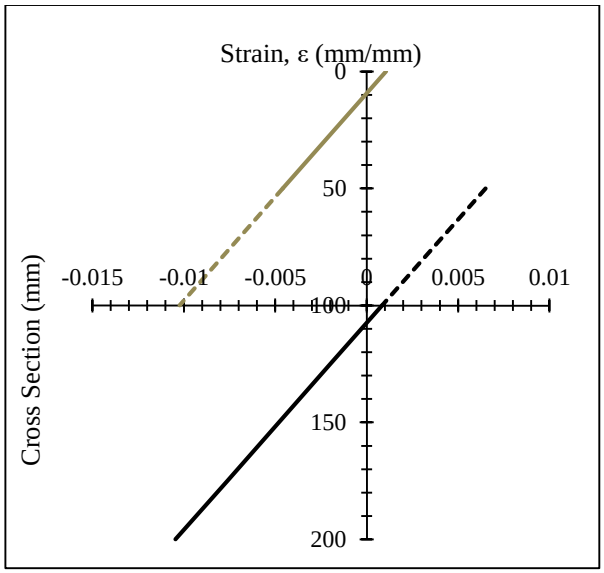

b) Shot 2: P_r = 98.0

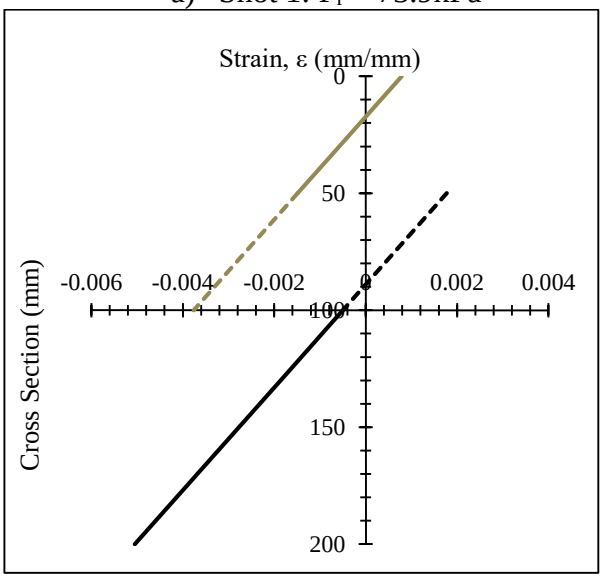

c) Shot 3: P_r = 88.6kPa

Figure 5.6 – NCTS-M: Equilibrated Section Strain Profile

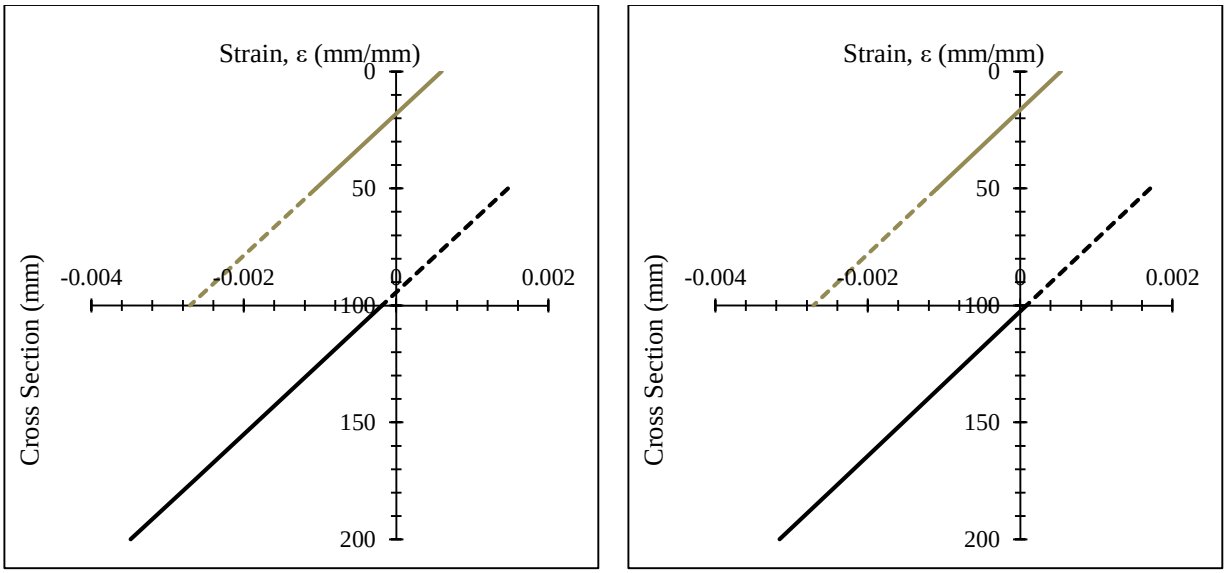

a) Shot 1: P_r = 74.9kPa b) Shot 2: P_r = 99.5kPa

Figure 5.7 – NCTS-R: Equilibrated Section Strain Profile

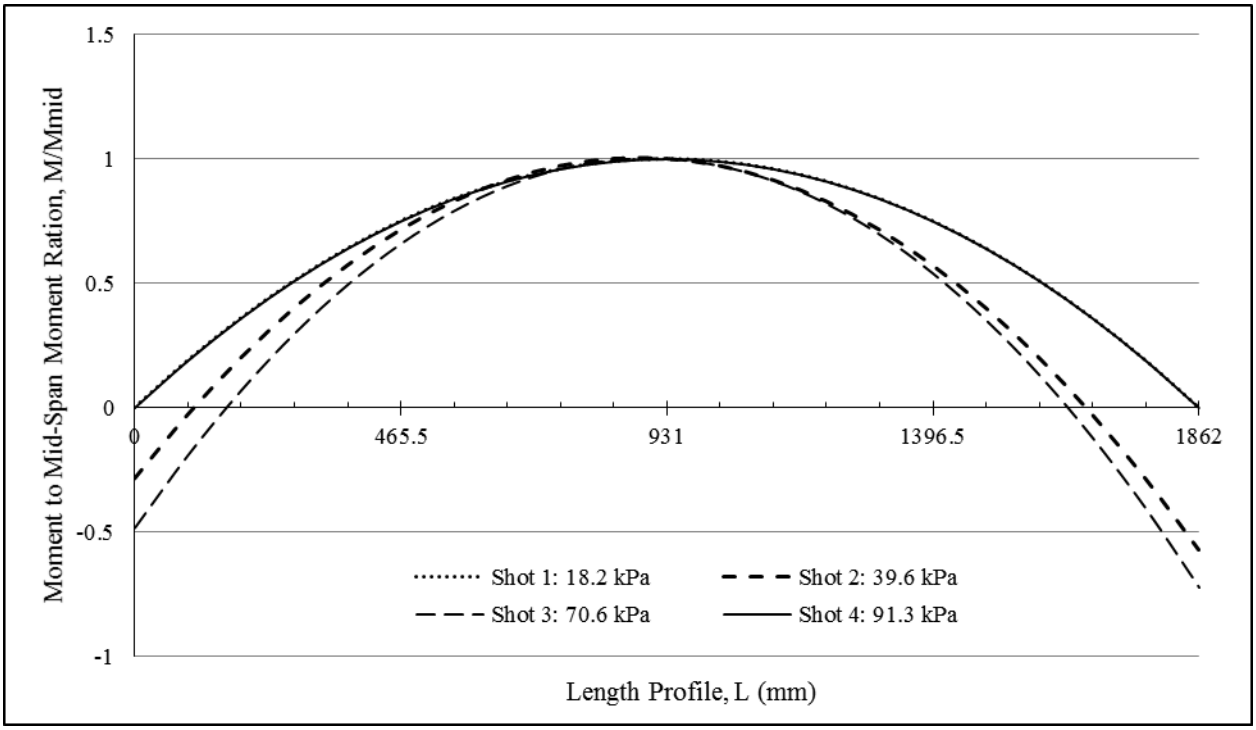

Figure 5.8 – SRC-1: Experimental Moment Distribution Strain Data

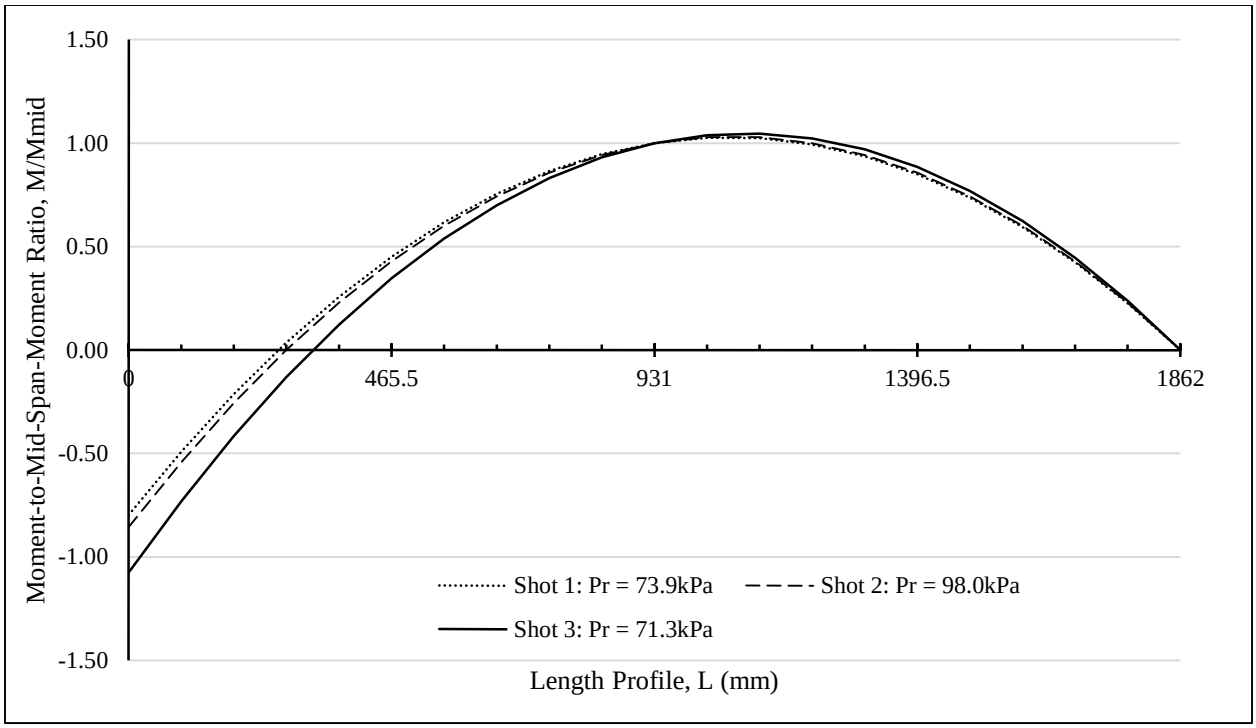

Figure 5.9 – NCTS: Typical Experimental Moment Distribution Strain Data

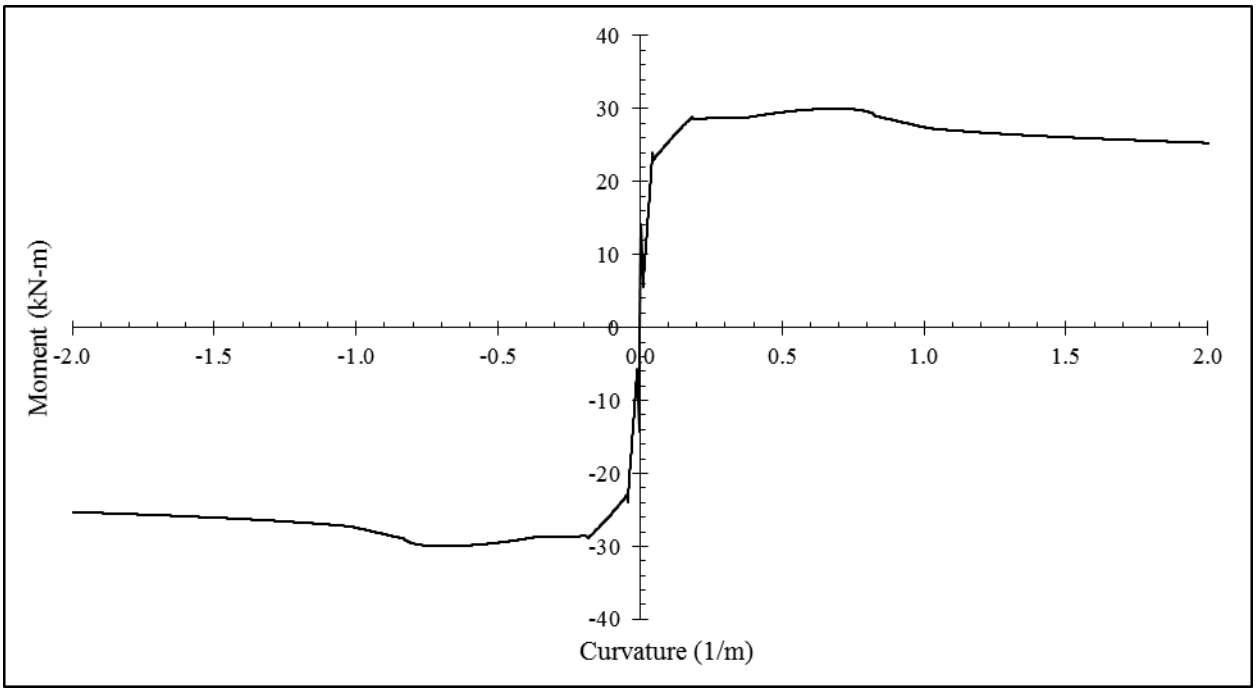

Figure 5.10 – Idealized Moment Curvature and Actual Moment Curvature for Non-Composite and Fully Composite Sandwich Panels

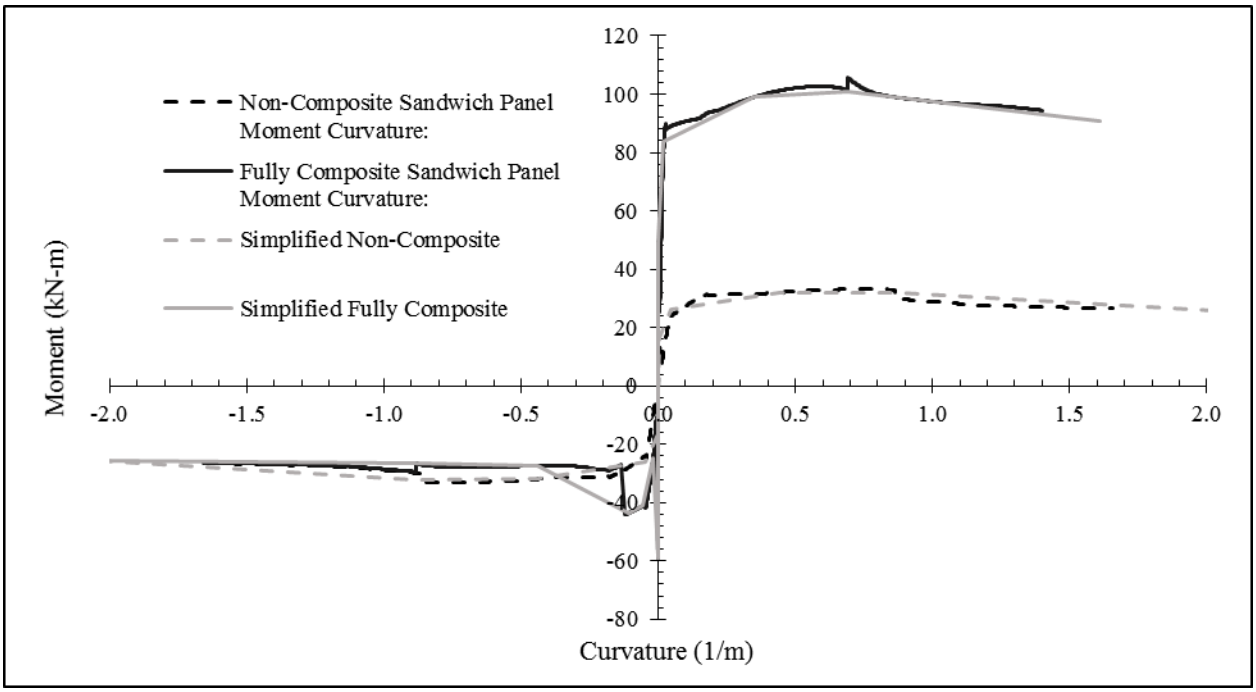

Figure 5.11 – SRC-1 Moment-Curvature Relationship

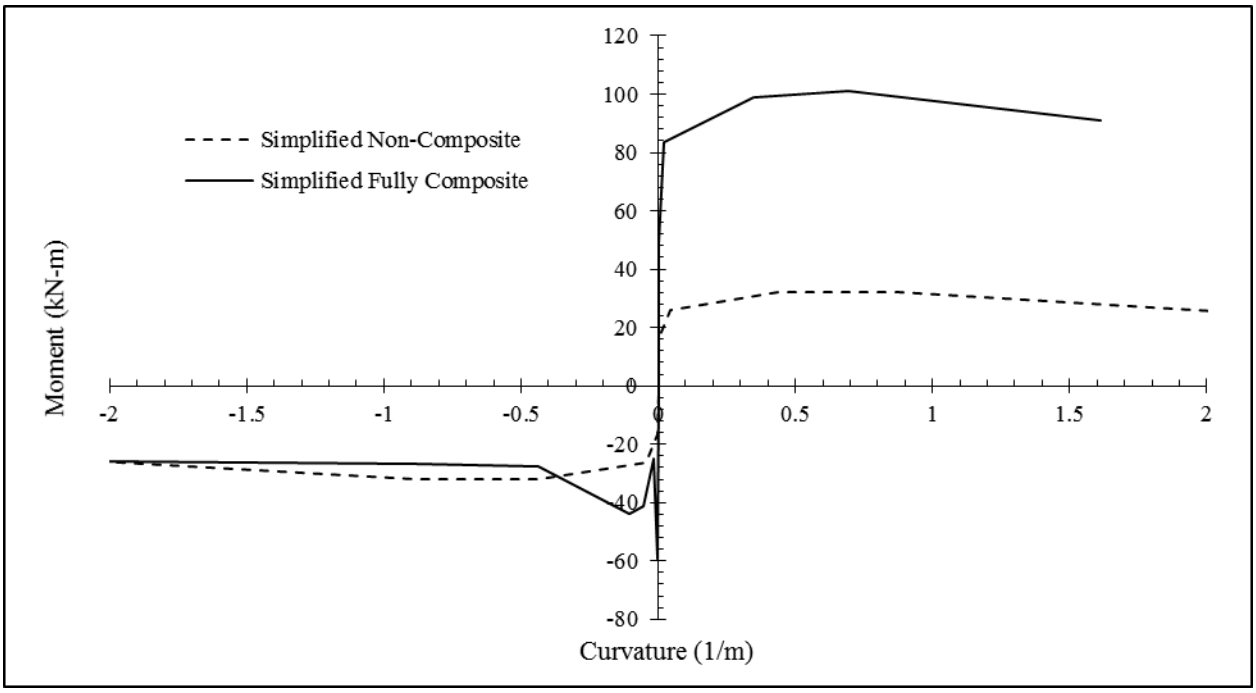

Figure 5.12 – NCTS-1: Idealized Moment-Curvature Diagram

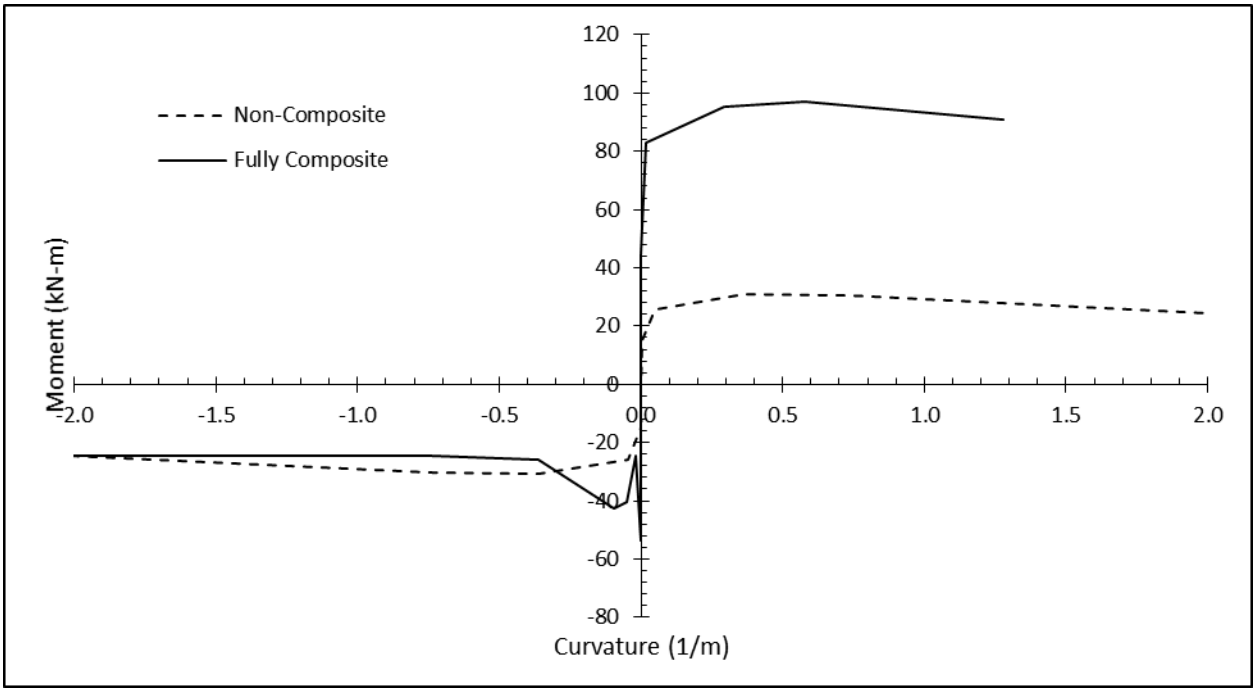

Figure 5.13 – NCTS-2: Idealized Moment-Curvature Diagram

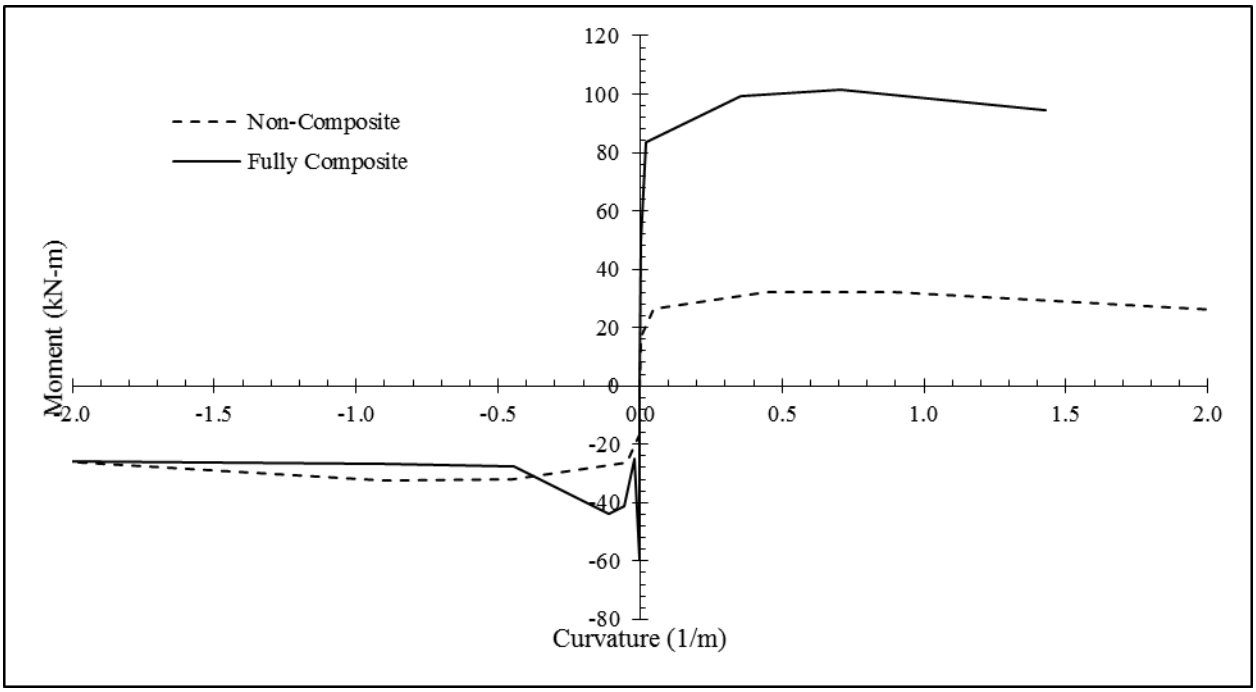

Figure 5.14 – NCTS-M: Idealized Moment-Curvature Diagram

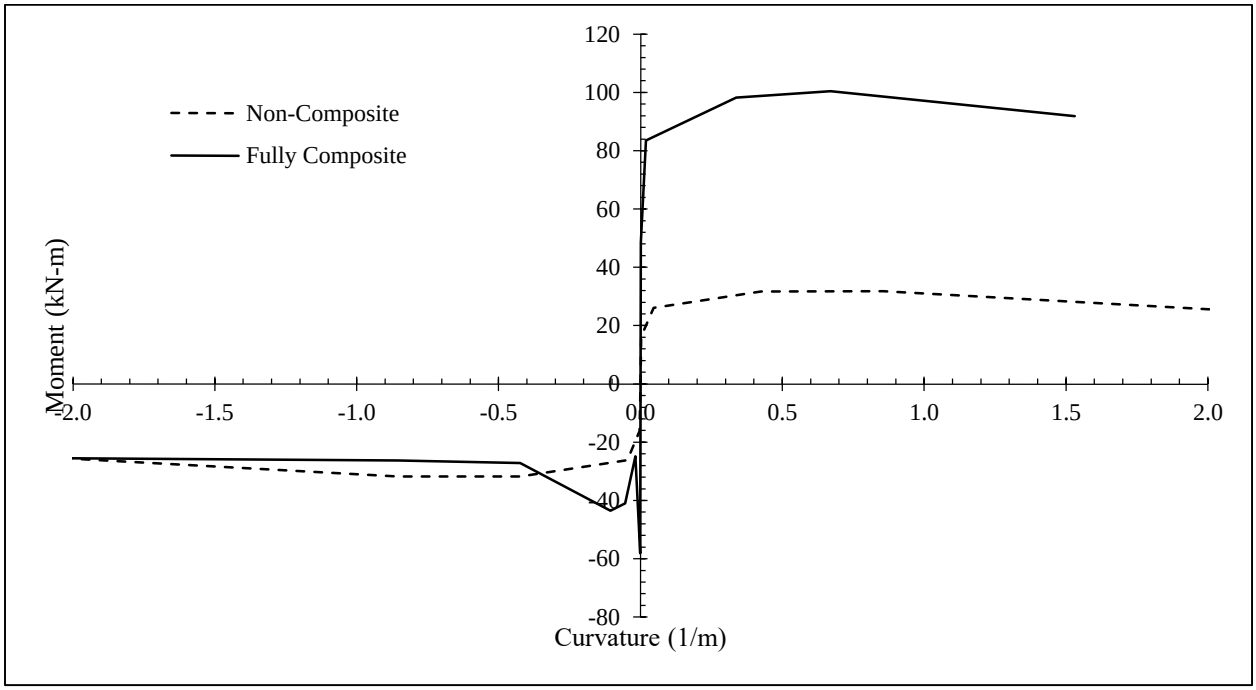

Figure 5.15 – NCTS-R: Idealized Moment Curvature Diagram

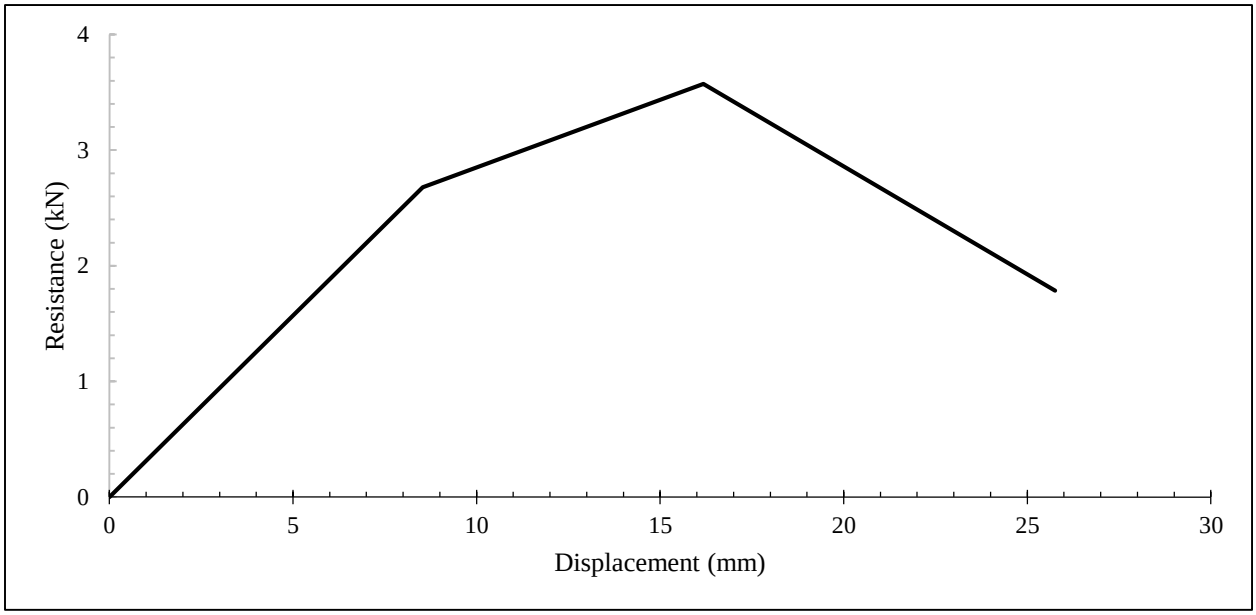

Figure 5.16 – Backbone of Shear Tie Force-Deformation Relationship (Reproduced from Naito et Al. [11])

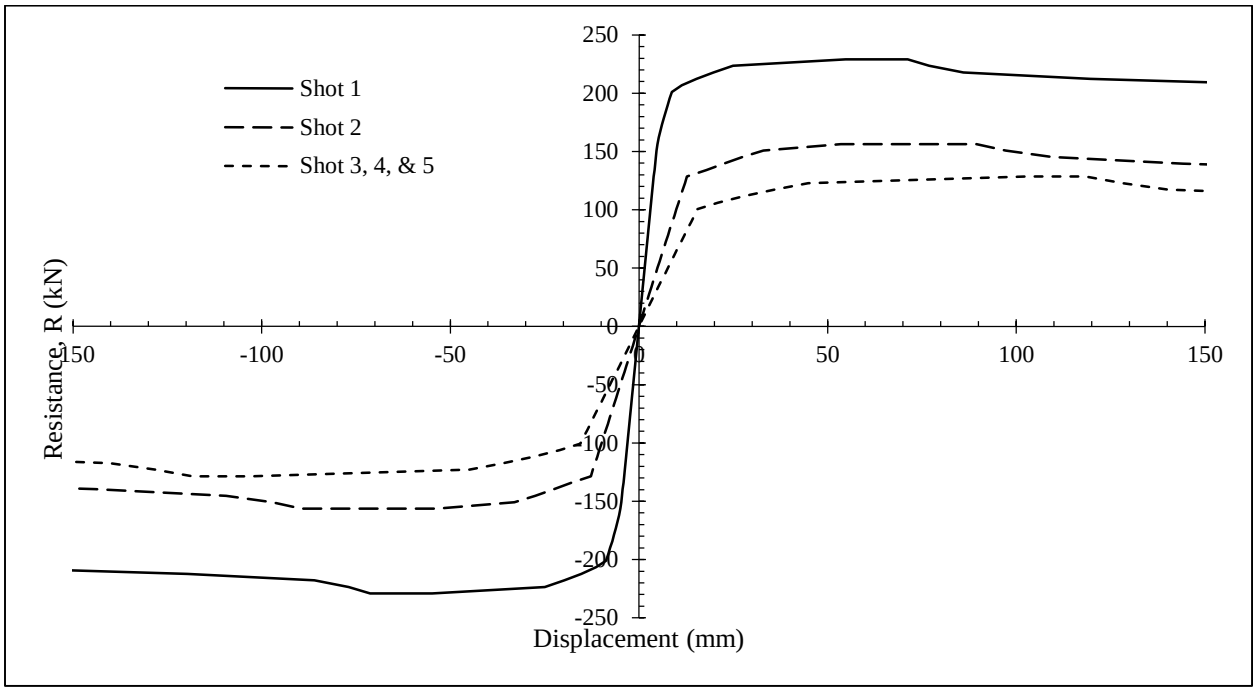

Figure 5.17 – SRC-1: Resistance Curve

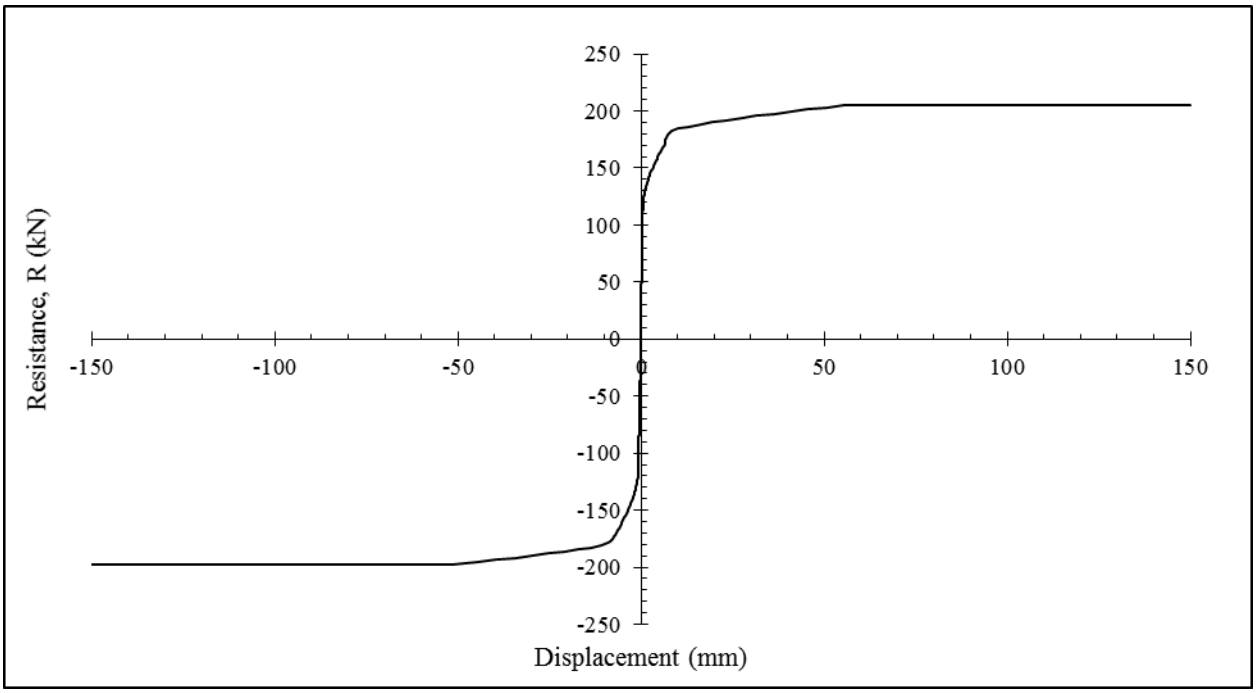

Figure 5.18 – NCTS-1 Resistance Curve

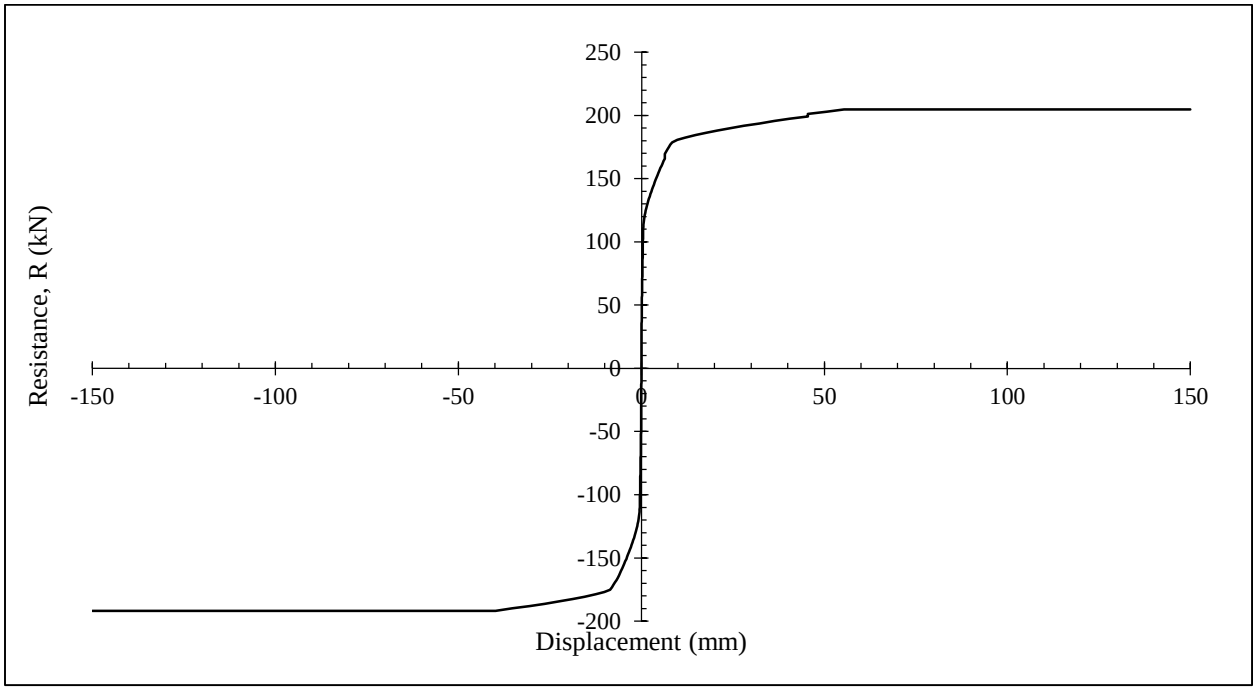

Figure 5.19 – NCTS-2 Resistance Curve

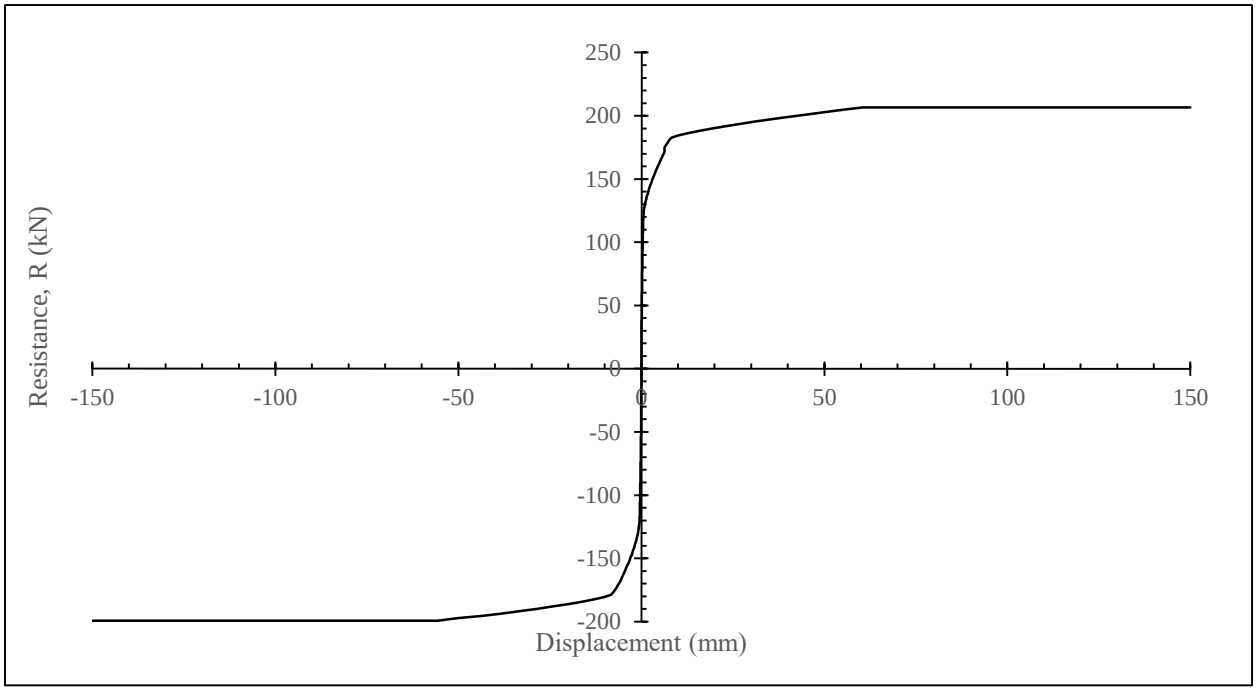

Figure 5.20 – NCTS-M Resistance Curve

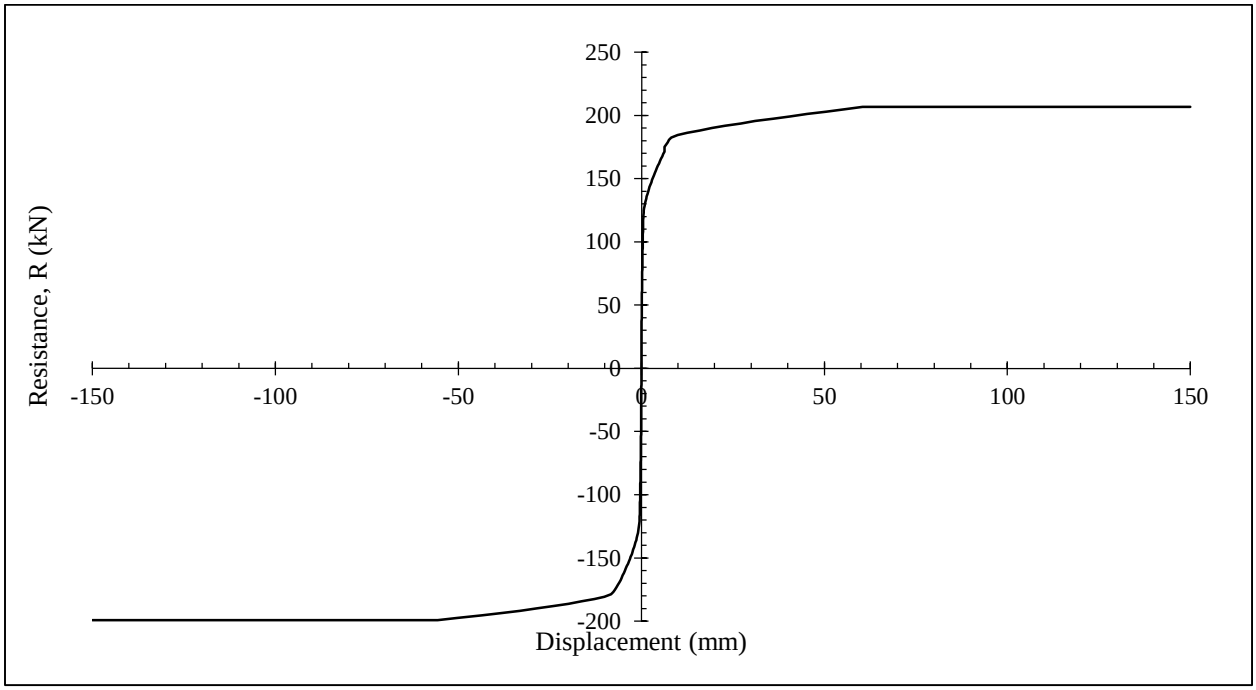

Figure 5.21 – NCTS-R Resistance Curve

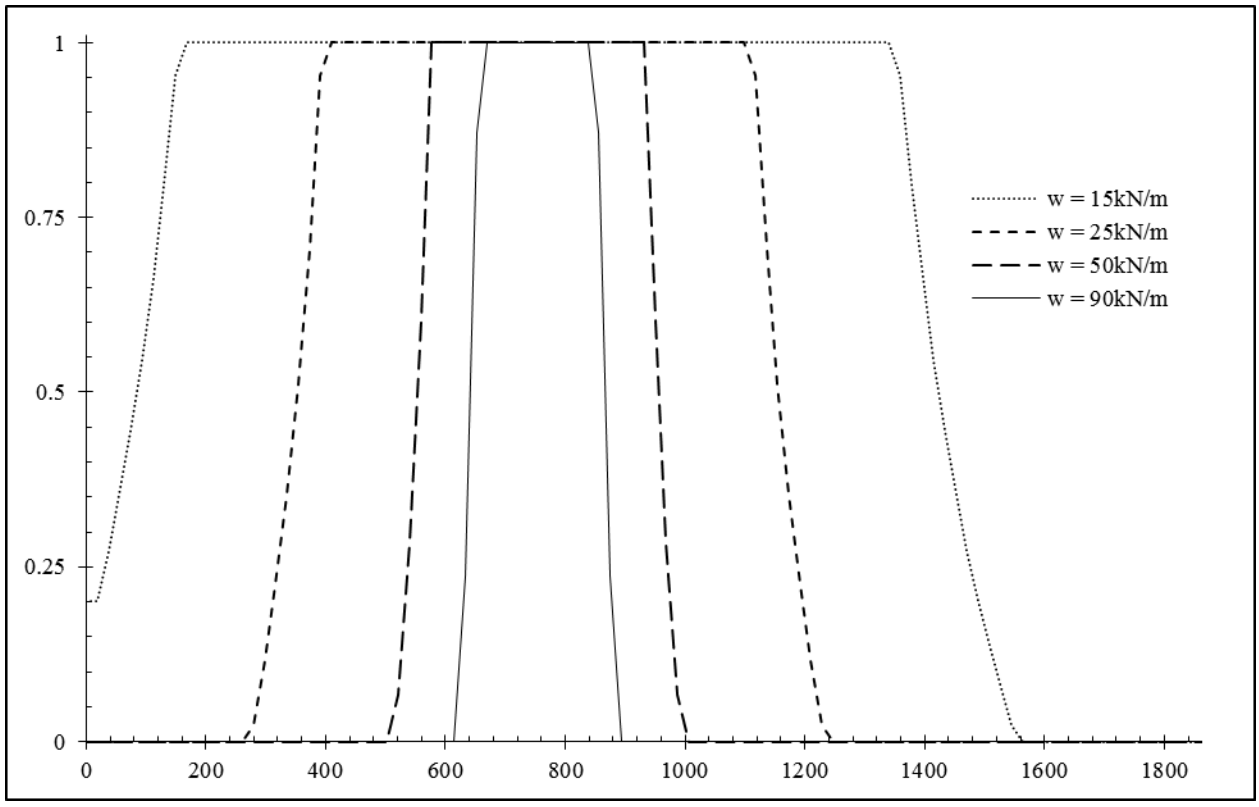

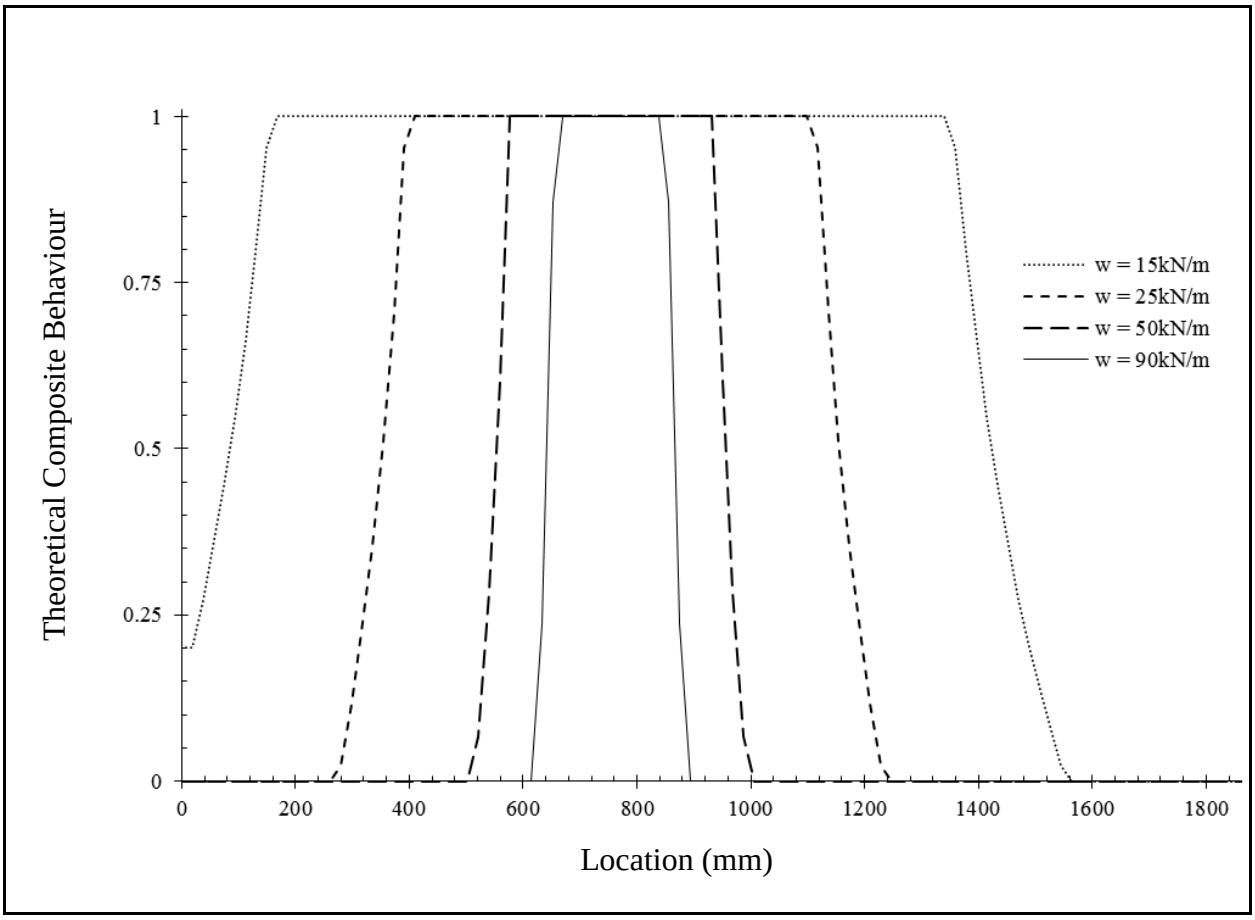

Figure 5.22 – Typical Theoretical Degradation of Composite Behaviour in a NCTS Panel

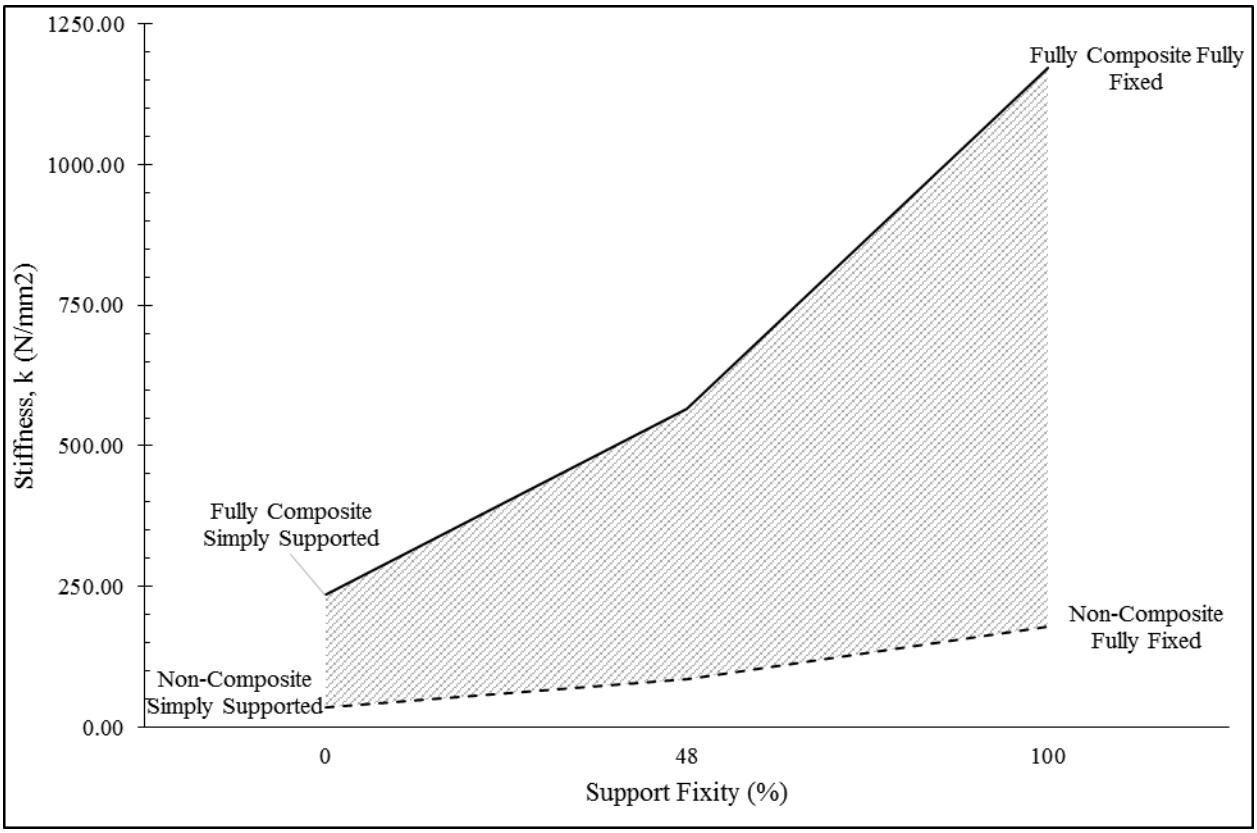

Figure 5.23 – Distribution of Member Stiffness based on Composite Behaviour and Boundary Conditions

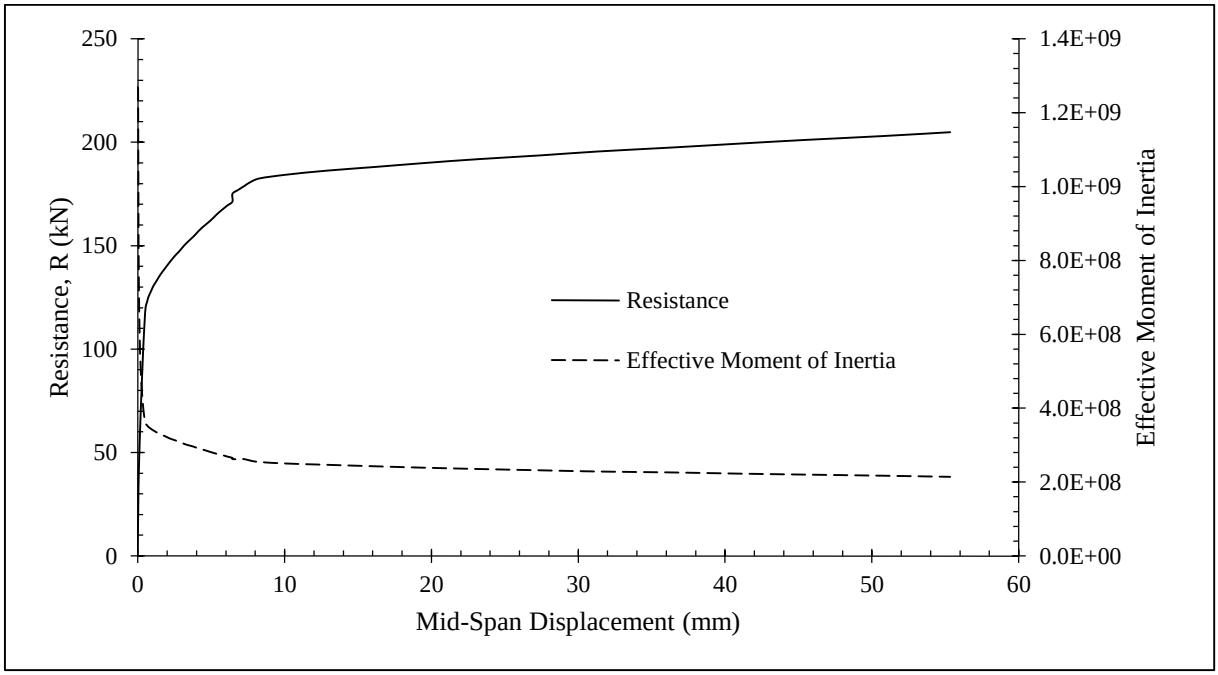

Figure 5.24 – Resistance Curve vs. Effective Moment of Inertia for Typical NCTS Panel

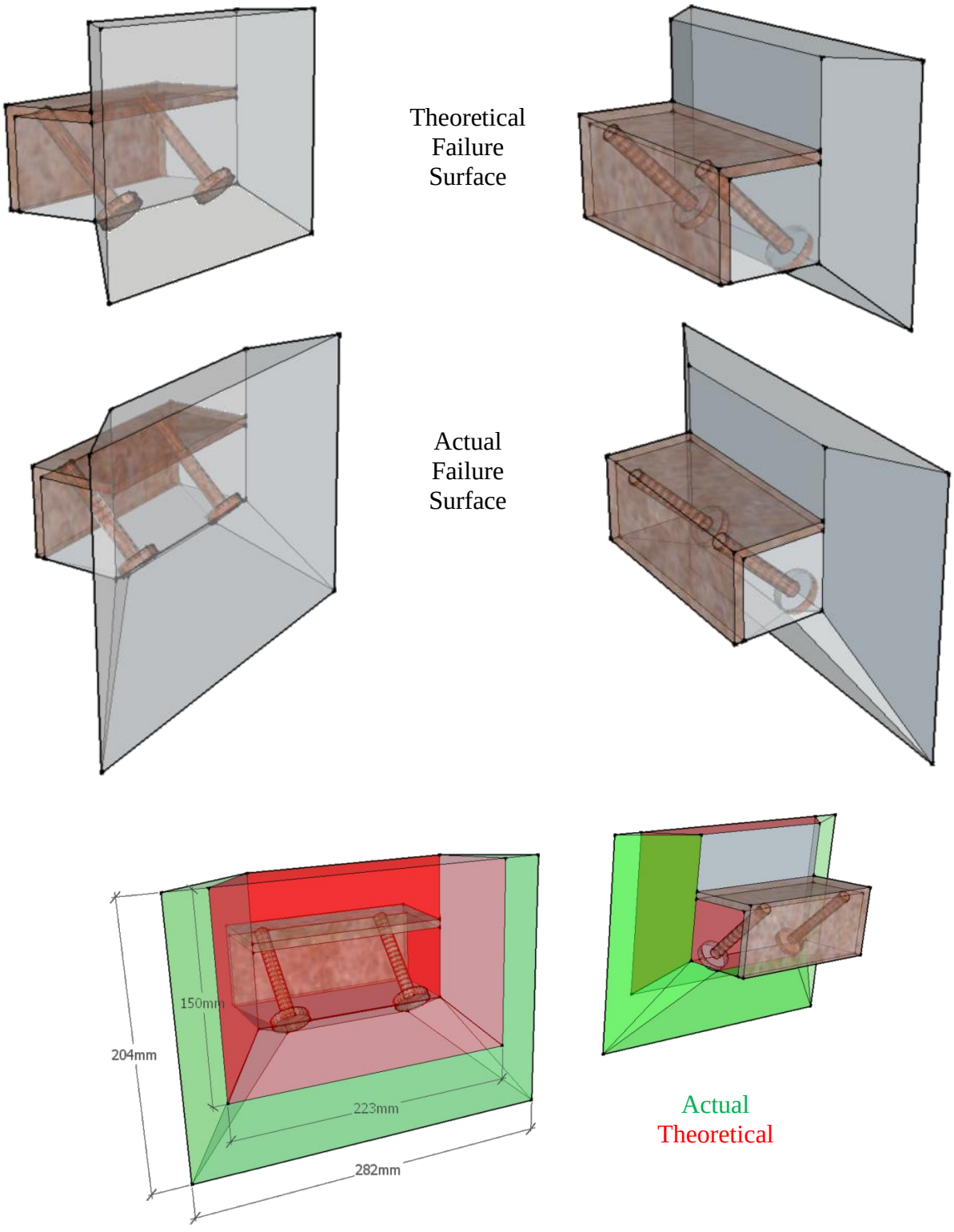

Figure 5.25 – Three-Dimensional Comparison of NCTS-1 Average Failure Surface and Approximate Punching Shear Failure Surface

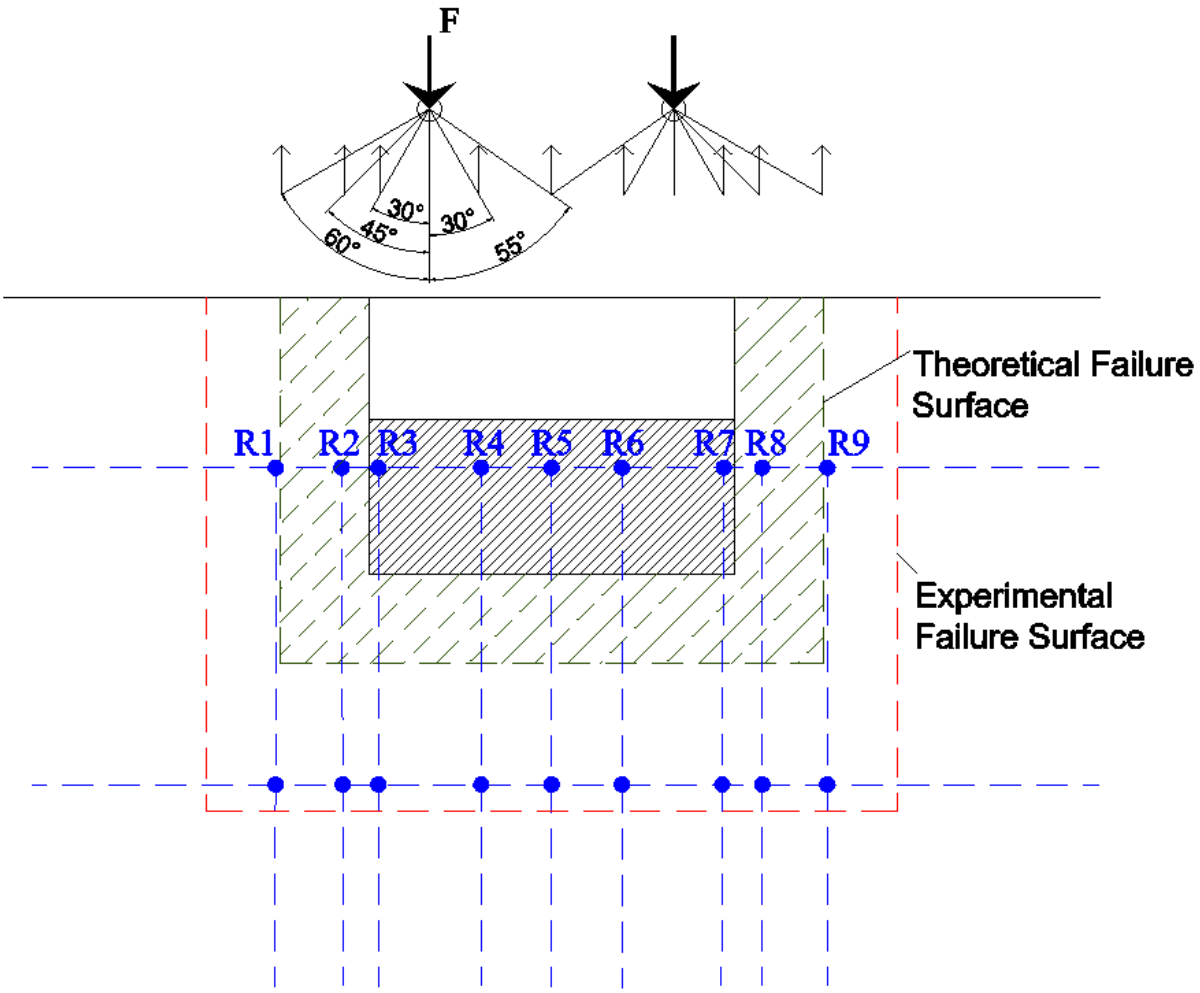

Figure 5.26 – Theoretical Force Distribution of Modified Support Reinforcement

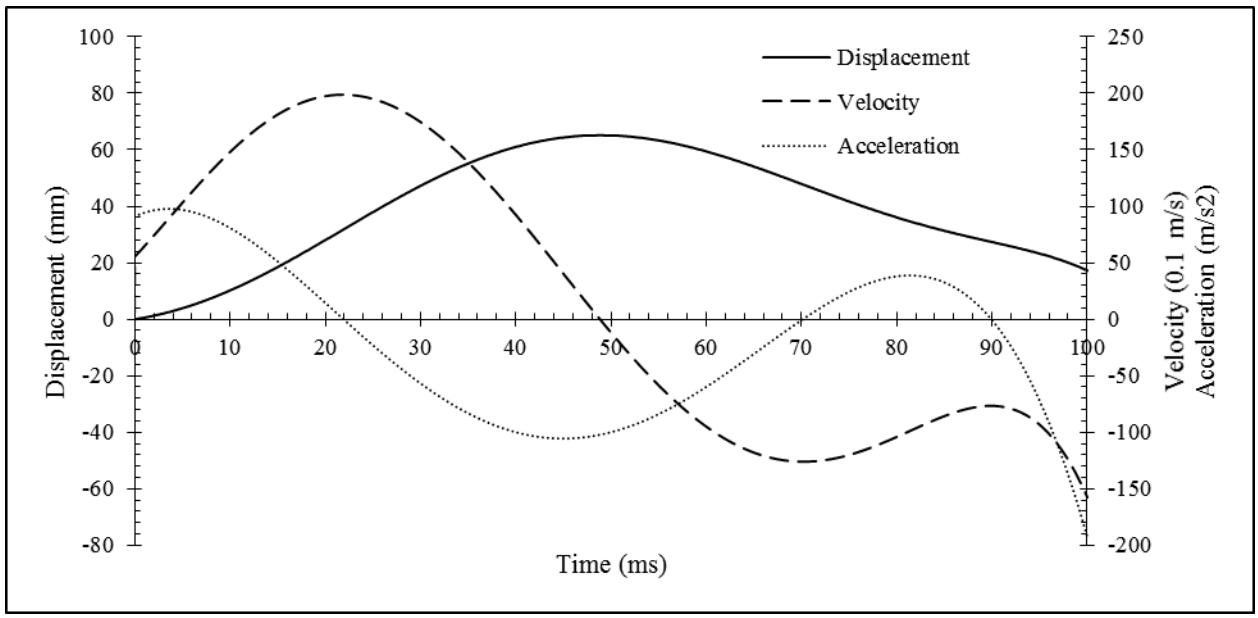

Figure 5.27 – Typical Theoretical Displacement-Time, Velocity-Time, and Acceleration-Time Histories

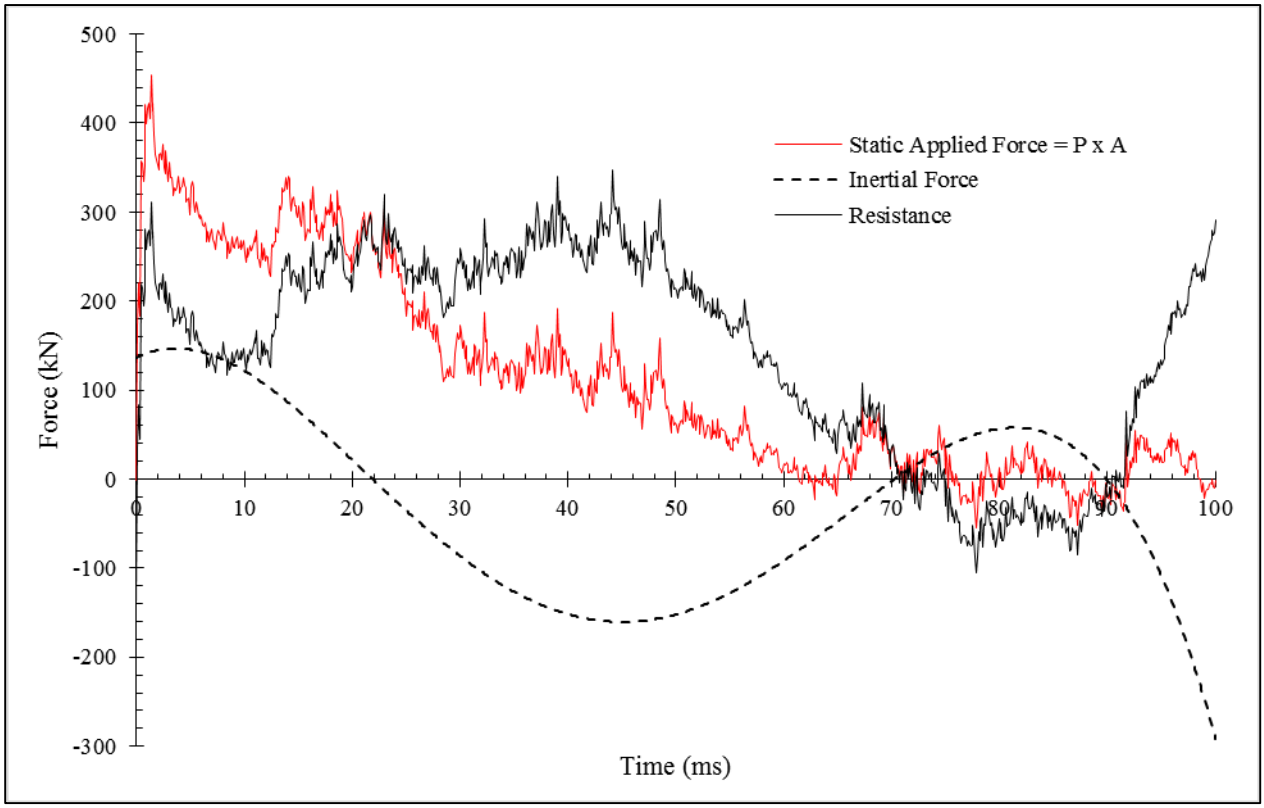

Figure 5.28 – Typical Theoretical Force-Time, Inertial Force-Time, and Resistance-Time Histories

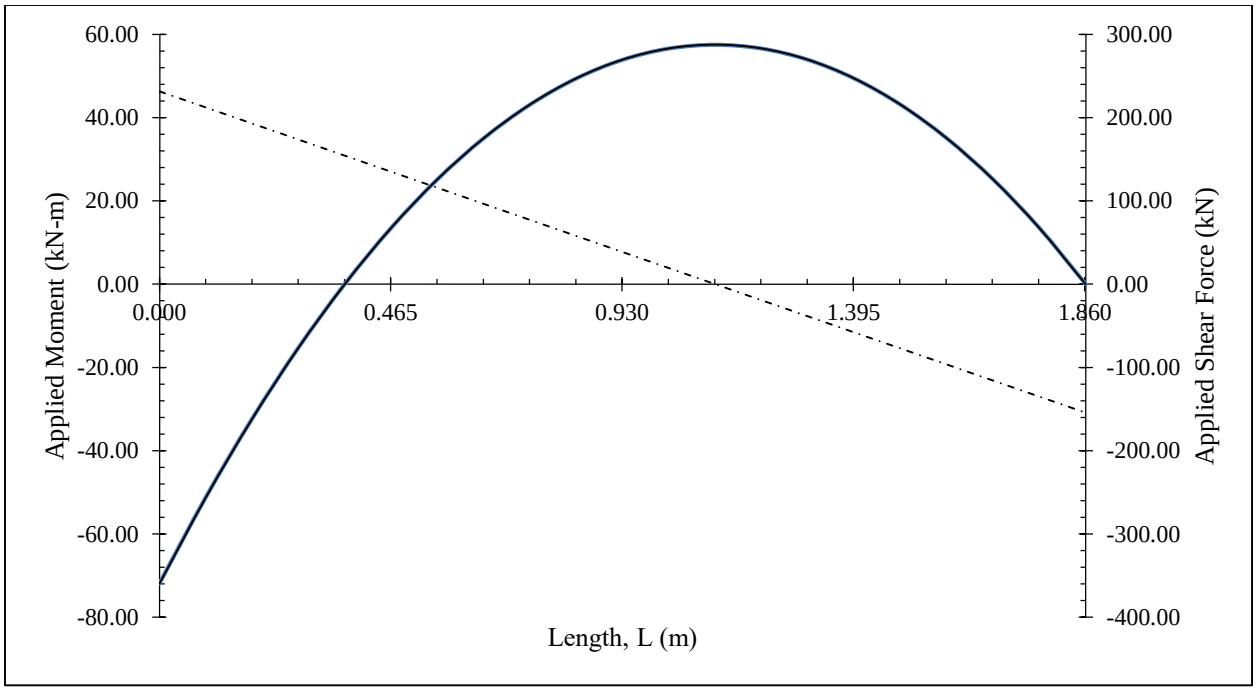

Figure 5.29 – NCTS: Typical Moment and Shear Force Diagram

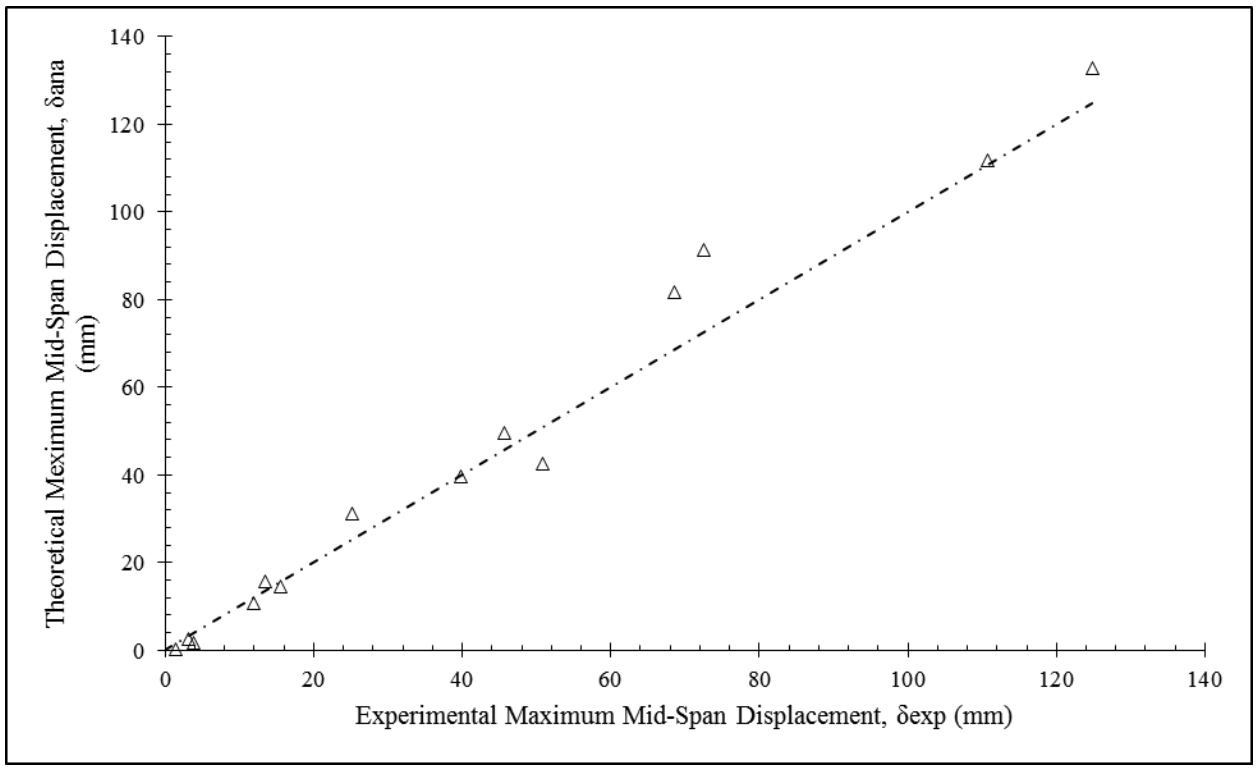

Figure 5.30 – Analytical vs. Experimental Maximum Mid-Span Displacement

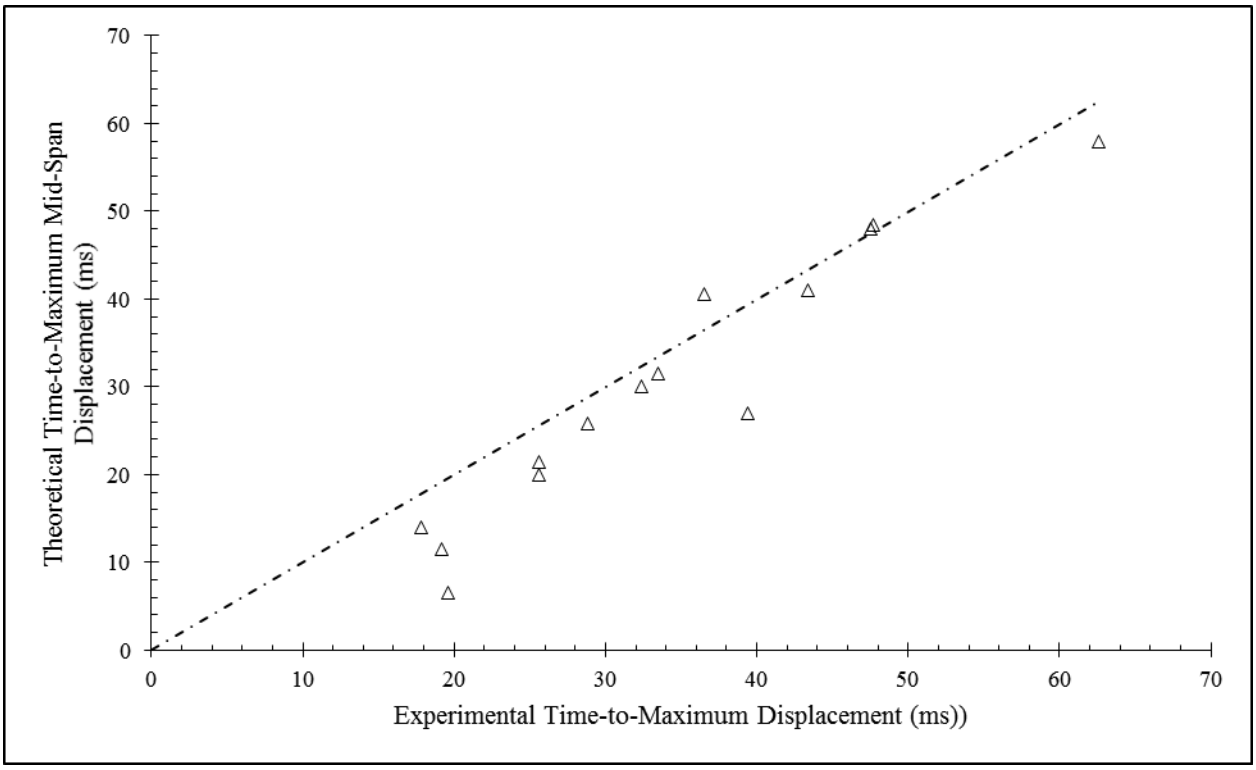

Figure 5.31 – Analytical vs. Experimental Time-to Maximum Mid-Span Displacement

6.0 Application of Analytical Findings

NCTS panel are inherently well suited to sustain blast loads due to the mass of thick concrete wythes and the flexural capacity required for erection. However, performing a blast assessment of any particular panel could indicate an inability to sustain the flexural forces associated with extreme blast pressures or the susceptibility of the panel's support system to large dynamic loads. Two full scale specimens were designed, one with an *8000mm* span and one with *4000mm* span, and analysed against blast loads similar to historical events. The *8000mm* single span panel, NCTS-FS8, is representative of a school auditorium or a warehouse. The *4000mm* single span panel, NCTS-FS4, is representative of a typical single span single storey wall. All calculations, excluding panel design, were performed using nominal resistance and did not incorporate material reduction factors.

6.1 Panel Design

CSA A23.3-04 employs the moment magnification method for the design of slender one-way NCTS panels. A design program written in Microsoft® Excel® was used to perform all necessary structural checks. A print screen of the design page is shown in Figure 6.1. A detailed drawing of each panel is provided in Figure 6.2 to Figure 6.4.

NCTS-FS8 and NCTS-FS4 each have a width of *4000mm* with a *165mm* structural wythe, a *50mm* layer of insulation, and a *75mm* architectural wythe. Each specimen is reinforced with two layers of eleven *15M* bars in each direction in the structural face and a single layer of *152x152xMW18.1/18.1* WWM. The panel is supported with three joist seats and direct bearing at the top and bottom of the panel, respectively. The joist seats, spaced at *1200mm*, consist of a *300mm* long *90x90x10mm* angle with two *16mm* diameter headed studs embedded *100mm* at *45º*. The base support consists of a *225mm* direct bearing area against the slab on grade.

6.2 Material Properties

6.2.1 Concrete

A specified cylinder strength of *40MPa* was selected for this example. Hognestad's stress-strain relationship was used to model concrete behaviour for sectional analysis. UFC [8] recommended DIF of *1.19* and *1.10* for concrete in bending and direct shear were applied to the dynamic analysis of NCTS-FS8 and NCTS-FS4.

6.2.2 Steel

15M deformed steel reinforcement was selected for this example. The empirical stress-strain relationship presented in Figure 3.15 was used in the analysis of NCTS-FS8 and NCTS-FS4. UFC [8] recommended DIF of *1.17* and *1.05* for the yield and ultimate capacity of steel in flexure were used in the dynamic analysis of NCTS-FS8 and NCTS-FS4.

6.3 Derivation of Load-Deformation Properties

6.3.1 Moment-Curvature

Similarly, to the analysis of the scaled test specimens a six line, five-point moment-curvature relationship was used to accurately reproduce the inbound and rebound response of fully composite panels. Moment-curvature diagrams were constructed for non-composite and fully-composite behaviour within the panel. Partial composite behaviour within the panel can be calculated through interpolation of these two extremes, based on the shear tie degradation at each data point of the resistance curve. For a detailed procedure please refer to Section 5.4.1. The moment-curvature for NCTS-FS8 and NCTS-FS4 are plotted in Figure 6.5.

6.3.2 Shear Tie Degradation

Shear tie degradation is a key component in accurately predicting the composite behaviour in a sandwich panel. Generic shear ties identical to those used in the scaled specimens were spaced at

400mm in each direction. The shear tie load-deformation curve is presented in Figure 5.16 and a detailed analytical procedure is provided in Section 5.4.2.

6.3.3 Resistance Curve

The resistance curves for NCTS-FS8 and NCTS-FS4 are plotted in Figure 6.6 and Figure 6.7, respectively. Each resistance curve was constructed by gradually increasing the applied uniformly distributed load in increments of *1kN/m* until failure of the panel occurred. A total of 251 data points along the panel were selected to build the curvature distribution for inbound and rebound pressures. A detailed outline of the procedure is provided in Section 5.4.3.

6.4 Modelling Displacement-Time Histories

An SDOF analysis was performed on panels NCTS-FS8 and NCTS-FS4 using RC Blast. Displacement-time histories and pressure-impulse diagrams were constructed for different blast loading scenarios. For more detail regarding the capabilities and use of RC Blast refer to Section 5.5.1.

6.4.1 Transformation Factors, System Damping, Mass, and Loaded Area

Transformation factors were applied to the full scale panels following the procedure outlined in 5.5.2. Load-mass transformation factors were assigned to the panel at each load increment during construction of the resistance curve. If no data point on the panel experienced moments in excess of its respective yield capacity the load-mass transformation factor was taken as *0.78*. Upon yielding of any point the load-mass transformation factor of the entire system was changed to *0.66*.

Similarly, system damping was determined following the procedure outlines in 5.5.3. Damping was calculated as *1%* critical damping using a moment of inertia of $2.691x10^9 mm^4$ and $2.267x10^9 mm^4$ for panel NCTS-FS8 and NCTS-FS4, respectively.

The mass of the NCTS-FS8 system was *22747kg* with a loaded area of $32m^2$ while NCTS-FS4 had a total mass of *11373kg* and an exposed surface area of $16m^2$.

6.4.2 Pressure-Time History

A functional characteristic of RC Blast is its ability to generate pressure-time histories for specified charge weight and stand-off distance combinations. NCTS-FS8 and NCTS-FS4 have been analysed under blast pressures similar to those subjected to surrounding structures in the 1995 Oklahoma City Bombing. In this particularly horrific event a truck filled with the equivalent of *2800kg* of TNT was detonated outside the Alfred P. Murrah Federal building in downtown Oklahoma. The blast, which could be heard and felt up to *55km* away, destroyed or damaged hundreds of building and took *168* human lives. This evaluation will determine the ability of NCTS panels to withstand extreme to moderate blast loads.

Shockwave parameters were generated for *2800kg* of TNT at *30m*, *50m*, *70m*, and *100m* stand-off distance.

6.5 Determining Support Loads and Assessing Strengthening Alternatives

The analytical procedure outlined in Section 5.6 specifies the methods used to predict support reactions based on the displacement-time history of the panel. For design purposes it is acceptable to consider the support reactions produced by static load (i.e. $P_r \, x \, A_{Load}$). This method will produce large pressures resulting in a conservative design. For this example, a dynamic analysis was performed to determine support loads.

Four strengthening alternatives were evaluated against the specified blast parameters. Three methods strengthen the member during construction; reinforcing with stirrups, reinforcing with headed bars, and thickening of concrete around the support. Retrofitting with surface bonded FRP laminates is a post-construction strengthening technique. Assessment followed the procedures specified in Section 5.6.

6.6 Discussion of Analytical Results

The displacement-time histories for each shot on NCTS-FS8 and NCTS-FS4 are plotted in Figure D.1 through Figure D.8 in Appendix D. This data is also tabulated in

Table 6.1 with support reaction data. Support resistance of unmodified supports is presented in Table 6.2 while details for modified and retrofitted supports are provided in Table 6.3 through Table 6.6. Pressure impulse diagrams for NCTS-FS8 and NCTS-FS4 are presented in Figure 6.8 and Figure 6.9.

The displacement-time history for all tests indicate that full-scale NCTS panels are capable of sustaining the flexural demands of even the most powerful blast parameters. The *NCTS-FS4* suffered lower mid-span displacements than NCTS-FS8, however both experienced very similar support rotations with only a *14%* difference on average. The maximum difference between the two panels support rotations was *1.36º*. Each specimen sustained loads near its peak resistance, however rotations are far below the failure criteria specified in CSA S850-12 [1].

The dynamic reactions presented in

Table 6.1 indicate that both full-scale NCTS panels suffer support failure for *30m*, *50m*, and *70m* stand-off distances. The panels are capable of sustaining the specified blast loads when the charge is placed *100m* or more from the panel. Otherwise modification is required. Thickening of the concrete surrounding the support is an effective method of increasing the punching shear resistance of the supports. Concrete can easily be added around the supports during casting with minimal cost increase. However, to produce significantly enhanced strength the concrete layer must be thick and will likely create a thermal bridge in the insulation layer. Also adding solid sections anywhere in the panel will decrease shear tie slip resulting in increased composite behaviour. This will make the panel stiffer, potentially inflating the support reactions.

Installing support reinforcement during panel construction is an efficient way to significantly increase support resistance. The two primary reinforcement methods involve installing either stirrups or headed bars along the perimeter of the support. Table 6.3 and Table 6.4 show that each method successfully strengthens the supports against the specified blast loads to within a *50m* stand-off distance. However, design specifications outlined in CSA A23.3-04 [5] limit the

punching shear resistance of supports reinforced with stirrups to $0.55\lambda\phi_c\sqrt{f_c'}$. As a result, stirrup reinforced supports can only sustain the specified blast loads at a stand-off distance of *70m* or greater. Another disadvantage of stirrup reinforcement is the design limitations of $0.19\lambda\phi_c\sqrt{f_c'}$ to concrete stress within the reinforced zone. The limitation placed on headed bars is less stringent allowing a punching shear resistance up to $0.75\lambda\phi_c\sqrt{f_c'}$ and concrete stress of $0.28\lambda\phi_c\sqrt{f_c'}$. As a result, supports reinforced with headed bars are capable of sustaining the specified blast loads to within *50m* of the panel.

Retrofitting NCTS panels with FRP laminates surface bonded to the tensile face of the structural wythe is an effective means of increasing the support resistance of existing tilt-up structures. This process requires removal of the architectural wythe from a portion of the panel surrounding the support. Surface bonded FRP retrofits increase support resistance enough to maintain the specified the applied blast loads to within *50m*. However, the absence of specific design guidelines may warrant a conservative design with a higher factor of safety.

Limitations to the maximum capacity of the concrete within the reinforced zone, prevented any combination of strengthening techniques from resisting the specified blast loads within *30m* of the panel. Alternative engineer measures such as lower support spacing, increase plate size, or installation of a load distribution mechanism (i.e. concrete slab) on the roof decking could be incorporated into designs to sufficiently increase capacity.

Table 6.1 – Summary of Analytical Results

Specimen	*Shot*	*Peak Reflected Pressure* P_r *kPa*	*Positive Phase Duration* t_d^+ *ms*	*Impulse* I_r *kPa-ms*	*Maximum Mid-Span Displacement* δ_{max} *mm*	*Maximum Upper Support Rotation* θ_{max} *Degrees*	*Upper Support Reaction* V_f *kN*
NCTS-FS8	2800kg @ 30m	876.1	29.3	4745.1	216.2	5.17	8024.7
	2800kg @ 50m	215.5	45.0	2600.5	115.6	2.76	847.2
	2800kg @ 70m	102.1	53.1	1780.3	76.1	1.82	443.0
	2800kg @ 100m	53.5	60.3	1205.1	49.1	1.17	256.3
NCTS-FS4	2800kg @ 30m	876.1	29.3	4745.1	136.5	6.53	9109.1
	2800kg @ 50m	215.5	45.0	2600.5	58.0	2.77	737.9
	2800kg @ 70m	102.1	53.1	1780.3	31.1	1.48	410.2
	2800kg @ 100m	53.5	60.3	1205.1	15.7	0.75	205.1

Table 6.2 – Punching Shear Resistance of Unmodified Support

Panel		βc	α_c			*Shear Resistance*			

	Compressive Strength f_c' *MPa*			*Depth of Shear Plane* d *mm*	*Critical Section Perimeter* b_0 *mm*	*CSA A23.4 (13-5)* v_{r1} *MPa*	*CSA A23.4 (13-6)* v_{r2} *MPa*	*CSA A23.4 (13-7)* v_{r3} *MPa*	*Shear Resistance per Support* V_r *(kN)*	*Total Shear Resistance* V_r *(kN)*
FS	40	3.33	3	65	940	2.10	2.74	2.62	128.1	384.4

Table 6.3 – Punching Shear Resistance of Modified Support Reinforced with Stirrups

Specimen	*Shot*	*Upper Support Reaction* V_1 *kN*	*Load per Support* V_{sup} *kN*	*Concrete Resistance per Support* V_c *kN*	V_{sup}-V_c *kN*	*Stirrup Spacing* δ_{max} *mm*	*Area of Shear Reinforcement* A_{vs} mm^2	*Modified Support Resistance* V_s *kN*	*Maximum Support Resistance* $V_{r,max}$ *kN*
NCTS-FS8	2800kg @ 30m	8024.7	2674.9	69.0	**2605.9**	25	2200	2814.62	**199.8**
	2800kg @ 50m	847.2	282.4		**213.4**	100	800	318.62	
	2800kg @ 70m	443.0	147.7		**78.6**	100	400	193.82	
	2800kg @ 100m	256.3	85.43		**N/A**	N/A	N/A	N/A	
NCTS-FS4	2800kg @ 30m	9109.1	3036.4		**2967.3**	25	2400	3064.22	
	2800kg @ 50m	737.9	246.0		**176.9**	150	800	277.02	
	2800kg @ 70m	410.2	136.7		**67.7**	200	400	162.62	
	2800kg @ 100m	205.1	68.4		**N/A**	N/A	N/A	N/A	

Table 6.4 – Punching Shear Resistance of Modified Support Reinforced with Headed Bars

Specimen	*Shot*	*Upper Support Reaction* V_f *kN*	*Load per Support* V_{sup} *kN*	*Concrete Resistance per Support* V_c *kN*	V_{sup}-V_c *kN*	*Stirrup Spacing* δ_{max} *mm*	*Area of Shear Reinforcment* A_{vs} mm^2	*Modified Support Resistance* V_r *kN*	*Maximum Support Resistance* $V_{r,max}$ *kN*
NCTS-FS8	2800kg @ 30m	8024.7	2674.9	101.7	**2573.2**	25	2200	2847.3	**272.4**
	2800kg @ 50m	847.2	282.4		**180.7**	100	600	288.91	
	2800kg @ 70m	443.0	147.7		**46.0**	200	400	164.11	
	2800kg @ 100m	256.3	85.43		**N/A**	N/A	N/A	N/A	
NCTS-FS4	2800kg @ 30m	9109.1	3036.4		**2934.7**	25	2400	3096.9	
	2800kg @ 50m	737.9	246.0		**144.3**	100	800	288.9	
	2800kg @ 70m	410.2	136.7		**35.0**	200	400	164.1	
	2800kg @ 100m	205.1	68.4		**N/A**	N/A	N/A	N/A	

Table 6.5 – Punching Shear Resistance of Support Retrofitted with Surface Bonded FRP Laminates

Specimen	*Shot*	*Upper Support Reaction* V_f *kN*	*Load per Support* V_{sup} *kN*	*Concrete Resistance per Support* V_c *kN*	*Number of FRP Layers Required* n_{frp}	*Retrofitted Support Capacity* V_f *kN*
NCTS-FS8	2800kg @ 30m	8024.7	**2674.9**	110.4	N/A	**N/A**
	2800kg @ 50m	847.2	**282.4**		3	**289.95**
	2800kg @ 70m	443.0	**147.7**		2	**165.17**
	2800kg @ 100m	256.3	**85.43**		N/A	**N/A**
NCTS-FS4	2800kg @ 30m	9109.1	**3036.4**		N/A	**N/A**
	2800kg @ 50m	737.9	**246.0**		3	**289.95**
	2800kg @ 70m	410.2	**136.7**		2	**165.17**
	2800kg @ 100m	205.1	**68.4**		N/A	**N/A**

Table 6.6 – Punching Shear Resistance of Support with Thickened Concrete Section

Specimen	*Shot*	*Upper Support Reaction* V_f *kN*	*Load per Support* V_{sup} *kN*	*Increase in Thickness Required* d^+ *mm*	*Retrofitted Support Capacity* V_r *kN*
NCTS-FS8	2800kg @ 30m	8024.7	**2674.9**	N/A	**N/A**
	2800kg @ 50m	847.2	**282.4**	80	**295.3**
	2800kg @ 70m	443.0	**147.7**	20	**151.5**
	2800kg @ 100m	256.3	**85.43**	N/A	**N/A**
NCTS-FS4	2800kg @ 30m	9109.1	**3036.4**	N/A	**N/A**
	2800kg @ 50m	737.9	**246.0**	65	**246.4**
	2800kg @ 70m	410.2	**136.7**	15	**140.9**
	2800kg @ 100m	205.1	**68.4**	N/A	**N/A**

Design Summary:		
Controlling L Load Case 7		
Vertical Rein	15	375
Resisting Mc	32.6	

Lifting Design Summary		
Maximum Lif	11.3	
Lifting Line L	3025	6625
Resisting Mc	14.4	

Concrete Properties	
Normal Weight Concrete	
Φc	1
fc' (MPa):	28
fr (Mpa):	3.17
Ec (MPa):	23812
Specific Grav (kN/m^3)	24
Φm	1
	1
α1 = 0.85 - 0.0015 x fc' =	0.808
β1 = 0.97 - 0.0025 x fc' =	0.9
Eccentricity (mm):	0.0825
	0.1

Steel Properties	
fy (MPa):	400
Es (MPa):	200000
Φs	1
Tensile Steel	
Rebar Diameter, db (mm):	15
Rebar spacing, s (mm):	375
Bar Area, Abar (mm^2):	200
As Tension Face, (mm^2/m):	533.33
Minimum Cover (mm):	25.00
Tens. Rebar Depth, dst (mm):	132.5
Steel Ratio:	0.003232
As Compression Face, (mm^2/m):	533.3333
Comp. Rebar Depth, dsc (mm):	30

Panel Properties	
Height (mm)	8000
Structural Wythe Thickness (mm)	165
Architectural Wythe Thickness (mm)	75
Total Panel Thickness	290
Width (mm)	8000
Joist Span(mm)	5450
l/t = Height / Thickness =	48
	Single Reinforcement Mat
Select No. of Reinf. Layers:	Two
Effect. Moment of Inertia, Ie (mm^4):	3.01E+08
Gross Moment of Inertia, Ig (mm^4):	3.74E+08
Cracked Moment of Inertia, Icr (mm^4):	6.71E+07
Bending Stiffness (kN-m/m)	
Kbf = 48 x Ec x Icr / 5 x L^2 =	239.6

Serviceability Check	
Cracking Moment (kN-m/m):	14.41
Effective Moment of Inertia, Ie (mm^4):	3.74E+08
Serviceability Bending Stiffness	
Kbs (kN-m) = 48 x Ec x Ie/ (5 x L^2) =	1337.07
viceability Bending Moment, Mbs (kN-m	11.44
Moment Mag. Fact, δbs:	1.03
Serviceability Moment, Ms (kN-m/m):	11.75
	Mcr > Ms
Serviceability Displacement, Δs (mm):	8.8

Load Properties/Resistance								
Self Weight (kPa):	192							
Unfactored Dead Load (kPa):	1.30							
Unfactored Snow Load (kPa):	2.16							
UnfactoredWind Load (kPa):	1.35							
	Load Case 1	Load Case 2	Load Case 3	Load Case 4	Load Case 5	Load Case 6	Load Case 7	Load Case 8
Superimposed, Ptf (kN/m):	9.9	14.7	8.9	26.5	26.5	8.9	14.7	6.4
Half Panel W, Pwf (kN/m):	32.26	28.80	28.80	28.80	28.80	28.80	28.80	20.74
Lateral Load, wf (kPa):	0	0	0.542	0	0.542	1.896	1.896	1.896
Deflection-PΔ Effect, Δ0	0.002	0.003	0.022	0.006	0.028	0.074	0.077	0.070
	Converges	Converges	Converges	Converges	Converges	Converges	Converges	Converges
Mb (kN-m/m)	0.49	0.74	5.56	1.41	7.01	18.38	19.20	17.41
Moment Mag. Fact, δb:	1.21	1.22	1.19	1.30	1.30	1.19	1.22	1.13
Fact. Moment, Mb (kNm/m):	0.6	0.9	6.6	1.8	9.1	21.8	23.5	19.6
Equiv. Steel Area, Ase (mm^2):	639	642	627	672	672	627	642	601
ae (mm):	11.3	11.4	11.1	11.9	11.9	11.1	11.4	10.6
Resisting Moment, Mr (kN-m/m):	32.4	32.6	31.9	34.0	34.0	31.9	32.6	30.6
	Mr > Mf	Mr > Mf	Mr > Mf	Mr > Mf	Mr > Mf	Mr > Mf	Mr > Mf	Mr > Mf

Figure 6.1 – NCTS Panel Design Software

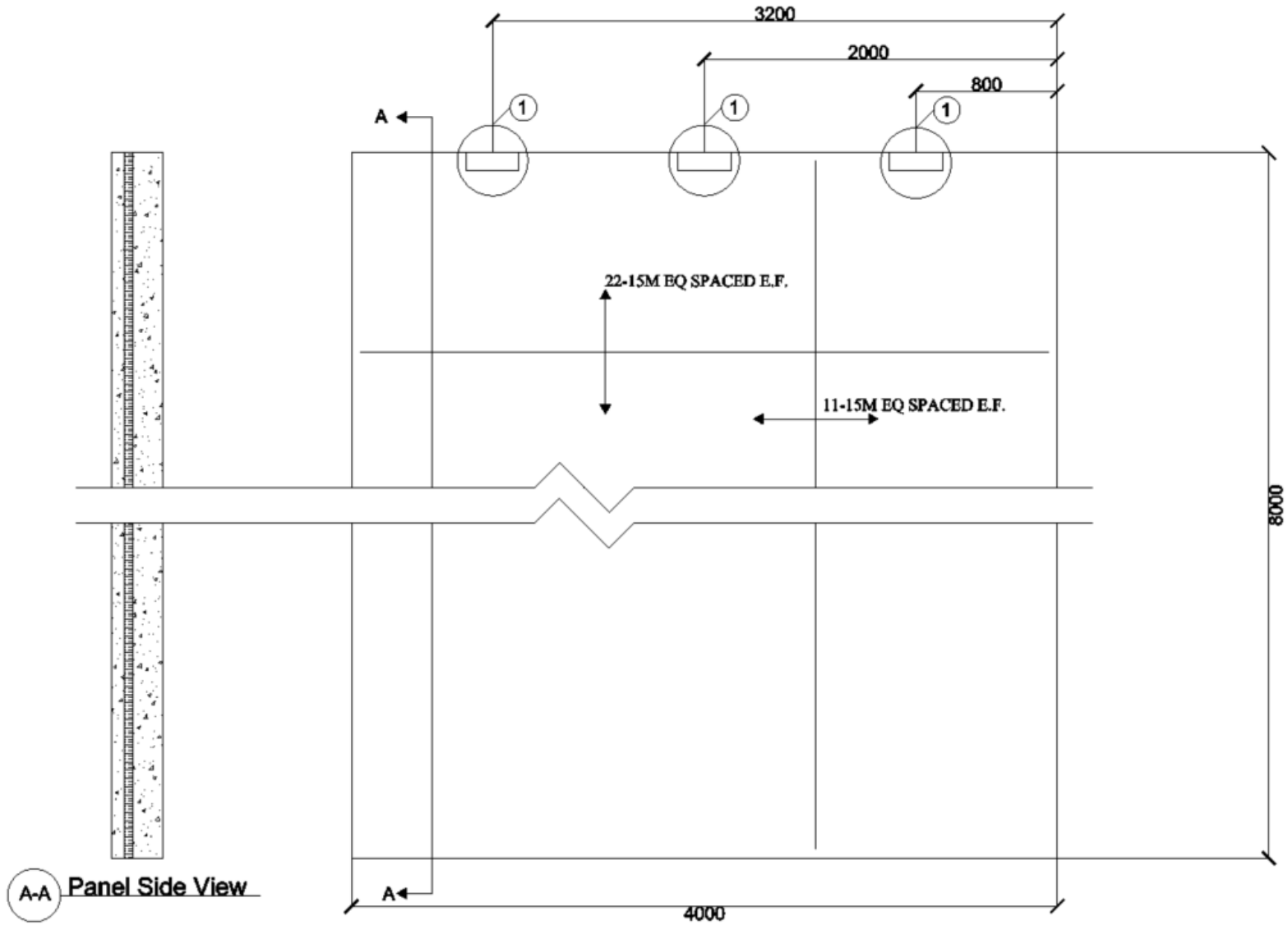

Figure 6.2 – NCTS-FS8 Details

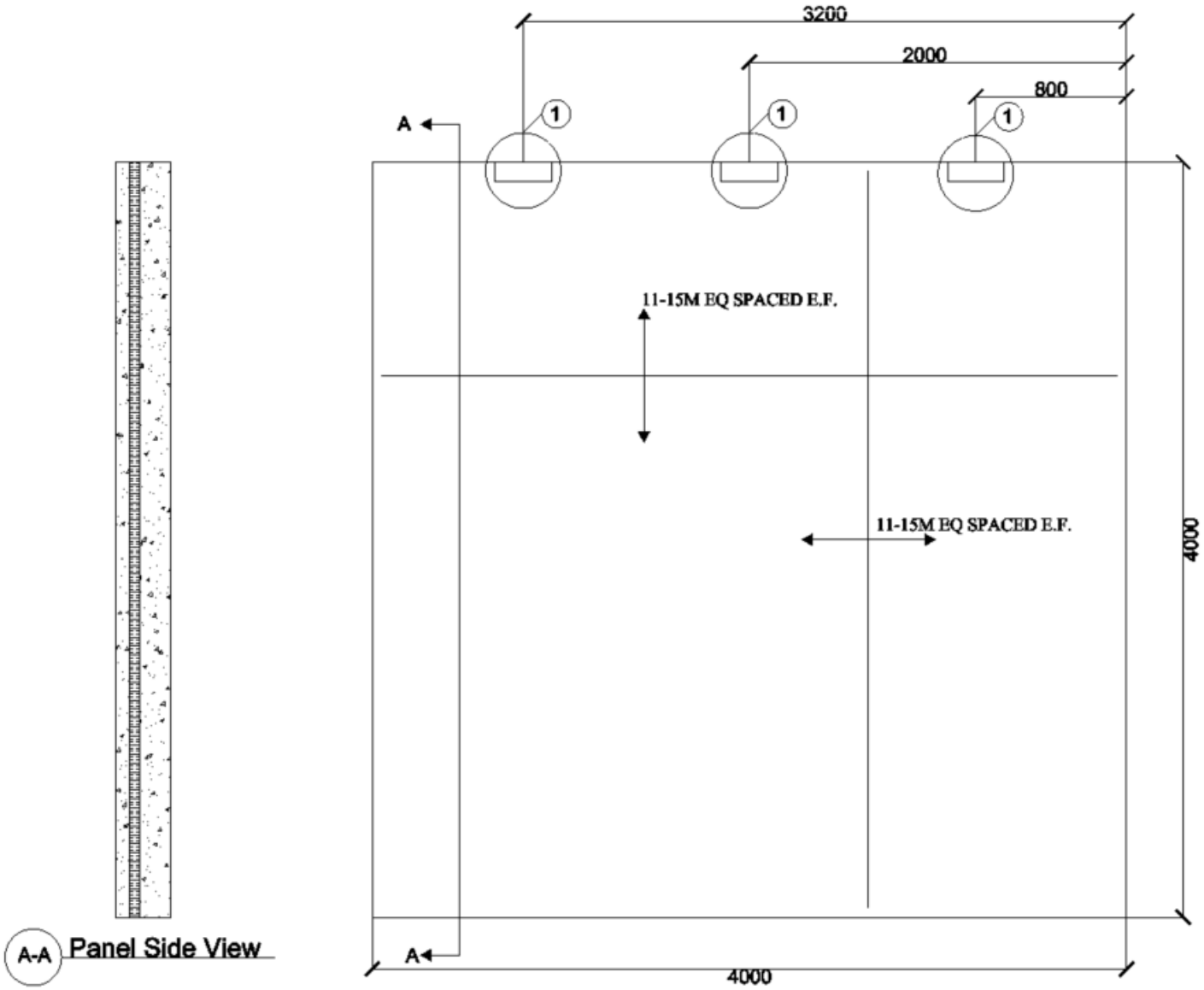

Figure 6.3 – NCTS-FS4 Details

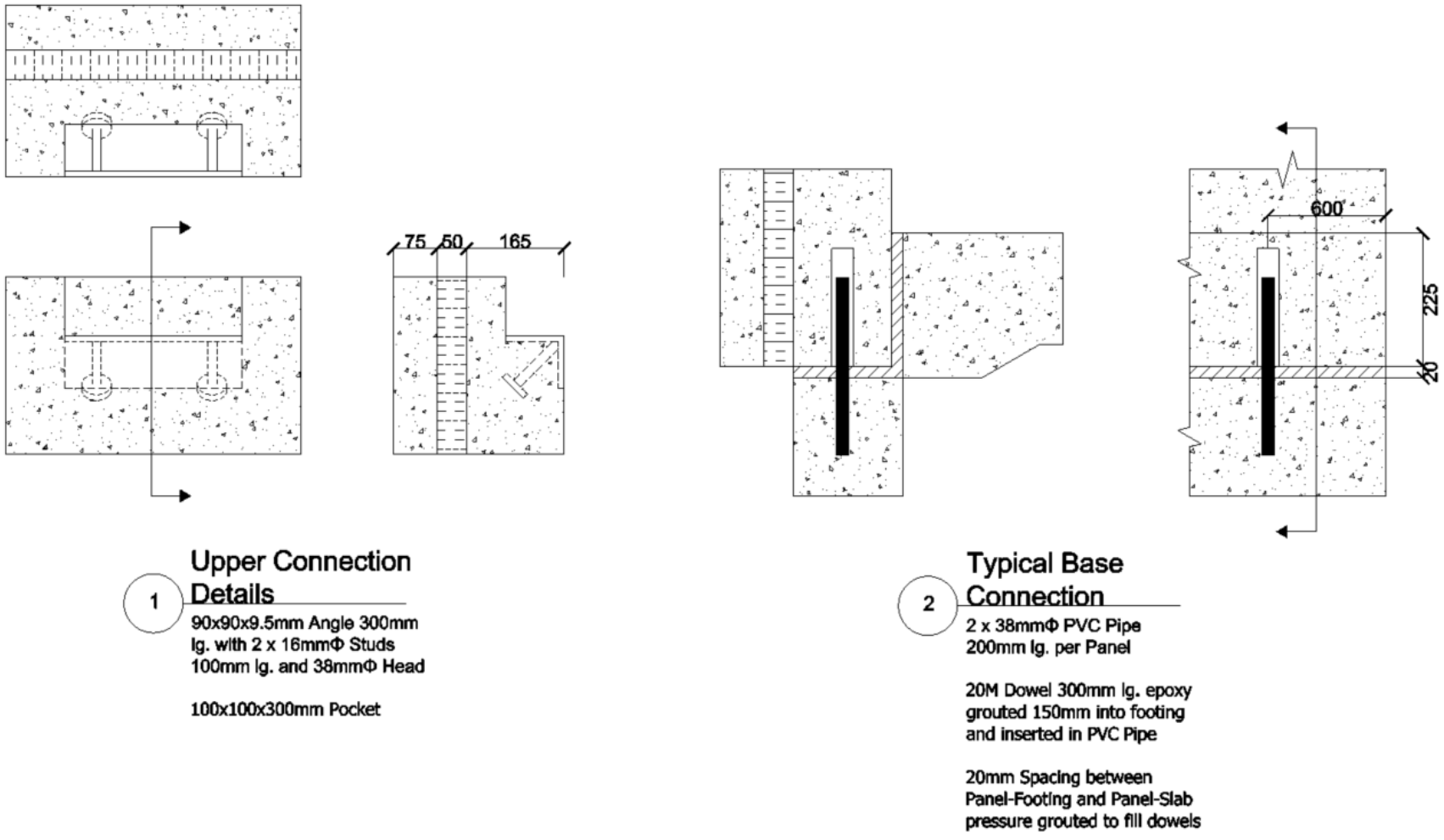

Figure 6.4 – NCTS-FS8 & NCTS-FS4: Panel Details

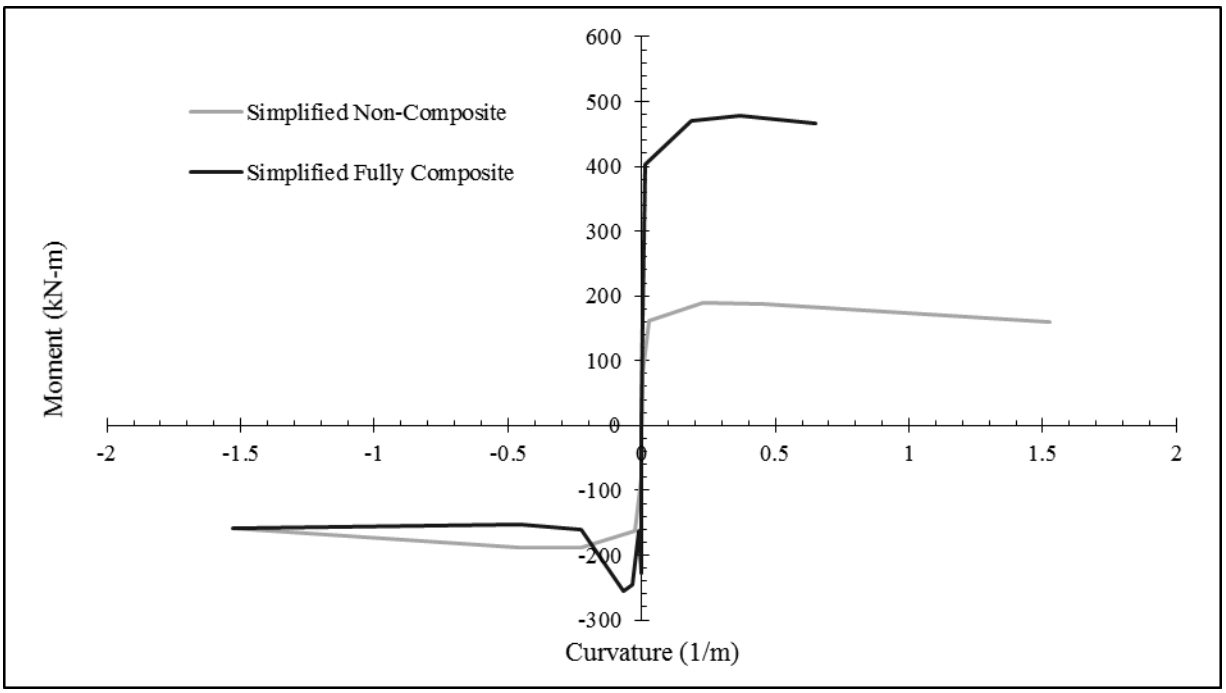

Figure 6.5 – NCTS-FS8 & -FS4: Moment-Curvature Relationship

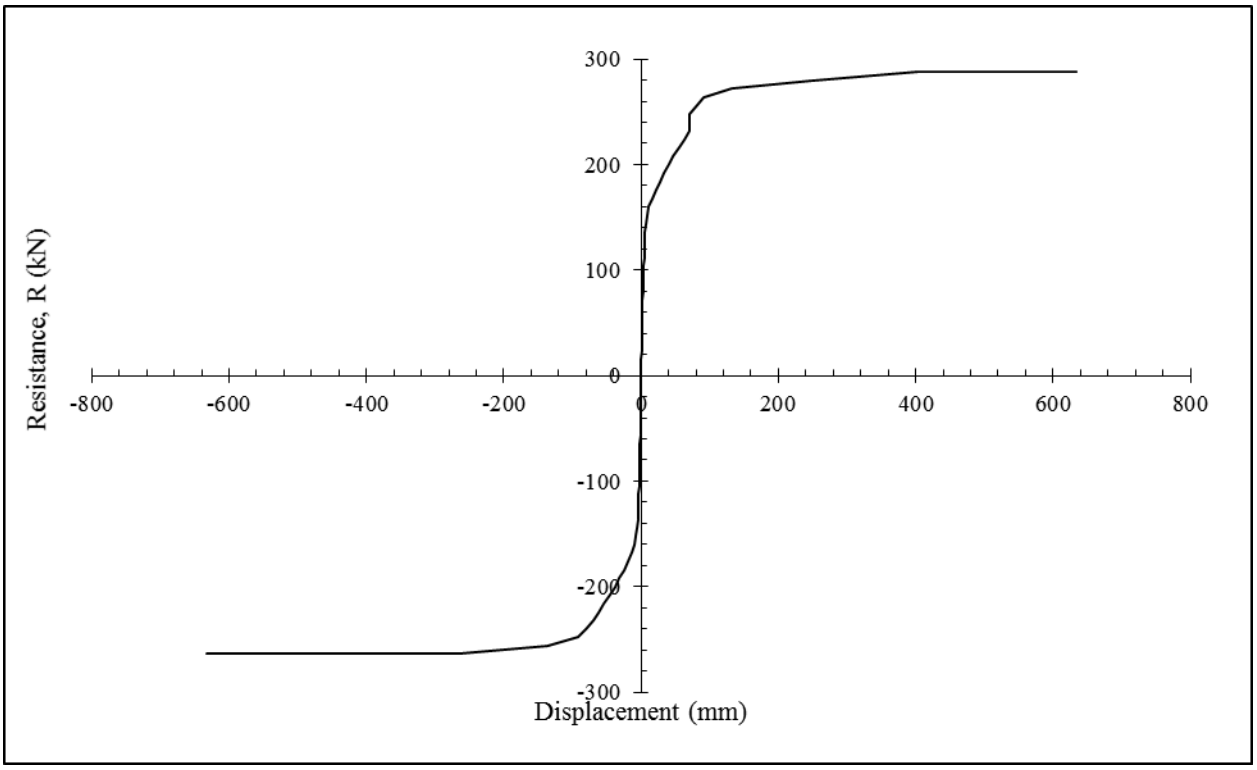

Figure 6.6 – NCTS-FS8: Load-Deformation Characteristics

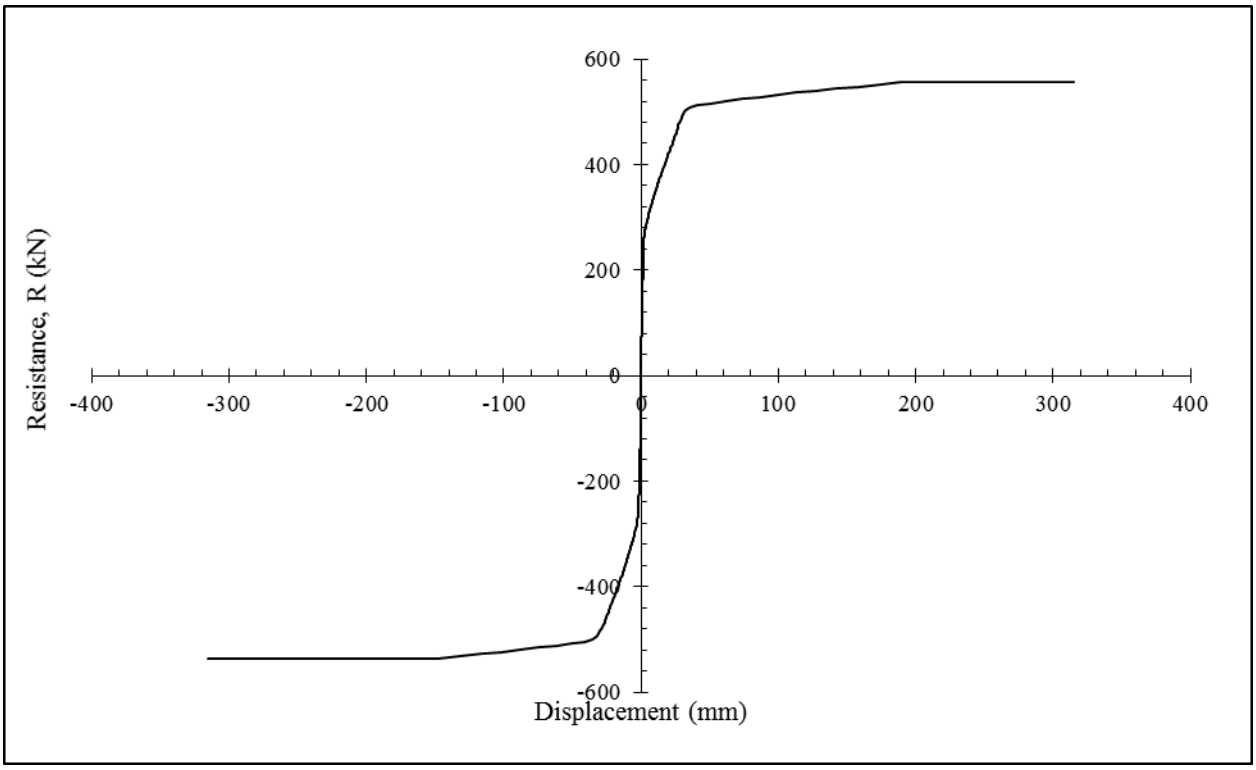

Figure 6.7 – NCTS-FS4: Load-Deformation Characteristics

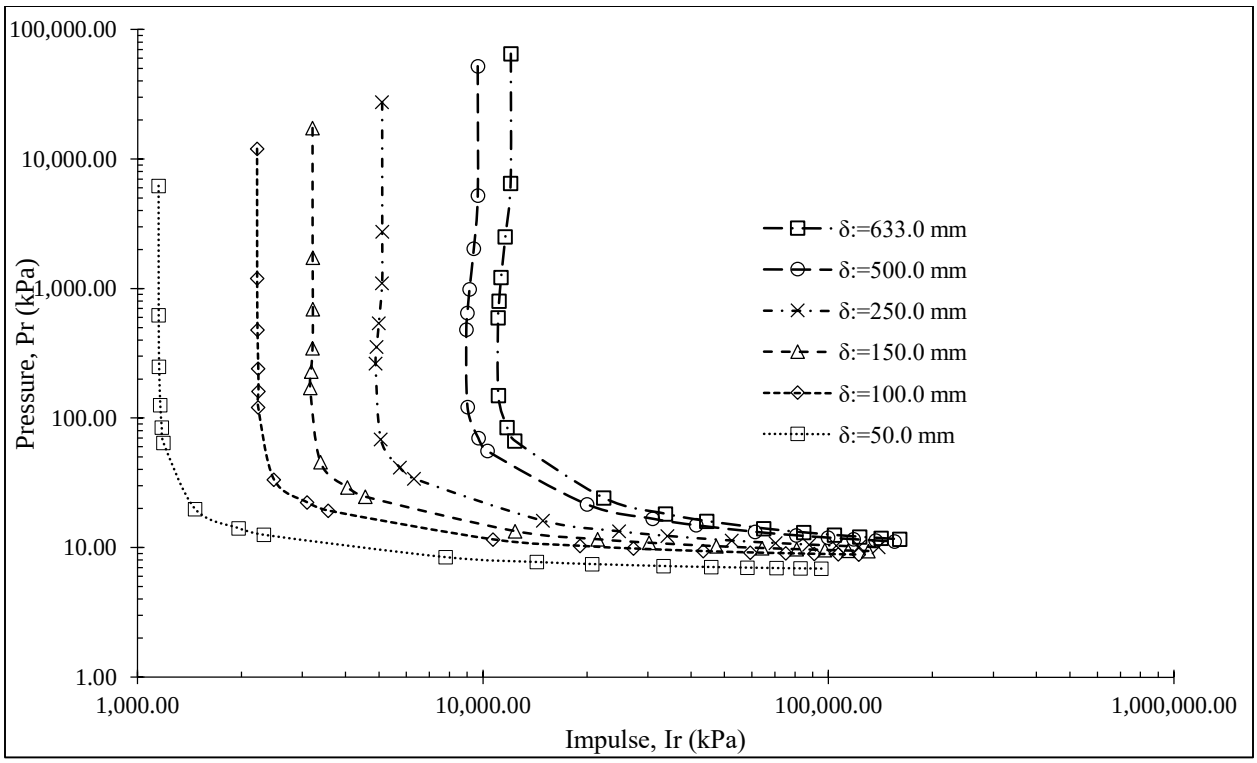

Figure 6.8 – NCTS-FS8: Pressure-Impulse Diagram

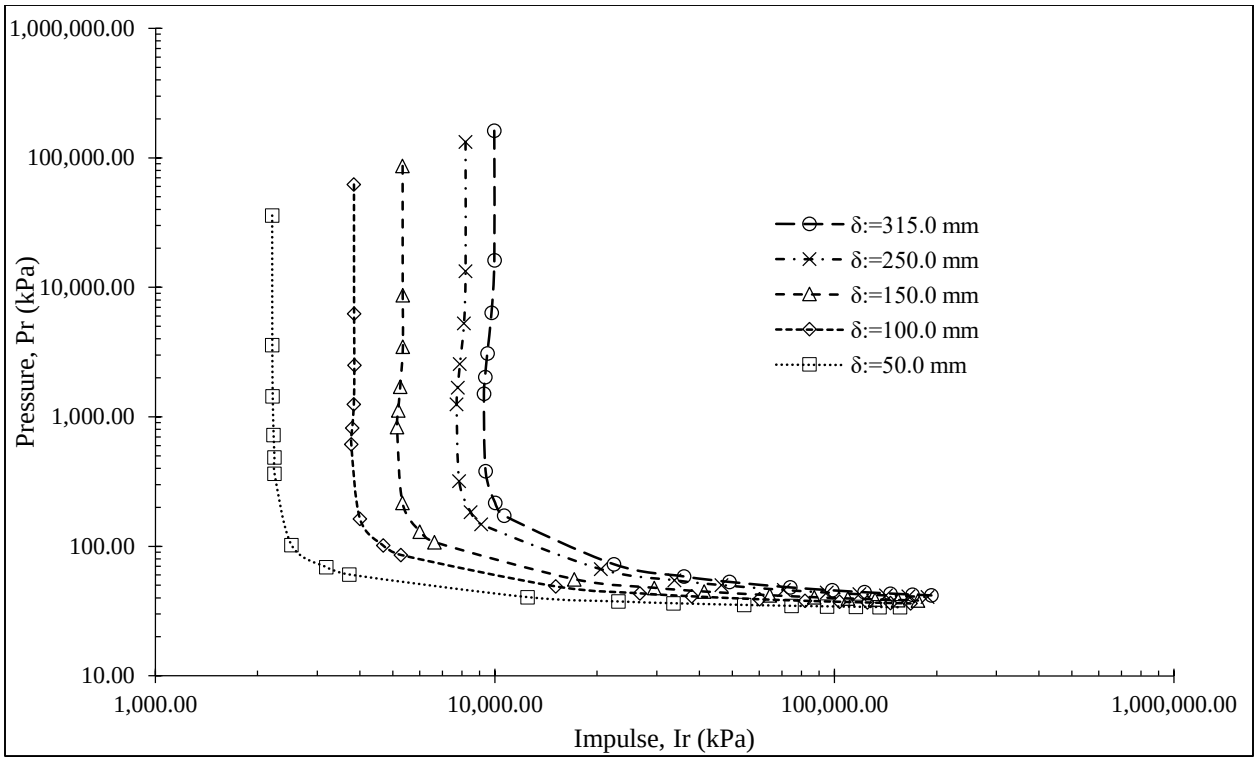

Figure 6.9 – NCTS-FS4: Pressure-Impulse Diagram

7.0 Conclusions

7.1 Summary

An experimental and analytical investigation was performed on the blast resistance of solid reinforced concrete and non-composite tilt-up sandwich panels. The experimental portion examined the flexural behaviour of the panel under simulated blast loads and the development of damage in common supports. Five specimens were constructed and tested under simulated blast loads in the shock tube testing facility at the University of Ottawa's Structural Engineering Research Laboratory.

One control panel consisting of a *100mm* solid reinforced concrete section was subjected to five shots of gradually increased pressure-impulse combinations until failure. Three non-composite tilt-up panels consisting of a *100mm* structural wythe, a *50mm* thick insulation layer, and a *50mm* thick architectural wythe were subjected to several shots of gradually increase pressure-impulse combinations until failure. One panel was repaired and tested as a fifth specimen under similar loading conditions. Two of the NCTS panels, NCTS-1 and NCTS-2, were supported by unmodified, non-retrofitted joist seats along the upper edge and direct bearing in the lower. The fourth specimen, NCTS-M, was supported by modified joist seats containing shear reinforcement along the upper edge and direct bearing in the lower. Finally, NCTS-R was a repaired panel retrofitted with surface bonded FRP laminate on the tensile face of the structure wythe surrounding the upper supports. A data acquisition system recorded displacement, pressure, longitudinal strain, and sectional strain data for each test to facilitate a complete assessment of the specimens.

RC Blast, a SDOF analysis software, was used to construction displacement-time histories for every test on each panel based on specified load-deformation characteristics, panel properties, and impulsive forcing functions. Hysteretic panel behaviour was predicted by RC Blast, accounting for residual damage and additional effects associated with consecutive shots. A detailed sectional analysis was conducted to assess the composite behaviour of NCTS panels under extreme blast loads. Shear tie degradation was modelled to capture the distribution of composite deterioration along the span of the panel under incrementally increased uniformly distributed loads. Analytical

displacement-time histories are compared to experimental data in terms of maximum mid-span displacement, time-to-maximum mid-span displacement, and behaviour in free vibration.

An analytical investigation was performed to determine dynamic reactions and predict support behaviour under extreme blast loads. CSA A23.3-04 guidelines for determining punching shear capacity of flat slabs with columns were applied to tilt-up panel supports. Theoretical support capacities were compared with empirical observations and approximate dynamic reactions. Modified and retrofitted supports examined in the experimental study were evaluated against unmodified support capacities and dynamic reactions.

Finally, a practical design evaluation was performed on two full-scaled non-composite tilt-up panels subjected to blast induced shock waves. Two NCTS Panels, NCTS-FS8 spanning *8m* and NCTS-FS4 spanning *4m*, with identical cross-sectional properties were designed and analysed under the same blast parameters. Blast parameters for a *2800kg* TNT charge weight, similar to the 1995 Oklahoma City Bombing, at *30m*, *50m*, *70m*, and *100m* were generated using RC Blast. RC Blast generated displacement-time histories and pressure-impulse relationships were compared and assessed based on maximum mid-span displacements and corresponding support rotations. Dynamic support reactions were calculated and strengthening alternatives were designed for each blast scenario using stirrup reinforcement, headed bar reinforcement, surface bonded FRP laminate, and concrete thickening in support regions. The design limitations for each alternative were examined and discussed in detail.

7.2 Conclusions

The following conclusions can be drawn from the literature review, experimental data, and analytical results presented in this thesis:

- NCTS panels performed considerably better in flexure than the SRC control panel sustaining substantially less damage under similar shock wave pressures. This can be attributed to several characteristics including the additional mass of the architectural wythe, additional flexural capacity of the architectural wythe, and composite behaviour within the panel. In the current experimental program, Panel SRC-1 developed *110.8mm* of deflection opposed to the *25.2mm* mid-span deflection suffered by NCTS-1. On average, the

maximum displacements of NCTS-1 were *27.3%* of those exhibited by SRC-1 under similar test pressures. The maximum mid-span displacement in NCTS-1 was *45.6mm* prior to support failure.

- The longitudinal displacement and strain distributions demonstrated by NCTS specimens were highly comparable. Data consistently indicated partially fixed and pinned boundary condition for the NCTS specimens as shown by the moment distribution plotted in Figure 5.9. Contrastingly, displacement and strain data from the SRC-1 specimen were indicative boundary conditions ranging from simply supported to fully fixed. Rotation in the base support was repaired following the tests conducted on SRC-1 and is the suspected cause of these discrepancies.
- NCTS-2 and NCTS-M reached failure criteria for support rotations of *9.0º* with mid-span displacements of *72.5mm* and *85mm*, respectively. NCTS-R suffered an upper support rotation of *14.7º* a displacement of *122.0mm*. The resistance of NCTS-R was compromised due to the repair joint at approximately three-quarter-span and performed considerably worse than other NCTS panels as a result. Consequentially, the support reactions experienced by the retrofitted NCTS-R were less than other panels under similar pressures.
- Incorporating shear tie degradation into the derivation of load-deformation characteristics increases the accuracy of the predicted composite behaviour within the panel. Proper models of shear tie deterioration yield a distribution of composite behaviour along the span of the panel.
- RC Blast's SDOF analysis accurately predicted the displacement-time history prior to peak displacements. Maximum displacements were consistently predicted to *0.93* of experimental peaks for all tests with a standard deviation of *0.27*. Maximum displacements were more conservatively predicted with greater accuracy for powerful blasts. On average, maximum displacements were predicted to *1.08* of the experimental peaks for shots with an impulse greater than *1000kPa-ms*.
- The post-peak behaviour of NCTS panels was poorly predicted due to the inability to accurately model the transformation of panel stiffness. RC Blast interprets specimen

damping and unloading stiffness as constant parameters and does not capture the gradual loss of composite strength and the resulting change in sectional properties.

- Support capacities predicted with conventional punching shear analysis formulas accurately reflected experimental behaviour and corresponded with dynamic support reactions. This approach produces conservative results due to the assumed failure plain.
- Modified supports exhibited a significant increase in punching shear capacity representative of experimental behaviour. Stirrup reinforced specimens produced the greatest improvements with a theoretical increase in punching shear capacity of *196.9kN* per support. Supports retrofitted with surface bonded FRP laminates experienced an increase resistance to punching shear failure of *73.2kN* per support.
- Full-scale panels, designed follow CSA A23.3-04 [5] guidelines, analytically evaluated against blast pressures similar to those induced by the 1995 Oklahoma City bombing. Support modifications were designed to improve punching shear capacity to acceptable levels. As a result, panels were capable of sustaining blast loads in which unmodified supports failed prior to the development of significant flexural damage.

7.3 Recommendations

Based on the findings of presented in this research thesis the following recommendations have been drafted for the design and analysis of NCTS panels subjected to blast loads:

- Composite behaviour of NCTS panels should be modelled by interpolating between fully composite and non-composite moment-curvature relationships based on shear tie degradation. Empirical load-deformation characteristics for shear ties presented by Naito et Al. [11] are recommended for analytical purposes.
- NCTS panel resistance should not be underestimated in an attempt to conservatively predict panel behaviour. Displacement-time histories are sensitive to variations in resistance curves and could result in miscalculated support reactions.

- In the absence of a detailed dynamic analysis simple support boundary conditions should be assumed for a conservative design approach and support reactions should be calculated using static loading conditions. (i.e. $F = P_r \, x \, A_L$)
- Support capacities should be calculated using conventional punching shear analysis techniques for flat slabs specified in CSA A23.3-04. This includes supports modified with steel reinforcement.
- Punching shear capacity limitations specified by CSA A23.3-04 for steel reinforced supports are more stringent for stirrup reinforcement. Supports modified by headed steel bars are limited to a capacity of $0.75\lambda\phi_c\sqrt{f_c'}$ opposed to $0.55\lambda\phi_c\sqrt{f_c'}$ for stirrup reinforcement. Headed steel bars achieve the required resistance with less area, A_{vs}, than stirrups.

7.4 Recommendations for Future Research

Based on the experimental data and analytical results presented in this document the following subjects of future research are recommended:

- This experimental study investigated the behaviour of SRC and NCTS panels with different mass. Similar research should be conducted to evaluate the effect of the additional mass of the architectural wythe on the resistance of sandwich panels. There are several methods of doing this. Distributed mass could be installed on the panel such that the sectional behaviour of the section would not change. An SRC panel could be designed with an inbound moment-curvature relationship and mass similar to a fully composite and non-composite panel.
- The displacement-time analysis of NCTS panels following maximum displacements are extremely sensitive to unloading stiffness and damping. The degradation of composite behaviour, the change in sectional properties, and its effect on panel stiffness require more detailed examination. These parameters are difficult to capture within the current analysis which would need to capture change in stiffness and ultimately the critical damping of the system. The inability to do this with the current analytical software is evidenced by the difference in frequency of the analytical and experimental displacement-time histories

shown in Annex C. Future research should incorporate this degradation into the scope of the analysis to more accurately estimate post-peak displacements.

- A more detailed study different support types and embedment details should be investigated to determine failure criteria and evaluate performance.
- The longitudinal moment distributions found in the experimental portion of this study may have been influenced by the size of the panel and distribution of composite behaviour. Research of specimens with real asymmetric connection details is necessary in determining the moment distribution properties of full-scale panels.
- Additional research is required to evaluate the benefits of surface bonded FRP retrofits on tilt-up panel support capacity.

References

[1] Canadian Standards Association, Design and Assessment of Buildings Subjected to Blast Loads, Mississauga Ontario: CSA Group, 2012.

[2] Naito, Clay J., Robert J. Dinan, Jeff W. Fisher, and John M. Hoemann ,"Precast/Prestressed Concrete Experiments - Series 1 (Volume 1)," Air Force Research Laboratory, Tyndall Air Force Base, FL, 2008.

[3] Naito, Clay J., John M. Hoemann, Jonathon S. Shull, Aaron Saucier, Hani A. Salim, Bryan T. Berwick, and Michael I. Hammons, "Precast/Prestressed Concrete Experiments Performance on Non-Load Bearing Sandwich Wall Panels," 2011.

[4] Cement and Concrete Association of New Zealand, Technical Manual 34 0 Tilt-up Technical Manual, Wellington, NZ: Cement and Concrete Associaion of New Zealand, 2004.

[5] Cement Association of Canada, Concrete Design Handbook, Third Edition ed., Ottawa, ON: Cement Association of Canada, 2010.

[6] Lloyd, Alan, M. Saatcioglu, I. Nistor, and D. Palermo, "New Shock Tube Testing Facilities for Simulated Blast Loading of Structural and Non-Structural Components," University of Ottawa, Ottawa, 2010.

[7] B. Shadravan, "Investigation of Surface Bond Behaviour of FRP Sheets on Concrete and Masonry Substrates," Ph.D. Thesis, University of Ottawa, Ottawa, 2009.

[8] United States of America Department of National Defence, Unified Facilities Code (UFC) 03-340-02: Structures to Resist the Effects of accidental Explosions, Washington, DC, 2008.

[9] Benayoune A., A.A. Abdul Samad, D.N. Trikha, A.A. Abang Ali, and S.H.M. Ellinna, "Flexural Behaviour of Pre-Cast Concrete Sandwich Composite Panel - Experimental and Theoretical Investigations," *Construction and Building Materials*, vol. 22, pp. 580-592, 2008.

[10] Dayton Superior, Precast Concrete Handbook, Dayton Superior, 2014.

[11] Naite, Clay J., John Hoemann, Mark Beacraft, and Bryan Bewick, "Performance and Characterization of Shear Ties for Use in Insulated Precast Sandwich Wall Panels," *Journal of Structural Engineering*, vol. 138, no. 1, pp. 52-61, 2012.

[12] Jacques, Eric, Alan Lloyd, and Murat Saatcioglu, "Predicting Reinforced Concrete Response to Blast Loads," *Canadian Journal of Civil Engineering*, vol. 39, pp. 1-18, 2012.

[13] J. M. Biggs, Introduction to Structural Dynamics, New York, NY: McGraw-Hill, 1964.

[14] El-Salakawy E., K. Soudki, and M. Polak, "Punching Shear Behaviour of Flat Slabs Strengthened with Fiber Reinforced Polymer Laminates," *Journal of Composites for Construction*, vol. 8, no. 5, pp. 384-392, 2004.

[15] Farghaly A. and Ueda T., "Prediction of Punching Shear Strength of Two-Way Slabs Strengthened Externally with FRP Sheets," *Journal of Composites for Construction*, vol. 15, no. 2, pp. 181-193, 2011.

[16] Jacques, Eric, *Blast Retrofit of Reinforced Concrete Walls and Slabs*, Ottawa, Ontario: University of Ottawa, 2010.

[17] Oswald C. and Bazan M., "Performance and Blast Design for Non-Load Bearing Precast Concrete Panels," in *SEI Structures Congress*, Boston, MA, 2014.

A. Comparison of Experimental Displacement-Time Histories

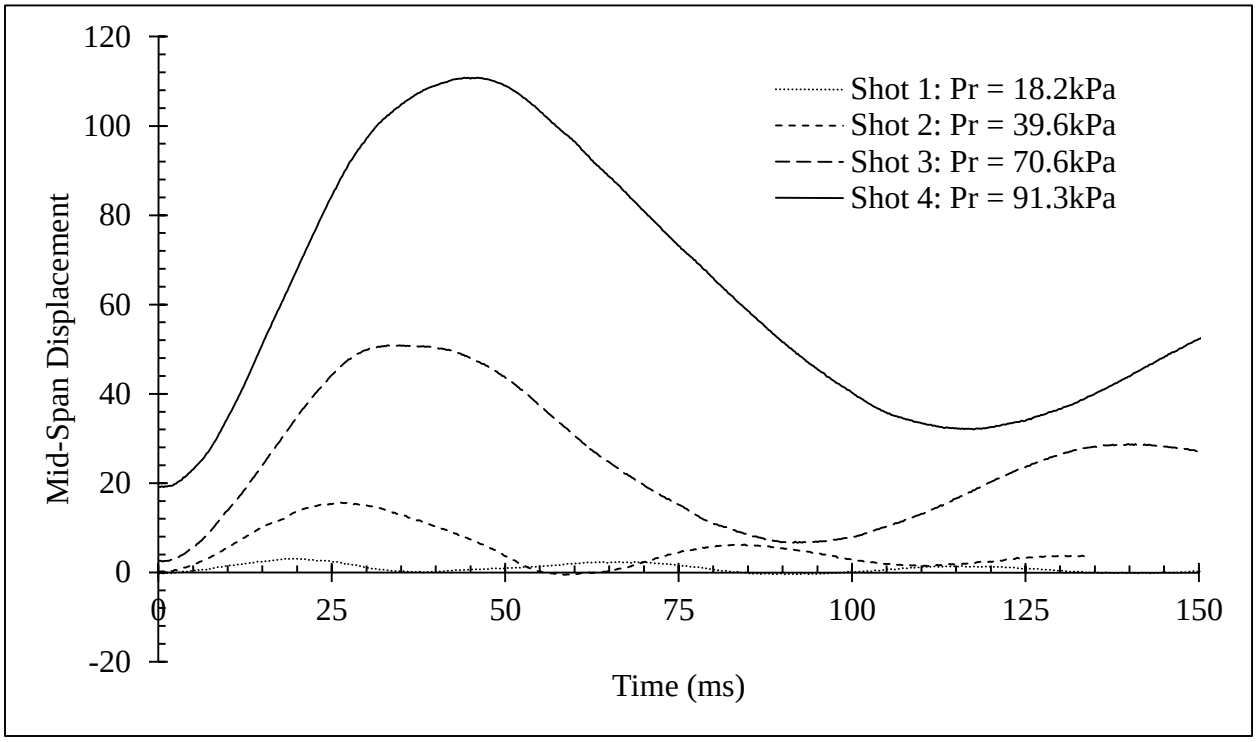

Figure A.1 – SRC-1: Experimental Mid-Span Displacement-Time Histories

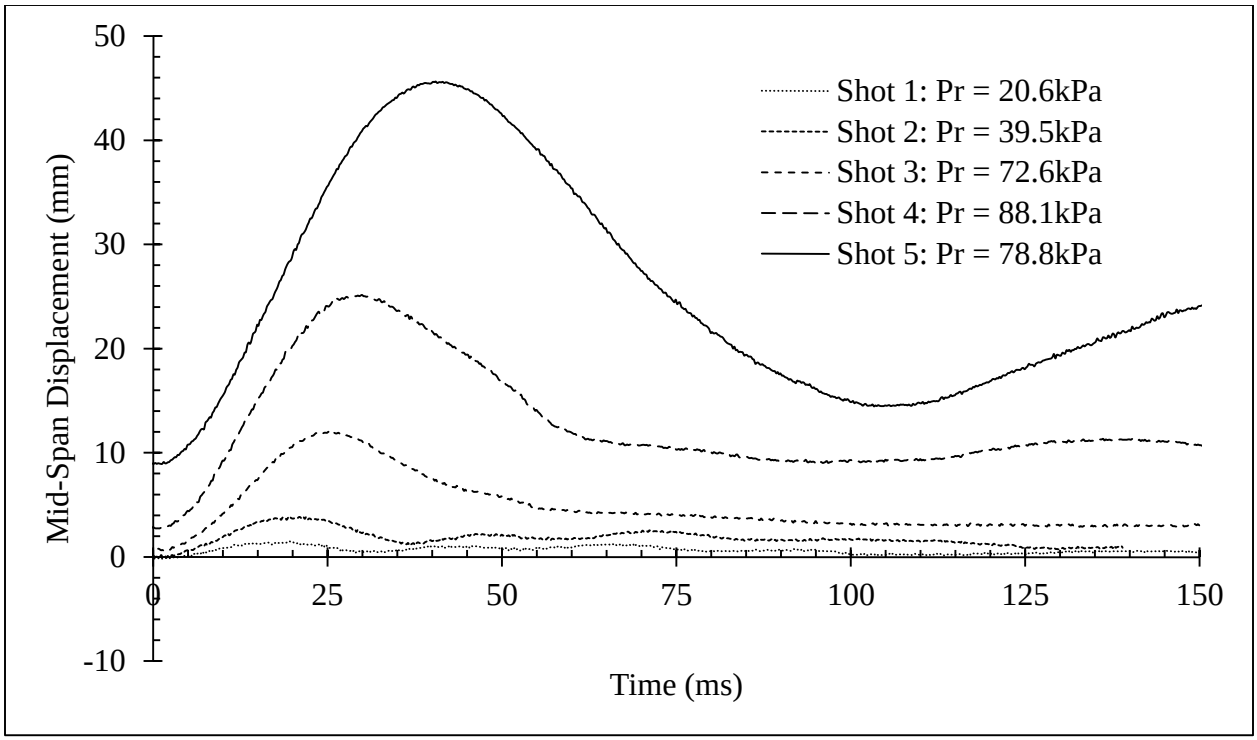

Figure A.2 – NCTS-1: Experimental Mid-Span Displacement-Time Histories

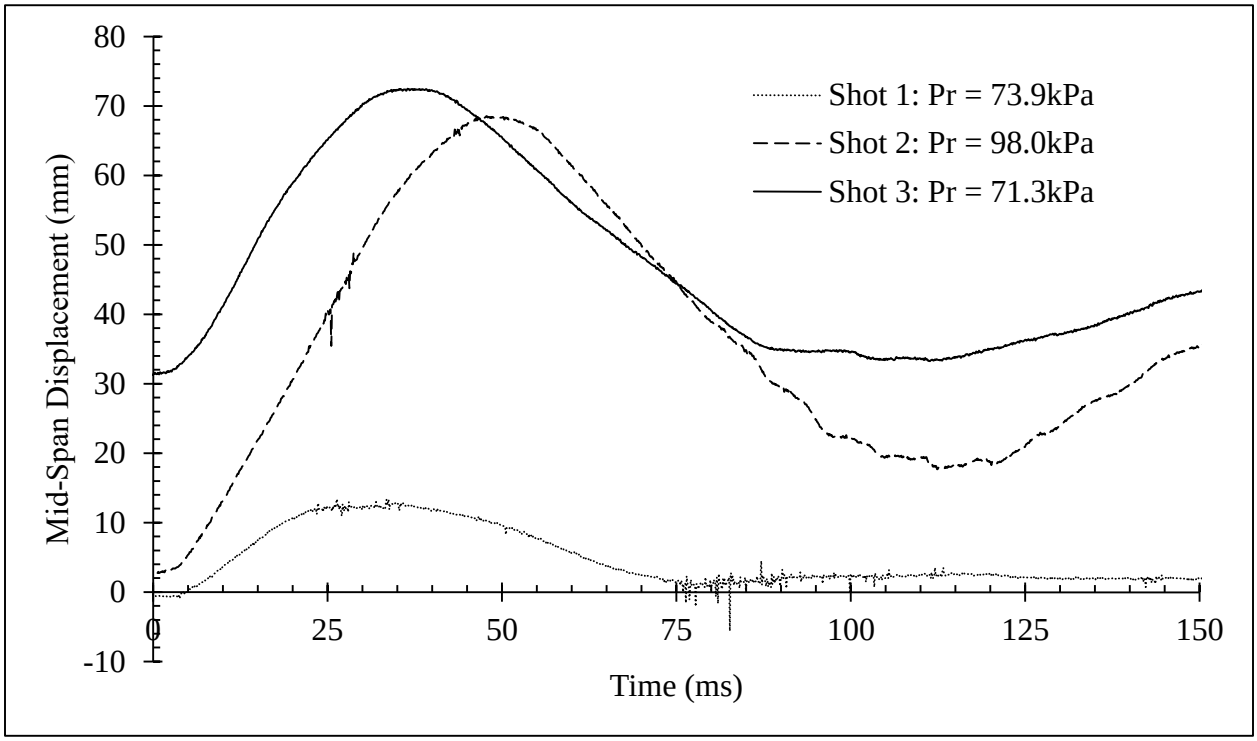

Figure A.3 – NCTS-M: Experimental Mid-Span Displacement-Time Histories

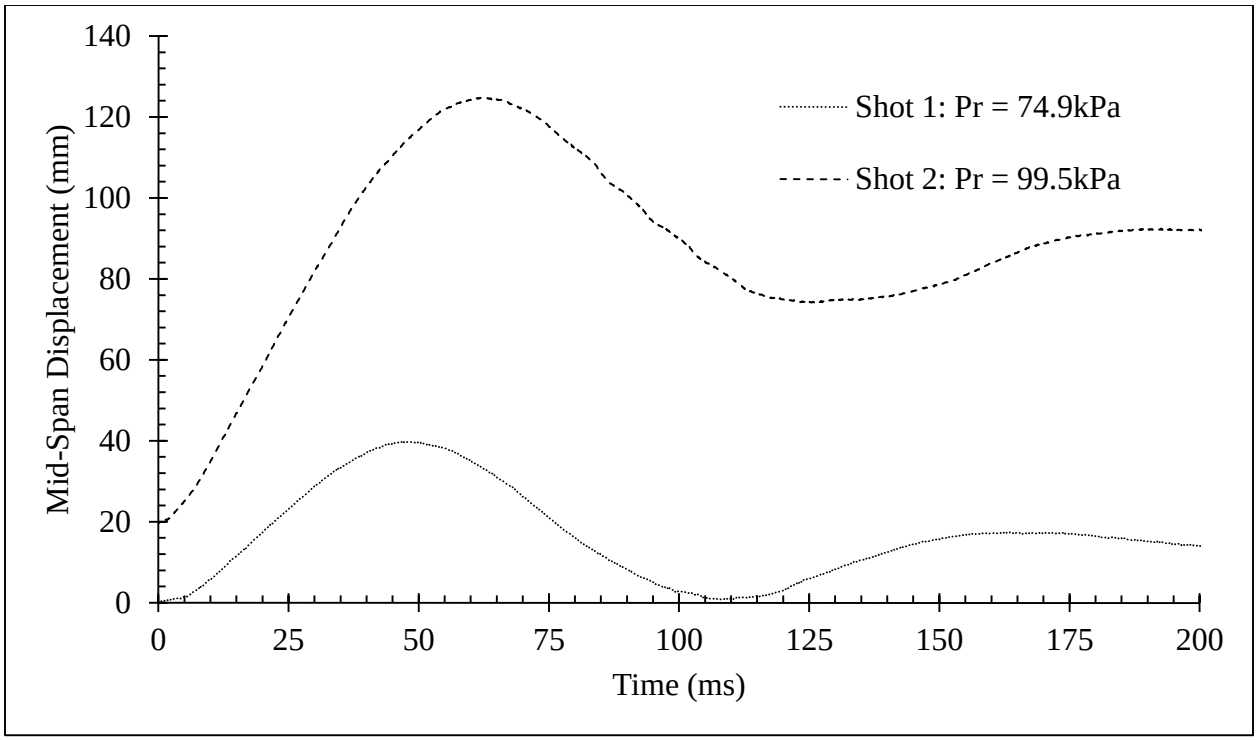

Figure A.4 – NCTS-R: Experimental Mid-Span Displacement-Time Histories

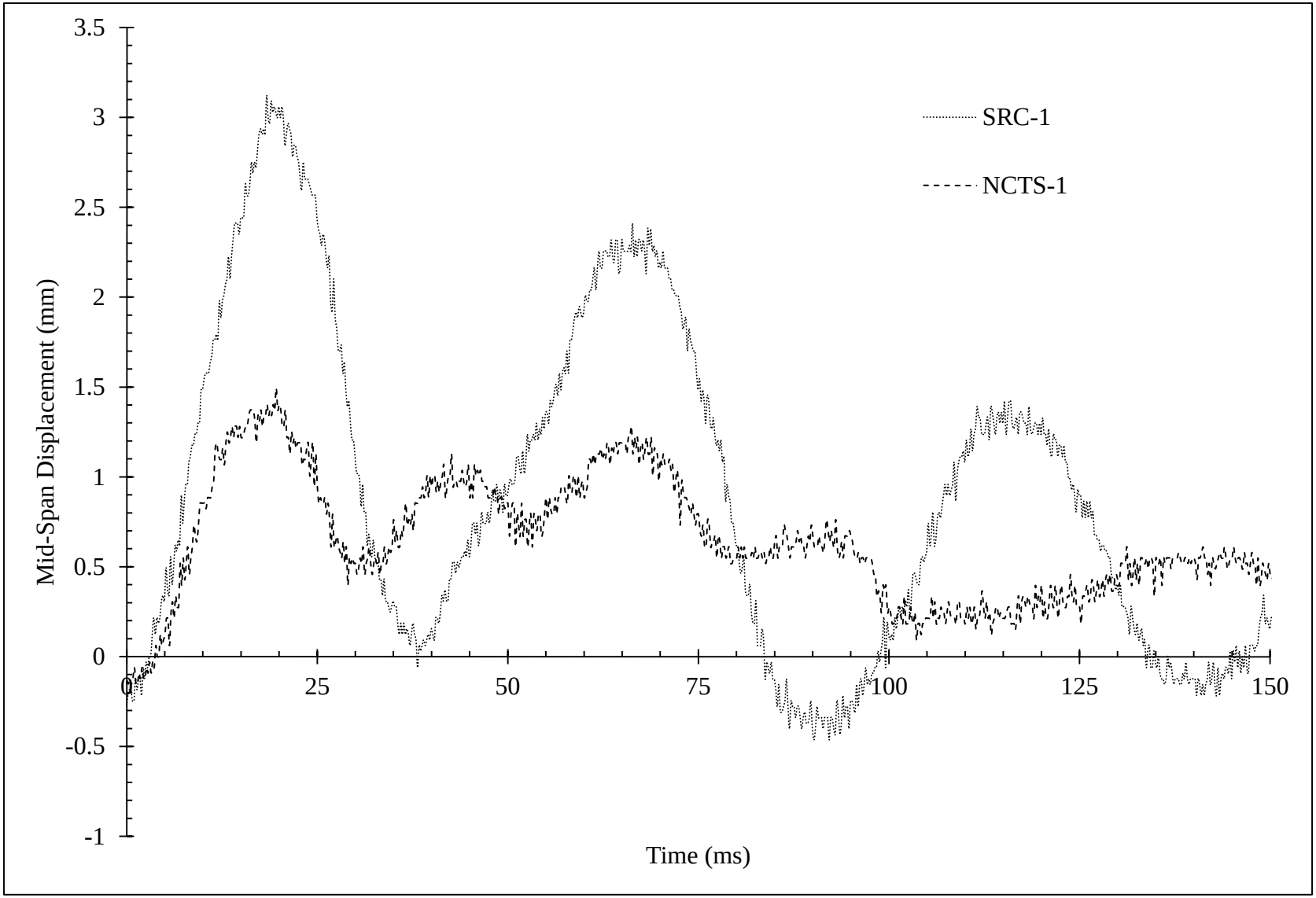

Figure A.5 – SRC-1 vs. NCTS-1 Shot 1: Experimental Mid-Span Displacement-Time Histories

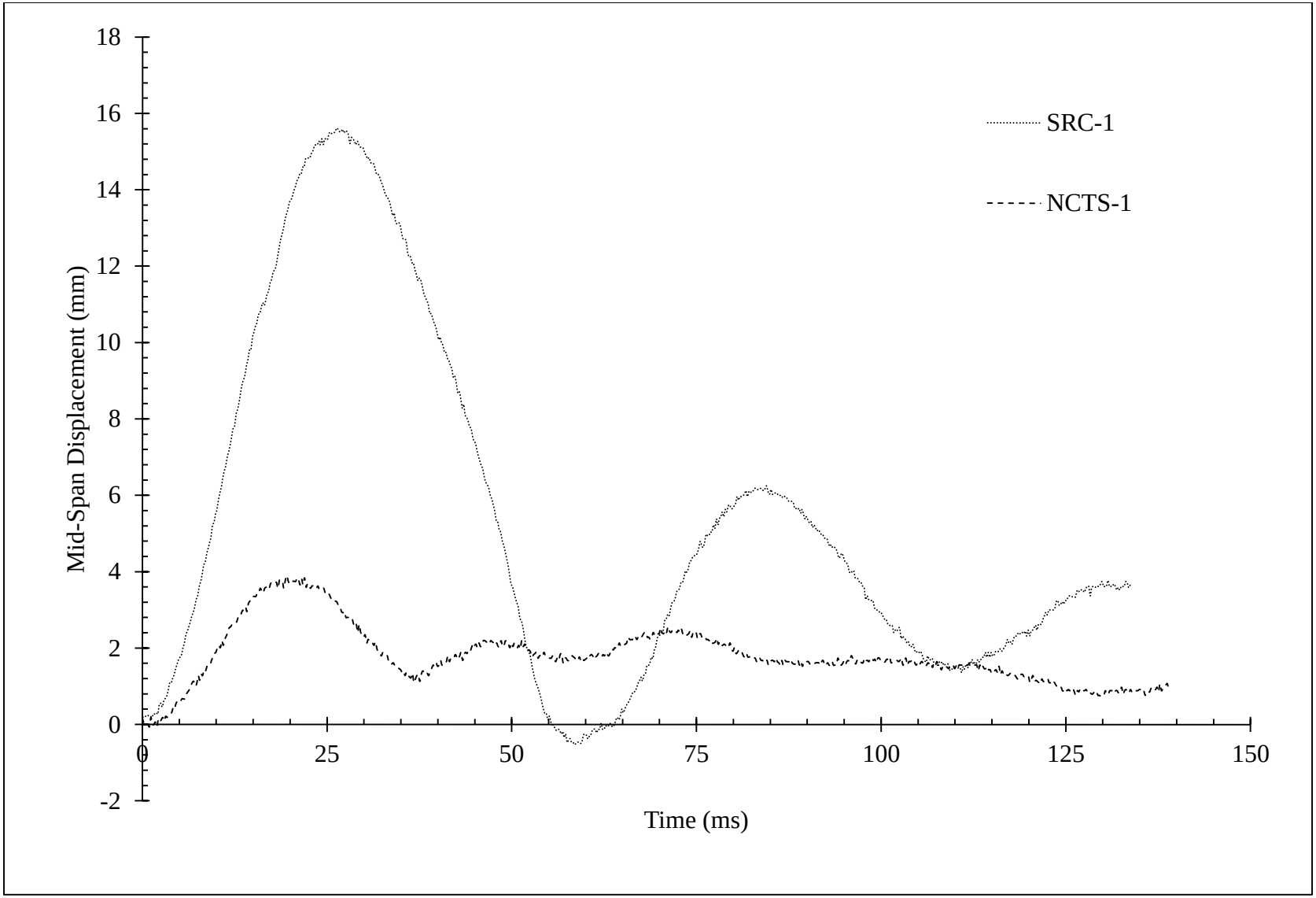

Figure A.6 – SRC-1 vs. NCTS-1 Shot 2: Experimental Mid-Span Displacement-Time Histories

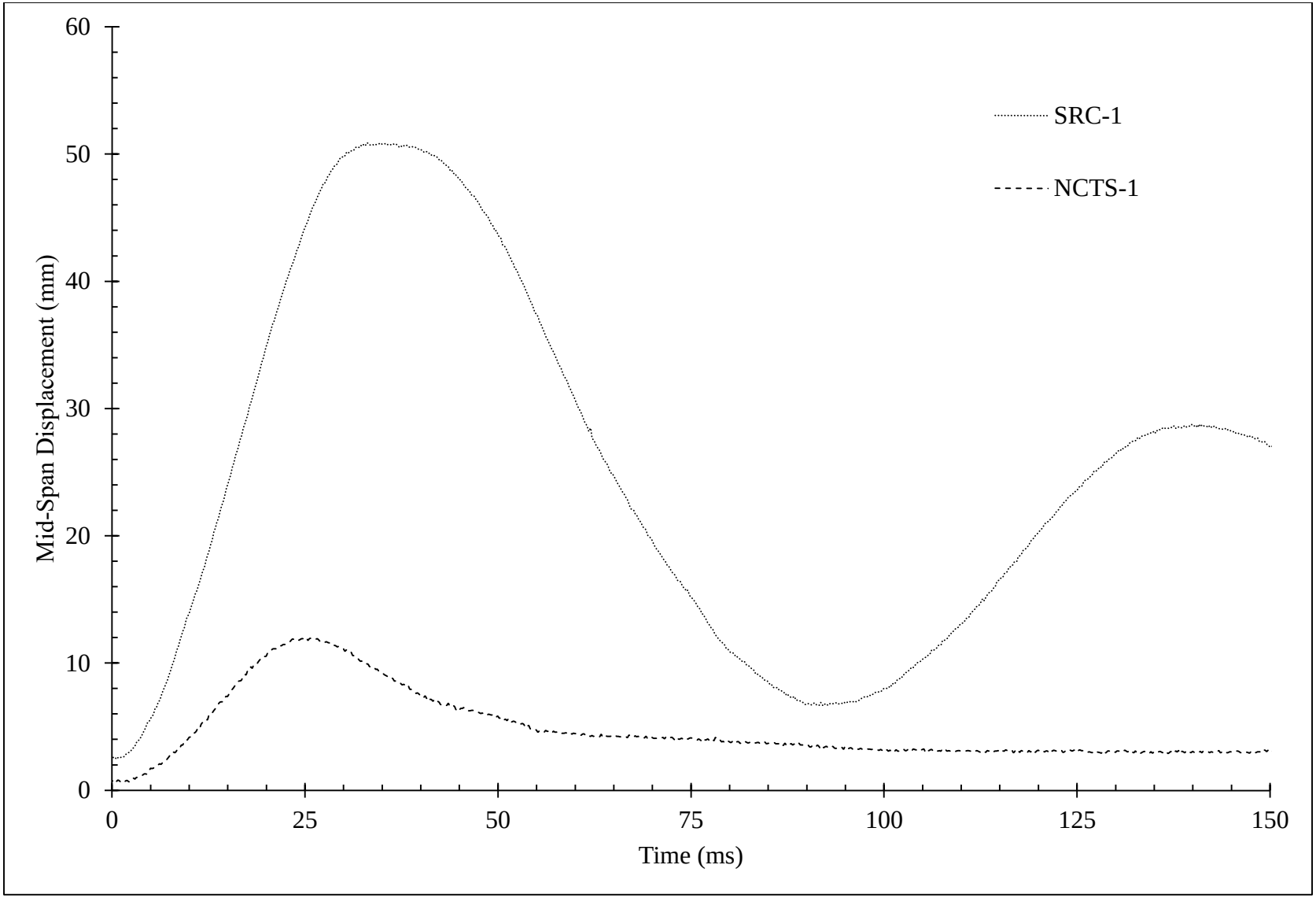

Figure A.7 – SRC-1 vs. NCTS-1 Shot 3: Experimental Mid-Span Displacement-Time Histories

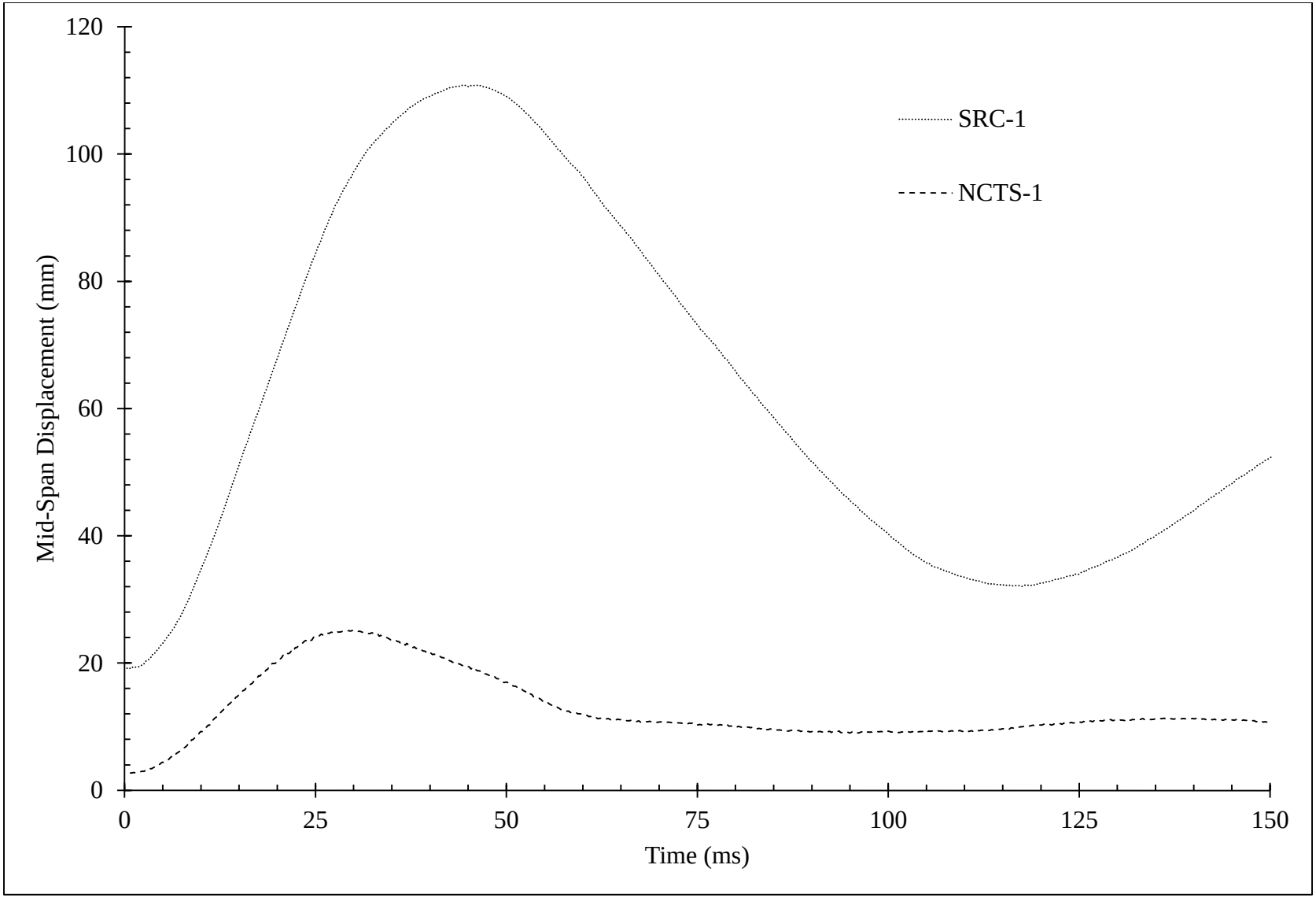

Figure A.8 – SRC-1 vs. NCTS-1 Shot 4: Experimental Mid-Span Displacement-Time Histories

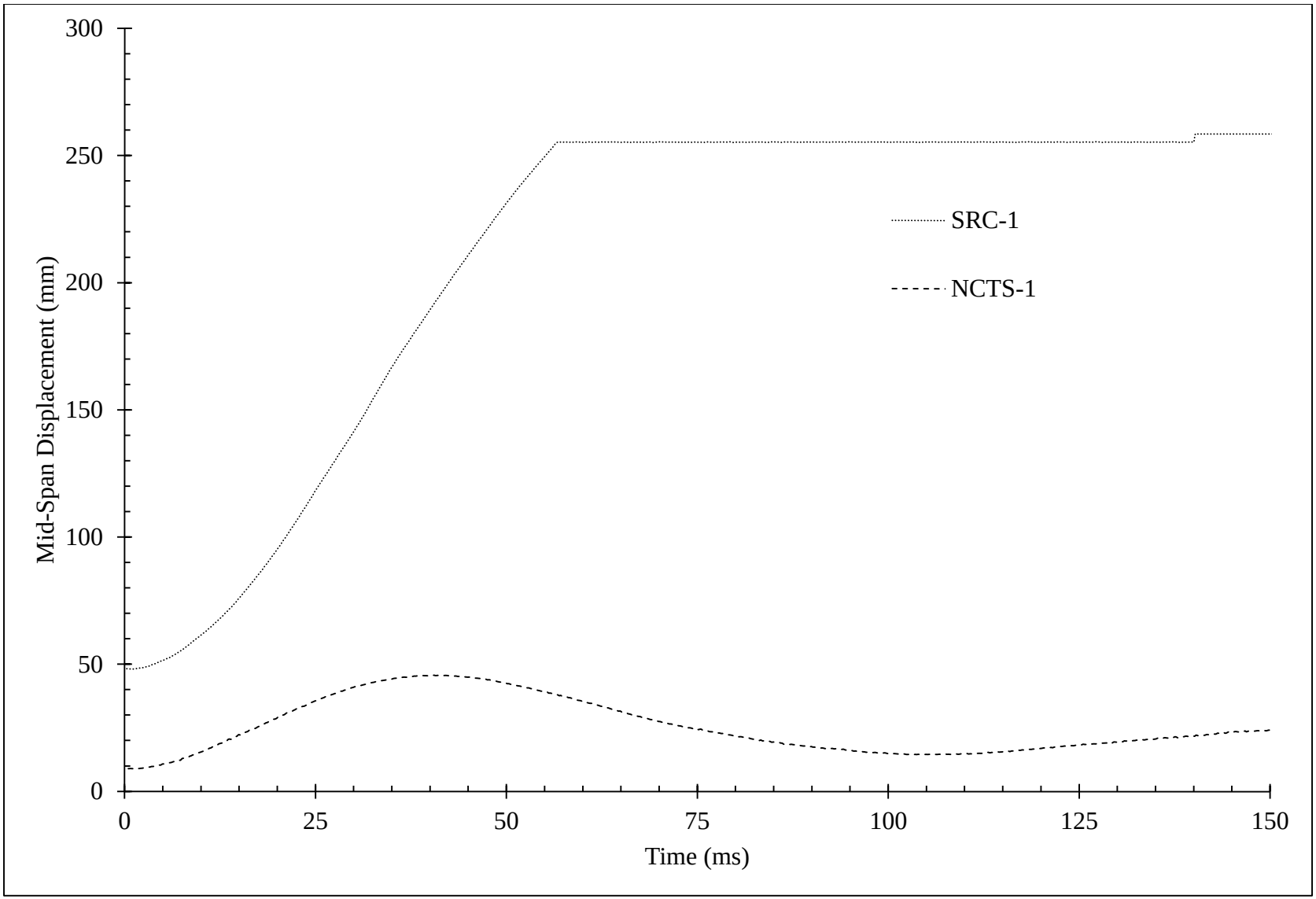

Figure A.9 – SRC-1 vs. NCTS-1 Shot 5: Experimental Mid-Span Displacement-Time Histories

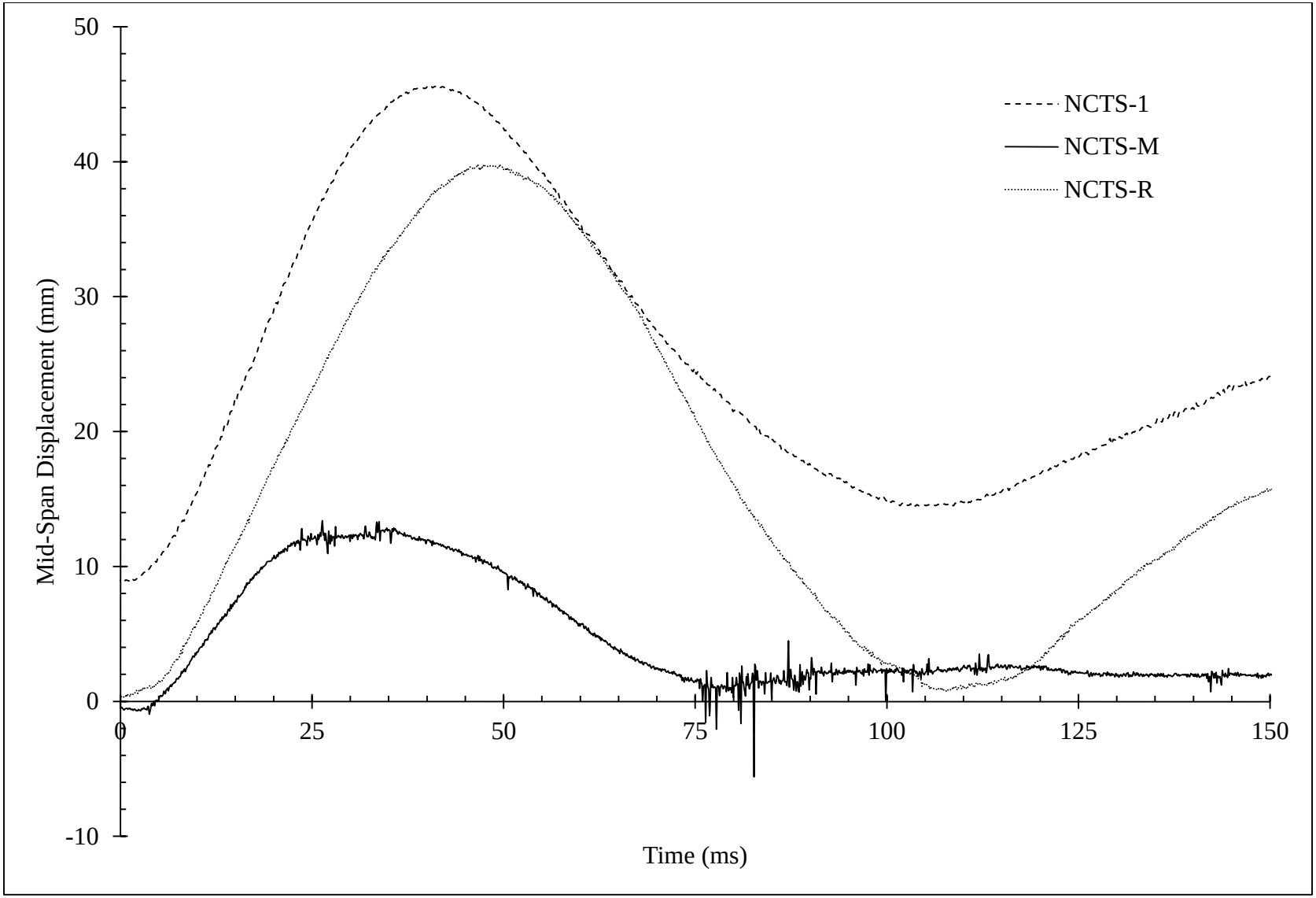

Figure A.10 – NCTS Shot 5: Experimental Mid-Span Displacement-Time Histories

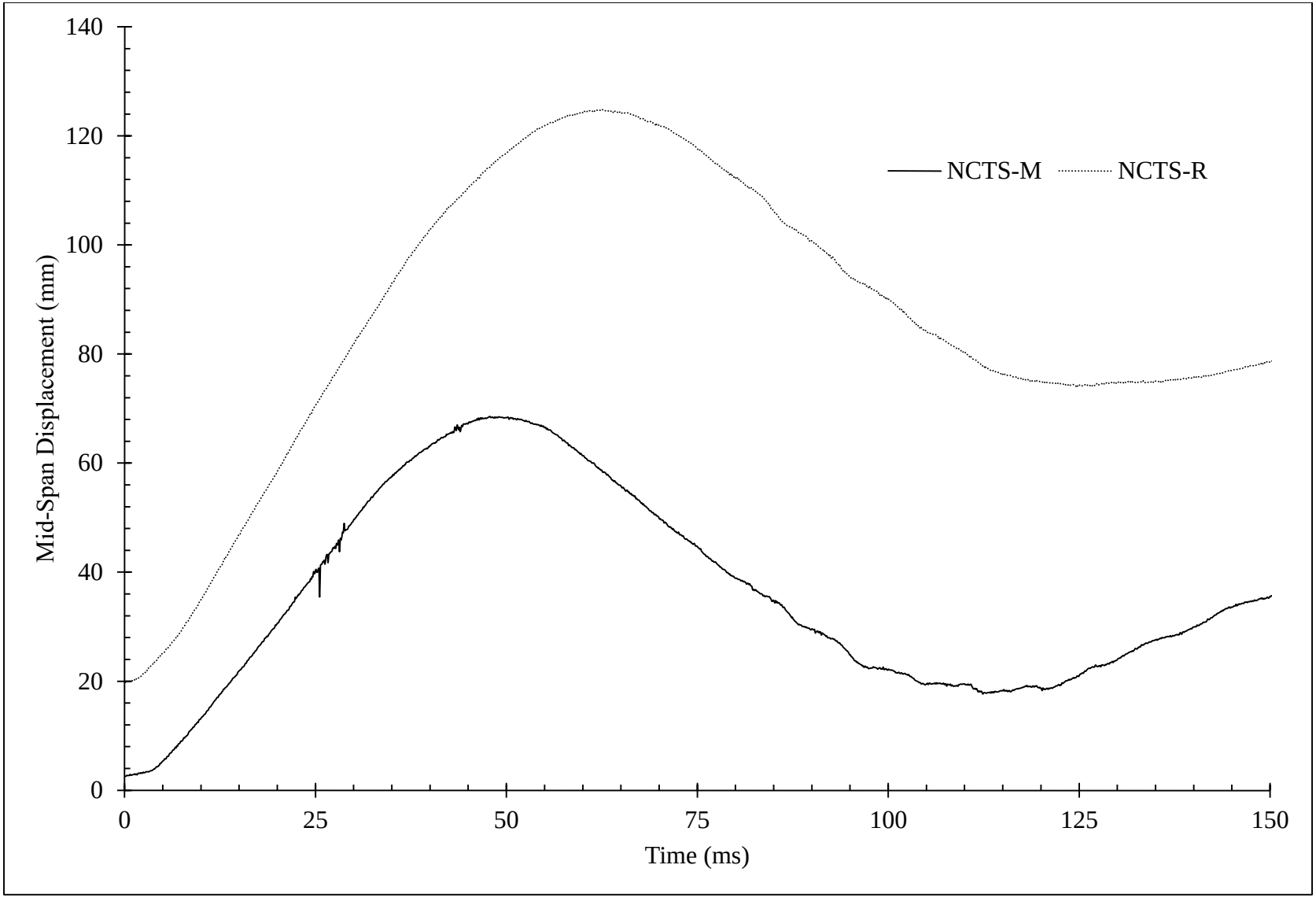

Figure A.11 – NCTS Shot 6: Experimental Mid-Span Displacement-Time Histories

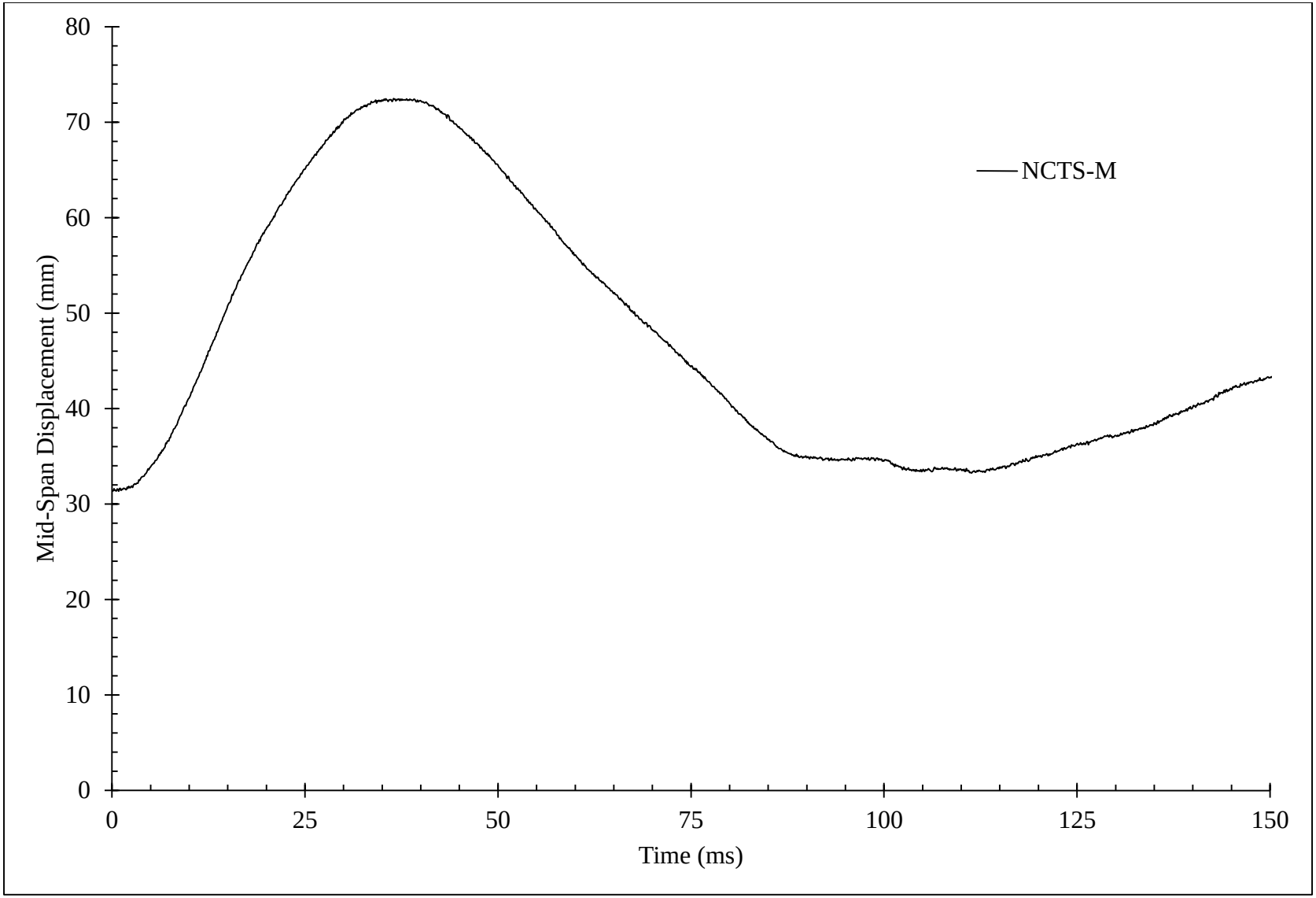

Figure A.12 – NCTS Shot 7: Experimental Mid-Span Displacement-Time Histories

B. Comparison of Experimental Pressure-Time Histories

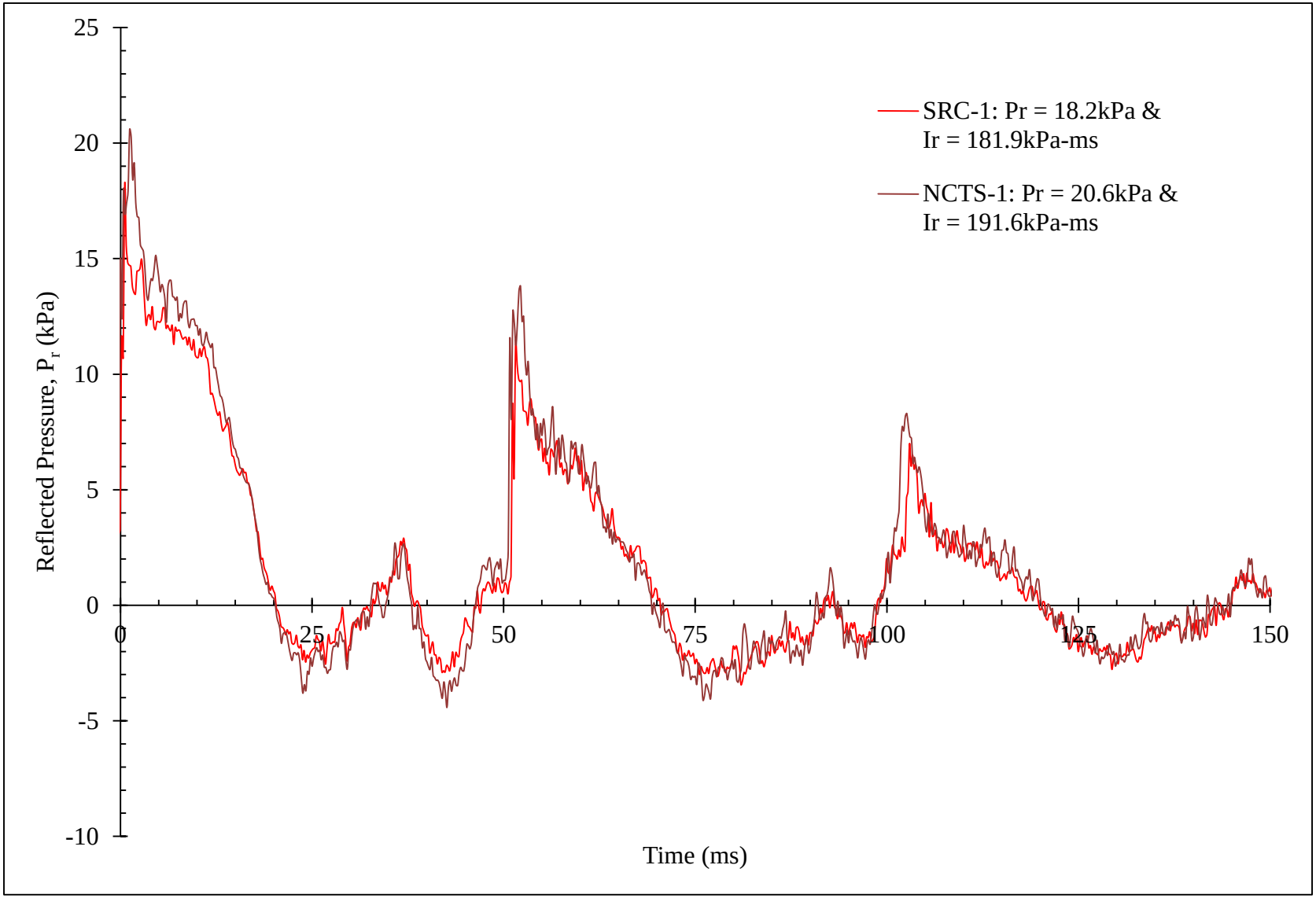

Figure B.1 – Shot-1: Experimental Pressure-Time Histories

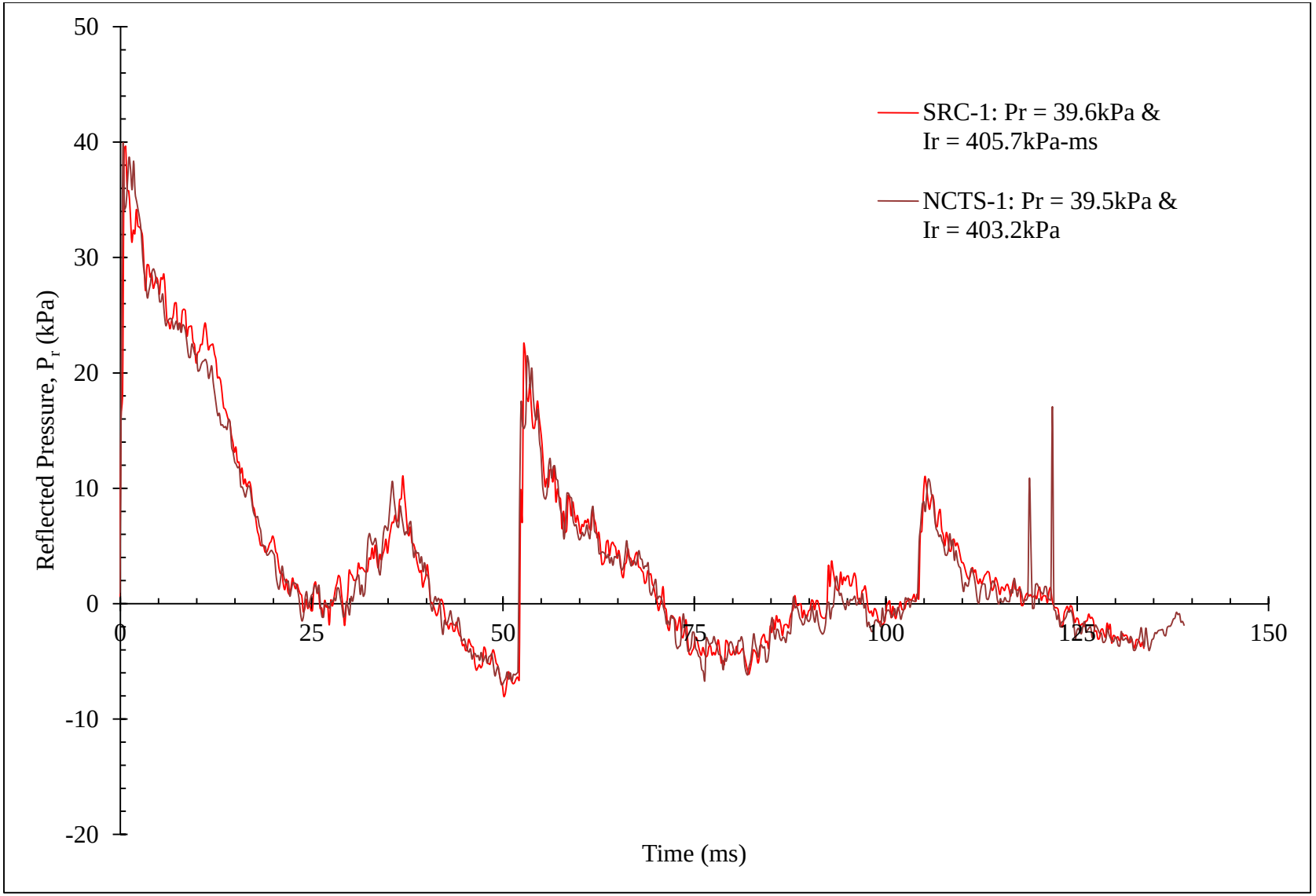

Figure B.2 – Shot 2: Experimental Pressure-Time Histories

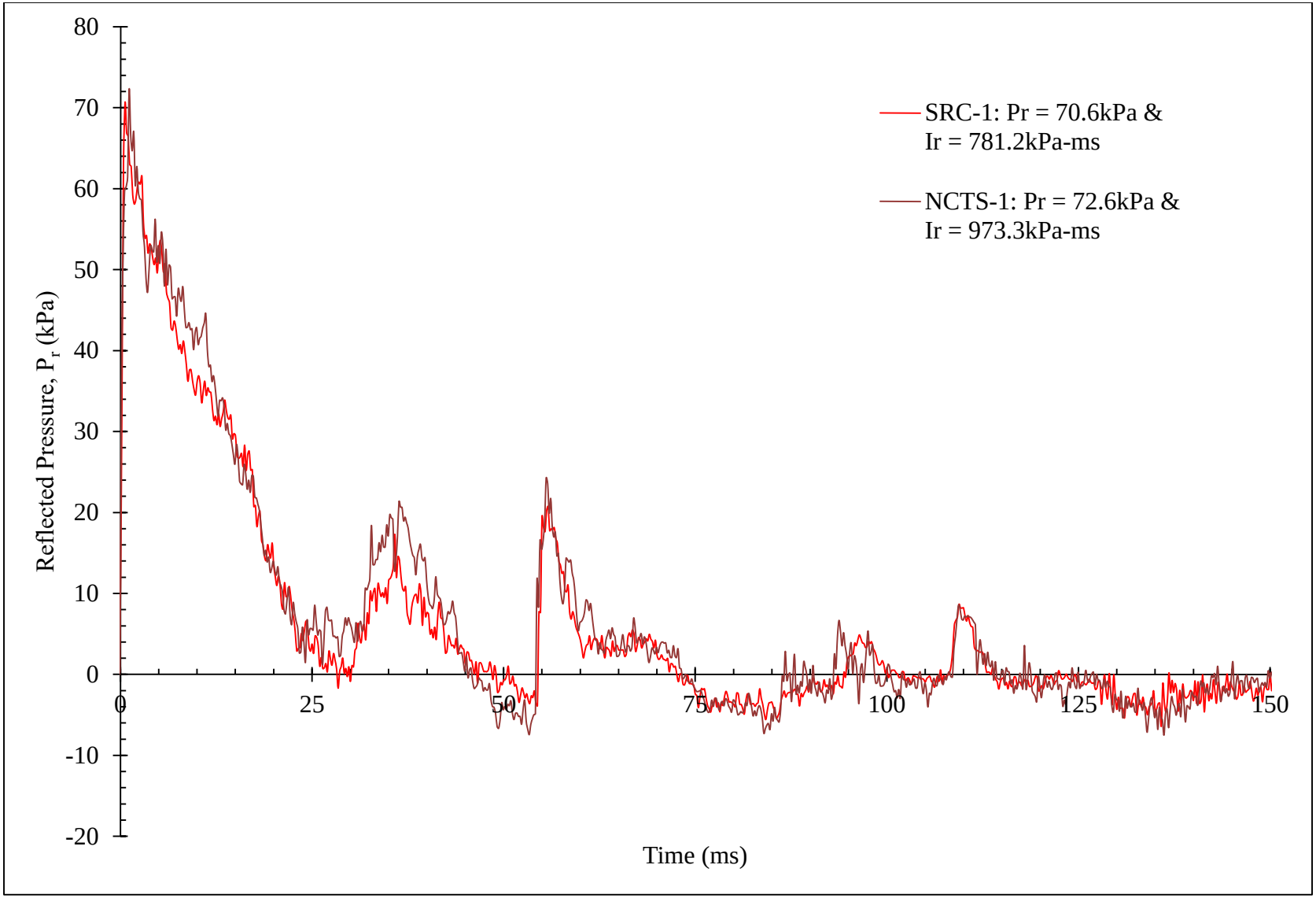

Figure B.3 Shot 3: Experimental Pressure-Time Histories

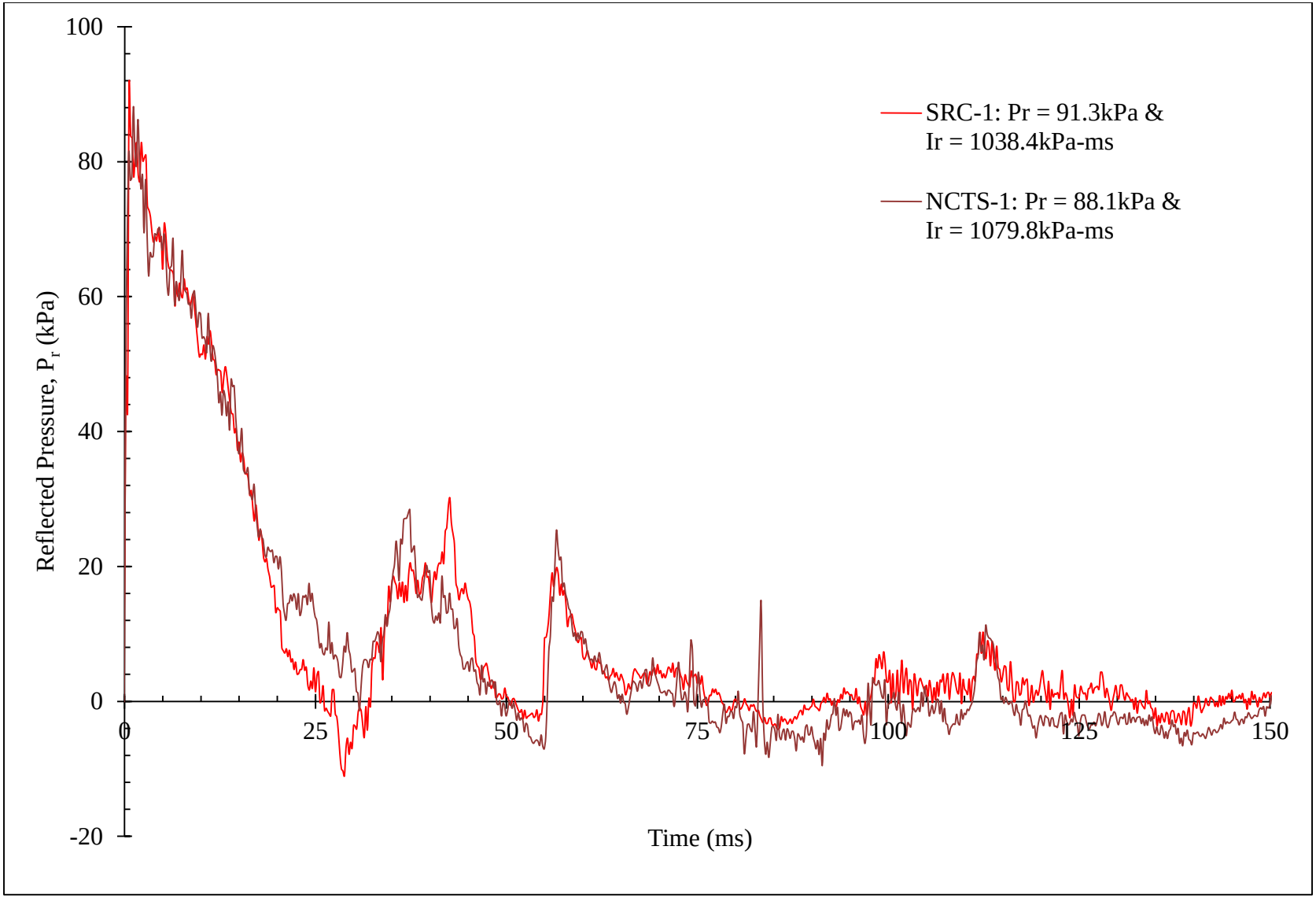

Figure B.4 – Shot 4: Experimental Pressure-Time Histories

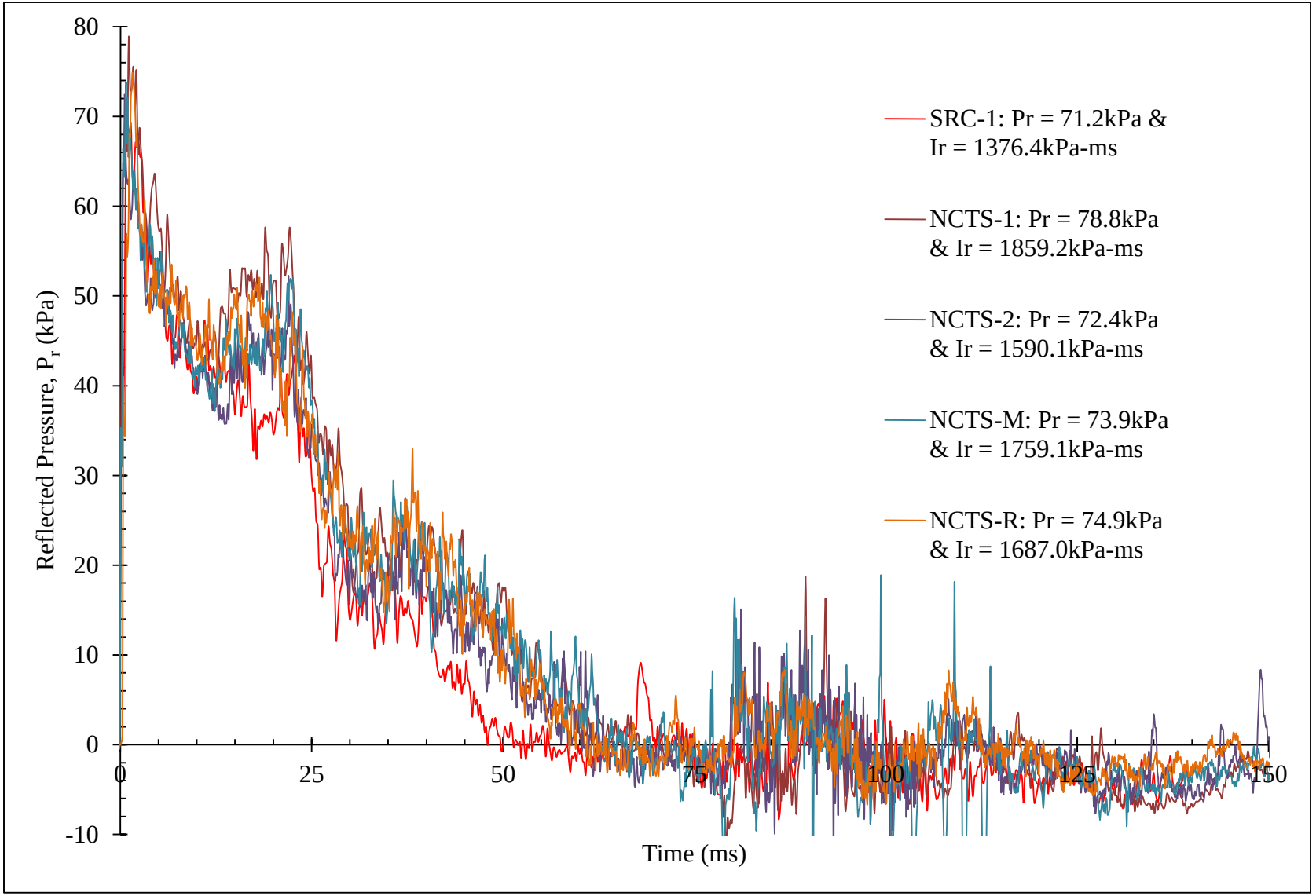

Figure B.5 – Shot 5: Experimental Pressure-Time Histories

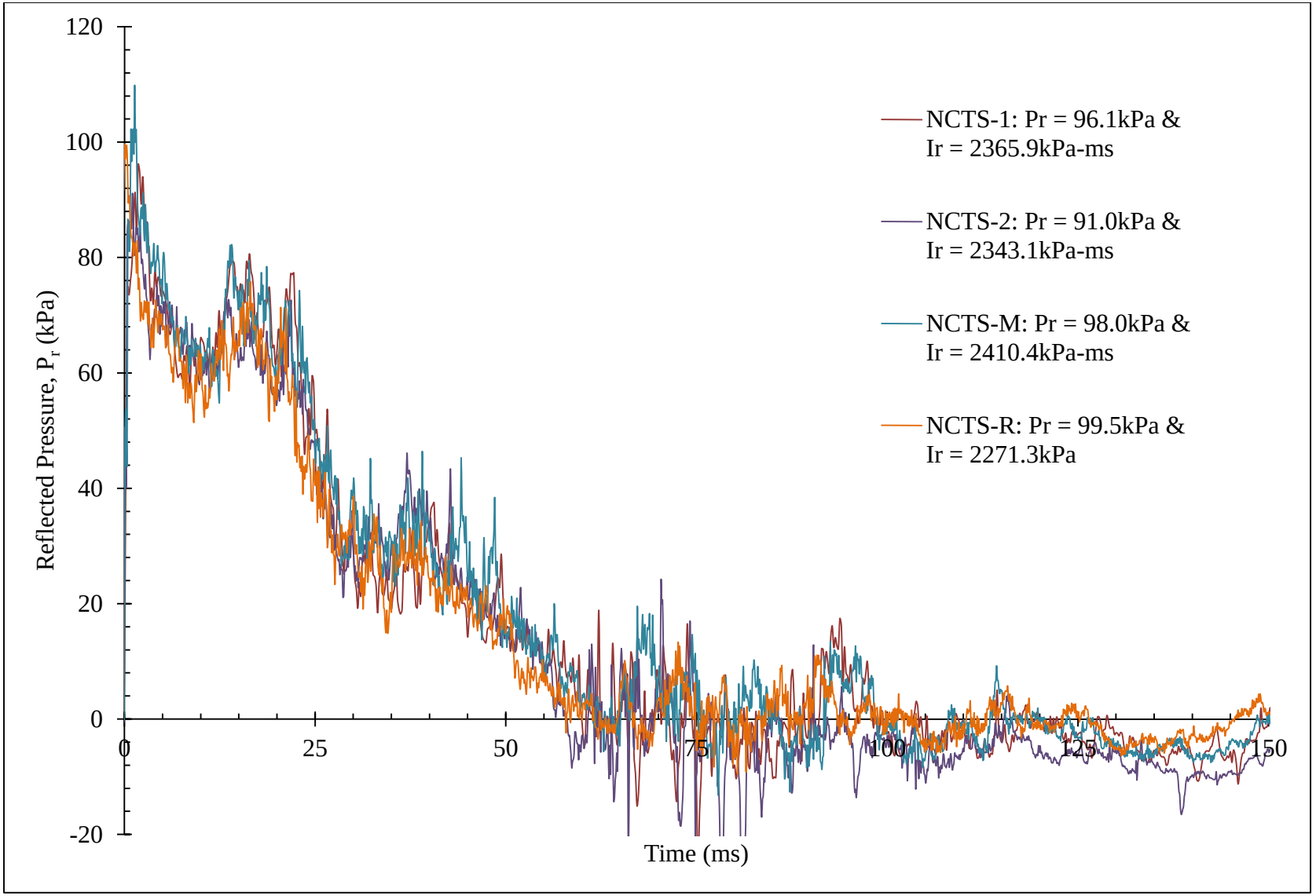

Figure B.6 – Shot 6: Experimental Pressure-Time Histories

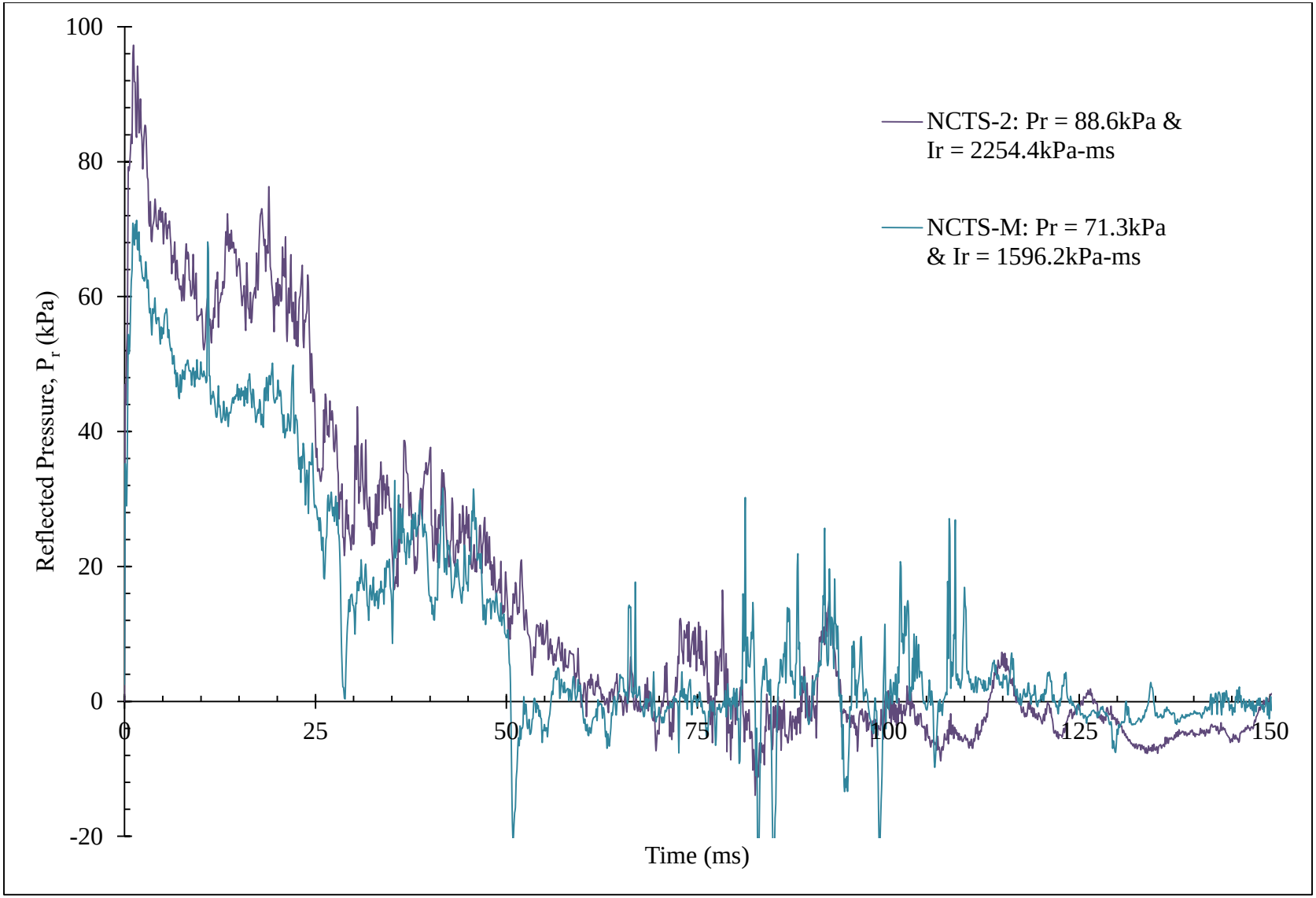

Figure B.7 – Shot 7: Experimental Pressure-Time Histories

C. Theoretical and Experimental Displacement-Time Histories

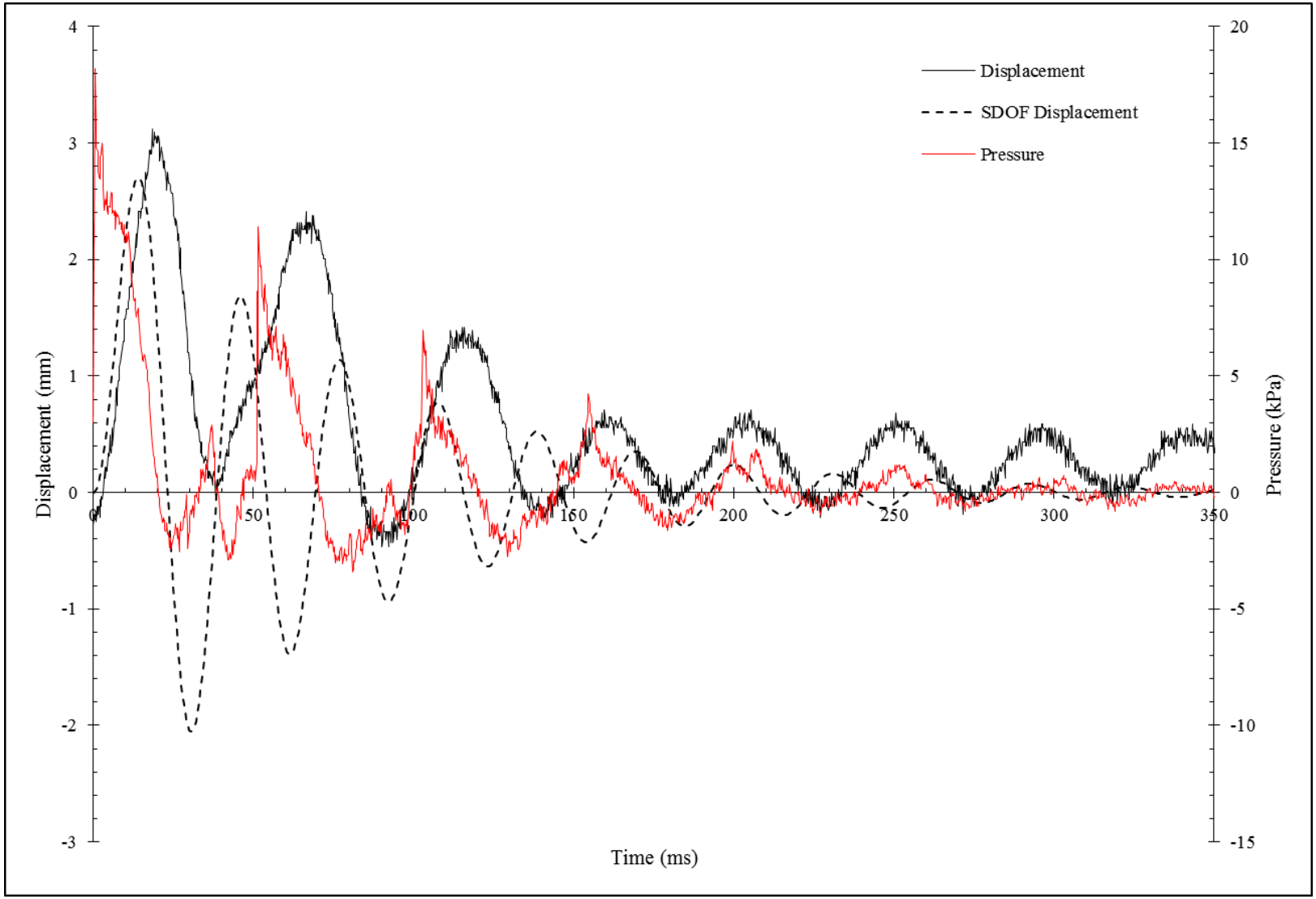

Figure C.1 – SRC-1 Shot 1: Pressure-Time History, Predicted and Experimental Displacement-Time Histories

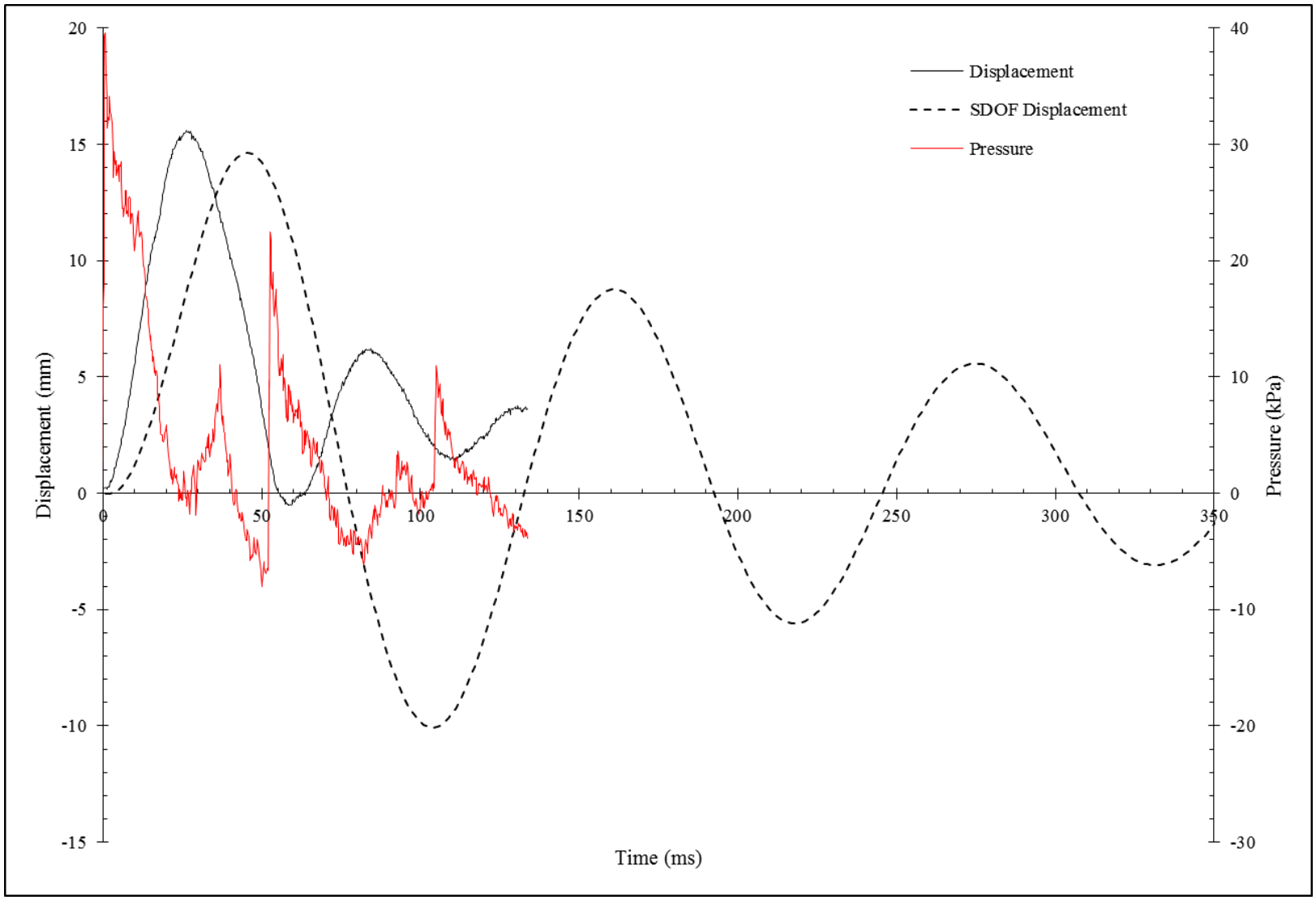

Figure C.2 – SRC-1 Shot 2: Pressure-Time History, Predicted and Experimental Displacement-Time Histories

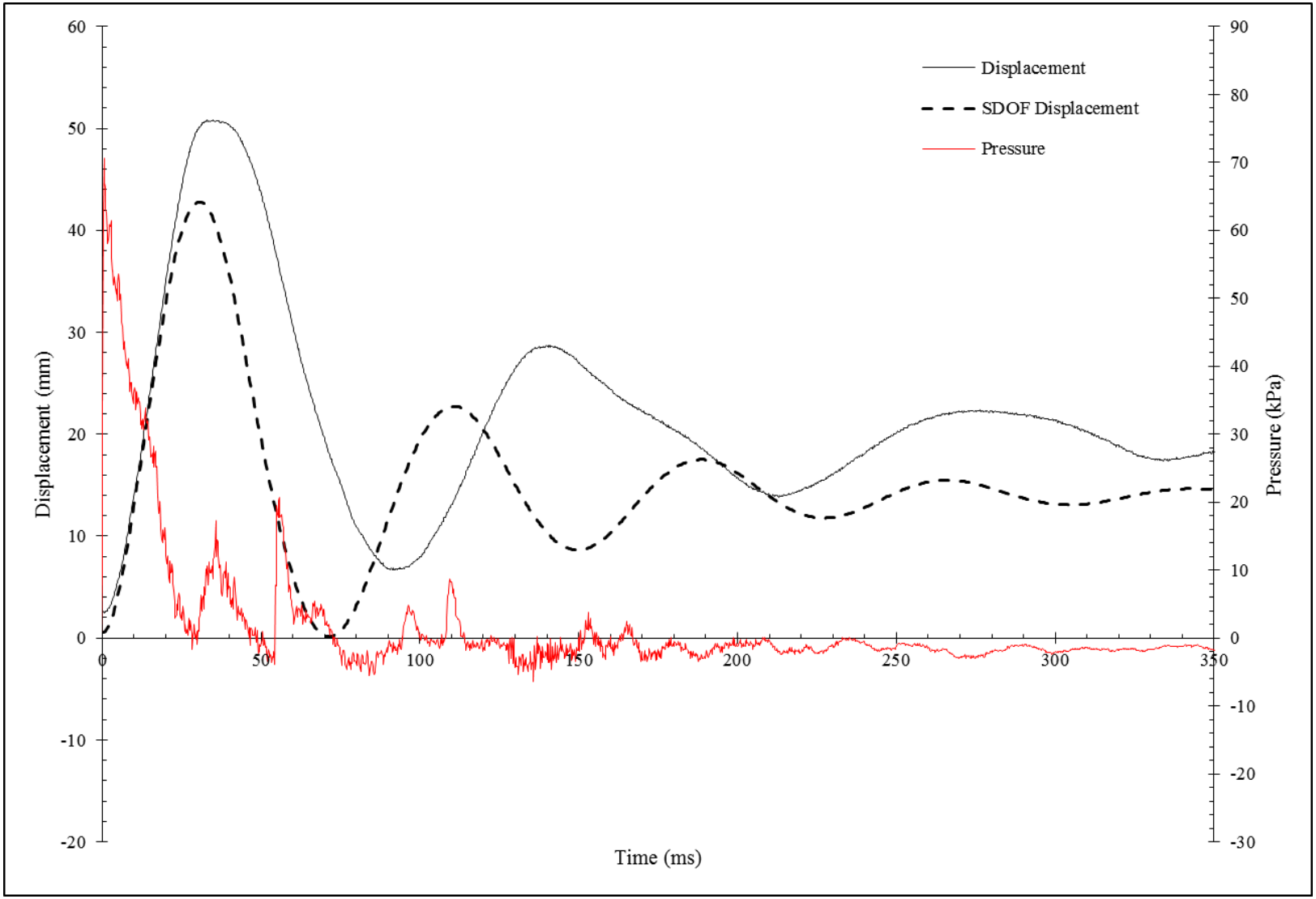

Figure C.3 – SRC-1 Shot 3: Pressure-Time History, Predicted and Experimental Displacement-Time Histories

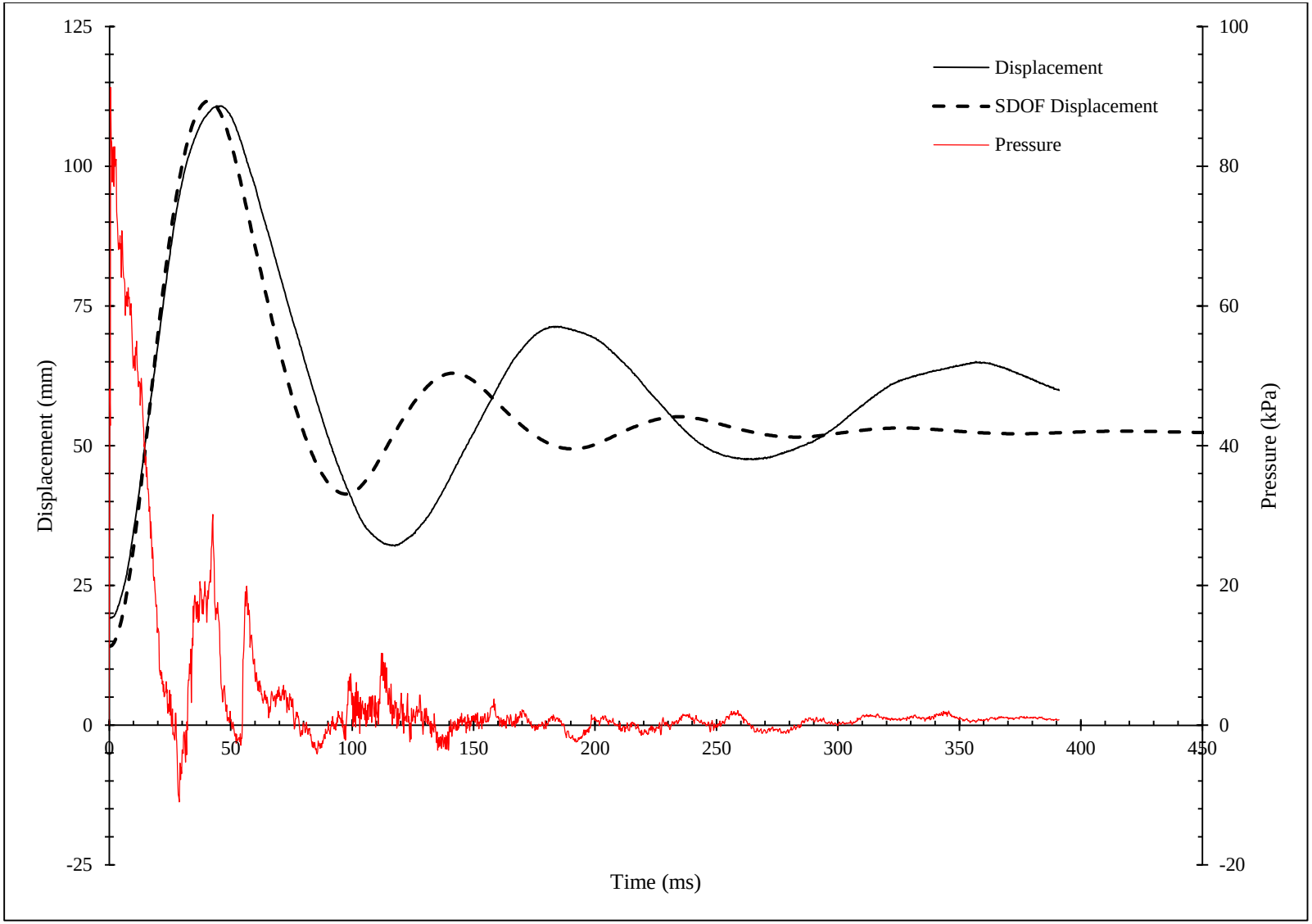

Figure C.4 – SRC-1 Shot 4: Pressure-Time History, Predicted and Experimental Displacement-Time Histories

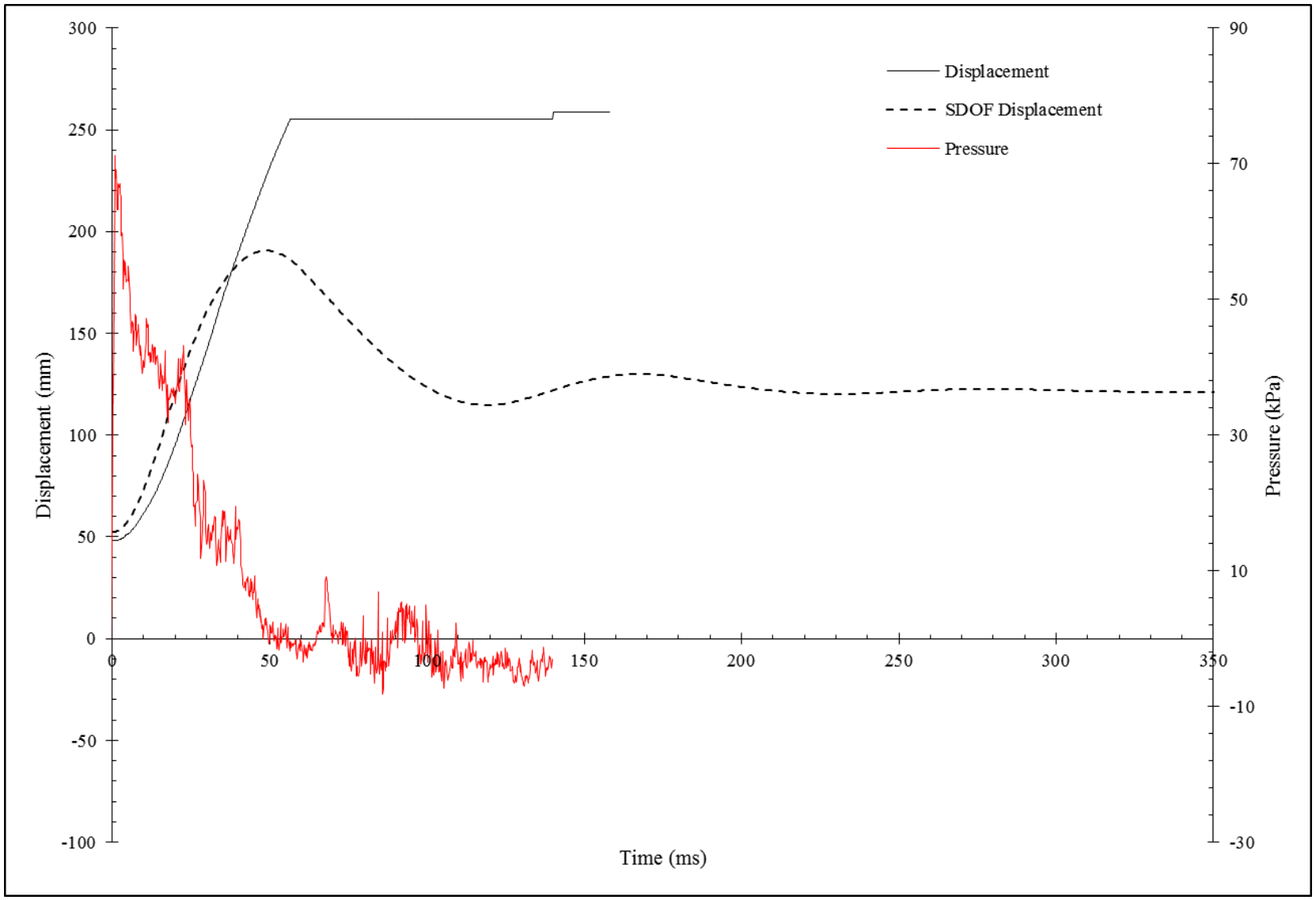

Figure C.5 – SRC-1 Shot 5: Pressure-Time History, Predicted and Experimental Displacement-Time Histories

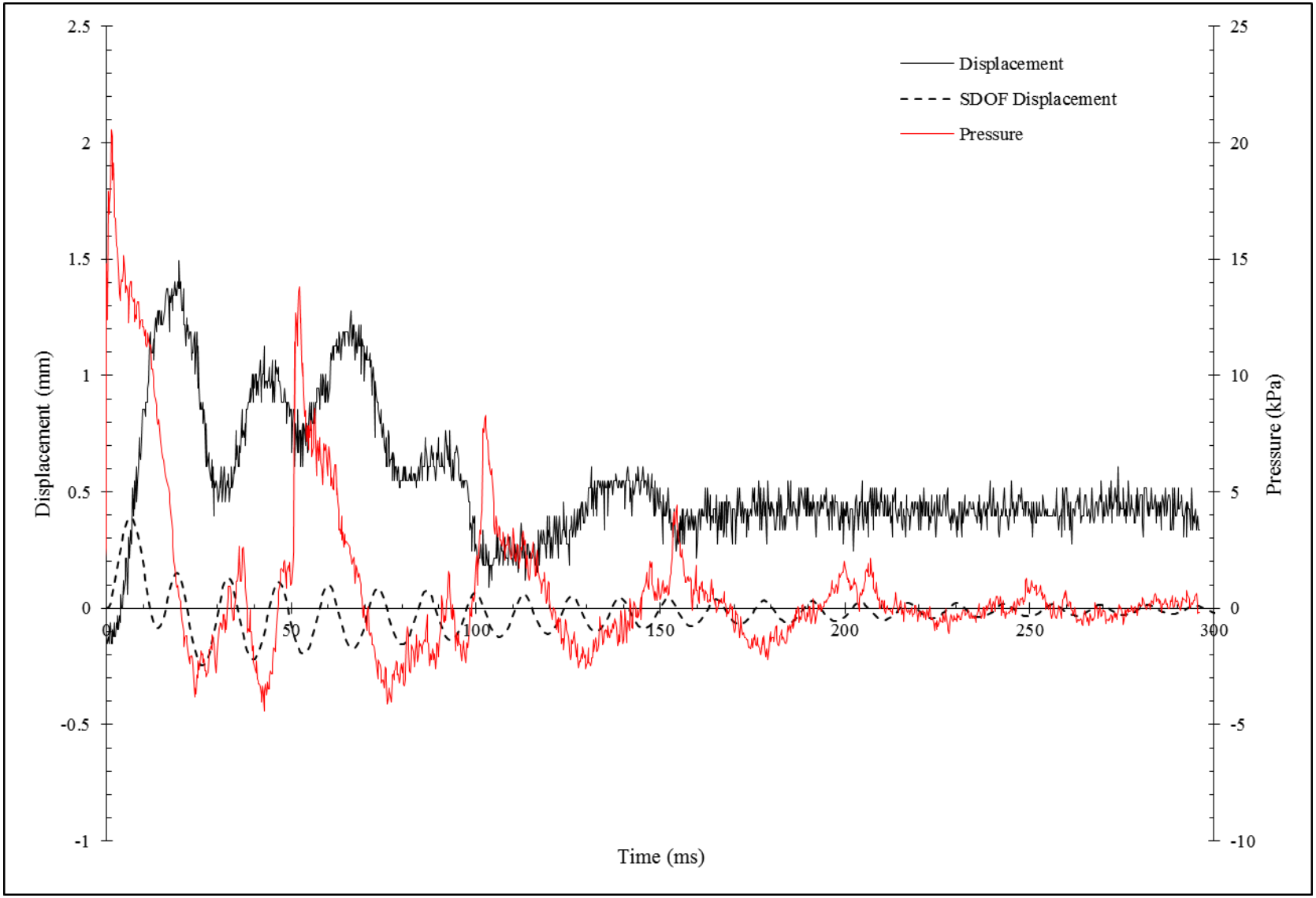

Figure C.6 – NCTS-1 Shot 1: Pressure-Time History, Predicted and Experimental Displacement-Time Histories

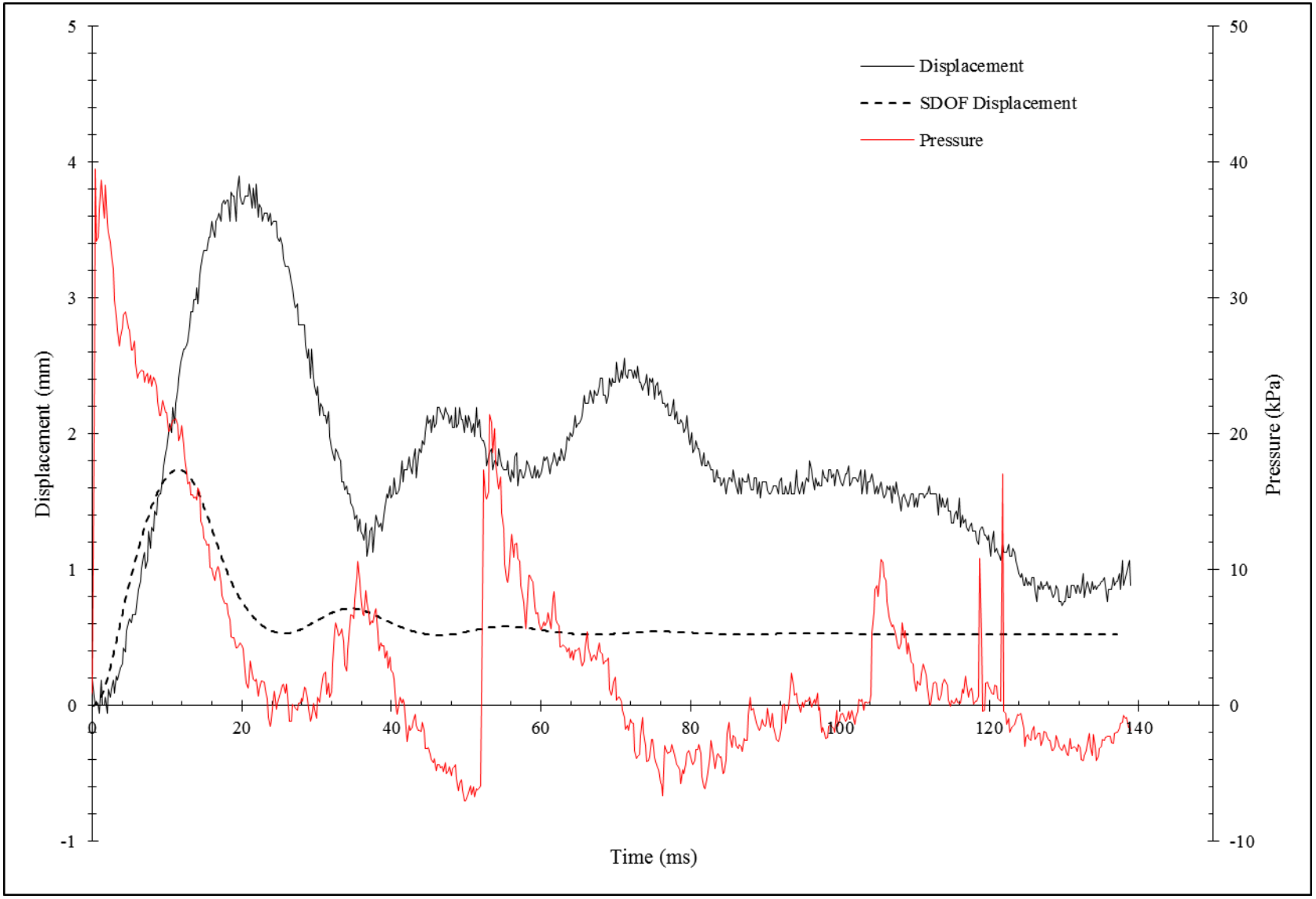

Figure C.7 – NCTS-1 Shot 2: Pressure-Time History, Predicted and Experimental Displacement-Time Histories

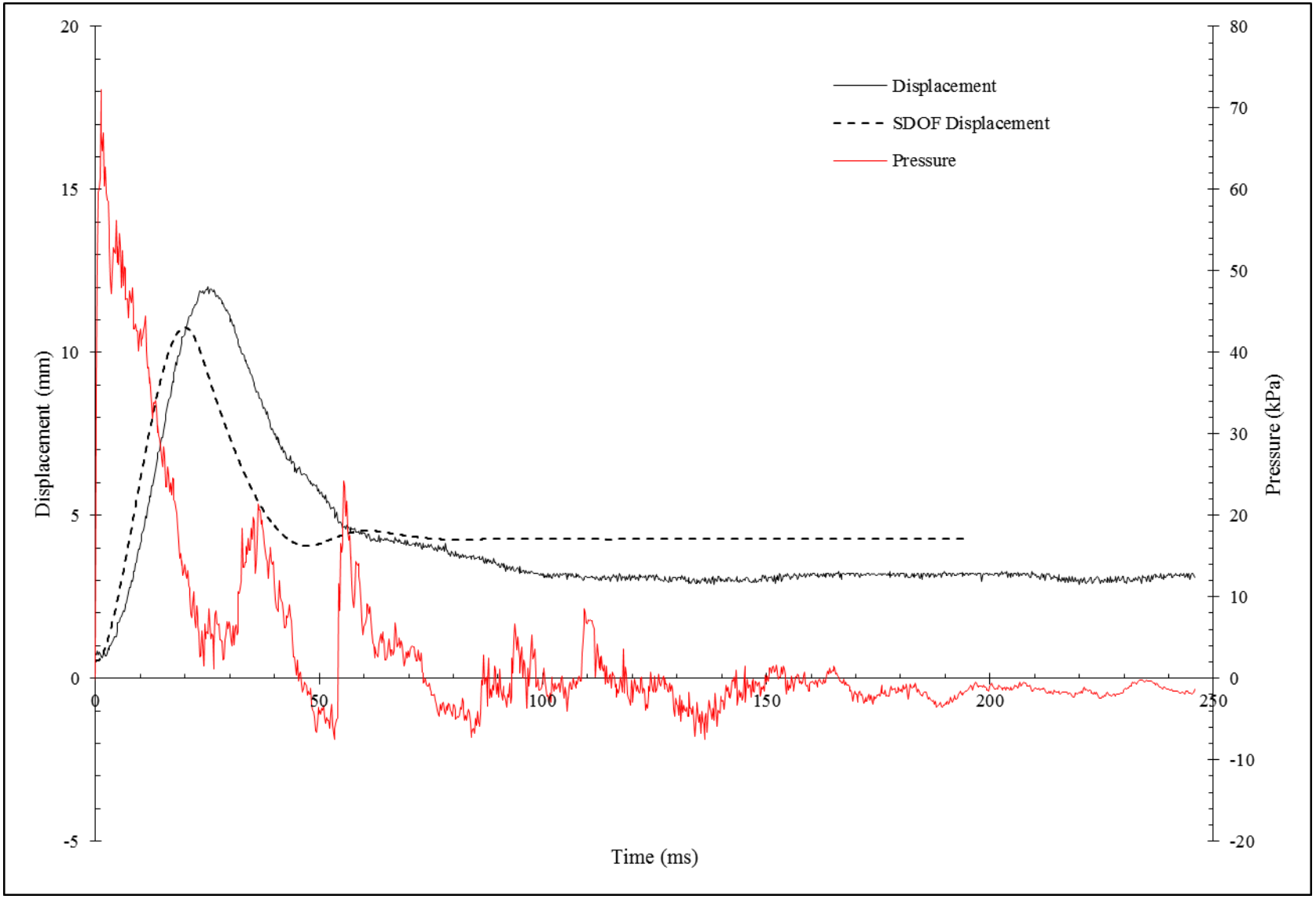

Figure C.8 – NCTS-1 Shot 3: Pressure-Time History, Predicted and Experimental Displacement-Time Histories

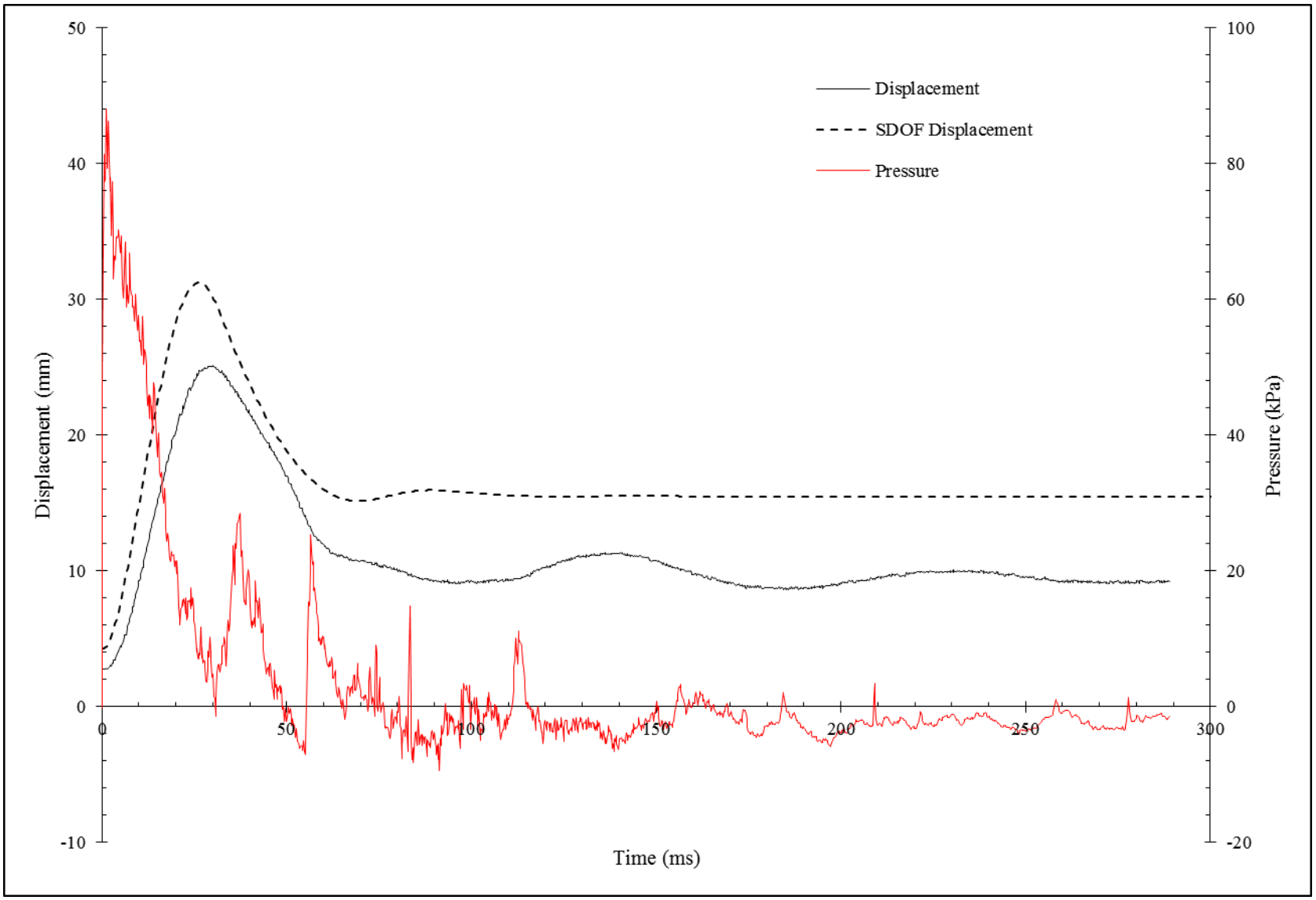

Figure C.9 – NCTS-1 Shot 4: Pressure-Time History, Predicted and Experimental Displacement-Time Histories

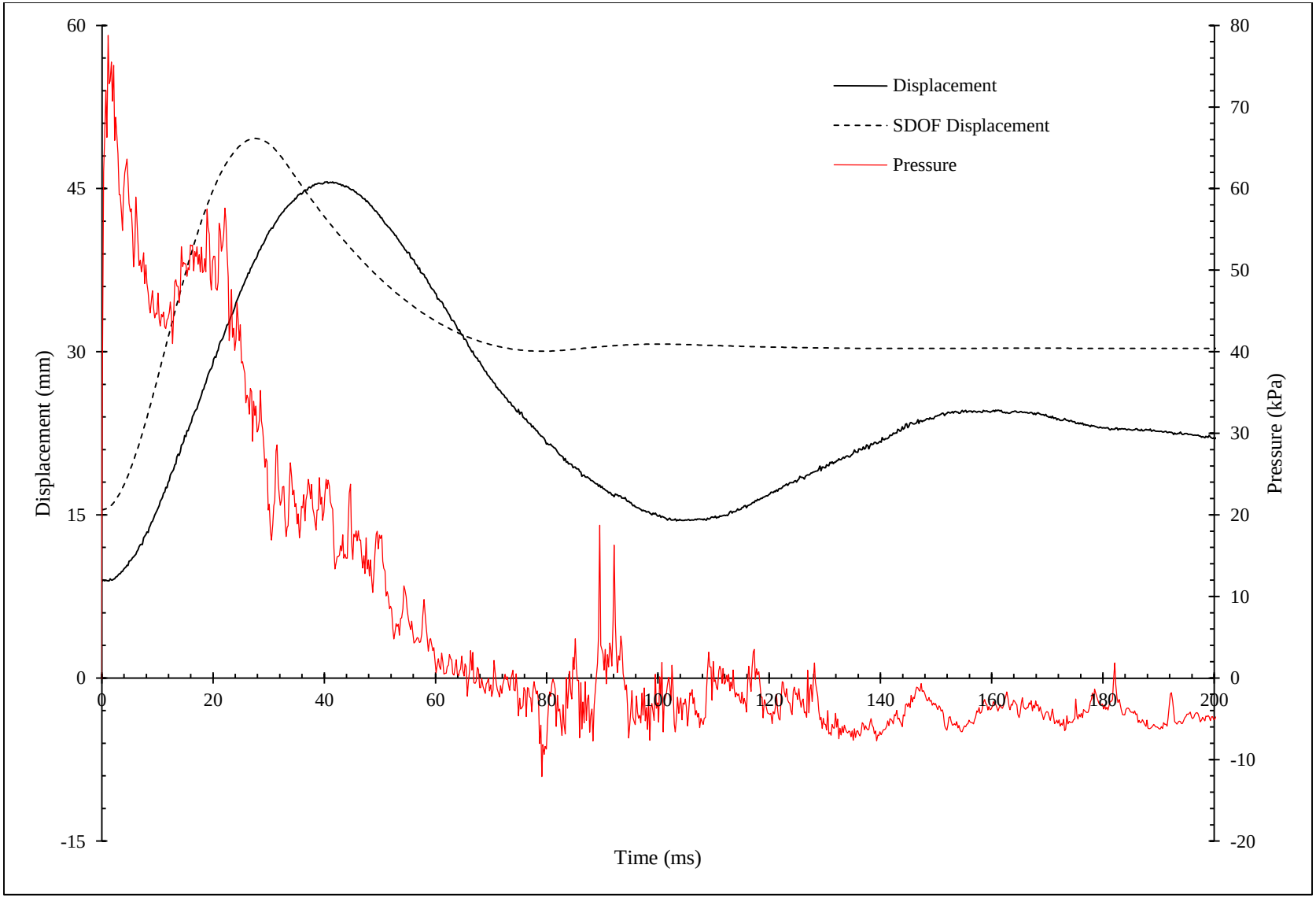

Figure C.10 – NCTS-1 Shot 5: Pressure-Time History, Predicted and Experimental Displacement-Time Histories

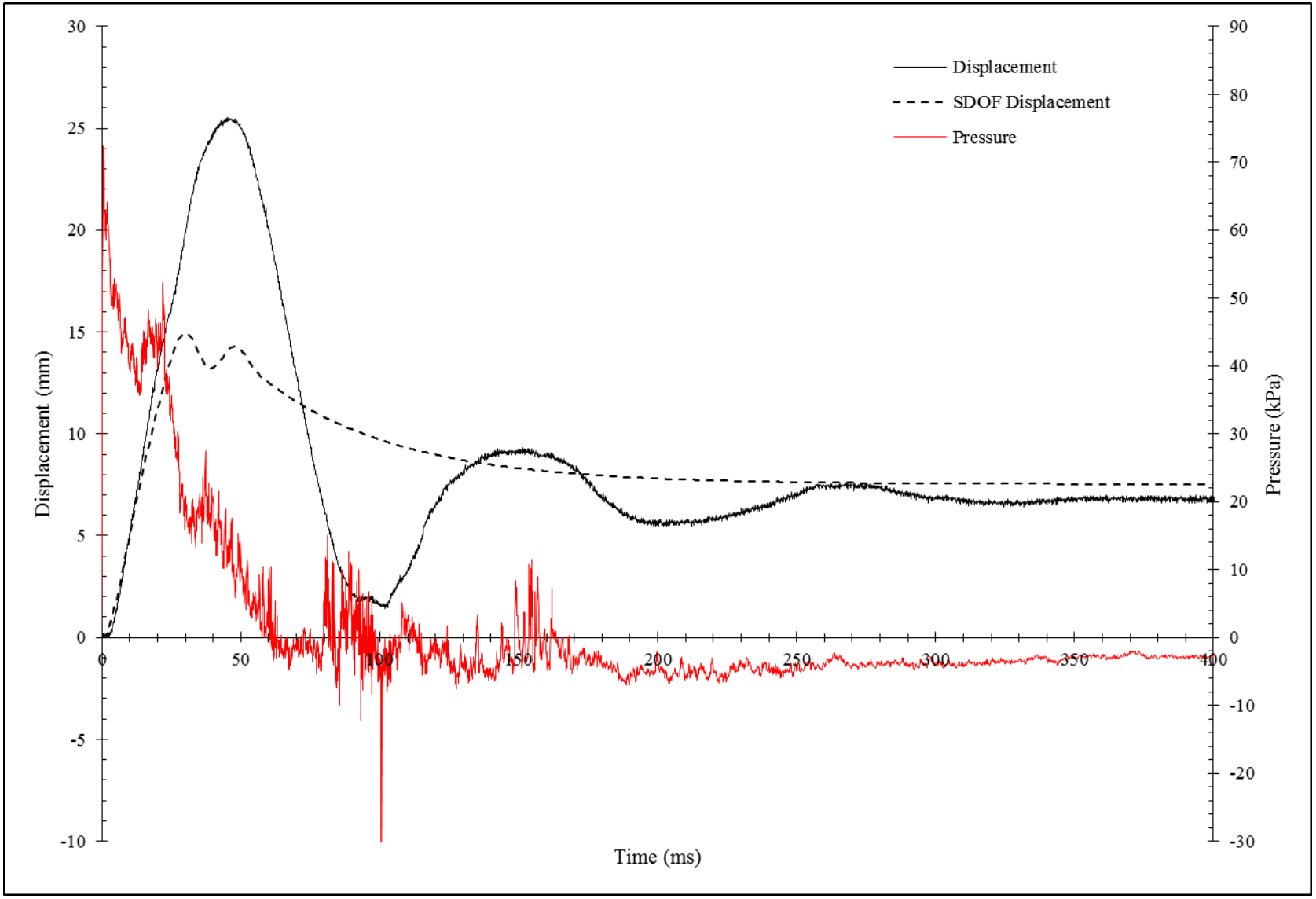

Figure C.11 – NCTS-2 Shot 1: Pressure-Time History, Predicted and Experimental Displacement-Time Histories

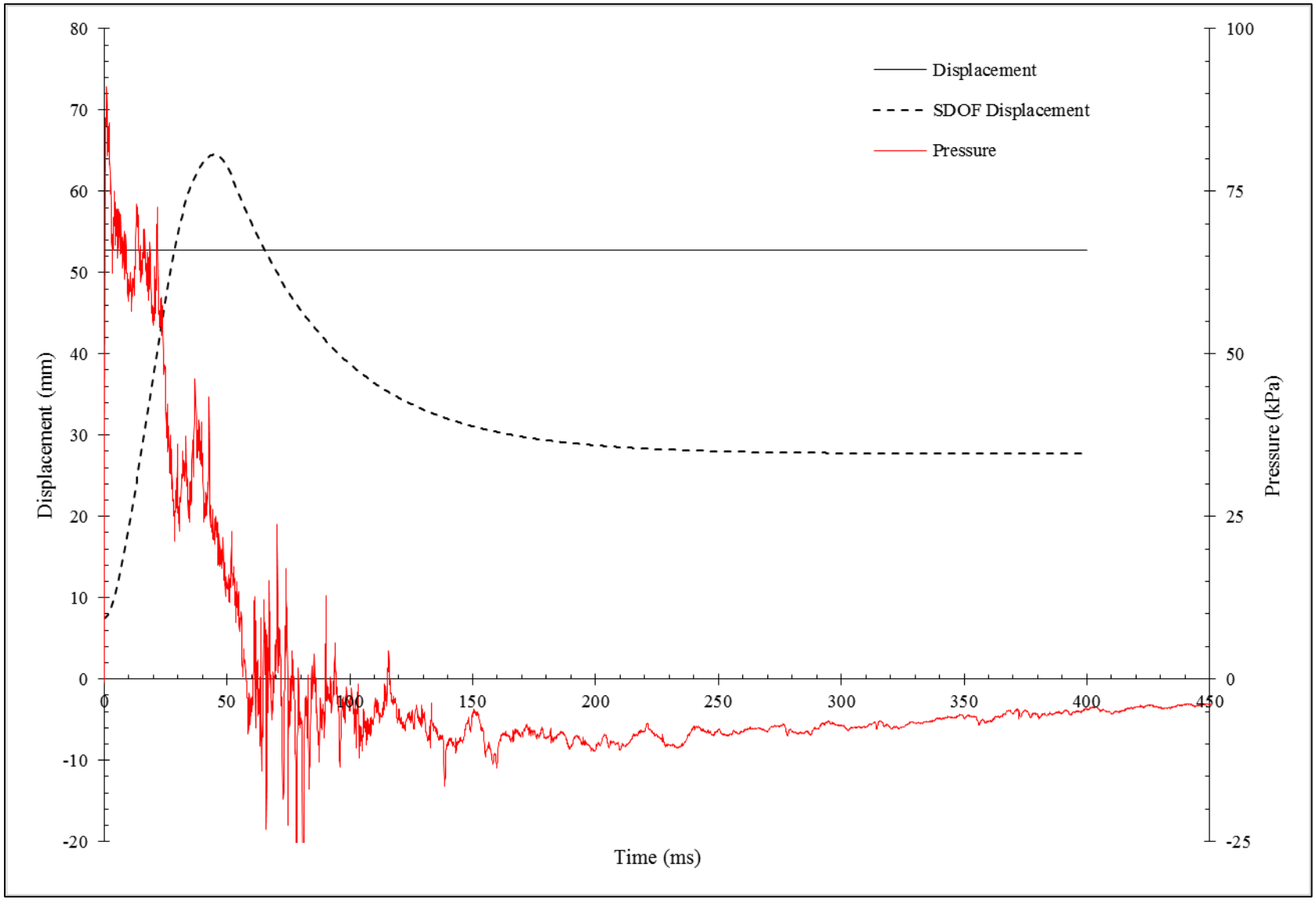

Figure C.12 – NCTS-2 Shot 2: Pressure-Time History, Predicted and Experimental Displacement-Time Histories

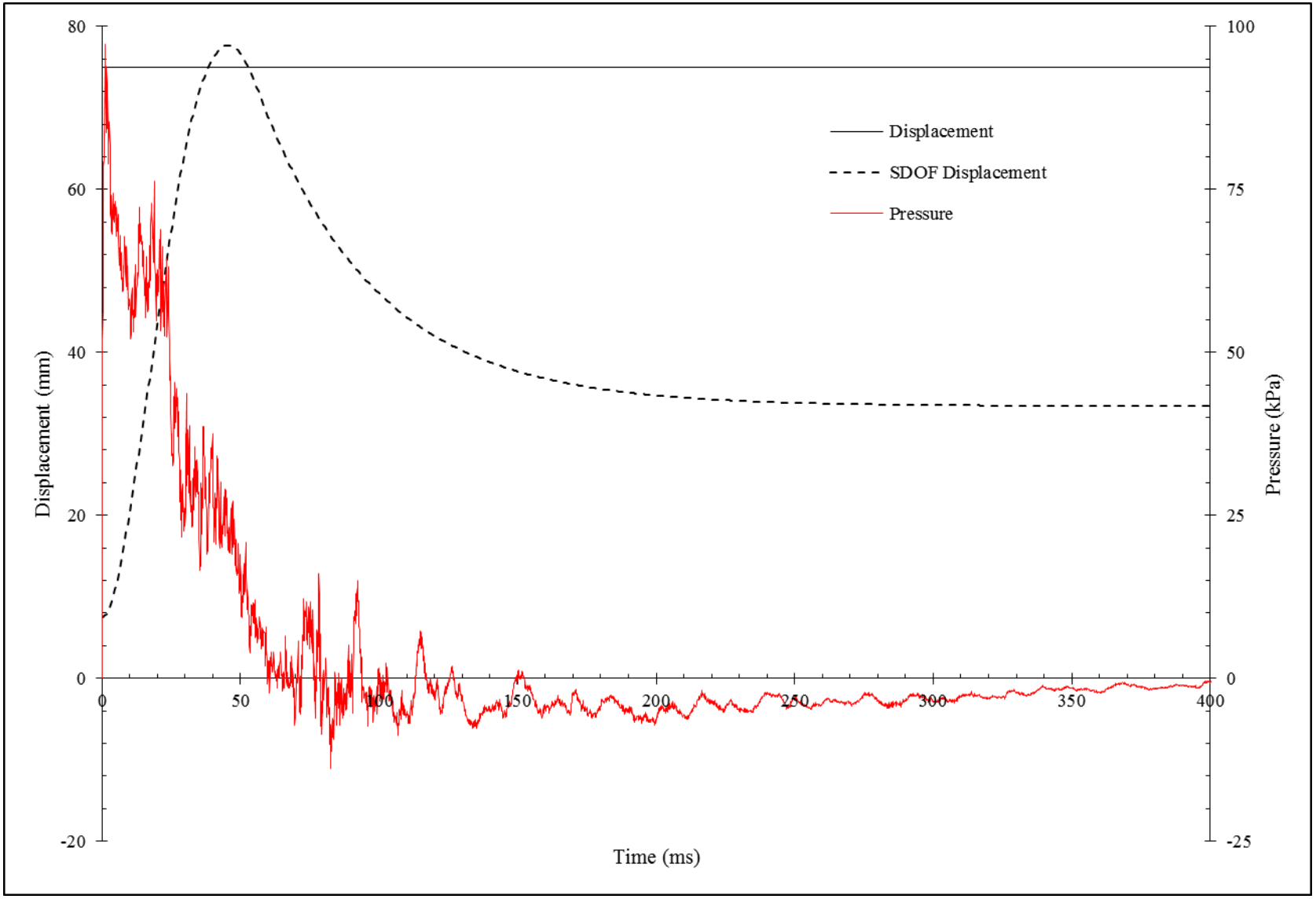

Figure C.13 – NCTS-2 Shot 3: Pressure-Time History, Predicted and Experimental Displacement-Time Histories

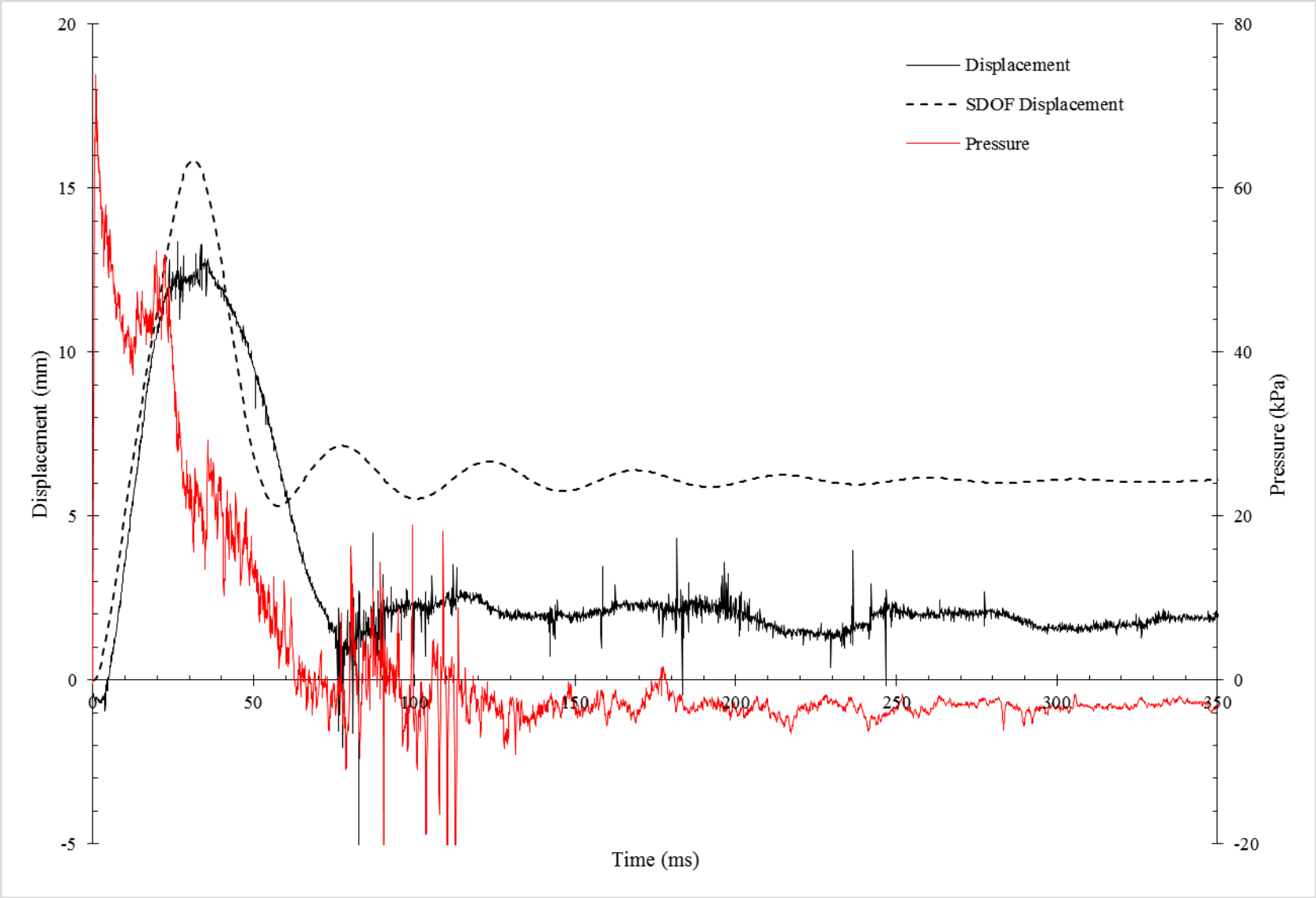

Figure C.14 – NCTS-M Shot 1: Pressure-Time History, Predicted and Experimental Displacement-Time Histories

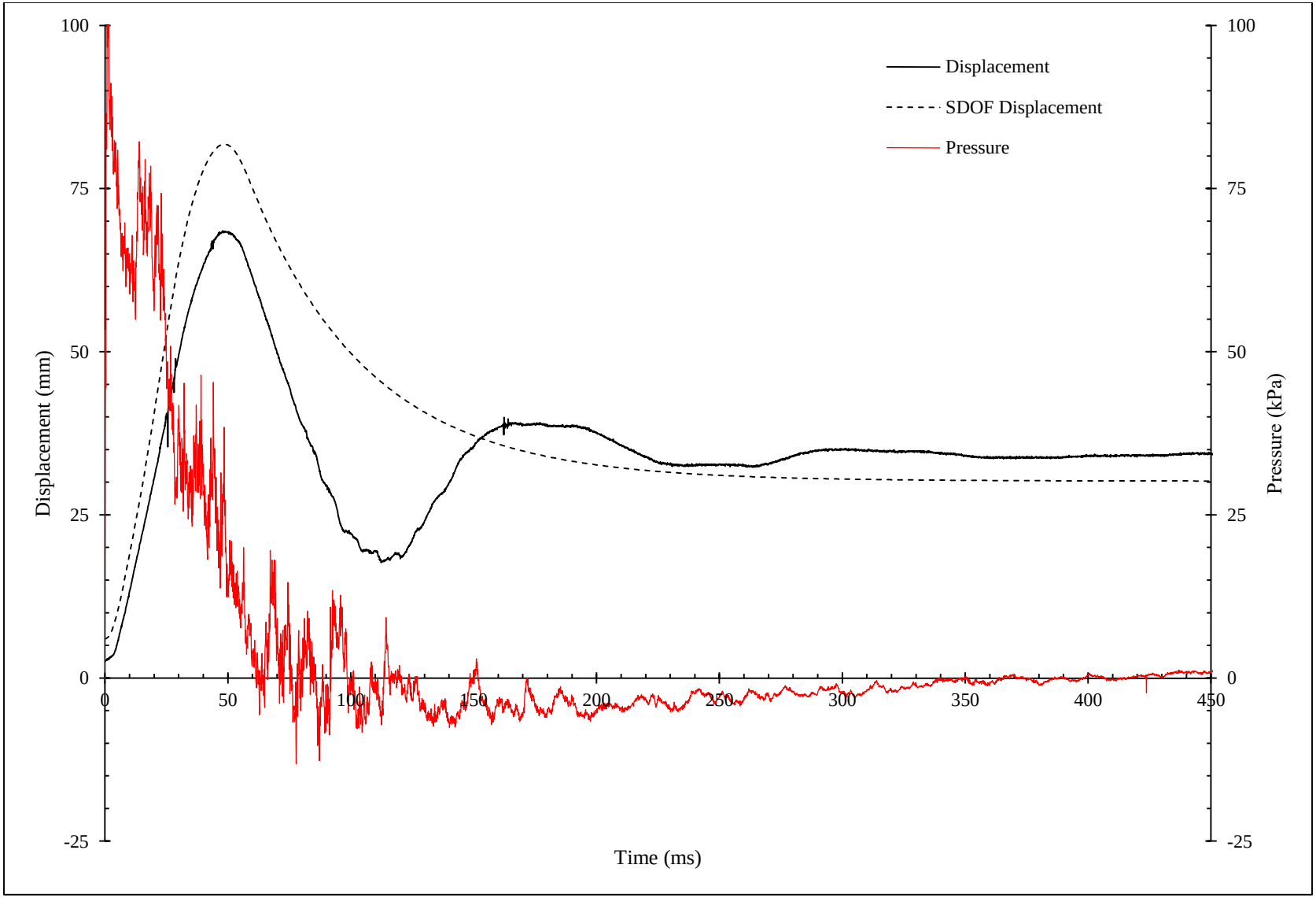

Figure C.15 – NCTS-M Shot 2: Pressure-Time History, Predicted and Experimental Displacement-Time Histories

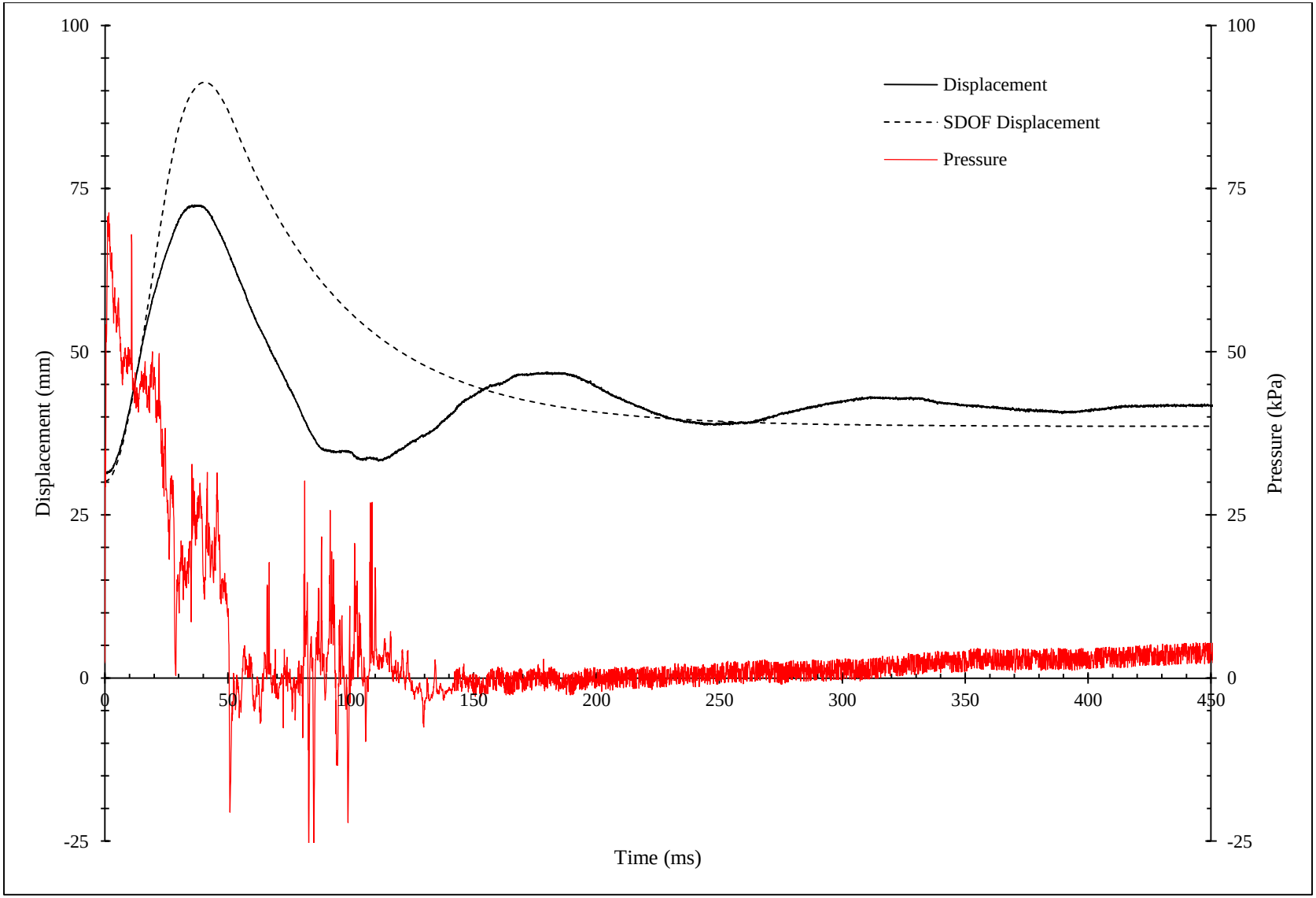

Figure C.16 – NCTS-M Shot 3: Pressure-Time History, Predicted and Experimental Displacement-Time Histories

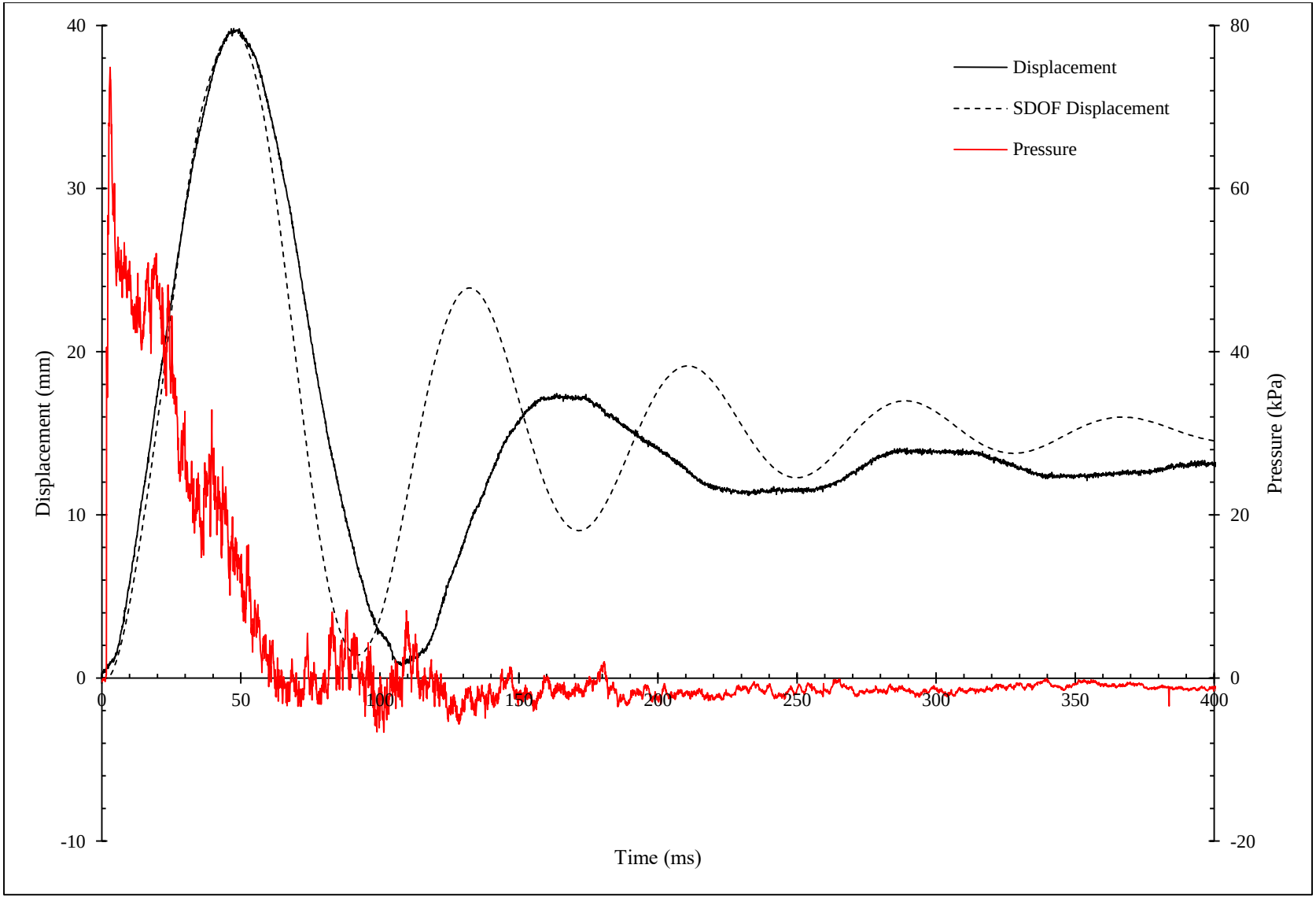

Figure C.17 – NCTS-R Shot 1: Pressure-Time History, Predicted and Experimental Displacement-Time Histories

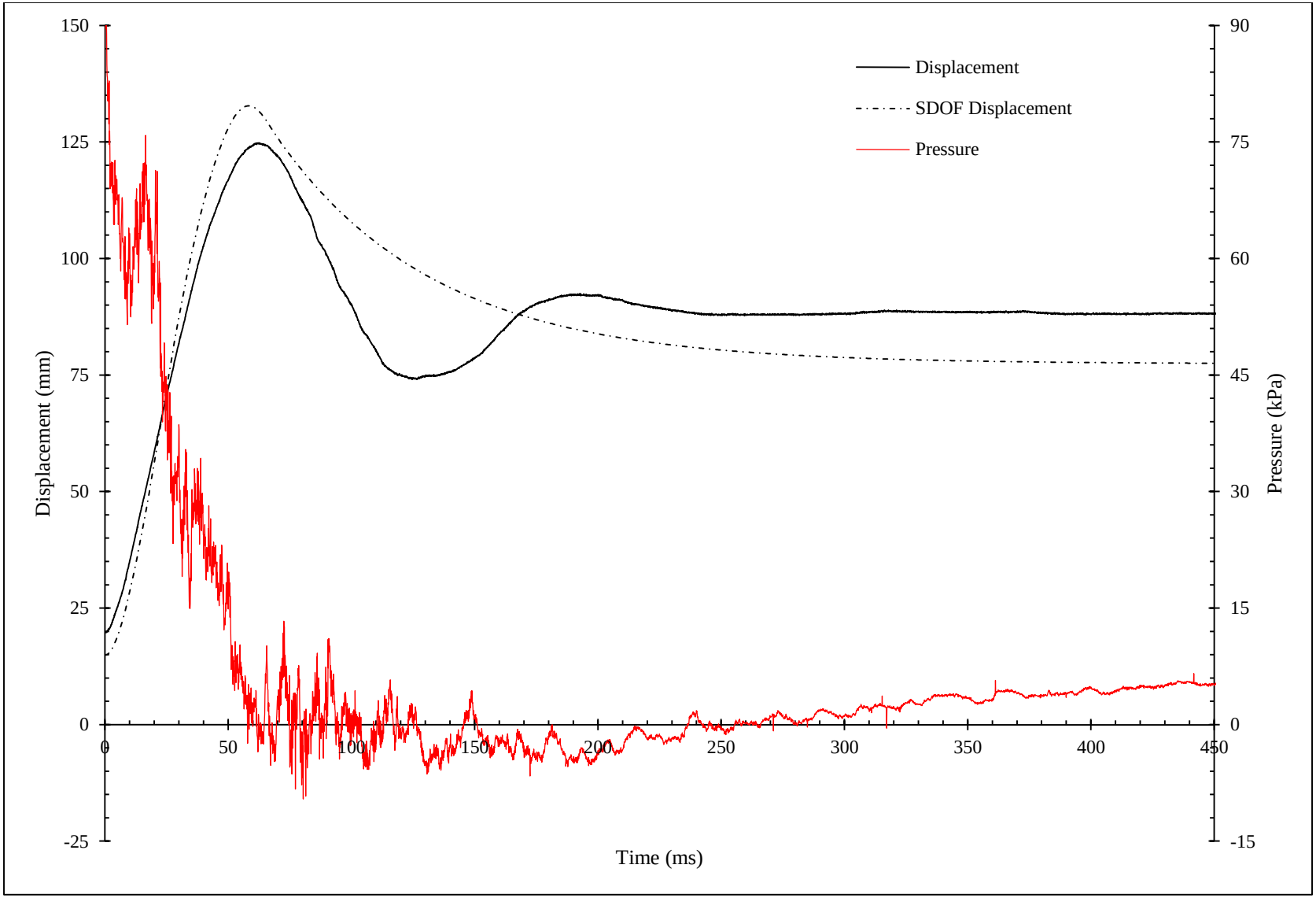

Figure C.18 – NCTS-4 Shot 2: Pressure-Time History, Predicted and Experimental Displacement-Time Histories

D. NCTS-FS8 and NCTS-FS4 Theoretical Displacement-Time Histories

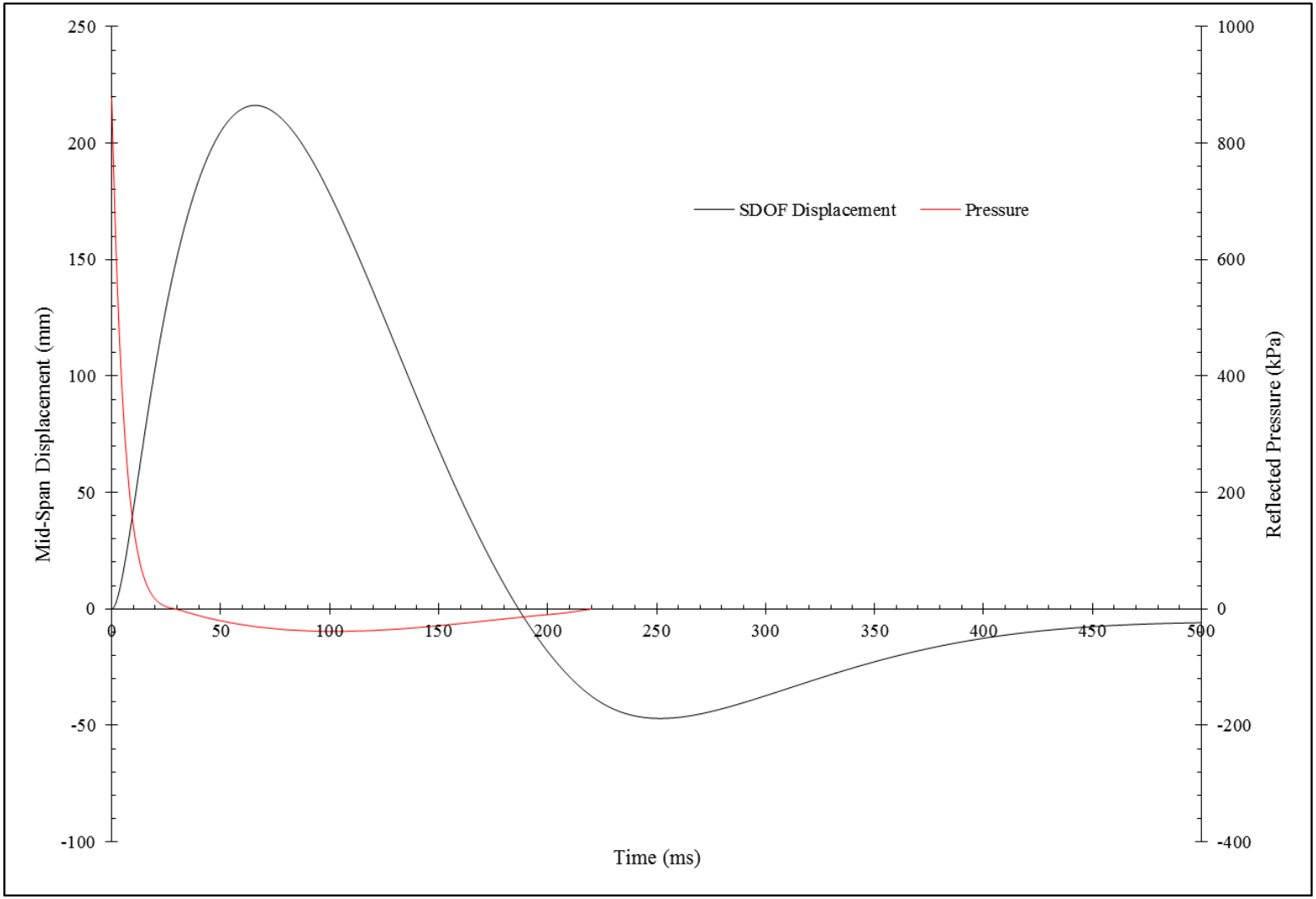

Figure D.1 – NCTS-FS8 2800kg TNT @ 30m: Pressure-Time and Displacement-Time Histories

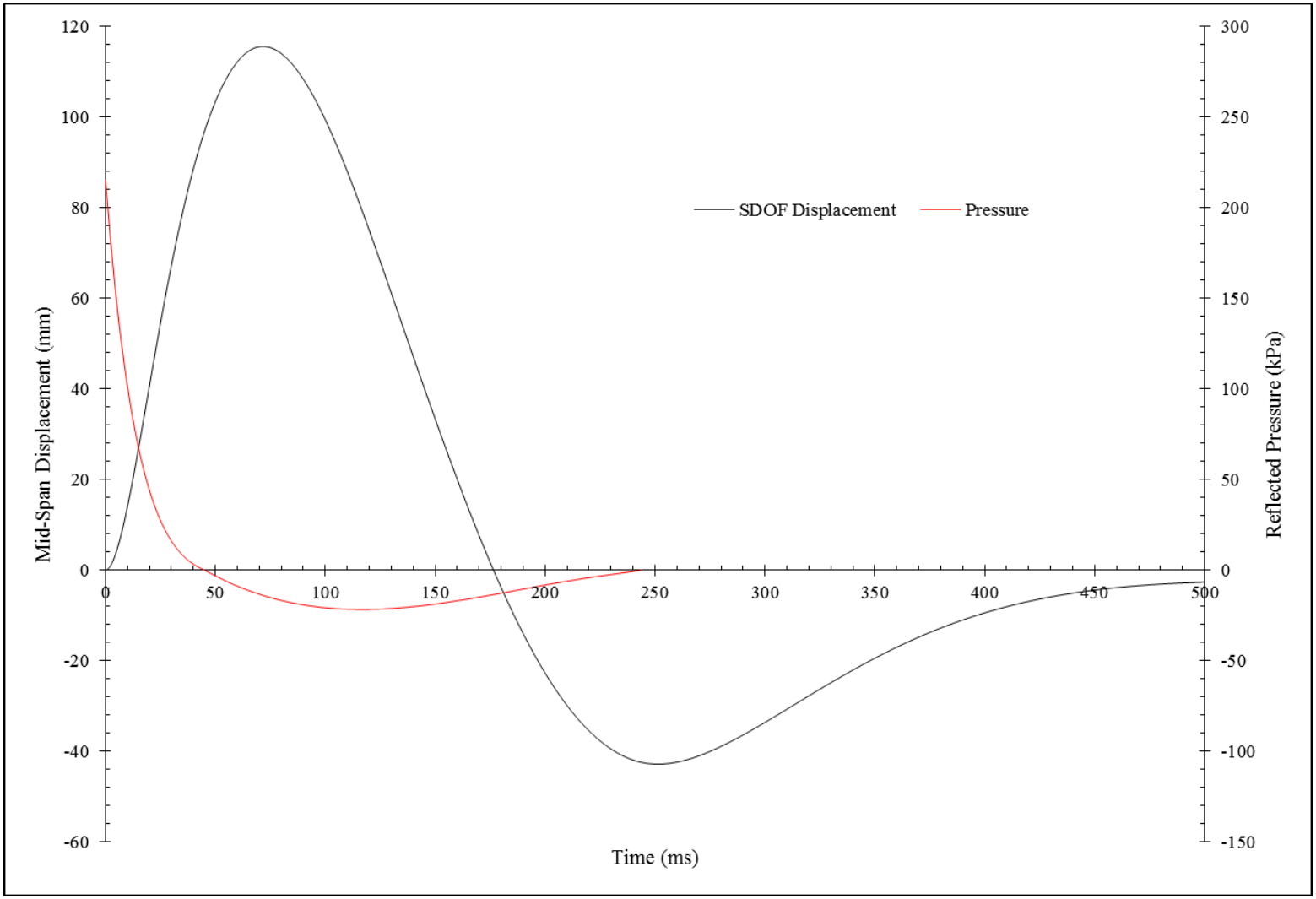

Figure D.2 – NCTS-FS8 2800kg TNT @ 50m: Pressure-Time and Displacement-Time Histories

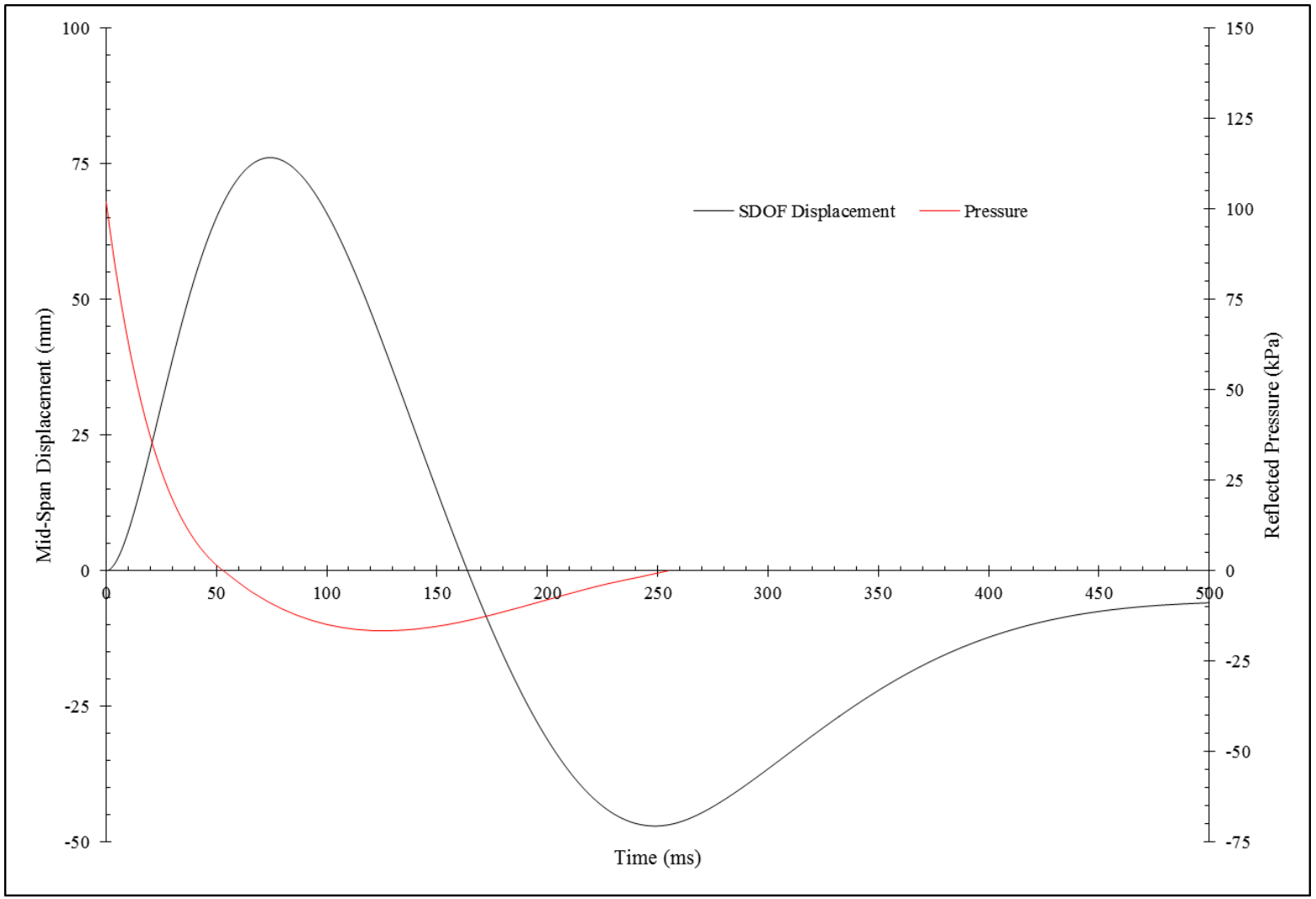

Figure D.3– NCTS-FS8 2800kg TNT @ 70m: Pressure-Time and Displacement-Time Histories

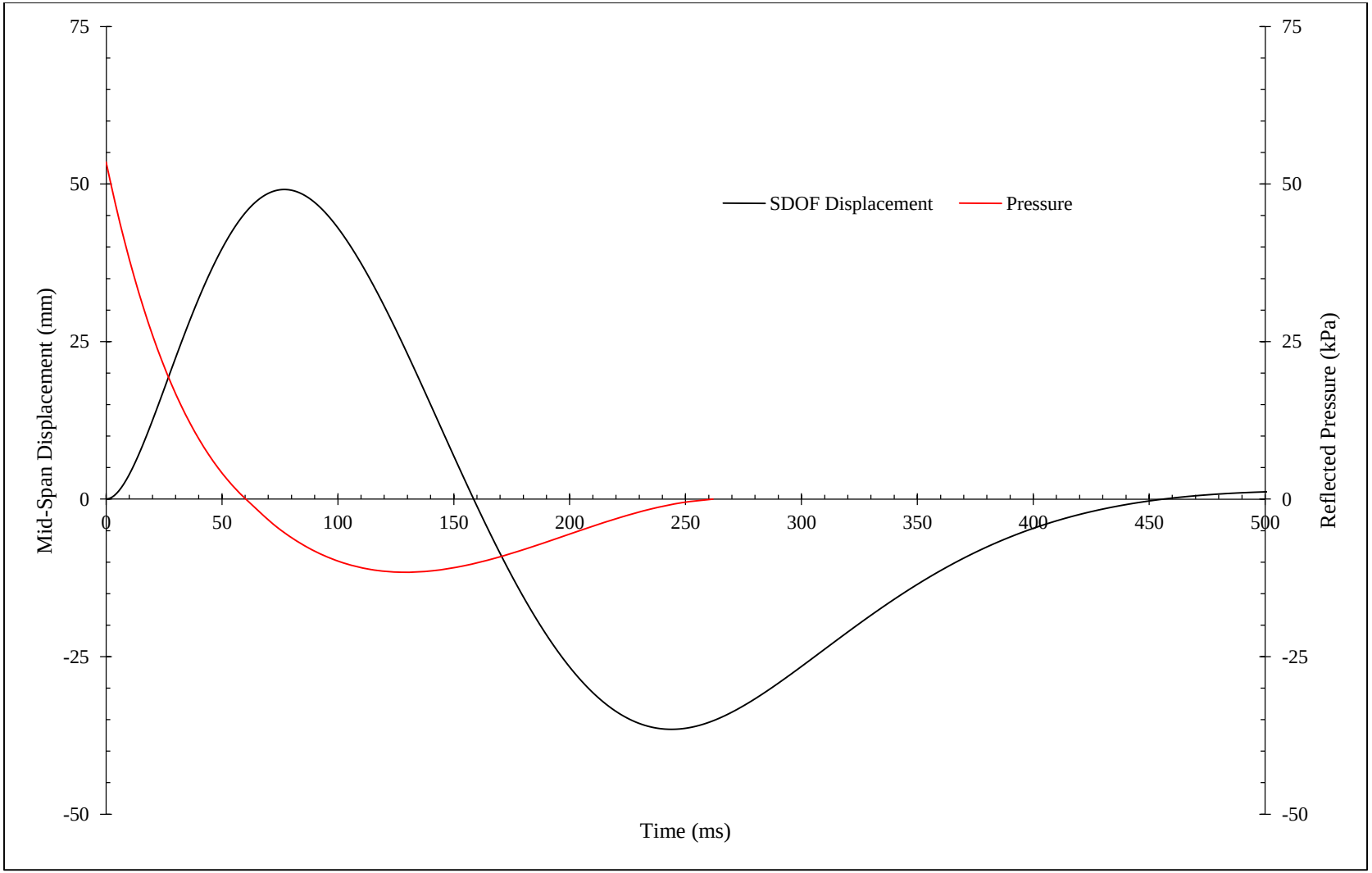

Figure D.4 – NCTS-FS8 2800kg TNT @ 100m: Pressure-Time and Displacement-Time Histories

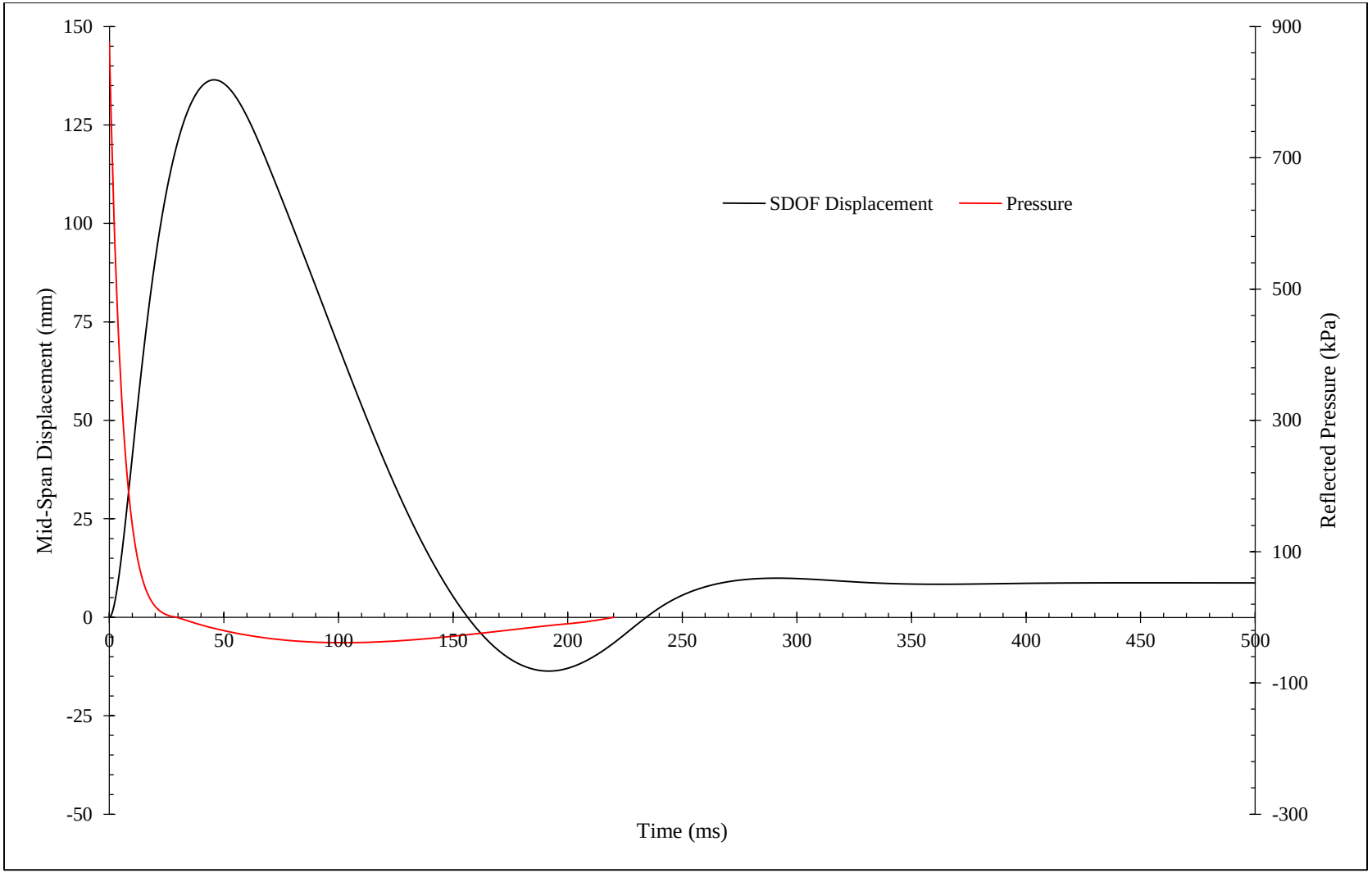

Figure D.5 – NCTS-FS4 2800kg TNT @ 30m: Pressure-Time and Displacement-Time Histories

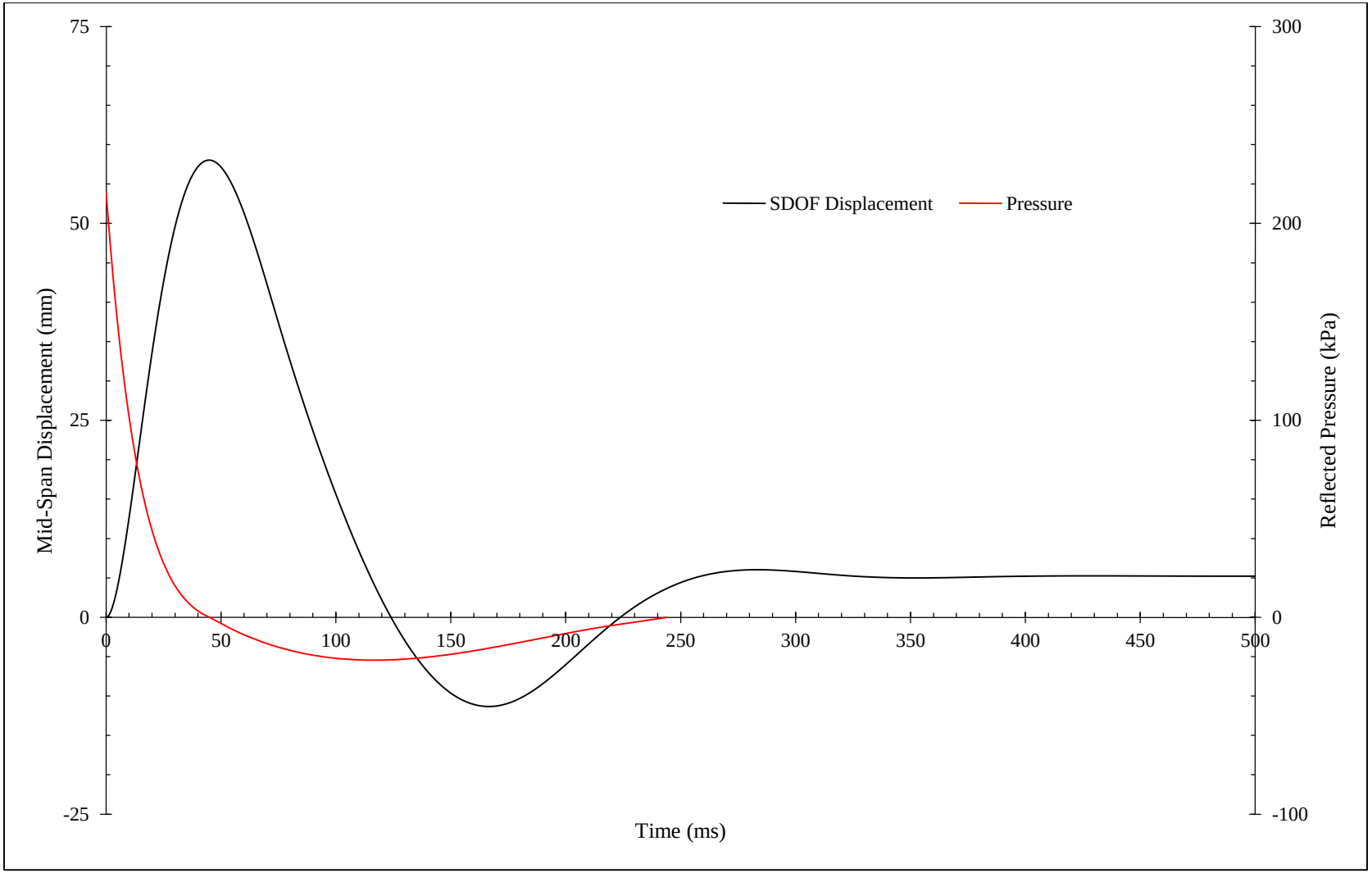

Figure D.6 – NCTS-FS4 2800kg TNT @ 50m: Pressure-Time and Displacement-Time Histories

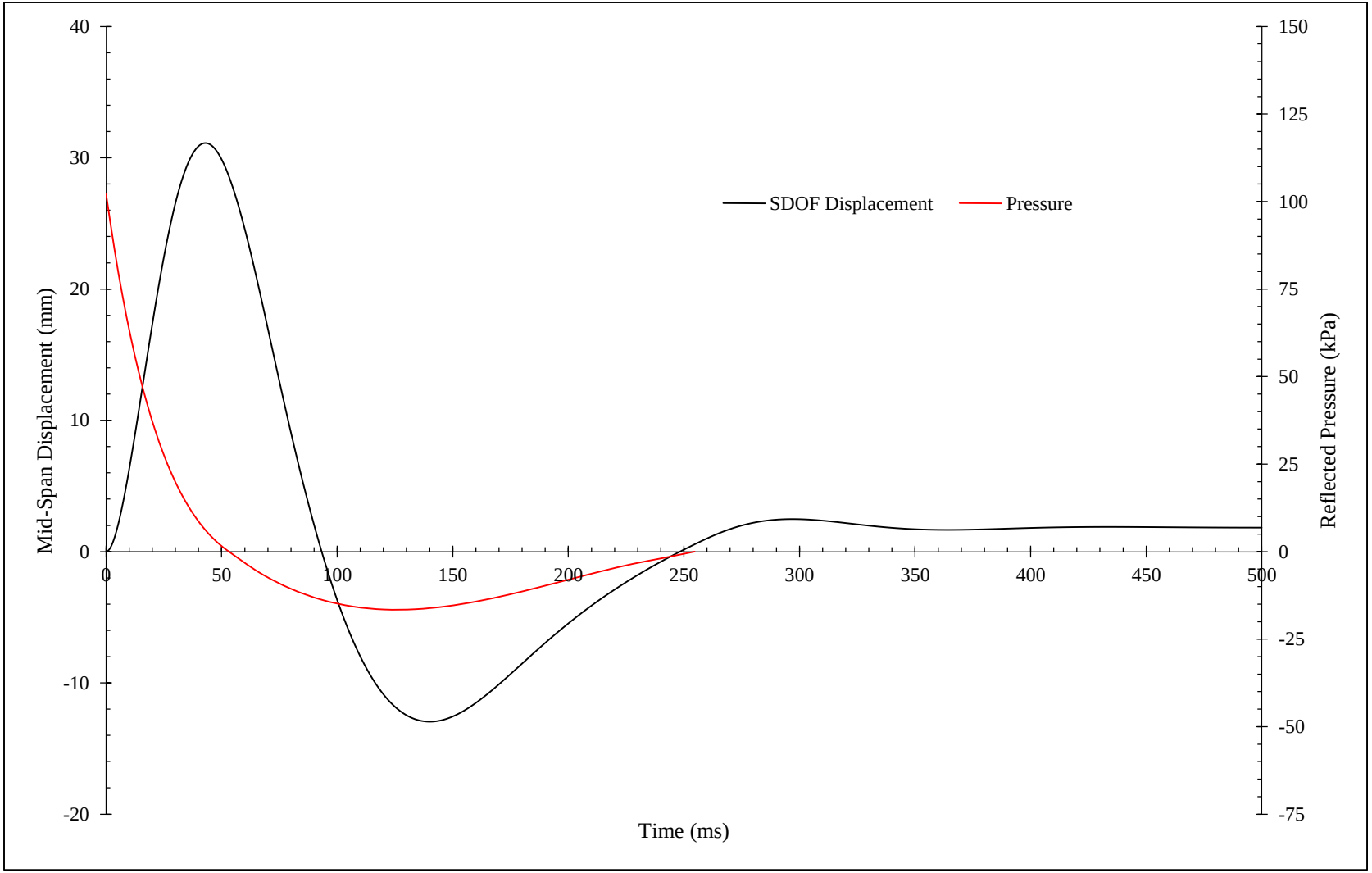

Figure D.7 – NCTS-FS4 2800kg TNT @ 70m: Pressure-Time and Displacement-Time Histories

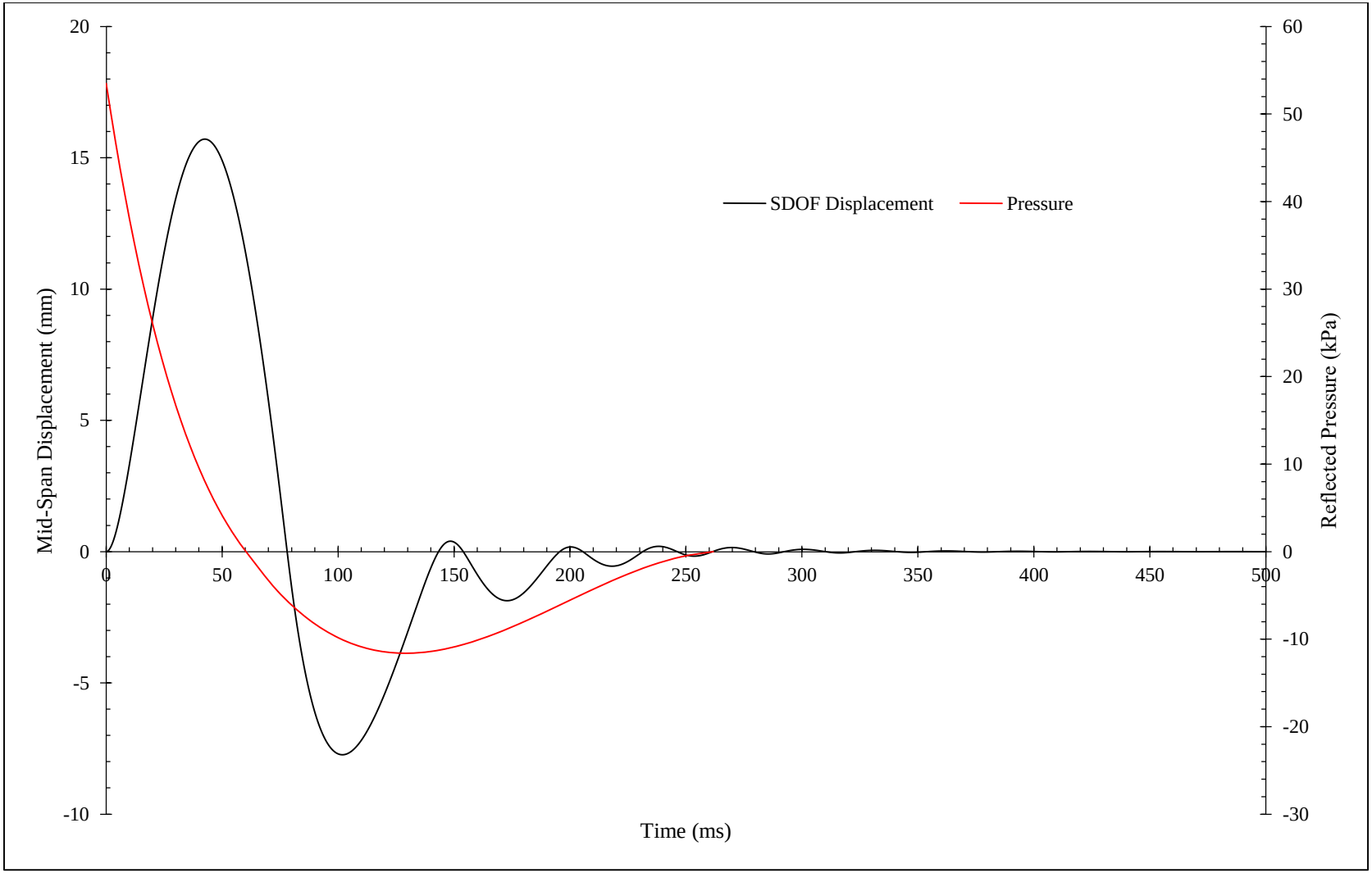

Figure D.8 – NCTS-FS4 2800kg TNT @ 100m: Pressure-Time and Displacement-Time Histories